THE JOURNAL
OF
CHEMICAL PHYSICS

VOLUME 19, NUMBER 5 MAY, 1951

On the Energetic Treatment of Non-Isothermal Processes. The Principle of Thermal Interaction

HANS HOLTAN, JR.
*Institutt for Teoretisk Kjemi, Norges Tekniske Hoegskole, Trondheim, Norway**

(Received December 15, 1950)

1. The existing theories for non-isothermal processes are discussed. They can be divided into two kinds, depending upon whether or not they take the flow of heat into account. None are able to predict experimental results.

2. A new hypothesis, "the principle of thermal interaction" is introduced by employing Onsager's principle of reciprocity and is expressed in terms of Brønsted's energetics.

It states that *there is an interaction between the flow of heat and the transport phenomena in a non-isothermal process in such a way that the loss of work* (loss of potential energy) *for the transport of entropy bound to chemical substance can be compensated partly or completely by the transport of free entropy contained in the flow of heat in the opposite direction.* The result is that any particle will tend to move against the temperature gradient.

3. The new principle is applied to thermocells with a solid electrolyte, and the results predicted are shown to be in agreement with experimental data.

4. The Knudsen equation, applicable to a thermal transpiration cell, is derived without employing the kinetic theory of gases.

INTRODUCTION

THE first thermodynamic treatment of a non-isothermal system was carried out by W. Thomson.[1-4] (For a review of his ideas see references 5 and 6.) His treatment was based upon the important assumption that the thermoelectric effect is a reversible one, not influenced by the irreversible flow of heat and the evolution of Joule heat always present in such a system.

During the past 100 years, this hypothesis has been discussed frequently, without establishing whether or not the hypothesis is correct. The Thomson equations appear, however, to agree with experiment. These equations are derived by setting the amounts of heat reversibly added to the system during a cycle equal to the electric work performed, according to the first law, and assuming, according to the second law, that there are no changes in entropy during the process. Thus:

$$dE/dT=\pi/T, \tag{1}$$

and

$$d^2E/dT^2=(\sigma_b-\sigma_a)/T, \tag{2}$$

where E is the thermoelectric force, π is the Peltier-coefficient for the reversible heat effect occurring at the junctions between the two metals a and b, and σ_a and σ_b are the Thomson coefficients for the reversible heat effect occuring in the temperature gradient of the two electric conductors.

L. Boltzmann[7] was the first to criticize Thomson's hypothesis. He stated that the irreversible flow of heat and the Joule heat cannot be ignored because it is impossible to eliminate both of them by any kind of experiment. His treatment leads to an inequality not subject to experimental test.

N. Bohr[8] found the Thomson equations as a by-product of his theoretical investigations on the electronic theory of metals. He, too, disagreed with Thomson on the fundamental hypothesis. The reason why he found the same equations resides in the fact that the equations for the movement of individual particles are symmetric to the past and the future, or,

* Present address: c/o Prof. Victor K. La Mer, Columbia University, New York 27, New York.

[1] W. Thomson, Proc. Roy. Soc. Edinburgh, December 15, 1851.
[2] W. Thomson, Proc. Roy. Soc. (London), VII, May, 1854.
[3] W. Thomson, Trans. Roy. Soc. Edinburgh 21, 123 (1857).
[4] W. Thomson, Mat. Fys. Papers I 232, 316 (1882); II 192 (1884).
[5] Wm. Roeser, J. Appl. Phys. 11, 388 (1940).
[6] Handbuch der Exp. Physik XI², 397 (1935).
[7] L. Boltzmann, Sitzber. Akad. Wiss. Wien, Math.-naturw. Klasse. Abt. II. 96, 1258 (1887).
[8] Niels Bohr, "Studier over metallernes elektroneteori," dissertation, Copenhagen, 1911, p. 72.

expressed mathematically, that they are invariant to the transformation

$$(t)\rightarrow(-t). \tag{3}$$

L. Onsager[9] has also disagreed with Thomson's hypothesis. He introduced his principle of reciprocity, which he proved by a statistical treatment based upon the principle of microscopic reversibility. If there were no interaction between the flow of heat and the flow of electricity, we would have

$$X_1=R_1I_1, \tag{4}$$

and

$$X_2=R_2I_2, \tag{5}$$

where X_1, R_1, and I_1 are the electric potential difference, the electric resistance, and the electric current; and the symbols with the subscript 2 are the corresponding properties for the heat flow.

If they interact with each other, we have

$$X_1=R_{11}I_1+R_{12}I_2, \tag{6}$$

$$X_2=R_{21}I_1+R_{22}I_2. \tag{7}$$

The principle of reciprocity states that $R_{12}=R_{21}$.

This principle has been applied more recently by Prigogine[10] to the calculation of different macroscopic effects. Even if R_{12} is equal to R_{21}, it is not possible to get rid of both of them in the final expressions. (In many cases, we have more than two such equations, and, therefore, more coefficients.) This means that this method, likewise, is not able to predict experimental results from known data. De Groot[11,12] has applied Onsager's principle of reciprocity to the Soret effect.

Eastman[13] based his theory upon the original Thomson hypothesis, treating the phenomena in the stationary states as reversible processes. The concept of a transfer of entropy is an important part of his presentation. Entropy of transfer is ascribed to the non-ideality of solutions and of membranes in the different systems. Application of this concept to processes such as, for example, thermal endosmosis, leads to the conclusion that the effects should disappear for ideal systems. Wagner[14] has treated the phenomena in a similar way. We shall show that there is no good reason for believing that this is the case.

Recently, Tolman and Fine[15] and Tuck[16] have published papers where various types of non-isothermal processes are treated as irreversible. Actually, their treatments tacitly imply Thomson's hypothesis, because no use is made of any principle of interaction between the flow of heat and the non-isothermal process. Bridgman[17] has discussed the thermocouple from a similar point of view.

Rodebush[18,19] many years ago published two interesting papers indicating that he was not certain that Eastman's treatment was correct. Brønsted,[20] making the Thomson assumption, has again discussed the thermoelectric effect in his last publication on energetics. Recently, a paper from five of Eastman's pupils[21] has been published. It contains a report of many experiments performed with thermocells. The old Eastman equation is again used in the interpretation of the experiments.

THE PRINCIPLE OF THERMAL INTERACTION IN NON-ISOTHERMAL SYSTEMS

The author of this paper considers the processes involved in all non-isothermal systems as being fundamentally of an irreversible nature. According to Onsager's principle of reciprocity, an interaction between the different irreversible processes has to be taken into account. The new idea is to express the interaction by means of known thermodynamic functions. A new hypothesis, given the name "principle of thermal interaction," will be introduced. In presenting this principle, Brønsted's energetics becomes particularly appropriate for the purpose. The following references (written in English) are recommended for readers not familiar with his new presentations.[22–24] A complete bibliography is also given in references 25 and 26. The relations to classical thermodynamics will, of course, be kept in mind at all times.

It is helpful to consider some ideas, discussed in Brønsted's first paper on energetics.[27] Since a chemical substance consists of a complex of quantities (chemical matter, volume, entropy, electrical charge, surface, etc.), the amount of chemical matter transported between different chemical potentials is not the only quantity which, in the general case, has to be taken into account

Consider two systems I and II consisting of the same chemical substance and defined by the variables pressure, temperature, chemical potential and the molal

[9] L. Onsager, Phys. Rev. **37**, 405 (1931); **38**, 2265 (1931).
[10] J. Prigogine, *Étude Thermodynamique des Phénomènes Irréversibles* (Dunod, Paris, 1947).
[11] S. R. de Groot, "L'effet Soret," theses, Amsterdam, 1945.
[12] S. R. de Groot, J. phys. radium (8) **8**, 193 (1947).
[13] E. D. Eastman, J. Am. Chem. Soc. **48**, 1482 (1926); **50**, 283 (1928).
[14] C. Wagner, Ann. Physik (5) **3**, 629 (1929); **6**, 370 (1930).
[15] R. C. Tolman and P. C. Fine, Revs. Modern Phys. **20**, 51 (1948).
[16] L. D. Tuck, J. Chem. Phys. **18**, 1128 (1950).
[17] P. W. Bridgman, *The Thermodynamics of Electrical Phenomena in Metals* (The Macmillan Company, New York, 1934).
[18] W. Rodebush, Chem. Rev. **4**, 255 (1927).
[19] W. Rodebush, J. Am. Chem. Soc. **49**, 792 (1927).
[20] J. N. Brønsted, Festskr. Koeb. Univ. November, 1946.
[21] Goodrich, Goyan, Morse, Preston, and Young, J. Am. Chem. Soc. **72**, 4411 (1950).
[22] J. N. Brønsted, Phil. Mag. **7**, **29**, 449 (1940).
[23] J. N. Brønsted, Kgl. Danske Videnskab. Selskabs, Mat.-fys. Medd. XIX, 8 (1941).
[24] La Mer, Foss, and Reiss, Ann. N. Y. Acad. Sci. **6**, 605 (1949), reprinted in Acta. Chem. Scand. **3**, 1238 (1950).
[25] K. Sandved and H. Holtan, Jr., J. Chem. Educ. **26**, 288 (1949).
[26] H. Holtan, Jr., Tids. Kjemi, Bergvesen, Met. **8**, 124 (1948); reprinted in Tekn. Ukeblad **95**, 6241 (1948).
[27] J. N. Brønsted, Kgl. Danske Vidsenskab. Selskab, Mat.-fys. Medd XV, No. 4 (1937).

quantities energy, entropy, and volume:

I. p_1, T_1, μ_1, E_1, S_1, and V_1;
II. p_2, T_2, μ_2, E_2, S_2, and V_2.

A surrounding vacuum is also included in the total system. Using the classical method of Carnot–van't Hoff, Brønsted obtains the following expressions for A, the maximum external work gained by a reversible transport of one mole of substance from system I to system II:

$$A=\mu_1-\mu_2+S_1(T_1-T_2). \tag{8}$$

Various intermediate states of type III, differing from I and II in certain values of the variables, are used in the derivation of (8). Brønsted shows that the final expression (8) for a finite process I→II, does not depend upon the choice of the intermediate state, i.e., the path followed, as long as the entropy necessary for the transformations involved in passing through the different intermediate states III, is taken in every case from system II. Since the transport of chemical substance automatically involves a transport of entropy bound to the substance, the work connected with the transport of the complex will be the sum of a chemical and a thermal term. According to Brønsted's work principle, we should expect a corresponding pressure-volume term to be added to Eq. (8). The complete symmetry which generally characterizes the different energy and work terms is, consequently, not involved in Eq. (8). This is due to the fact that the transport phenomena in the system is not symmetric, because no net transport of volume has taken place. He, therefore, states that the transport of volume has been compensated by a transport of free volume in the opposite direction.

If now the transport of entropy is compensated by a transport of free entropy (entropy not bound to matter) from II to I, we may say that no transport of entropy has taken place, and the work will be equal to the pure chemical term. Brønsted seems not to have had the entropy connected to the heat flow, which always is present in such a system, in mind when he wrote this, because in his later (1946) treatment of the thermoelectric phenomena, he employs Thomson's hypothesis, assuming that there is no interference between the heat flow and the thermoelectric effect. In the case discussed previously, the compensating entropy must, therefore, have been taken from system II and led reversibly and added to system I.

According to Onsager's principle of reciprocity, the heat flow *does* interfere with the transport phenomena, and the new hypothesis which we introduce states that the flow of heat interacts with the transport phenomena inside a non-isothermal system in such a way that the thermal loss of work (loss in thermal potential energy) for the transport of thermal quantity bound to the substance (the entropy) is compensated for partly or completely by the transport of free entropy in the opposite direction. This means that the term $S_1(T_1-T_2)$ in Eq. (8) disappears partly or completely.

In the derivation of Eq. (8), it is assumed that the entropy (S_2-S_1) necessary for the transformations is taken from system II. If this entropy is taken from system I instead of from system II, the thermal term will be $S_2(T_1-T_2)$ instead of $S_1(T_1-T_2)$. The expression for the loss of work will, consequently, depend upon the source of (S_2-S_1). In actual transport processes in non-isothermal systems, this arbitrariness does not introduce any difficulty, because the path of the transport process is known. In these systems, the entropy necessary for raising the temperature of a complex of quantities, is always taken from Thomson reservoirs, i.e., from heat reservoirs outside the system. Thus, the Thomson entropy is defined by:[20]

$$dS=(\partial S/\partial T)dT=\sigma' dT,\dagger \tag{9}$$

where the Thomson entropy coefficient σ' is related to the ordinary Thomson coefficient σ by the equation

$$\sigma'=\sigma/T. \tag{10}$$

For two systems which differ infinitesimally with respect to the temperature, we have for the total loss of work

$$SdT+d\mu=0. \tag{11}$$

Equation (11) is, of course, one of Gibbs' energy equations. Brønsted has shown that the sum of the thermal and the chemical losses of work (losses of potential energy) during a transport of substance in such a system is equal to zero also for finite temperature differences (pressure is constant) when the entropy variation according to Eq. (9) is exchanged between the system and the surroundings (Thomson reservoirs along the temperature gradient). The result is that in such a system there is no tendency for matter to be transported from one point to another, because a reversible transport is accompanied by no loss in potential energy. There will, consequently, not be any tendency for an irreversible process to take place. This statement becomes correct only if there is no interaction between the flow of heat and the transport of the complex of quantities in the system. We assert that there is interaction, and, consequently, a movement of particles against the temperature gradient exists when the particles are not hindered by any external constraint, because a part or all of the term SdT cancels as a result of the flow of heat in the opposite direction. The transport of matter, consequently, depends not only upon the temperature gradient but also upon the actual flow of heat. This is the *principle of thermal interaction.*

Now in certain systems, this transport against the temperature difference is hindered if the cycle is not complete, as, for example, is the case in a thermocell involving a solid electrolyte. In other cases, for example in the gaseous thermocell or in a non-isothermal solution

† No restriction on the partial differential coefficient in Eq. (9) is given, as it differs from case to case.

(Soret-effect), the processes will run irreversibly. If all of the entropy bound to substance is compensated, as it is in certain systems where the irreversible processes are not allowed to proceed, it means that in this case $-\Delta F$ becomes the measure for the maximum obtainable work.

During the formulation of this principle of thermal interaction, we have had at all times a one-component system in mind, but extension to polycomponent systems is not difficult.

THERMOCELLS WITH SOLID ELECTROLYTE

All the thermocells considered here will be of the type

$$\underset{T_1}{\text{Me}};\ \text{MeX};\ \underset{T_2}{\text{Me}} \qquad (12)$$

or

$$\underset{T_1}{\text{X}_2};\ \text{MeX};\ \underset{T_2}{\text{X}_2}, \qquad (13)$$

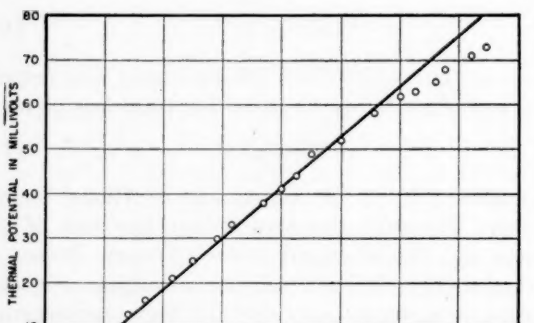

FIG. 1. Thermopotential as a function of the temperature difference for the system $\underset{T_1}{\text{Pb}};\ \text{PbCl}_2;\ \underset{T_2}{\text{Pb}}$. One electrode is maintained at 350°C. Circles are Reinhold's (reference 28) results. The line is drawn for the theoretical limiting slope at 350°C.

where Me stands for metal, MeX for solid (or fused) salt and X_2 for gas (halogen), as in the following cell:

$$\underset{T}{\text{Pb}};\ \text{PbCl}_2;\ \underset{T+dT}{\text{Pb}} \qquad (14)$$

$PbCl_2$ is an anion conductor, i.e., the transference number for the anion equals unity. Passage of one faraday of electricity through this cell produces the following cell reaction:

$$\tfrac{1}{2}\text{Pb}_T+\tfrac{1}{2}\text{PbCl}_{2T+dT}\rightarrow\tfrac{1}{2}\text{Pb}_{T+dT}+\tfrac{1}{2}\text{PbCl}_{2T}. \qquad (15)$$

The thermopotential will be given by

$$dE/dT=(S'''_{\text{Pb}}-S'''_{\text{PbCl}_2})/2f, \qquad (16)$$

where S''' refers to the compensated entropy, and f is 96,500 coulomb.

Brønsted's entropy symbols (1) to (3) are extended to (4); thus:

(1) S: general symbol for entropy

(2) S': transported or communicated entropy

(3) S'': entropy produced by an irreversible process

(4) S''': compensated entropy.

Inserting the absolute entropies for lead and lead chloride in this equation, we obtain a result which is in complete agreement with the experimental results obtained by Reinhold;[28] see Fig. 1. This means that all of the entropy bound to the substance is compensated in this case. It also means that $-\Delta F$, in this case as in isothermal reactions, gives the maximum obtainable external work.

Since the entropy of lead chloride is greater than that of lead, it follows from Eq. (16) that the colder electrode will be positive, in agreement with experiment.

Next consider the thermocell

$$\underset{T}{\text{Ag}};\ \text{AgCl};\ \underset{T+dT}{\text{Ag}}, \qquad (17)$$

where the electrolyte is a cation conductor; i.e., the transference number for the cation is equal to one.

In this cell we might expect the thermopotential to be

$$dE/dT=S_{\text{Ag}}/f, \qquad (18)$$

the metal, according to the principle of thermal interaction, being transported against the temperature gradient, making the warmer electrode positive. This is, however, not the case. If we consider the cell more carefully, we see that this cell reaction has no opportunity to take place, because both electrodes and electrolyte are solid. We see that one mole of salt has to be transported in the opposite direction. This is also pointed out by Reinhold.[29] He, however, never took this transport into consideration, stating that it was a purely mechanical one. According to our point of view, it has to be taken into consideration, because it is accompanied by changes in thermal energy. As a result, the thermopotential will be:

$$dE/dT=(S_{\text{Ag}}-S_{\text{AgCl}})/f. \qquad (19)$$

We have again inserted the absolute entropies for the compensated entropies. The calculated thermopotential is now in complete agreement with experimental results, Fig. 2.

The results of many such calculations (unpublished) leads to a principle for stationary and nonstationary electrodes. According to this principle:

1. A solid metal electrode is stationary. If substance is removed from this electrode, this empty space cannot be filled by the electrode itself; it has to be filled with electrolyte. In addition, there is no place for adding substance to the electrode without moving the electrolyte away.

2. A fused metal electrode is nonstationary. It can itself fill such an empty space. This space might also be filled with electrolyte.

[28] H. Reinhold, Z. anorg. Chem. **171**, 193 (1928).
[29] H. Reinhold, Z. Electrochem. **30**, 294 (1933).

3. A gas electrode, constructed in such a way that the gas is absorbed in a suitable metal, is not stationary. An empty space here has to be filled with electrolyte.

By considering cells with solid metal electrodes and solid electrolyte, we have, thus, seen that the colder electrode will always be positive, because a transport of electrolyte has to take place. If we consider thermocells where the electrodes melt at lower temperatures than the salt and if the salt has a sufficiently small anionic transference number, we will expect the metal to move against the temperature gradient. This is the case in the cell

$$\underset{T}{Pb_{(l)}};\ \underset{T}{\underset{T+dT}{PbI_{2(s)}}};\ \underset{T+dT}{Pb}, \qquad (20)$$

where Reinhold[29] found that the warmer electrode to be positive; in the other cases he found the colder electrode to be positive. If only the cation carried the current, the potential would be

$$dE_1/dT = S_{Pb}/2f = 0.48_3 \text{ mv/degree at } 350°C, \qquad (21)$$

but if only the cation carried the current, the potential would be

$$dE_2/dT = -(S_{PbI_2} - S_{Pb})/2f = -0.75_3 \text{ mv/degree at the same temperature.} \qquad (22)$$

We have, therefore, for the resulting potential

$$t^+(0.48_3) - t^-(0.75_3) = dE_{exp}. \qquad (23)$$

The transference numbers are known approximately and can be inserted into Eq. (23) for predicting the thermopotential. Here we will use the experimental thermopotential for calculating the transference numbers. The thermopotential determined by Reinhold[29] is 0.23 mv/degree at 350°C, yielding

$$t^+ = 0.80 \quad \text{and} \quad t^- = 0.20. \qquad (24)$$

G. V. Hevesy and W. Seith[30] found for the transference numbers using diffusion and conductance measurements the values:

T°C	t_{Pb}
338	0.79–0.85
376	0.93–1.00.

The results conform within the limits set by the following errors:

1. Errors involved in determining the thermopotential.
2. Errors involved in determining the entropies and specific heats of lead and lead iodide.
3. Errors involved in determining the transference numbers by diffusion and conduction measurements.

THE GASEOUS THERMOCELL

Experiments on the thermal transpiration cell were carried out as early as 1879 by Osborne Reynolds[31] using porous plugs. He found that

$$p_1/p_2 = (T_1/T_2)^{\frac{1}{2}} \qquad (25)$$

was valid for gases at low pressures.

In 1907 Lippmann[32] discovered that when a pure substance, for example, a liquid, is placed in two chambers separated by a membrane, the substance will flow from one chamber to the other when the temperatures in the two chambers are unequal. He experimented with many membranes and substances, and always found that the substances moved against the temperature gradient. This effect has been called thermal endosmosis. It has been treated thermodynamically by Eastman.[13]

Knudsen[33] derived the equation of Osborne Reynolds from the kinetic theory of gases, under the assumption that the parts of the system at different temperatures are separated by a capillary so narrow that the dimensions are of the same order of magnitude as the mean free path of the molecules.

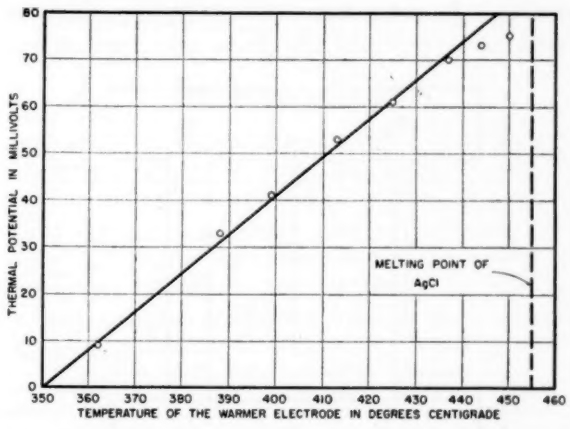

FIG. 2. Thermopotential as a function of the temperature difference for the system Ag; AgCl; Ag maintained at 327°C. $\underset{T_1}{\underset{T_2}{}}$ Circles are Reinhold's results (see reference 28). The line is drawn for the theoretical limiting slope of the curve at 327°C.

In differential form, Eq. (25) reads:

$$d \ln p = 1/2(d \ln T). \qquad (26)$$

Prigogine[10] has tried to derive Eq. (26) using Onsager's principle of reciprocity and de Donder's theory of affinity. His formula contains, however, an unknown coefficient. This coefficient can, of course, be evaluated by comparing the equation with Knudsen's kinetic expression, which is found to be in agreement with experimental results when the pressures are low. Recently, Brønsted and Koefoed[34] have reinvestigated this

[30] G. V. Hevesy and W. Seith, Z. Physik **56**, 790 (1929).
[31] Osborne Reynolds, Phil. Trans. **170**, II, 727 (1879).
[32] Lippmann, Compt. rend. **145**, 104, 105 (1907).
[33] M. Knudsen, Overs. Kgl. Danske Videnskab. Selskabs, Forh. 1909, 603, 1910, 1. Die Theorie der Strahlung und der Quanten. (Abh. d. Deutschen Bunsengeseschaft). Nr. 7. 116 (1913).
[34] Brønsted and Koefoed, Presented by Koefoed at Colloquium Brussels January, 1948.

effect experimentally using a plug of ZnO powder instead of a membrane.

The fountain effect in liquid helium II is a special case of the Reynolds-Lippmann effect, even though it is probably more complicated (two liquid flow). It is treated thermodynamically by London[35] on the assumption that it is a simple effect.

We will consider first Brønsted's interpretation[20] using the apparatus of Fig. 3. This gaseous thermocell consists of three containers B_0, B_1, and B_2 filled with the same pure gas. The states in the different containers are defined by the variables (temperature, pressure, entropy, volume, and chemical potential):

$$B_0\colon T_0,\ p_0,\ S_0,\ V_0, \text{ and } \mu_0.$$
$$B_1\colon T_1,\ p_0,\ S_1,\ V_1, \text{ and } \mu_1.$$
$$B_2\colon T_1,\ p_2,\ S_2,\ V_2, \text{ and } \mu_2.$$

That the pressures in B_1 and B_0 are the same means that the tube r_1 is wide, while the difference between the pressures in B_0 and B_2 means that the tube r_2 is narrow.

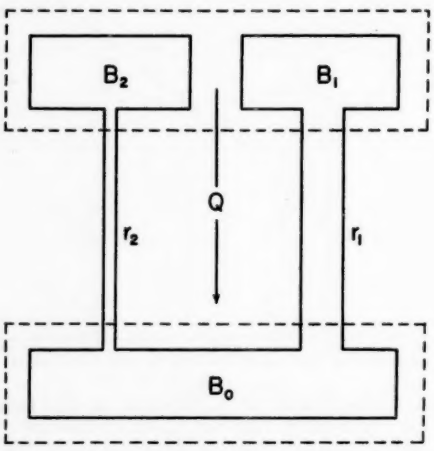

FIG. 3. Schematic representation of a thermal transparation cell with a narrow and a large tube.

According to Brønsted, the following expression will now be valid in the right side of the apparatus:

$$d\mu+SdT=0. \tag{27}$$

Since

$$dS=C_p d\ln T, \tag{28}$$

we will have

$$S-S_0=C_p \ln T/T_0, \tag{29}$$

and the chemical potential difference will be

$$\mu_1-\mu_0=S_0(T_0-T_1)+C_p[T_1-T_0-T_1 \ln(T_1/T_0)]. \tag{30}$$

If now the difference in entropy between B_1 and B_2 is communicated between r_1 and the surroundings, Brønsted shows that the losses of work (losses of potential energy), i.e., the chemical and the thermal loss of work, involved in a reversible transport of substance from B_0 to B_1, or vice versa, are equal and of opposite sign. This means that there is no tendency for the complex of quantity to move in any direction. This is also evident from Eq. (27), which may be taken as an expression for the sum of the losses of work in an infinitesimally diverging system. Consequently, there is no tendency for an irreversible process to take place. This statement becomes correct only if there is no interaction between the flow of heat and the transport of the quantities in the system. According to the principle of thermal interaction, the particles will tend to move up the temperature gradient. Since, however, the tube r_1 is wide, no pressure difference can be established, and the result in this case will be *convection*.

By considering the left part of the apparatus,‡ Brønsted used Knudsen's equation, and calculated the different losses of work by a reversible transport from B_0 to B_2 or vice versa. The result is, of course, that the sum of the chemical, spatial, and thermal terms are equal to zero. The only thing this tells us is that there is no macroscopic transport of matter in the stationary state.

Eastman[13] treats the thermal endosmosis in a similar way. According to his treatment, the effect is due to the occurence of heat effects when the substance passes through the membrane; the result is a transport of entropy in the surroundings, since this heat effect is different for leaving and entering the membrane. His final expression for this effect is

$$dp/dT=-\bar{L}_M/VT, \tag{31}$$

where $\bar{L}_M$ is the heat absorbed when one mole of the substance dissolves in a large amount of the saturated membrane. It is evident from Eq. (31) that the effect disappears when the membrane is ideal.

This discussion, based upon Thomson's hypothesis, leads to the conclusion that the effect is due to the capillary (Brønsted) or to the non-ideality of the membrane (Eastman).

APPLICATION OF THE PRINCIPLE OF THERMAL INTERACTION TO THE GASEOUS THERMOCELL

According to the principle of thermal interaction, a substance situated in a temperature gradient will tend to move up this gradient because of interaction with the flow of heat or because the loss of thermal work for the substance is compensated partly or completely by the transport of free entropy in the opposite direction. This tendency exists whether or not a membrane or a capillary is present. A pressure gradient, however, cannot be maintained without the insertion of a membrane or a capillary, and, as already mentioned, a convection between the cooler and the warmer zones will result in these cases. After insertion of a membrane or a capillary, we will expect the substance to move against the temperature gradient until the pressure is raised enough to hinder further transport. This is in agreement with experiment. The highest pressure is found in that region

[35] H. London, Proc. Roy. Soc. (London) **A171**, 484 (1939).

‡ Brønsted's treatment in this paper (1946) is not in agreement with the treatment in his first (1937) paper; see reference 27.

where the temperature is highest. However, the effect may be complicated when using a nonporous membrane in which the substance is slightly soluble.[36]

Consider the same pure substance in two different states I and II. In state I we have the temperature T and the pressure p, and in II we have the temperature $T+dT$ and the pressure $p+dp$. The two systems are separated by a membrane. The substance has moved against the temperature gradient because of the interaction of the flow of heat and has raised the pressure in system II. Since no external work is performed this process has run irreversibly. The entropy of n moles in system II is given by

$$nS_2=nS_1+n(\partial S/\partial T)_p dT+n(\partial S/\partial p)_T dp, \quad (32)$$

where S represents the molal entropy. If the substance is an ideal gas, no heat effects will occur except for the Thomson heat added during the passage through the membrane. This heat effect equals $C_v dT$ for the passage of one mole.

Since it follows from Eq. (8) that the difference in entropy between n moles of substance in state II and in state I is given by

$$ndS=nC_p/TdT-n(\partial V/\partial T)_p dp, \quad (33)$$

it follows that the entropy irreversibly produced by transport of n moles against the temperature gradient is equal to

$$ndS''=n(C_p-C_v)/T-n(\partial V/\partial T)_p dp, \quad (34)$$

where S'' stands for entropy irreversibly produced per mole.

According to the principle of thermal interaction, the loss in potential thermal energy will be equal to $S'''dT$, where S''' is the entropy bound to the substance which is compensated by the flow of free entropy in the opposite direction. In the stationary state, there is no macroscopic transport of substance, and we will have

$$-nSdT-nd\mu+nS'''dT=0, \quad (35)$$

or

$$nS'''dT=nVdp. \quad (36)$$

Since

$$nS'''dT=nTdS'', \quad (37)$$

we obtain from Eqs. (34), (36), and (37)

$$(C_p-C_v)dT-T(\partial V/\partial T)_p dp=Vdp, \quad (38)$$

and by inserting the values for an ideal gas, we obtain

$$RdT=(RT/p)dp+Vdp=2Vdp, \quad (39)$$

or

$$d\ln p=\tfrac{1}{2}d\ln T. \quad (40)$$

This is the Knudsen Eq. (26) in differential form.

Equation (40) has been derived here on the assumption that both gas and membrane are ideal, i.e., for the same case for which the effect according to Eastman's theory should disappear, see Eq. (31).§

In our treatment we have sought for potential differences as a driving force in accordance with Brønsted's fundamental postulate, rather than assuming the driving forces to arise from equipotential communicated heat.

ACKNOWLEDGMENT

The author is indebted to Professor Karl Sandved, Norwegian Institute of Technology, Trondheim, Norway, for extensive and valuable discussions on the subject during three years, and to Professor V. K. LaMer, Columbia University, for many critical and constructive discussions and for his aid in composing the manuscript while holding a Smith-Mundt Fellowship in his laboratory.

[36] K. G. Denbigh, Nature **163**, 60 (1949).

§ For the osmotic temperature effect Eastman obtains an equation similar to Eq. (31). It is based upon the assumption that the decrease in activity of the solvent produced by the presence of a solute might be compensated by an increase in temperature as well as by an increase in pressure as in the ordinary osmotic equilibrium. Eastman concludes after deriving this equation: "Furthermore, resort to ideal membranes showing no heat effects fails to generalize the concept, for it then appears that, in perfect solutions, equilibrium can result only when there is no difference in composition of the solution of the two components. The conception, therefore, has no general meaning or application in thermodynamics."

Molecular Orbital Calculations for H_3

J. M. WALSH AND F. A. MATSEN
Departments of Physics and Chemistry, The University of Texas, Austin, Texas
(Received November 30, 1950)

Calculations are made on the binding energy of H_3 using the several methods of calculation based on molecular orbitals. The results are compared to the valence bond-plus-ionic-terms treatment of Hirschfelder *et al.*, which employs the most general linear combination of products of atomic orbitals. The antisymmetrized molecular orbital treatment with configuration interaction is only slightly inferior to this treatment, while the other molecular orbital calculations are considerably inferior. These conclusions probably apply to calculations on more complex molecules.

WITH few exceptions[1,2] the wave functions for molecules are taken to be linear combinations of products of atomic orbitals. These functions must satisfy the Pauli principle and must belong to one of the irreducible representations of the molecular point group. The most general expansion of this type is that used in the complete valence bond-plus-ionic-terms treatment, since the number of independent structures is always equal to the number of the several products. For polyatomic molecules[3] all other product expansion treatments are less general and lead to a poorer description as a consequence of restrictions imposed on the variation parameters. One of these treatments, the antisymmetrized molecular orbital product, has been used extensively in calculations on conjugated unsaturated molecules.[4] For H_2 and H_3^+ the calculation[5,6] has been improved by the use of "generalized" molecular orbitals. Further improvement in the treatment has been obtained by a consideration of the interaction between the several electron configurations.[7–9] While both of these devices give improved descriptions, these must always be poorer than that resulting from the most general expansion as obtained with the valence bond-plus-ionic-terms treatment.

The valence bond treatment alone and with ionic terms for H_3 has been given by Hirschfelder.[10] In the present paper are presented the antisymmetrized molecular orbital product, the generalized molecular orbital, and the molecular orbital with configuration interaction treatments for the same molecule. The five calculations are compared both from the standpoint of the generality of the wave functions and by the calculated binding energies. The latter quantity appears to be a good criterion for wave function quality.

The three orthogonal molecular orbitals for the linear symmetrical configuration of H_3 are

$$\begin{aligned}\psi_{\mathrm{I}}(i)&=a_1(i)+\lambda a_2(i)+a_3(i),\\ \psi_{\mathrm{II}}(i)&=a_1(i)-a_3(i),\\ \psi_{\mathrm{III}}(i)&=a_1(i)-\lambda' a_2(i)+a_3(i),\end{aligned}\tag{1}$$

where

$$\lambda'=\frac{2(1+S_{13}+\lambda S_{12})}{\lambda+2S_{12}},$$

and S_{ij} are the overlap integrals;

$$S_{ij}=\int a_i(k)a_j(k)d\tau_k.$$

These orbitals represent the ground, first excited, and second excited one-electron orbitals, since they contain zero, one, and two nodal surfaces, respectively.[11] Thus, the antisymmetrized molecular orbital representation of this system is written

$$\psi=\Sigma(-1)^P P\psi_{\mathrm{I}}(1)\psi_{\mathrm{I}}(2)\psi_{\mathrm{II}}(3)\alpha(1)\beta(2)\alpha(3).$$

This function may be expanded and written in terms of the atomic orbital wave functions. It is then seen to differ from the most general wave function in that certain of the coefficients are no longer independent and arbitrary (see Table I).

The integrals that arise from the variation treatment of this wave function are either available as familiar types or may be obtained from the tables[12] of Hirschfelder and Weygandt, compiled by use of a differential analyzer. Calculations were made both with and without inclusion of a variable screening constant in the atomic orbitals. For $Z=1$ (no screening) a binding energy of 38.5 kcal/mole with respect to the infinitely spaced hydrogen atoms is obtained. The predicted internuclear separation is $R=2.00a_0$, and the associated value of the λ-parameter is $\lambda=1.6$. When Z is varied as a parameter the energy expression is minimized for $R=1.82a_0$,

[1] H. M. James and A. S. Coolidge, J. Chem. Phys. **1**, 825 (1933).
[2] Frost, Braunstein, and Schwemer, J. Am. Chem. Soc. **70**, 3292 (1948).
[3] For H_2, the valence bond-plus-ionic-terms, the generalized molecular orbital, and the molecular orbital with configuration interaction treatments are identical, while the antisymmetrized molecular orbital product and the valence bond treatments are less general.
[4] For example: M. G. Mayer and A. L. Sklar, J. Chem. Phys. **6**, 645 (1938).
[5] C. A. Coulson, Phil. Mag. **40**, 393 (1949).
[6] Walsh, Moore, and Matsen, J. Chem. Phys. **18**, 1070 (1950).
[7] D. P. Craig, Proc. Roy. Soc. (London) **200A**, 474 (1950).
[8] Parr, Craig, and Ross, J. Chem. Phys. **18**, 1561 (1950).
[9] Configuration interaction is implicit in the treatment of ethylene by R. G. Parr and B. L. Crawford, J. Chem. Phys. **16**, 526 (1950).
[10] J. Hirschfelder, J. Chem. Phys. **6**, 795 (1938).
[11] K. F. Herzfeld, Revs. Modern Phys. **21**, 527 (1949).
[12] J. Hirschfelder and C. N. Weygandt, J. Chem. Phys. **6**, 806 (1938).

$Z=1.10$ and $\lambda=1.5$, and the total binding[13] is 46.0 kcal/mole, an improvement of only 7.5 kcal/mole over that obtained without a screening constant. In obtaining these minima, only integral and half-integral values of $\rho=ZR$ were used, since some of the integrals are tabulated only for these values.

Use of the most general possible (non-orthogonal) one-electron orbitals

$$\psi_1(i)=a_1(i)+\lambda_2 a_2(i)+\lambda_3 a_3(i),$$
$$\psi_2(i)=a_1(i)+\eta_2 a_2(i)+\eta_3 a_3(i),$$
$$\psi_3(i)=a_1(i)+\mu_2 a_2(i)+\mu_3 a_3(i),$$

to formulate a molecular wave function leads to only a slight improvement over the simple molecular orbitals. When this function is written in valence bond-plus-ionic-terms form, the coefficients given in the fourth column of Table I are obtained. As seen by comparison to the third column, this function differs from the simple molecular orbital only in that the coefficient of the first term is not restricted to the value two. Now in the valence bond-plus-ionic-terms analysis this quantity was varied and found to be two. It seems logical to conclude, then, that the generalized molecular orbitals for H_3 would give only a slight, if any, improvement over the simpler antisymmetrized molecular orbital treatment.

The allowed electron configurations for H_3 are

$$\begin{aligned}
&\psi_{\rm I}(1)\psi_{\rm I}(2)\psi_{\rm II}(3) && \text{a}\\
&\psi_{\rm I}(1)\psi_{\rm II}(2)\psi_{\rm II}(3) && \text{b}\\
&\psi_{\rm I}(1)\psi_{\rm II}(2)\psi_{\rm III}(3) && \text{c}\\
&\psi_{\rm II}(1)\psi_{\rm II}(2)\psi_{\rm III}(3) && \text{d}\\
&\psi_{\rm II}(1)\psi_{\rm III}(2)\psi_{\rm III}(3). && \text{e}
\end{aligned} \qquad (2)$$

TABLE I. Comparison of valence bond-plus-ionic-terms coefficients (obtained by variation as arbitrary parameters) to the analogous molecular orbital quantities obtained upon writing molecular orbital wave functions in valence bond form.

Term [See Eq. (4)]	Arbitrary coefficients (Reference 10)	Analogous molecular orbital parameters	Analogous generalized molecular orbital parameters	Analogous configuration interaction parameters
$a_1a_2a_3\beta(2)$ type terms	2.0	2.0	B_1B_2	2.0
$a_1a_2a_3\beta(1)$ and $\beta(3)$ terms	−1.0	−1.0	−1.0	$-(1+C_1)$
$a_2a_2a_1$ and $a_1a_3a_3$ terms	0.31	$\lambda=1.5$	B_1	C_2
$a_1a_1a_2$ and $a_2a_3a_3$ terms	0.25	1.0	1.0	$(1-C_1)$
$a_1a_1a_3$ and $a_2a_3a_1$ terms	0.13	$2/\lambda=1.33$	B_2	C_3
	Calculated energy 67.09 kcal/mole	Calculated energy 45.97 kcal/mole	~46	~64 kcal/mole

[13] R. G. Pearson, J. Chem. Phys. **16**, 502 (1948). A molecular orbital treatment of H_3 is given, neglecting antisymmetrization. An instability of 28 kcal/mole with respect to the separate atoms is obtained. A stability of 46 kcal/mole is obtained above when the function is antisymmetrized. This 74 kcal/mole improvement may be regarded as electron correlation brought about by the antisymmetrization process.

The molecular orbitals are given explicitly in (1). The configurations, 2a, 2c, and 2e, are antisymmetric, while 2b and 2d are symmetric with respect to an interchange of the end nuclei so the two groups will not interact. Since 2a is the configuration of lowest energy, the antisymmetric set will contain the ground state. The configuration interaction wave function is then

$$\begin{aligned}
\psi=&\Sigma(-1)^P P\{\psi_{\rm I}(1)\psi_{\rm I}(2)\psi_{\rm II}(3)\alpha(1)\beta(2)\alpha(3)\}\\
&+A\Sigma(-1)^P P\{\psi_{\rm III}(1)\psi_{\rm III}(2)\psi_{\rm II}(3)\alpha(1)\beta(2)\alpha(3)\\
&+B\Sigma(-1)^P P\{\psi_{\rm I}(1)\psi_{\rm II}(2)\psi_{\rm III}(3)\alpha(1)\beta(2)\alpha(3)\}. \qquad (3)
\end{aligned}$$

Upon expanding and regrouping, this function may be written in the equivalent form

$$\begin{aligned}
\psi=&2.0[\Sigma(-1)^P P\{a_1(1)a_2(2)a_3(3)\alpha(1)\beta(2)\alpha(3)\}]\\
&-(1+C_1)[\Sigma(-1)^P P\{a_1(1)a_2(2)a_3(3)\beta(1)\alpha(2)\alpha(3)\}\\
&+\Sigma(-1)^P P\{a_1(1)a_2(2)a_3(3)\alpha(1)\alpha(2)\beta(3)\}]\\
&+C_2[\Sigma(-1)^P P\{a_2(1)a_2(2)a_1(3)\alpha(1)\beta(2)\alpha(3)\}\\
&-\Sigma(-1)^P P\{a_2(1)a_2(2)a_3(3)\alpha(1)\beta(2)\alpha(3)\}]\\
&+(1-C_1)[\Sigma(-1)^P P\{a_1(1)a_1(2)a_2(3)\alpha(1)\beta(2)\alpha(3)\}\\
&-\Sigma(-1)^P P\{a_3(1)a_3(2)a_2(3)\alpha(1)\beta(2)\alpha(3)\}]\\
&+C_3[\Sigma(-1)^P P\{a_1(1)a_1(2)a_3(3)\alpha(1)\beta(2)\alpha(3)\}\\
&-\Sigma(-1)^P P\{a_3(1)a_3(2)a_1(3)\alpha(1)\beta(2)\alpha(3)\}]. \qquad (4)
\end{aligned}$$

This function differs[14] from the most general which can be expanded in terms of the type atomic orbital products only in that the coefficients of the second and fourth terms above are not independent. For the purpose of the discussion, an estimate of the binding energy,[15] 63 ± 1 kcal/mole,[15] by this method is sufficient. This represents an improvement of some 18 kcal/mole over the simple molecular orbital treatment as a consequence of the de-emphasis of ionic terms. In the valence bond-plus-ionic-terms treatment all coefficients in equation are varied independently, which gives a binding energy 67.09 kcal/mole.

SUMMARY AND CONCLUSIONS

The simple, generalized, and configuration interaction molecular orbital methods have been applied to H_2, H_3^+, and H_3. For two electrons on two atoms, the generalized and configuration interaction molecular orbitals are considerably superior to the simple molecular orbital method and are equivalent to the most general ex-

[14] It is of interest to note that the analogous wave function for H_3^+, just as for H_2 above, is equivalent to the most general which can be expanded in terms of atomic orbitals; i.e., it is equivalent to the valence bond-plus-ionic-terms treatment for this linear symmetrical model. Hirschfelder, Eyring, and Rosen, J. Chem. Phys. **4**, 130 (1936). This corresponds to an energy calculation of 155.35 kcal/mole as compared to 136.8 kcal/mole for the simple molecular orbital treatment of that molecule.

[15] This estimate is obtained as follows: The difference between the valence bond and simple molecular orbital energy calculations is 67.09 minus 45.97 or 21.12 kcal/mole. The latter function differs from the valence bond function in that the coefficients of the third, fourth, and fifth terms are too large (see Table I). By picking $C_1=0$ in the configuration interaction column, only the fourth term coefficient (which is least exaggerated) remains too large. Hence, the discrepancy between the valence bond result and that of the present function is considerably less than one-third of 21 kcal/mole, probably 3 or 4 kcal/mole.

pansion in terms of atomic orbitals (i.e., the valence bond-plus-ionic-terms function).

For two electrons on three atoms, the generalized molecular orbital is superior to the simple molecular-orbital method but is inferior to the valence bond-plus-ionic-terms method. In this case, the configuration interaction method is again equivalent to the valence bond-plus-ionic-terms treatment.

For three electrons on three atoms, the generalized molecular orbital analysis gives only a slight improvement over use of simple molecular orbitals. The configuration interaction treatment, however, represents considerable improvement over the simple molecular orbital method, and is only slightly inferior to the valence bond-plus-ionic-terms analysis.

These results can probably be extrapolated to more complex systems. They indicate that judgment must be exercised in drawing conclusions from the antisymmetrized molecular orbital product treatments, and they are in accord with conclusions drawn from some of the recent calculations on conjugated unsaturated molecules.[7,8]

THE JOURNAL OF CHEMICAL PHYSICS VOLUME 19, NUMBER 5 MAY, 1951

The General Valence Orbitals Derivable by sp_3 Hybridization

P. TORKINGTON
British Rayon Research Association, Manchester, England
(Received November 26, 1950)

An examination is made of the allowed sets of four sp_3-hybrid orbitals satisfying the symmetry requirements of the point groups C_{2v} and C_{3v}, the object of the analysis being to aid in the formalization of the study of deviations from the ideal tetrahedral valence angle, found in systems of symmetry lower than T_d. Tables of allowed interorbital angles are given.

I. INTRODUCTION

MEASUREMENTS of molecular dimensions over the last few years have confirmed that comparatively few systems with the ideal hybrid bonds of quantum mechanics exist.* In particular, it would appear that if a hybrid set had a certain symmetry, then only if this symmetry was also present in the system of bonded atoms supposed containing the set would the valence angles be the ideal ones. Thus, the exact tetrahedral bonding angle is almost certainly only to be found in systems of symmetry T_d; CH_4 and CCl_4 can be assumed exactly tetrahedral, but this is certainly not true of CH_2Cl_2, of symmetry C_{2v}, or of CH_3Cl and $CHCl_3$, of symmetry C_{3v}. Asymmetrical van der Waals' repulsions would, of course, distort the valence angles; the orbitals would presumably adapt themselves, if this were allowable. Linnett (1)† has examined the dynamics of orbital-following which occurs during molecular vibrations; in some of the bending modes of methane and the deutero-methanes, orbital-following is allowed, so that the energy required to distort the bonds is less than in other modes in which orbital-following is forbidden. Non-tetrahedral orbitals for the carbon atom have been considered by Duffey (2), who applied his results to cyclo-butane and cyclo-pentane. His conclusions were criticized by Kilpatrick and Spitzer (3). In the present paper the two general sets of four orbitals having symmetries C_{2v} and C_{3v}, respectively, are examined. The approach is quite straightforward, but the results seem worth summarizing, as follows.

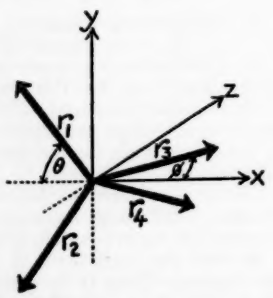

FIG. 1. Vector representation for systems of orbitals of symmetry C_{2v}.

II. SETS OF FOUR sp_3 HYBRID ORBITALS OF SYMMETRY C_{2v}

The coordinate axes used are shown in Fig. 1. The initial p orbitals ψ_{2p_x}, ψ_{2p_y} and ψ_{2p_z} can be represented by vectors along the x, y, and z axes. The s orbital ψ_{2s} will be spherically symmetrical about the origin of the system. The vectors r_1, r_2, r_3, and r_4 represent four hybrid orbitals, ψ_1 and ψ_2, ψ_3 and ψ_4. ψ_1 and ψ_2 form a pair of equivalent orbitals in the x–y plane, (σ_{xy}), symmetrical about σ_{xz}. ψ_3 and ψ_4 form another pair, in σ_{xz}, symmetrical about σ_{xy}. 2θ and 2ϕ are the inter-bonding angles for the two pairs of orbitals; they are related to the third angle, that between r_1 and r_3, as follows:

$$\cos\alpha_{13} = -\cos\theta\cdot\cos\phi. \qquad (1)$$

The direction cosines for the four hybrid orbitals in

* See the recent review by Wilson (7) (see Bibliography) on microwave spectroscopy, where references will be found. See also a note by the author (8).

† See Bibliography.

TABLE I. Direction cosines for the four hybrid orbitals of symmetry C_{2v}.

i	1	2	3	4
l_i	$-\cos\theta$	$-\cos\theta$	$\cos\phi$	$\cos\phi$
m_i	$\sin\theta$	$-\sin\theta$	0	0
n_i	0	0	$\sin\phi$	$-\sin\phi$

this vector representation are given in Table I. For hybridization to give resultants along r_1, r_2, r_3, and r_4, the three p orbitals must be combined as follows:

$$\begin{bmatrix}\psi_{2p_1}\\ \psi_{2p_2}\\ \psi_{2p_3}\\ \psi_{2p_4}\end{bmatrix}=\begin{bmatrix}-\cos\theta & \sin\theta & 0\\ -\cos\theta & -\sin\theta & 0\\ \cos\phi & 0 & \sin\phi\\ \cos\phi & 0 & -\sin\phi\end{bmatrix}\begin{bmatrix}\psi_{2p_x}\\ \psi_{2p_y}\\ \psi_{2p_z}\end{bmatrix}, \quad (2)$$

where ψ_{2p_i} is the component from the $2p$ orbitals to ψ_i. Now, including the $2s$ orbital, the final hybrids can be expressed as:

$$\psi_i=a_i\psi_{2s}+b_i\psi_{2p_i}, \quad (3)$$

with the coefficients a_i, b_i determined by the following necessary and sufficient condition for the orbitals to be an orthogonal normalized set (2):

$$a_ia_j+b_ib_j\cos\alpha_{ij}=\delta_{ij} \quad (i=1 \text{ to } 4,\ j=1 \text{ to } 4), \quad (4)$$

where α_{ij} is the angle between the vectors r_i and r_j, and δ_{ij} is the Kroenecker delta, ($\delta_{ij}=0$, $i\neq j$; $\delta_{ii}=1$, $i=1$ to 4). To satisfy the symmetry requirements of the present case,

$$a_1=a_2, \quad a_3=a_4; \quad b_1=b_2, \quad b_3=b_4. \quad (5)$$

Solving for the four constants‡ in terms of the angles θ, ϕ:

$$\left.\begin{aligned} a_1^2&=(1-\cot^2\theta)/2 \quad b_1^2=1/2\sin^2\theta\\ a_3^2&=(1-\cot^2\phi)/2 \quad b_3^2=1/2\sin^2\phi\end{aligned}\right\} \quad (6)$$

with the condition that the angles θ, ϕ should satisfy the following symmetrical relation:

$$3\cos2\theta\cdot\cos2\phi-\cos2\theta-\cos2\phi=1, \quad (7)$$

or:

$$\cot^2\theta+\cot^2\phi=1. \quad (7a)$$

The matrix equation for the transformation to the general set of orbitals of symmetry C_{2v} is then found to be as follows:

$$\begin{bmatrix}\psi_1\\ \psi_2\\ \psi_3\\ \psi_4\end{bmatrix}=\begin{bmatrix}\{(1-\cot^2\theta)/2\}^{\frac{1}{2}} & -(1/\sqrt{2})\cot\theta & 1/\sqrt{2} & 0\\ \{(1-\cot^2\theta)/2\}^{\frac{1}{2}} & -(1/\sqrt{2})\cot\theta & -1/\sqrt{2} & 0\\ \{(1-\cot^2\phi)/2\}^{\frac{1}{2}} & (1/\sqrt{2})\cot\phi & 0 & 1/\sqrt{2}\\ \{(1-\cot^2\phi)/2\}^{\frac{1}{2}} & (1/\sqrt{2})\cot\phi & 0 & -1/\sqrt{2}\end{bmatrix}\begin{bmatrix}\psi_{2s}\\ \psi_{2p_x}\\ \psi_{2p_y}\\ \psi_{2p_z}\end{bmatrix}. \quad (8)$$

In the above, the positive roots for a_i and b_i from Eq. (6) are used; apart from the sign, the coefficients are completely determined for a given value of either θ or ϕ. [See Eq. (7).] The form of the coefficients a_i restricts each angle to the range 45° to 135°. For a given value of ϕ, say, there will be two values allowed to θ, $\theta_1(<\pi/2)$ and $\theta_2=\pi-\theta_1$. The relation between the angles is shown in Fig. 2. The bond-forming power can be taken as proportional§ to the amplitude function P_i; for the ith orbital,

$$P_i=a_i\times1+(3\times b_i^2)^{\frac{1}{2}}, \quad (9)$$

where the value for the $2s$ orbital is unity. Substituting for the present problem from Eq. (6), we obtain

$$\left.\begin{aligned} P_1=P_2&=(3/2)^{\frac{1}{2}}\operatorname{cosec}\theta+\{(1-\cot^2\theta)/2\}^{\frac{1}{2}}\\ P_3=P_4&=(3/2)^{\frac{1}{2}}\operatorname{cosec}\phi+\{(1-\cot^2\phi)/2\}^{\frac{1}{2}}\end{aligned}\right\}. \quad (10)$$

It is convenient to define P_θ as the amplitude function for either of a pair of equivalent bonds, with interbonding angle 2θ; and similarly, P_ϕ with angle 2ϕ. Plots of P_θ and P_ϕ for the present problem are given in Fig. 3 as functions of the angle 2ϕ. From Eq. (10) it follows that, for a given value of ϕ, $P_{\theta_1}=P_{\theta_2}$. For $\phi<\pi/2<\theta$, or $\phi>\pi/2>\theta$, the orbitals have pyramidal form.

It appears that deviations from the tetrahedral bonding angle over the range of about 100° to 120° affect the bonding power of each bond only slightly. A small increase in one of the two angles is accompanied by a small decrease in the other; thus, opening up 2ϕ from the tetrahedral value (109°28′) to 120° closes 2θ to 101°32′ (arc cos $-1/5$), and the bonding-power amplitude functions go from $P=2$ to $P_\phi=1.992$, $P_\theta=1.989$.

The three matrices for the transformation of Eq. (8) for $2\phi=90°$, 109°28′, and 120° are given below:

$\phi=45°$, $\theta=90°$

$$\begin{bmatrix}1/\sqrt{2} & 0 & 1/\sqrt{2} & 0\\ 1/\sqrt{2} & 0 & -1/\sqrt{2} & 0\\ \cdots & \cdots & \cdots & \cdots\\ 0 & 1/\sqrt{2} & 0 & 1/\sqrt{2}\\ 0 & 1/\sqrt{2} & 0 & -1/\sqrt{2}\end{bmatrix}$$

$\phi=\theta=54°44'$

$$\begin{bmatrix}1/2 & -1/2 & 1/\sqrt{2} & 0\\ 1/2 & -1/2 & -1/\sqrt{2} & 0\\ \cdots & \cdots & \cdots & \cdots\\ 1/2 & 1/2 & 0 & 1/\sqrt{2}\\ 1/2 & 1/2 & 0 & -1/\sqrt{2}\end{bmatrix}$$

$\phi=60°$, $\theta=50°46'$

$$\begin{bmatrix}1/(6)^{\frac{1}{2}} & -1/\sqrt{3} & 1/\sqrt{2} & 0\\ 1/(6)^{\frac{1}{2}} & -1/\sqrt{3} & -1/\sqrt{2} & 0\\ \cdots & \cdots & \cdots & \cdots\\ 1/\sqrt{3} & 1/(6)^{\frac{1}{2}} & 0 & 1/\sqrt{2}\\ 1/\sqrt{3} & 1/(6)^{\frac{1}{2}} & 0 & -1/\sqrt{2}\end{bmatrix}.$$

‡ Since the ψ_{2p_i} are normalized, the ratios (b_i/a_i) are, of course, identical with the hybridization ratios λ_i (also called the coefficients of mixing).

§ The bond-forming power is usually taken as directly proportional to the amplitude function P in the sense that the strength of a bond $A-B$, as measured by its dissociation energy, is proportional to P_AP_B, the product of the amplitudes of the overlapping orbitals forming the bond (9).

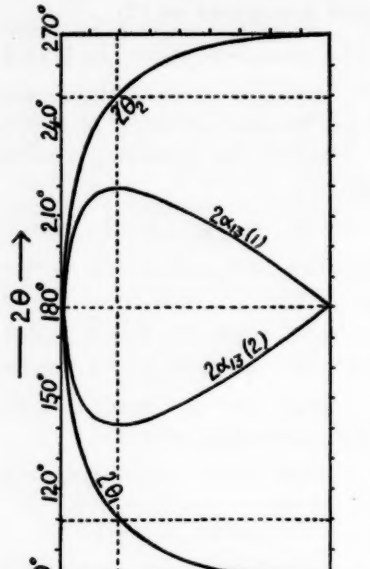

FIG. 2. Relation between the orbital valence angles 2θ and 2ϕ in the allowed structures for systems of orbitals of symmetry C_{2v}; the corresponding values allowed to the third valence angle α_{13} are also indicated. The curves are symmetrical about $2\phi=180°$, $2\theta=180°$.

The coefficients for the s orbital are in the first column; the first two rows are for the two hybrids whose vector representations subtend an angle 2θ, the second two rows for the two hybrids with valence angle 2ϕ. Decrease in the angle between two tetrahedral bonds gives less s orbital and more p orbital in the two hybrids concerned; increase of the angle gives more s and less p.|| With a bonding angle of 90°, ($\phi=45°$), the hybrids are pure p, all the s orbital going into the other pair of hybrids to form two equivalent orbitals directed in opposite senses, as in the usual divalent sp system. The orbitals with a bonding angle of 120° are a pair from the set of three trigonal orbitals obtained by trigonal hybridization. But for the latter, the odd p orbital is left as such, while here it is combined with the third trigonal orbital to give another pair of equivalent sp hybrid orbitals, with bonding angle 101°32′.

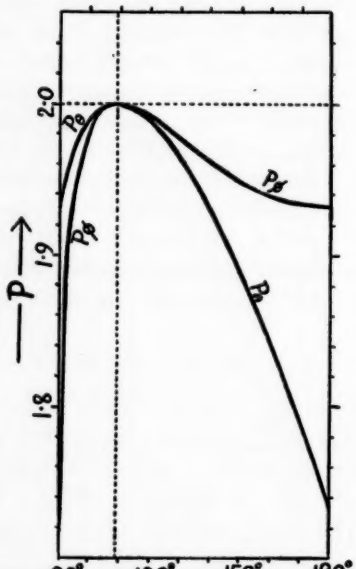

FIG. 3. Variation of bond-forming amplitude function with structure, for systems of orbitals of symmetry C_{2v}.

III. SETS OF FOUR sp_3 HYBRID ORBITALS OF SYMMETRY C_{3v}

The coordinate system shown in Fig. 4 is convenient. As before, the initial p orbitals are represented by vectors along the x, y, and z axes, the s orbital being spherically symmetrical about the origin of the system. The vectors r_1, r_2, and r_3 represent three equivalent hybrid orbitals, the angle between any two being α. The fourth orbital, r_4, is directed along the x axis; and r_1, r_2, and r_3 are each inclined to it at a bonding angle β. r_3 is contained in σ_{xy}, which is a plane of symmetry bisecting

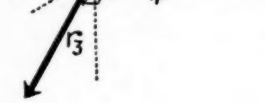

FIG. 4. Vector representation for systems of orbitals of symmetry C_{3v}.

α_{12}. The relation between α and β required by the geometry of the system is:

$$\left.\begin{aligned} 2\sin(\alpha/2) &= \sqrt{3}\sin\beta \\ 4\cos^2(\alpha/2) &= 1+3\cos^2\beta \end{aligned}\right\}. \tag{11}$$

The direction cosines for the four hybrid orbitals are given in Table II. The hybrid $2p$ orbitals corresponding to those in Eq. (2) are as follows:

$$\begin{bmatrix}\psi_{2p1}\\ \psi_{2p2}\\ \psi_{2p3}\\ \psi_{2p4}\end{bmatrix} = \begin{bmatrix}\cos\beta & (1/2)\sin\beta & -(\sqrt{3}/2)\sin\beta\\ \cos\beta & (1/2)\sin\beta & (\sqrt{3}/2)\sin\beta\\ \cos\beta & -\sin\beta & 0\\ 1 & 0 & 0\end{bmatrix}\begin{bmatrix}\psi_{2p_x}\\ \psi_{2p_y}\\ \psi_{2p_z}\end{bmatrix}. \tag{12}$$

The general hybrid orbitals, including ψ_{2s}, are again given by Eqs. (3) and (4). Here, for r_1, r_2, and r_3 to be equivalent,

$$a_1=a_2=a_3; \quad b_1=b_2=b_3. \tag{13}$$

|| This fact is the basis of the interpretations of interactions occurring in molecular vibrations put forward by Coulson, Duchesne, and Manneback (10, 11) and by Heath and Linnett (12).

Solving for the constants a_1, a_4, b_1, and b_4, by applying the condition summarized in Eq. (4), to be satisfied by an orthogonal normalized set of hybrid orbitals, the following values are obtained:

$$\left.\begin{array}{ll} a_1^2=[-(2/3)\cos\alpha]/\sin^2\beta & b_1^2=1/2\sin^2(\alpha/2) \\ a_4^2=2\cot^2\beta & b_4^2=-(2\cos\alpha)/\sin^2\beta. \end{array}\right\} \quad (14)$$

There is no relation between the angles α and β arising from this solution, since they are dependent.

Using the positive roots of Eq. (14), the matrix equation for the transformation from the initial s and p orbitals to hybrids of symmetry C_{3v} is as follows:

$$\begin{bmatrix}\psi_1\\ \psi_2\\ \psi_3\\ \psi_4\end{bmatrix}=\begin{bmatrix}\{-(2/3)\cos\alpha\}^{\frac{1}{2}}\operatorname{cosec}\beta & (2/3)^{\frac{1}{2}}\cot\beta & 1/(6)^{\frac{1}{2}} & -1/\sqrt{2}\\ \{-(2/3)\cos\alpha\}^{\frac{1}{2}}\operatorname{cosec}\beta & (2/3)^{\frac{1}{2}}\cot\beta & 1/(6)^{\frac{1}{2}} & 1/\sqrt{2}\\ \{-(2/3)\cos\alpha\}^{\frac{1}{2}}\operatorname{cosec}\beta & (2/3)^{\frac{1}{2}}\cot\beta & -(2/3)^{\frac{1}{2}} & 0\\ -\sqrt{2}\cot\beta & (-2\cos\alpha)^{\frac{1}{2}}\operatorname{cosec}\beta & 0 & 0\end{bmatrix}\begin{bmatrix}\psi_{2s}\\ \psi_{2p_x}\\ \psi_{2p_y}\\ \psi_{2p_z}\end{bmatrix}. \quad (15)$$

TABLE II. Direction cosines for the four hybrid orbitals of symmetry C_{1v}.

i	1	2	3	4
l_i	$\cos\beta$	$\cos\beta$	$\cos\beta$	1
m_i	$(1/2)\sin\beta$	$(1/2)\sin\beta$	$-\sin\beta$	0
n_i	$-(\sqrt{3}/2)\sin\beta$	$(\sqrt{3}/2)\sin\beta$	0	0

The relation between the angles α and β is shown in Fig. 5. There are no real orbitals for $\alpha<90°$. At each value of α there are two values allowed to β; if the root greater than 90° is β_1, then the second root is $\beta_2=\pi-\beta_1$. The orbitals going with β_2 will be of the umbrella type. The expressions for the bond-forming amplitude function, analogous to Eq. (10), are

$$\left.\begin{array}{r} P_1=P_2=P_3=(2/3)^{\frac{1}{2}}[(-\cos\alpha)^{\frac{1}{2}}+\sqrt{3}]\operatorname{cosec}\beta \\ P_4=\sqrt{2}[(-3\cos\alpha)^{\frac{1}{2}}-\cos\beta]\operatorname{cosec}\beta. \end{array}\right\} \quad (16)$$

Here it should be noted that P_1 is independent of which value of β is chosen to go with a given value of α, but that P_4 is greater for roots β_1 than for corresponding roots β_2. Plots of P_1 and P_4 against α are shown in Fig. 6. P_4, for values of β less than 90°, becomes zero at about $\alpha=95°30'$, and the curve is actually continuous down to $P=-1$ at $\alpha=90°$; the curve in Fig. 6 has been taken to $P=+1$, the dotted segment being the reflection of the actual curve across $P=0$. Comparison with Fig. 3 shows that there is much more variation in the bond-forming power of the single orbital ψ_4 in the C_{3v} set than in others considered here. Figure 6 can be used to illustrate the course of the reaction (5) $X+H_3C-Y \rightarrow X\cdots C\cdots Y\rightarrow X-CH_3+Y$ as follows. $P_4(\beta_2)$ can be interpreted as the bond-forming power of the orbital available for the formation of the $C-X$ bond; this increases with opening of the angle $\alpha=\overset{\frown}{HCH}$ till, at $\alpha=120°$, the bond-forming power from C along the axis XCY is the same in both senses. Further motion of the system in the same direction then completes the reaction. Thus, the $C-Y$ bond "moves along" the curves $P_4(\beta_1)$, $P_4(\beta_2)$, in that direction, and the $C-X$ bond along the same curves, in the reverse

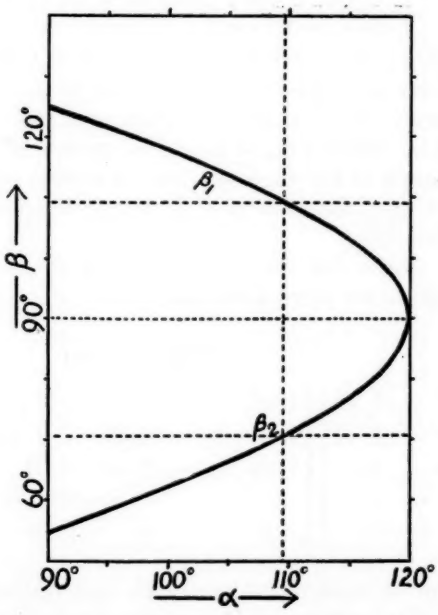

FIG. 5. Relation between the valence angles α and β for systems of orbitals of symmetry C_{3v}. The curve is symmetrical about $\beta=90°$. (It should be noted that, unlike the curves of Fig. 2 for the C_{2v} system, the curve of Fig. 5 does not demonstrate the inability of the system to exist with values of the parameter angle less than 90°. This is because the restriction on the range of values allowed to α does not enter into the geometrical relation between α and β. In the C_{2v} case, the formula relating 2θ and 2ϕ is obtained from the normalization condition.)

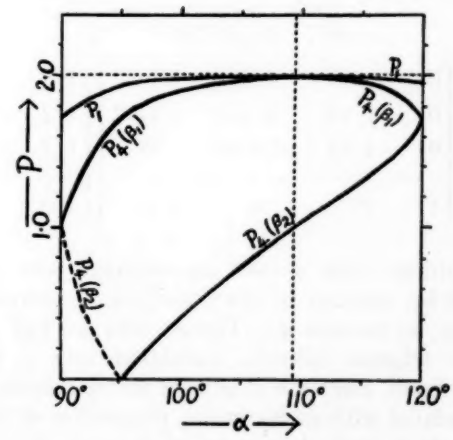

FIG. 6. Variation of bond-forming amplitude function with structure, for systems of orbitals of symmetry C_{3v}.

TABLE III.

2ϕ, α	C_{2v} 2θ	α_{13}	C_{3v} β	$\Delta(2\phi)$, $\Delta\alpha$	C_{2v} $\Delta(2\theta)$	$\Delta(\alpha_{13})$	C_{3v} $\Delta\beta$	$\lambda_{2\phi}$, α	C_{2v} $\lambda_{2\theta}$	C_{3v} λ_4
90° 0′	180° 0′	90° 0′	125°16′	−19°28′	+70°32′	−19°28′	+15°48′	∞	1.0000	0.0000
90°28′	165°31′	95° 6′	124°56′	−19° 0′	+56° 3′	−14°22′	+15°28′	11.081	1.0163	0.1576
91°28′	154°49′	98°45′	124°13′	−18° 0′	+45°21′	−10°43′	+14°45′	6.2506	1.0512	0.2845
92°28′	147°57′	101° 1′	123°30′	−17° 0′	+38°29′	−8°27′	+14° 2′	4.8203	1.0862	0.3759
93°28′	142°41′	102°40′	122°46′	−16° 0′	+33°13′	−6°48′	+13°18′	4.0667	1.1214	0.4543
94°28′	138°22′	103°58′	122° 2′	−15° 0′	+28°54′	−5°30′	+12°34′	3.5833	1.1566	0.5261
95°28′	134°43′	105° 0′	121°18′	−14° 0′	+25°15′	−4°28′	+11°50′	3.2399	1.1921	0.5942
96°28′	131°33′	105°51′	120°33′	−13° 0′	+22° 5′	−3°37′	+11° 5′	2.9798	1.2279	0.6604
97°28′	128°45′	106°35′	119°47′	−12° 0′	+19°17′	−2°53′	+10°19′	2.7740	1.2639	0.7258
98°28′	126°16′	107°10′	119° 0′	−11° 0′	+16°48′	−2°18′	+9°32′	2.6061	1.3002	0.7912
99°28′	124° 1′	107°39′	118°14′	−10° 0′	+14°33′	−1°49′	+8°46′	2.4658	1.3369	0.8575
100°28′	121°59′	108° 4′	117°26′	−9° 0′	+12°31′	−1°24′	+7°58′	2.3462	1.3740	0.9252
101°28′	120° 7′	108°25′	116°37′	−8° 0′	+10°39′	−1° 3′	+7° 9′	2.2428	1.4116	0.9950
102°28′	118°25′	108°42′	115°48′	−7° 0′	+8°57′	−0°46′	+6°20′	2.1523	1.4496	1.0675
103°28′	116°51′	108°55′	114°58′	−6° 0′	+7°23′	−0°33′	+5°30′	2.0722	1.4881	1.1436
104°28′	115°24′	109° 6′	114° 6′	−5° 0′	+5°56′	−0°22′	+4°38′	2.0007	1.5271	1.2239
105°28′	114° 2′	109°15′	113°14′	−4° 0′	+4°34′	−0°13′	+3°46′	1.9364	1.5667	1.3094
106°28′	112°47′	109°21′	112°20′	−3° 0′	+3°19′	−0° 7′	+2°52′	1.8783	1.6070	1.4013
107°28′	111°36′	109°25′	111°24′	−2° 0′	+2° 8′	−0° 3′	+1°56′	1.8253	1.6479	1.5009
108°28′	110°31′	109°28′	110°28′	−1° 0′	+1° 3′	−0° 0′	−1° 0′	1.7768	1.6895	1.6102
109°28′	109°28′	109°28′	109°28′	0° 0′	0° 0′	0° 0′	0° 0′	1.7321	1.7321	1.7321
110°28′	108°30′	109°28′	108°27′	+1° 0′	−0°58′	−0° 0′	−1° 1′	1.6911	1.7750	1.8678
111°28′	107°35′	109°26′	107°24′	+2° 0′	−1°53′	−0° 2′	−2° 4′	1.6530	1.8190	2.0237
112°28′	106°44′	109°22′	106°17′	+3° 0′	−2°44′	−0° 6′	−3°11′	1.6177	1.8639	2.2054
113°28′	105°55′	109°18′	105° 6′	+4° 0′	−3°33′	−0°10′	−4°22′	1.5847	1.9097	2.4226
114°28′	105° 9′	109°12′	103°50′	+5° 0′	−4°19′	−0°16′	−5°38′	1.5539	1.9565	2.6902
115°28′	104°25′	109° 6′	102°25′	+6° 0′	−5° 3′	−0°22′	−7° 3′	1.5250	2.0043	3.0353
116°28′	103°43′	108°58′	100°58′	+7° 0′	−5°45′	−0°30′	−8°30′	1.4979	2.0533	3.2303
117°28′	103° 4′	108°50′	99°15′	+8° 0′	−6°24′	−0°38′	−10°13′	1.4725	2.1034	4.2244
118°28′	102°26′	108°41′	97°10′	+9° 0′	−7° 2′	−0°47′	−12°18′	1.4484	2.1548	5.5335
119°28′	101°51′	108°31′	94°13′	+10° 0′	−7°37′	−0°57′	−15°15′	1.4258	2.2074	9.5563
120° 0′	101°32′	108°26′	90° 0′	+10°32′	−7°56′	−1° 2′	−19°28′	1.4142	2.2361	∞

direction. The probability factor for the reaction would appear to be determined by the probability that end-on motion of X towards the CH_3 group would coincide with the "opening" phase of the CH_3 symmetrical "breathing" vibration.

Small variations in α or β over the range 105° to 115° have very little effect on the bond-forming power. Thus, at $\alpha=105°$, β_1 takes the value 113°38′, and $P_1=1.997$, $P_4=1.979$; while at $\alpha=115°$, the values are $\beta_1=103°8'$, $P_1=1.997$ again, and $P_4=1.965$. It may be of interest in connection with studies of coupling and anharmonicity in molecular vibrations that a bond formed by overlapping of ψ_4 will be weakened¶ more in the opening of the angles α_{ij} between three equivalent bonds formed from the orbitals ψ_1, ψ_2, and ψ_3, than in their closing-up.

The matrix for the transformation of Eq. (15) is given below for three particular cases:

$\alpha=90°$, $\beta=125°16'$

$$\begin{bmatrix} 0 & -1/\sqrt{3} & 1/(6)^{\frac{1}{2}} & -1/\sqrt{2} \\ 0 & -1/\sqrt{3} & 1/(6)^{\frac{1}{2}} & 1/\sqrt{2} \\ 0 & -1/\sqrt{3} & -(2/3)^{\frac{1}{2}} & 0 \\ \cdots & \cdots & \cdots & \cdots \\ 1 & 0 & 0 & 0 \end{bmatrix}$$

$\alpha=\beta=109°28'$

$$\begin{bmatrix} 1/2 & -1/2\sqrt{3} & 1/(6)^{\frac{1}{2}} & -1/\sqrt{2} \\ 1/2 & -1/2\sqrt{3} & 1/(6)^{\frac{1}{2}} & 1/\sqrt{2} \\ 1/2 & -1/2\sqrt{3} & -(2/3)^{\frac{1}{2}} & 0 \\ \cdots & \cdots & \cdots & \cdots \\ 1/2 & \sqrt{3}/2 & 0 & 0 \end{bmatrix}$$

$\alpha=120°$, $\beta=90°$

$$\begin{bmatrix} 1/\sqrt{3} & 0 & 1/(6)^{\frac{1}{2}} & -1/\sqrt{2} \\ 1/\sqrt{3} & 0 & 1/(6)^{\frac{1}{2}} & 1/\sqrt{2} \\ 1/\sqrt{3} & 0 & -(2/3)^{\frac{1}{2}} & 0 \\ \cdots & \cdots & \cdots & \cdots \\ 0 & 1 & 0 & 0 \end{bmatrix}.$$

The orbitals with $\alpha=90°$ are identical with the set formed by rotation of the initial set of unhybridized orbitals; ψ_4 becomes ψ_{2s}. The set with $\alpha=120°$ are the normal trigonal hybrids, associated with a residual pure p bond. Decrease of α from the tetrahedral value is associated with an increasing proportion of p orbital in the three equivalent hybrids; increase of α is associated with decrease of p orbital in these.

The above work has been carried out as part of the program of fundamental research undertaken by the British Rayon Research Association.

¶ A decrease in P is interpreted here in this sense, rather than that the bond involved will shorten; this would not be possible, as then, in the vibrating molecule, the atom bonded by ψ_4 would have to oscillate with twice the frequency of those bonded by $\psi_{1,2,3}$. Such a combination of motions is forbidden in the normal modes. Further, in the reaction $X+H_3CY=XCH_3+Y$, discussed above, decrease of P must certainly be interpreted as leading to a weaker, and hence longer, bond.

APPENDIX I. TABLES OF BOND-ORBITAL ANGLES FOR SYSTEMS OF sp_3 HYBRIDS

The non-existence of sets of orbitals with bonding angles less than 90° and the stability of three-membered rings (e.g., cyclopropane) has led to the acceptance of the concept of "bent bonds" in constrained systems (6). It remains to be found whether bonds in which the line joining an atom-pair does not coincide with the direction in which the appropriate bonding orbital from either atom has its maximum are present in all non-ideal systems, or whether the apparent bond angles can be correlated with distortions of the ideal system of bonding orbitals. An alternative, if somewhat narrower, statement of the problem is "to what extent, if any, is intramolecular van der Waals' distortion accompanied by an adaptation of the system of bonding orbitals," (i.e., by orbital-following of the static type). Table III may be of some assistance in attempting such correlations.

Heading the columns of Table III are the symbols for the angles used in this paper; 2ϕ and α are the angles between two equivalent orbitals in the systems of symmetry C_{2v} and C_{3v} respectively, 2θ is the angle between the other pair of C_{2v} orbitals, α_{13} the remaining angle in this system, and β the second angle in the C_{3v} system. Values are given at one degree increments in 2ϕ and α, over the range 90° to 120°. The increments in the last four columns refer to the tetrahedral angle as null. The tabulated values call for no particular comment; but the degree of constancy of α_{13}, over a large range of values for 2ϕ, is perhaps somewhat unexpected.

APPENDIX II

It is of interest that there is no set of four sp_3 hybrid orbitals with symmetry C_s. Using Fig. 4, with σ_{xy} as the single plane of symmetry, so that ψ_1 and ψ_2 are equivalent orbitals, the hybrid $2p$ orbitals along r_1 to r_4 are

$$\begin{bmatrix}\psi_{2p_1}\\ \psi_{2p_2}\\ \psi_{2p_3}\\ \psi_{2p_4}\end{bmatrix}=\begin{bmatrix}-\cos\phi & [\sin^2\phi-\sin^2(\theta/2)]^{\frac{1}{2}} & -\sin(\theta/2)\\ -\cos\phi & [\sin^2\phi-\sin^2(\theta/2)]^{\frac{1}{2}} & \sin(\theta/2)\\ -\cos\psi & -\sin\psi & 0\\ 1 & 0 & 0\end{bmatrix}\begin{bmatrix}\psi_{2p_x}\\ \psi_{2p_y}\\ \psi_{2p_z}\end{bmatrix},$$

where θ is the angle between the two equivalent orbitals along r_1 and r_2; ϕ is the acute angle between r_1 and r_4, and between r_2 and r_4; and ψ is the acute angle between r_3 and r_4. There is no geometrical condition relating these three angles, and ψ_3 and ψ_4 are not assumed equivalent. For the above set to be orthogonal,

$$\sin\psi\cos\psi-2\cos\phi[\sin^2\phi-\sin^2(\theta/2)]^{\frac{1}{2}}=0.$$

The angle θ_{13} between r_1 and r_3, or r_2 and r_3, is given by

$$\cos\theta_{13}=\cos\phi\cos\psi-[\sin^2\phi-\sin^2(\theta/2)]^{\frac{1}{2}}\sin\psi$$

or, using the previous relation,

$$\cos\theta_{13}=\tfrac{1}{2}(2\cos^2\phi-\sin^2\psi)\cos\psi\sec\phi.$$

Now, solving for a_i, b_i in Eq. (4) of this paper, we find

$$a_4^2=(1-\cos\theta\sec^2\phi)^{-1}=[1-\sec\theta\cos^2\theta_{13}\sec^3\psi]^{-1}$$
$$b_4^2=(1-\cos^2\phi\sec\theta)^{-1}=(1-\cos\theta\cos^2\psi\sec^2\theta_{13})^{-1}.$$

Equating the two solutions for a_4^2 and b_4^2, we obtain another identity involving θ_{13}:

$$\cos\theta\cos\psi-\cos\phi\cos\theta_{13}=0.$$

Finally, eliminating θ_{13} between this identity and the previous one, we obtain the following equation relating ϕ and ψ:

$$2\sin^2\phi\cos^2\phi=(\cos^2\phi+\cos^2\psi)\sin^2\psi.$$

This equation is satisfied by roots $\psi=\phi$, or $\sin^2\psi=2\cos^2\phi$. The first root corresponds to a system of higher symmetry, C_{3v}, [giving $\cos\theta_{13}=\frac{1}{2}(3\cos^2\phi-1)$] and the second to $\theta=\theta_{13}=90°$, and this gives no real set of orbitals other than the one falling into the point group C_{3v}.

This absence of a set of C_s orbitals leads to an ambiguity in the structure of compounds of type CX_2YZ which is not present in CX_2Y_2 or CX_3Y.

For completeness the hybridization ratios of the three sets of orbitals are given in the last three columns of the table; the subscripts to λ refer to the angle between the equivalent orbitals, in the first two columns for λ, the four to the odd C_{3v} orbital, and the superscripts give the symmetry class.

BIBLIOGRAPHY

(1) J. W. Linnett and P. J. Wheatley, Trans. Faraday Soc. **45**, 33, 39 (1949); Nature **161**, 971 (1948).
(2) G. H. Duffey, J. Chem. Phys. **14**, 342 (1946).
(3) J. E. Kilpatrick and R. Spitzer, J. Chem. Phys. **14**, 463 (1946).
(4) N. F. Mott and I. N. Sneddon, *Wave Mechanics and Its Applications* (Clarendon Press, Oxford, 1948), p. 194 ff.
(5) E. A. Braude, Ann. Rep. Chem. Soc. 116 (1949); and see references to M. Polanyi and co-workers.
(6) C. A. Coulson and W. E. Moffitt, J. Chem. Phys. **15**, 151 (1947).
(7) E. B. Wilson, Jr., Trans. Faraday Soc. ("Discussion on Spectroscopy and Cell Structure," September, 1950).
(8) P. Torkington, Nature **163**, 446 (1949).
(9) Pauling and Sherman, J. Am. Chem. Soc. **59**, 1450 (1937).
(10) C. A. Coulson, J. Duchesne, and C. Manneback, Nature **160**, 793 (1947); *V. Henri Mem. Vol.* (Desoer, Liege, 1948), p. 33ff.
(11) J. Duchesne, *V. Henri Mem. Vol.* (Desoer, Liege, 1948), p. 47.
(12) D. F. Heath and J. W. Linnett, Nature **161**, 243 (1948); Trans. Faraday Soc. **44**, 556 (1948).

The Infrared Spectrum of Sulfur Hexafluoride*

R. T. LAGEMANN† AND E. A. JONES‡
K-25 Laboratories, Carbide and Carbon Chemicals Division, Union Carbide and Carbon Corporation, Oak Ridge, Tennessee
(Received September 19, 1950)

The infrared absorption spectrum of gaseous SF_6 has been investigated from 2 to 25μ with prism spectrometers of high resolution. The frequencies of the infrared active fundamentals found by earlier workers have been confirmed with the exception of one, formerly found at 965 cm^{-1}, which is shown to be at 940 cm^{-1}. However, the remainder of the spectrum differs considerably from previous work. With the aid of the Raman data, the observed spectrum has been interpreted in detail.

INTRODUCTION

THE Raman and infrared spectra of sulfur hexafluoride have been studied in some detail. The former has been investigated by Yost, Steffens, and Gross[1] and by Eucken and Ahrens,[2] both groups agreeing very well on the frequencies of the Raman shifts. Eucken and Ahrens also examined the infrared spectrum from 2 to 20μ, finding ten bands, two of which they identified as fundamental frequencies. With the help of the Raman active and infrared active fundamental frequencies and the measured specific heat of the liquid, they estimated the frequency of the inactive fundamental. However, their interpretation of certain of the bands as difference combination tones seems unsatisfactory and the value of the inactive frequency is used in interpreting only a few combination frequencies. It was therefore thought that a re-examination of the infrared spectrum, particularly with a view to finding more combination bands, might be worthwhile. This has resulted in the finding of many new bands under improved resolution, better values for two fundamental frequencies and a more satisfactory interpretation of the vibrational spectrum.

EXPERIMENTAL

The sample of sulfur hexafluoride was obtained from the Harshaw Chemical Company. It was described as being greater than 98 percent pure with F_2, HF, H_2O, and other sulfur fluorides as possible contaminants. The fact that it has been possible to interpret practically all of the observed infrared bands in terms of the assumed molecular structure indicates that the purity of the sample was high. This was further checked by comparing the spectrum with many other spectra of fluorine compounds available in this laboratory. Only evidence of SF_4 was found.

The infrared absorption spectrum of gaseous SF_6 was measured over the range 2 to 25μ by means of two Perkin-Elmer prism spectrometers, one a double-beam Model 21 covering the 2 to 15μ region, the other a Model 12C employing NaCl and KBr prisms alternatively. For most of the work, a ten-cm fluorothene[3] cell having KBr windows was used. The spectrum from 2–15μ was recorded at pressures of one and two atmospheres and regions of strong absorption at several lower pressures using the 10-cm cell. For some runs from 2 to 15μ a meter-long cell with thallium bromide-iodide (KRS-5) windows was used with the gas at one-atmosphere pressure. The region from 15–25μ was studied at one atmosphere pressure and at several lower pressures, using the meter cell. The gas transfer system and the cell, made principally of copper and fluorothene, were flushed several times with samples of the gas before a final sample for study was taken over into the absorption cell.

RESULTS

The infrared absorption of SF_6 gas between 2 and 25μ is shown in Fig. 1, which gives transmission curves for a variety of conditions. Some additional runs, used to substantiate the bands found, are not shown. The frequencies of the observed maxima of absorption are given in Table I. In the second column of the table are given the relative intensities, where "vs" means very strong, "s" strong, "m" medium, "w" weak, etc. In the last column are given the interpretations in terms of the permitted vibration species.

Table II lists the fundamental vibration frequencies along with their designation, type, and activity. The Raman frequencies listed are taken from Herzberg's[4] weighted averages of the data of Yost, *et al.*, and Eucken and Ahrens. The two infrared active fundamentals are from the present study. The inactive frequency is taken the same as that found by Eucken and Ahrens and will be discussed later.

DISCUSSION OF RESULTS

Most of the absorption regions reported by Eucken and Ahrens were found in the present study, although the intensities and frequency positions are in poor agreement in several cases. Some of their bands may

* This work is based on work performed for the AEC by Carbide and Carbon Chemicals Division, Union Carbide and Carbon Corporation, at Oak Ridge, Tennessee.
† Emory University, Emory University, Georgia.
‡ Now at Physics Department, Vanderbilt University, Nashville, Tennessee.
[1] Yost, Steffens, and Gross, J. Chem. Phys. **2**, 311 (1934).
[2] A. Eucken and H. Ahrens, Z. physik. Chem. **B26**, 297 (1934).
[3] J. S. Kirby-Smith and E. A. Jones, J. Opt. Soc. Am. **39**, 780 (1949).
[4] G. Herzberg, *Infrared and Raman Spectra of Polyatomic Molecules* (D. Van Nostrand and Company, New York, 1945), p. 337.

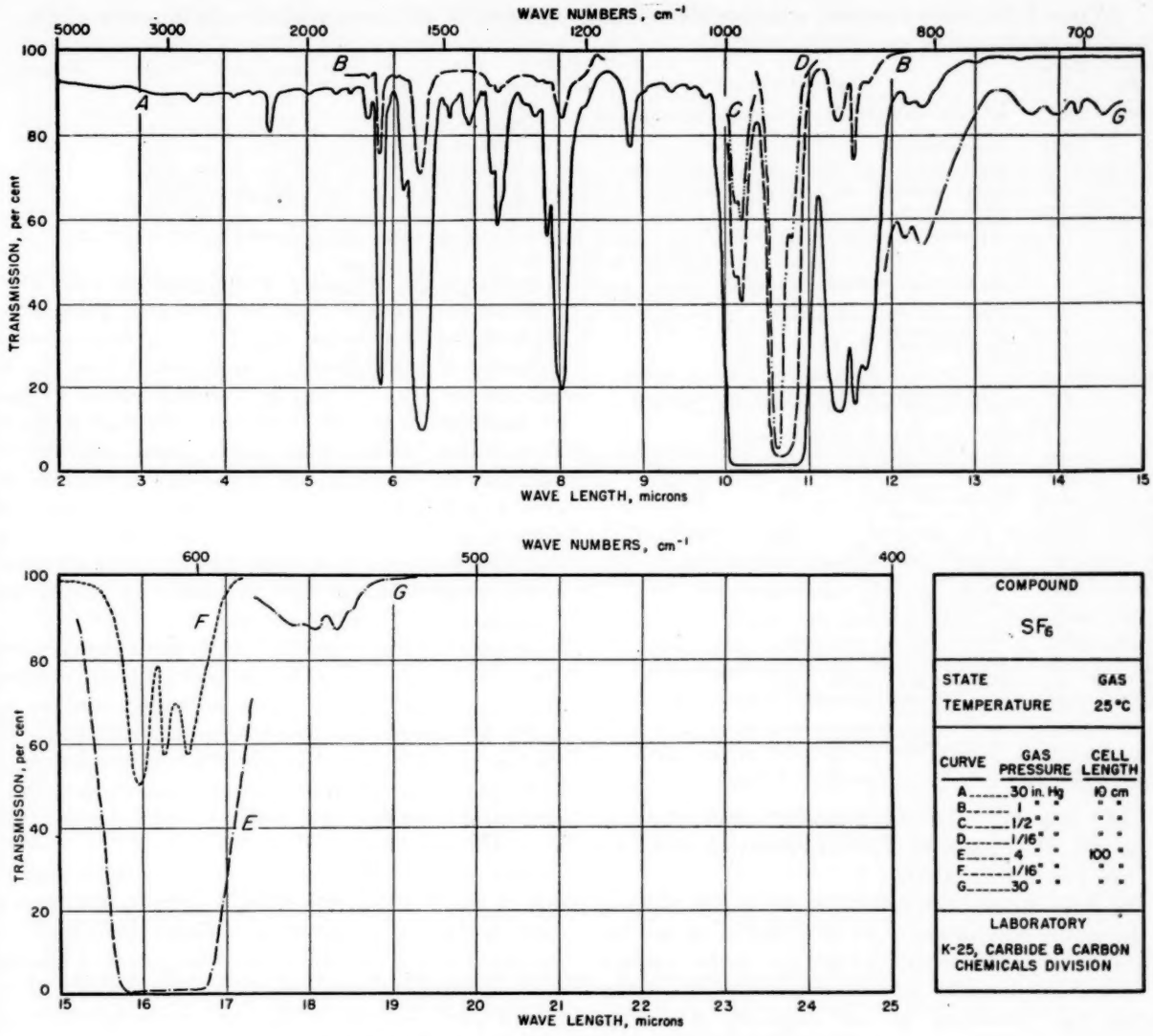

FIG. 1. Infrared absorption spectrum of sulfur hexafluoride gas.

have been due to an admixture of SF_4. A sample of SF_4 was studied by us and showed, in addition to other weaker bands, strong absorption at 723 and 738 cm^{-1}, a medium intensity band at 1163 cm^{-1}, and weak absorption at 1276 cm^{-1}. In our work on SF_6, we do not find a band at 1163 cm^{-1} although Eucken and Ahrens did; we do not observe absorption at 723 and 738 cm^{-1}, which is probably the resolved structure of the 730 region of Eucken and Ahrens. Thus, it is probable that our bands at 723 and 738 cm^{-1} and the bands found by Eucken and Ahrens at 730 and 1163 cm^{-1} are caused by SF_4. The absorption peak found in this work at 1276 cm^{-1} and at 1282 cm^{-1} by Eucken and Ahrens occurs weakly in SF_4; but since, in both studies, certain stronger SF_4 bands did not show up simultaneously, it it not ascribed to SF_4. The region which Eucken and Ahrens show as a single absorption peak at 965 cm^{-1} is resolved in this work into further structure, the strongest band of which is at 940 cm^{-1} and which is assigned to the fundamental ν_3. The infrared spectrum, as observed in the present work, is seen to be more complete than that found in the earlier study. The contours of several bands, notably the one at 615 cm^{-1} are better revealed.

INTERPRETATION OF THE SPECTRUM

Electron diffraction measurements[5,6] indicate that sulfur hexafluoride possesses a highly symmetrical structure with the sulfur at the center of a regular octahedron whose corners are occupied by the six fluorine atoms. Thus, the molecule belongs to point group O_h; and this is confirmed by the Raman investigations and the previous work on the infrared. For such a model one would expect six normal vibrations: three Raman active, one of species A_{1g}, one

[5] H. Braune and S. Knoke, Z. physik. Chem. **B21**, 297 (1933).
[6] L. O. Brockway and L. Pauling, Proc. Nat. Acad. Sci. U. S. **19**, 68 (1933).

TABLE I. The infrared spectrum of gaseous SF_6.

Wave number	Description	Interpretation
546 cm^{-1}	w	$644+524-615=553$ ($A_{1u}+A_{2u}+2E_u+2F_{1u}+2F_{2u}$
605		
615	vs	F_{1u} fundamental
626		
693	vw	$940+363-615=688$ ($A_{1u}+A_{2u}+2E_u+3F_{1u}+4F_{2u}$
705	vw	$2(524)-363=685$ ($A_{1u}+E_u+2F_{1u}+3F_{2u}$)
723	vw	SF_4?
738	vw	SF_4?
812	w	$644+940-775=809$ ($F_{1u}+F_{2u}$)
825	w	
865		
875	m	$524+363=887$ ($A_{1u}+E_u+F_{1u}+F_{2u}$)
887		
927	m	$2(644)-363=925$ ($F_{1u}+2F_{2u}$)
940	vs	F_{1u} fundamental
984	s	$644+363=1007$ ($F_{1u}+F_{2u}$)
995	s	
1026	vw	
1046	vw	$775+644-363=1056$ ($F_{1u}+F_{2u}$)
1072	vw	$3(363)=1089$ ($A_{1u}+F_{1u}+2F_{2u}$)
1114	vvw	
1132	w	$615+524=1139$ ($A_{2u}+E_u+F_{1u}+F_{2u}$)
1206	vw	$940+615-363=1192$ ($A_{1u}+A_{2u}+2E_u+3F_{1u}+4F_{2u}$)
1250	m	$644+615=1259$ ($F_{1u}+F_{2u}$)
1276	w	
1303	vw	$3(644)-615=1317$ ($2F_{1u}+2F_{2u}$)
1380	m	$775+615=1390$ (F_{1u})
1422	vvw	$2(524)+363=1411$ ($A_{1u}+E_u+2F_{1u}+3F_{2u}$)
1455	w	$940+524=1464$ ($A_{2u}+E_u+F_{1u}+F_{2u}$)
1502	w	$2(940)-363=1517$ ($A_{1u}+E_u+2F_{1u}+3F_{2u}$)
1580	m	$644+940=1584$ ($F_{1u}+F_{2u}$)
1635	w	$2(644)+363=1651$ ($F_{1u}+2F_{2u}$)
1710	m	$775+940=1715$ (F_{1u})
1756	w	$775+644+363=1782$ ($F_{1u}+F_{2u}$)
1830	vw	$3(615)=1845$ ($A_{2u}+2F_{1u}+F_{2u}$)
1880	vw	$2(644)+615=1903$ ($2F_{1u}+F_{2u}$)
2004	vw	$2(524)+940=1988$ ($A_{2u}+E_u+2F_{2u}+3F_{1u}$)
2220	w	$2(644)+940=2228$ ($2F_{1u}+F_{2u}$)
2315	vvw	$775+644+524+363=2306$ ($A_{1u}+A_{2u}+2E_u+2F_{1u}+2F_{2u}$)
2457	vw	$2(775)+940=2490$ (F_{1u})
2786	vw	$3(940)=2820$ ($A_{2u}+2F_{1u}+F_{2u}$)

E_g, and one F_{2g}; and two infrared active, both of species F_{1u}. There should also be a vibration of species F_{2u} inactive in both spectra.

The three Raman fundamentals previously assigned in the earlier studies are listed in Table II, as are the two infrared fundamentals which are chosen because of their high intensity and their usefulness in interpreting the remainder of the spectrum. The chief change from Eucken and Ahrens is to alter ν_3 from 965 to 940 cm^{-1}. The frequency of the inactive vibration ν_6 is taken from Eucken and Ahrens, who measured the specific heat and with the aid of knowledge of the other five fundamentals calculated ν_6 to be 363 cm^{-1}. Because the change from 965 to 940 cm^{-1} has little effect on the contribution of that vibration to the specific heat, we have not changed the value of ν_6, particularly since it is such an excellent value for explaining combination bands.

On the basis of the fundamental vibrational frequencies listed in Table II, it has been possible to interpret in a reasonable manner all but a few of the infrared bands. These interpretations are given in Table I. For a few bands more than one interpretation is given, but not all the possible alternative assignments have been indicated. In all cases, the interpretation proposed is consistent with the selection rules for the

TABLE II. The fundamental vibration frequencies of SF_6.

Activity	Frequency (cm^{-1})	Type	Designation
Raman (gas)	775	A_{1g}	ν_1
Raman (liquid)	644	E_g	ν_2
Infrared (gas)	940	F_{1u}	ν_3
Infrared (gas)	615	F_{1u}	ν_4
Raman (liquid)	524	F_{2g}	ν_5
Inactive	363	F_{2u}	ν_6

O_h point group. According to the selection rules for a molecule possessing a center of symmetry, none of the fundamental frequencies should have a first overtone appearing in the infrared. This is indeed found to be the case for SF_6. The finding of absorption peaks near the positions to be expected for the first overtones of some of the fundamentals is no doubt coincidental. Likewise, no combinations of the first harmonics are to be expected. It is also to be noted that no permitted infrared frequencies are found in the Raman spectrum and, conversely, no permitted Raman shifts are found in the infrared. Of the eight permitted infrared binary combinations all have been found.

Perhaps the least plausible of the interpretations are those for certain weak bands which invoke ternary difference combinations. Some of these coincide (or nearly so) with regions which were poorly explained by Eucken and Ahrens in that for many of the difference tones put forth as interpretations, the corresponding sum band is missing. For these, no better explanation seems to be available.

Some of the unsatisfactory interpretations may be due to the fact that the Raman data for two fundamentals is for the liquid state, whereas the other three measured bands were found for the gas. It is possible that an impurity, perhaps some sulfur fluoride, is responsible for such bands. This can only be decided when spectra of other sulfur fluorides become available.

Despite the improved resolution and improved accuracy of the frequency determinations, it is seen that the observed and calculated values found in Table I are not in as good agreement as might be hoped. The binary combinations, giving in general the more intense bands, are satisfactory, however. It appears that the anharmonicity is quite large and generally in the same direction for most of the combinations observed.

In conclusion, it can be said that the additional bands found in the present work furnish further confirmation of the regular octahedron model for SF_6.

ACKNOWLEDGMENT

It is a pleasure to acknowledge the generous assistance of Dr. John S. Kirby-Smith, Patricia Woltz, and George Burke.

The Calculation of Diffusion Coefficients from Sorption Data

STEPHEN PRAGER
Department of Chemistry, Cornell University, Ithaca, New York
(Received January 23, 1951)

A method is described for the calculation of the dependence of the diffusion coefficient on the concentration of diffusing material from data obtained by studying the rates of sorption of vapors by films. The principle of the method is to approximate the actual concentration dependence by a step function. For such a function the differential equations involved can be solved analytically, and the heights of the individual steps can be computed; the step function is then smoothed out by an averaging process. The method has been tried out for the sorption of isobutane by polyisobutylene at 35°C and found to be quite satisfactory.

INTRODUCTION

Of the methods available for the determination of the diffusion coefficients of vapors in polymers and other solids, the sorption method is experimentally one of the simplest and most accurate. A film of the material to be studied is suspended from a spring of known stiffness in an atmosphere of the vapor in question at a pressure p. The weight Q of vapor taken up by the film is then measured as a function of the time by observing the elongation of the spring with a traveling microscope. This experiment is repeated at several different values of p.

The experimental simplicity of this method is, unfortunately, offset to a considerable degree by the fact that if, as is usually the case, the diffusion coefficient governing the sorption process varies with the concentration of diffusing material, no analytic solution is known for the diffusion Eqs. (1) and (1a) below. The calculation of the diffusion coefficient from sorption data becomes, therefore, quite difficult. Indeed, until the publication of two recent papers by Crank and his associates,[1,2] there was no method of performing such a calculation. The present paper will present an alternative method involving a step function approximation to the concentration dependence of the diffusion coefficient.

DERIVATION OF THE METHOD

The diffusion of the vapor into the film is governed by Fick's second law, which, if one ignores diffusion through the edges of the film, may be expressed as follows:

$$\partial c/\partial t=\partial/\partial x[D(c)\partial c/\partial x] \tag{1}$$

with boundary conditions (assuming instantaneous surface equilibration)

$$\begin{aligned} &c(0,t)=c(l,t)=c_f,\\ &c(x,0)=0. \end{aligned} \tag{1a}$$

Here, $c(x,t)$ is the concentration of vapor at time t and at a distance x into the film normal to the surface, l is the film thickness, $D(c)$ is the diffusion coefficient, and c_f is the equilibrium concentration corresponding to the pressure p of the vapor.

[1] Crank and Park, Trans. Faraday Soc. **45**, 240 (1949).
[2] Crank and Henry, Trans. Faraday Soc. **45**, 1119 (1949).

For a film of area A normal to the direction of diffusion, the sorption method gives

$$Q=A\int_0^l c\,dx$$

as a function of t for various values of c_f, and our problem is to calculate $D(c)$ from this information.

The principle of the method is to approximate the true $D(c)$ by a step function, i.e., we divide up the concentration range into a number of intervals and assume that $D(c)$ has a constant (although as yet unknown) value in each. For such a step function $D(c)$, Eq. (1) can be solved for the early part of the diffusion process where the film can be treated as a semi-infinite solid. For the first interval, then, D is constant throughout and may readily be calculated if Q is known as a function of t for c_f corresponding to the end of the interval. For a diffusion process covering the first two intervals, $D(c)$ is given by a step function whose value in the first interval is now known from the previous calculation, and whose value in the second interval may be calculated from the $Q(t)$ for the process. This procedure may then be continued to calculate the value of $D(c)$ in the third interval, its values in the first two being known, and so on until the entire concentration range has been covered.

Before the concentration in the center of the film attains an appreciable value, we may regard the diffusion process in each half of the film as occurring in a semi-infinite solid. The boundary condition (1a) may then be replaced by

$$\begin{aligned} &c(0,t)=c_f, \quad c(\infty,t)=0,\\ &c(x,0)=0, \end{aligned} \tag{1b}$$

for the half of the film between $x=0$ and $x=\frac{1}{2}l$. (A precisely similar diffusion process takes place in the other half.) Boltzmann[3] has shown that for Eq. (1) with boundary conditions (1b), $c(x,t)$ is a function of $\lambda=x/t^{\frac{1}{2}}$ alone, and we may write Eq. (1) as an ordinary differential equation

$$-\tfrac{1}{2}\lambda\frac{dc}{d\lambda}=\frac{d}{d\lambda}\left[D(c)\frac{dc}{d\lambda}\right] \tag{2}$$

[3] L. Boltzmann, Ann. Physik Chem. **53**, 959 (1894).

with boundary conditions

$$c(0)=c_f, \quad c(l)=0. \tag{2a}$$

It follows then that

$$\begin{aligned} Q=A\int_0^l c(x,t)dx &= 2A\int_0^{\frac{1}{2}l} c(x,t)dx \\ &= 2At^{\frac{1}{2}}\int_0^{\infty} c(\lambda)d\lambda \\ &= 2AK(c_f)t^{\frac{1}{2}}. \end{aligned}$$

It must be remembered, of course, that all this holds only as long as there is no vapor in the center of the film; in most cases this is a good approximation up to the half time (time at which half the equilibrium amount of vapor has been taken up).

By plotting Q against $t^{\frac{1}{2}}$ for various values of c_f, we can then readily find $K(c_f)$ from the initial slope, and our problem is now to find $D(c)$ given $K(c_f)$.

Equation (2) may also be written

$$\frac{d\lambda}{dc}\int_0^c \lambda dc = -2D(c);$$

if we let

$$M(c)=\int_0^c \lambda dc,$$

$$Md^2M/dc^2=-2D(c). \tag{3}$$

From Eqs. (2a) and the definitions of M and K, we see that

$$\begin{aligned} &M(0)=0; \quad (dM/dc)_{c=c_f}=\lambda(c_f)=0, \\ &M(c_f)=\int_0^{c_f}\lambda dc=\int_0^{\infty} cd\lambda=K(c_f). \end{aligned} \tag{3a}$$

Equation (3) will be more convenient to use in what follows than Eq. (2).

We now approximate the true $D(c)$ with a step function, i.e., we assume that

$$D(c)=\begin{cases} D_1 & (0\leqslant c\leqslant c_1) \\ D_2 & (c_1\leqslant c\leqslant c_2) \\ \cdots & \cdots \\ D_k & (c_{k-1}\leqslant c\leqslant c_k) \\ \cdots & \cdots \\ D_N & (c_{N-1}\leqslant c\leqslant c_N), \end{cases} \tag{4}$$

where the constants D_k are yet to be calculated. For a sorption process in which $c_f=c_1$, we have

$$c=c_1\left[1-\operatorname{erf}\left(\ln\frac{2c_1D_1^{\frac{1}{2}}}{\pi^{\frac{1}{2}}M}\right)^{\frac{1}{2}}\right], \tag{5}$$

where

$$\operatorname{erf}x=\frac{2}{\pi^{\frac{1}{2}}}\int_0^x \exp(-v^2)dv.$$

This is simply the solution of Eq. (3) subject to the boundary condition given by the first two Eqs. of (3a), when $D(c)=D_1$ is constant throughout.[4] Using Eq. (5) and the third equation of (3a), we get for $c=c_1$,

$$D_1=\frac{\pi}{4}\frac{(M(c_1))^2}{c_1^2}=\frac{\pi}{4}\frac{(K(c_1))^2}{c_1^2}. \tag{6}$$

Thus, we can easily evaluate D_1 from $K(c_1)$.

To evaluate D_2, we consider a sorption process with $c_f=c_2$. $D(c)$ is then given by

$$D(c)=\begin{cases} D_1 & (0\leqslant c\leqslant c_1) \\ D_2 & (c_1\leqslant c\leqslant c_2), \end{cases} \tag{7}$$

where D_1 has been evaluated from Eq. (6), and D_2 remains to be computed. $M(c)$ must also be written in two parts:

$$M(c)=\begin{cases} M_1(c) & (0\leqslant c\leqslant c_1) \\ M_2(c) & (c_1\leqslant c\leqslant c_2), \end{cases} \tag{8}$$

where M_1 and M_2 satisfy the differential equations

$$\begin{aligned} M_1(d^2M_1/dc^2)&=-2D_1, \\ M_2(d^2M_2/dc^2)&=-2D_2, \end{aligned} \tag{9}$$

with boundary conditions

$$\begin{aligned} &M_1(0)=0, \quad M_2(c_2)=K(c_2), \quad \left(\frac{dM_2}{dc}\right)_{c_2}=0, \\ &M_1(c_1)=M_2(c_1), \left(\frac{dM_1}{dc}\right)_{c_1}=\left(\frac{dM_2}{dc}\right)_{c_1}. \end{aligned} \tag{9a}$$

The last two conditions of Eq. (9a) stem from the fact that d^2M/dc^2 must be everywhere finite, since otherwise $D(c)$ would be infinite [see Eq. (3)]; this means that M and its first derivative must be everywhere continuous.

For convenience, we now adopt the following notation:

$$\begin{aligned} &\mu_k=(c-c_{k-1})/(c_k-c_{k-1}), \\ &\Lambda_k(\mu_k)=M_k(c)/[D_k^{\frac{1}{2}}(c_k-c_{k-1})], \\ &\Lambda_k(0)=\Gamma_k, \quad \Lambda_k(1)=\gamma_k, \end{aligned} \tag{10}$$

$$\frac{1}{2}\left(\frac{d\Lambda_k}{d\mu_k}\right)_{\mu_k=0}=B_k, \quad \frac{1}{2}\left(\frac{d\Lambda_k}{d\mu_k}\right)_{\mu_k=1}=\beta_k.$$

Equations (9) and (9a) become then

$$\Lambda_k d^2\Lambda_k/d\mu_k^2+2=0, \quad (k=1, 2) \tag{11}$$

and

$$\begin{aligned} &\Gamma_1=0, \quad \gamma_2=K(c_2)/[D_2^{\frac{1}{2}}(c_2-c_1)], \quad \beta_2=0; \\ &\gamma_1=(D_2/D_1)^{\frac{1}{2}}\Gamma_2, \quad \beta_1=(D_2/D_1)^{\frac{1}{2}}B_2. \end{aligned} \tag{11a}$$

(In writing the last two equations of (11a) we have chosen $c_k-c_{k-1}=\Delta c$ constant for all k; the slight generalization involved in passing to the case of unequal intervals may, however, be made without difficulty.)

If we make a guess at D_2, then γ_2 can be evaluated; knowing β_2 and γ_2 we can then with the aid of Eq. (11)

[4] For example, E. L. Ince, *Ordinary Differential Equations* (Dover Publications, New York), p. 36.

evaluate B_2 and Γ_2:

$$\begin{aligned} \text{erf}B_2 &= \text{erf}\beta_2 + F(\beta_2)/\gamma_2, \\ \Gamma_2 &= [F(B_2)/F(\beta_2)]\gamma_2, \end{aligned} \tag{12}$$

where

$$F(y) = (2/\pi^{\frac{1}{2}}) \exp(-y^2).$$

Erf$y$ and $F(y)$ have been extensively tabulated,[5] and the above calculation may, therefore, be performed without difficulty. Using the last two Eqs. of (11a), we can then compute β_1 and γ_1, from which, in turn, we can, by the use of equations analogous to Eq. (12), calculate B_1 and Γ_1. If we have chosen D_2 correctly, then $\Gamma_1 = 0$, which means that $F(B_1) = 0$ or $\text{erf}(B_1) = 1$. Knowing D_1 and D_2, this procedure may be extended to calculate D_3 from $K(c_3)$, and so on.

In general, we wish to calculate D_N knowing $D_1, D_2, \cdots D_{N-1}$ and $K(c_N)$. We make a guess at D_N, which enables us to calculate γ_N:

$$\gamma_N = K(c_N)/D_N^{\frac{1}{2}}\Delta c; \tag{13}$$

β_N is always zero. We can then calculate erfB_1 by means of the recursion formulas,

$$\begin{aligned} \text{erf}B_k &= \text{erf}\beta_k + F(\beta_k)/\gamma_k, \\ \Gamma_k &= [F(B_k)/F(\beta_k)]\gamma_k, \\ \gamma_{k-1} &= (D_k/D_{k-1})^{\frac{1}{2}}\Gamma_k, \quad \beta_{k-1} = (D_k/D_{k-1})^{\frac{1}{2}}B_k. \end{aligned} \tag{14}$$

Our object is to choose D_N so that erf$B_1 = 1$. In order to make this choice in a systematic fashion, we first make two guesses $[D_N]_1$ and $[D_N]_2$ at random and then improve on them by the following successive approximations procedure:

$$[D_N]_{k+1} = \frac{[D_N]_k(1-[\text{erf}(B_1)]_{k-1}) - [D_N]_{k-1}(1-[\text{erf}(B_1)]_k)}{[\text{erf}(B_1)]_k - [\text{erf}(B_1)]_{k-1}}, \tag{15}$$

where $[\text{erf}(B_1)]_k$ is the value of erfB_1 corresponding to $[D_N]_k$. Equation (15) merely represents linear interpolation (or extrapolation) between $[D_N]_k$ and $[D_N]_{k-1}$ to find $[D_N]_{k+1}$ so that $[\text{erf}(B_1)]_{k+1} = 1$; four or five steps are usually enough to yield a sufficiently accurate value for D_N.

The $D(c)$ obtained in this fashion yields a $K(c_f)$ which coincides with the experimental $K(c_f)$ at the points $c_1, c_2, \cdots c_N$. Since, however, the step function character of our $D(c)$ does not correspond to physical reality, we smooth it out by calculating the average $\bar{D}(c)$ at $c_1, c_2, \cdots c_N$:

$$\begin{aligned} \bar{D}(c_k) &= \frac{1}{c_k}\int_0^{ck} D(c)dc \\ &= \frac{1}{k}\sum_{i=1}^{k} D_i. \end{aligned} \tag{16}$$

[5] *Tables of Probability Functions* (Works Projects Administration, New York, 1941), Vol. I.

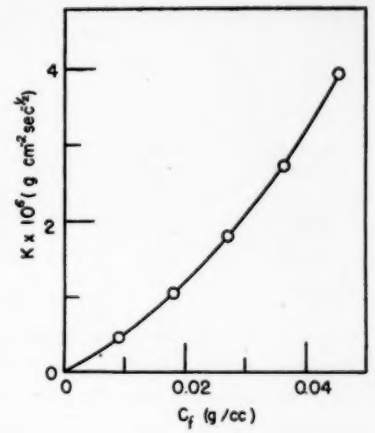

FIG. 1. K *vs* c_f for the polyisobutylene-isobutane system at 35°C.

We then fit $\bar{D}$ with a polynomial in c and recalculate $D(c)$ as indicated by Eq. (17) below:

$$D_r(c) = d/dc(c\bar{D}) = \bar{D} + cd\bar{D}/dc. \tag{17}$$

APPLICATION OF THE METHOD

To demonstrate the above method, we have used sorption data obtained by us on the isobutane-polyisobutylene system. We have divided the concentration range covered in our measurements into five equal intervals. Figure 1 gives the experimental values of K as a function of c_f; Fig. 2 is a plot of the calculated values of $\bar{D}$, D, and D_r *vs* c. In Table I we have tabulated K, D, $\bar{D}$, and D_r for the values $c_k = k\Delta c$. Table II is an actual calculation of D for the third interval, illustrating the approximation procedure.

To check our calculations, we computed the $c(\lambda)$ corresponding to $D_r(c)$ using a method developed by

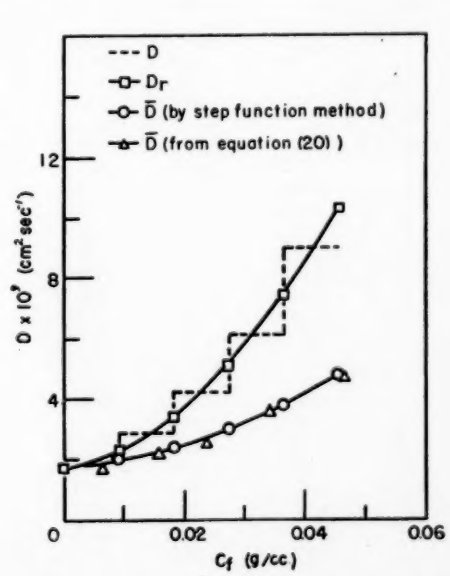

FIG. 2. D, D_r, and $\bar{D}$ *vs* c_f for the polyisobutylene-isobutane system at 35°C.

TABLE I. Calculated D values for the polyisobutylene-isobutane system at 35°C.

$c_k(\Delta c=0.0091$ g/cc)	$K\times10^6$ (g cm^{-2} sec$^{-\frac{1}{2}}$)	$D\times10^9$ (cm^2 sec^{-1})	$\bar{D}\times10^9$ (cm^2 sec^{-1})	$D_r\times10^9$ (cm^2 sec^{-1})
0.0000	0.00	—	—	1.8
0.0091	0.45	2.0	2.0	2.3
0.0182	1.05	2.9	2.4	3.4
0.0273	1.79	4.2	3.0	5.1
0.0364	2.73	6.1	3.8	7.4
0.0455	3.93	9.0	4.8	10.3

Crank and Henry[6] and compared it with the $c(\lambda)$ obtained from our step function $D(c)$. The latter $c(\lambda)$ may be readily obtained from calculations already performed in the course of computing $D(c)$:

$$\lambda(c_k)=2D_k^{\frac{1}{2}}\beta_k. \tag{18}$$

(See Eqs. (3a) and (10).) The method of Crank and Henry consists of a series of successive approximations as follows:

$$[c(\lambda)]_{n+1}=c_f-A\int_0^\lambda \frac{1}{D_r\{[c(w)]_n\}} \times\exp\left[-\frac{1}{2}\int_0^w \frac{v}{D_r\{[c(v)]_n\}}dv\right]dw, \tag{19}$$

where A is chosen so that $[c(\infty)]_{n+1}=0$. For the first approximation $[c(\lambda)]_1$ to $c(\lambda)$, we used the relationship given by Eq. (18); we then computed the second approximation $[c(\lambda)]_2$ as indicated by Eq. (19). The

TABLE II. Calculation of D_3 from $K(c_3)$, D_1 and D_2 having been found previously.

[$K(c_3)=1.79\times10^{-6}$ g cm^{-2} sec$^{-\frac{1}{2}}$, $D_1=1.963\times10^{-9}$ cm^2 sec^{-1}, $D_2=2.879\times10^{-9}$ cm^2 sec^{-1}.]

	$(D_3^{\frac{1}{2}})_1=0.7\times10^{-4}$	$(D_3^{\frac{1}{2}})_2=0.68\times10^{-4}$	$(D_3^{\frac{1}{2}})_3=0.64\times10^{-4}$	$(D_3^{\frac{1}{2}})_4=0.6474\times10^{-4}$
γ_3	2.814	2.897	3.078	3.043
β_3	0	0	0	0
$F(\beta_3)/\gamma_3=\text{erf}B_3$	0.4009	0.3894	0.3665	0.3707
B_3	0.3717	0.3601	0.3372	0.3413
$F(B_3)$	0.9828	0.9911	1.007	1.0043
Γ_3	2.451	2.545	2.748	2.709
$(D_3/D_2)^{\frac{1}{2}}$	1.305	1.267	1.193	1.206
γ_2	3.197	3.225	3.278	3.268
β_2	0.4849	0.4562	0.4023	0.4117
$\text{erf}\beta_2$	0.5071	0.4812	0.4306	0.4396
$F(\beta_2)$	0.8919	0.9164	0.9598	0.9525
$F(\beta_2)/\gamma_2$	0.2790	0.2842	0.2928	0.2915
$\text{erf}B_2$	0.7861	0.7654	0.7234	0.7311
B_2	0.8789	0.8405	0.7693	0.7818
$F(B_2)$	0.5212	0.5567	0.6244	0.6124
Γ_2	1.868	1.959	2.133	2.101
γ_1	2.262	2.372	2.583	2.544
β_1	1.064	1.018	0.9316	0.9468
$\text{erf}\beta_1$	0.8676	0.8500	0.8123	0.8194
$F(\beta_1)$	0.3637	0.4003	0.4737	0.4604
$F(\beta_1)/\gamma_1$	0.1608	0.1688	0.1834	0.1810
$\text{erf}B_1$	1.0284	1.0188	0.9957	1.0004

[6] Crank and Henry, Trans. Faraday Soc. 45, 636 (1949).

TABLE III. Comparison of $[c(\lambda)]_1$ computed by the step function method with $[c(\lambda)]_2$ computed by the method of Crank and Henry.

λ (cm sec$^{-\frac{1}{2}}$)	$[c(\lambda)]_1$ (g cm^{-3})	$[c(\lambda)]_2$ (g cm^{-3})
0	0.0364	0.0364
4.15×10^{-5}	0.0273	0.0274
7.47×10^{-5}	0.0182	0.0183
10.74×10^{-5}	0.0091	0.0087

results for the case of a sorption process covering four intervals ($N=4$) are shown in Table III. It will be seen that $[c(\lambda)]_1$ and $[c(\lambda)]_2$ agree very well, thus justifying our step function approximation to $D_r(c)$.

As a further check on our calculations, we also computed $D(c)$ by an approximate method suggested by Crank and Park.[1,6] According to these authors, if one carries out a sorption process from 0 to c_f together with the corresponding desorption process from c_f to 0, then $\bar{D}(c_f)$ can be calculated from the formula

$$\bar{D}(c_f)=0.0247l^2[(1/\tau_s)+(1/\tau_d)], \tag{20}$$

where τ_s and τ_d are the half times for the sorption and desorption processes, respectively. The two $\bar{D}$'s are compared in Fig. 2; it will be seen that they agree quite well. The method just outlined is, of course, much faster than the one previously described; in order to be able to use it, however, one has to have desorption as well as sorption data, which may be inconvenient to obtain. Furthermore, it may be pointed out that so far at least the method has been verified only empirically for a number of hypothetical $D(c)$ functions.

The principal defect of our method is that as the number of intervals increases, $\text{erf}B_1$ becomes rapidly less sensitive to D_N, as indicated in Fig. 3. This means that the accuracy in D_N possible with a given set of error function tables decreases rapidly with increasing N; it was these circumstances that limited us to the use of five intervals in the above calculations. Nevertheless, as can be seen from Table III and Fig. 2 the results are accurate within experimental error. Figure 3 also shows that for values of D_N which are considerably too large, $\text{erf}B_1$ approaches 1 again. This region is to be avoided,

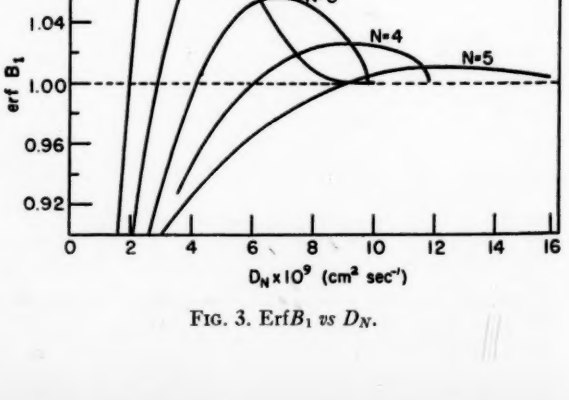

FIG. 3. ErfB_1 *vs* D_N.

because it yields values of D_N which are only apparently correct; the true value of D_N occurs where the plot of $\text{erf}B_1$ *vs* D_N crosses the line $\text{erf}B_1=1$.

In conclusion, it may be remarked that the concentration intervals do not necessarily have to be chosen equal; one may take smaller intervals in regions where $D(c)$ varies rapidly than in regions where it varies more slowly.

ACKNOWLEDGMENT

This work was carried out as part of a research project sponsored by Army Ordnance.

THE JOURNAL OF CHEMICAL PHYSICS VOLUME 19, NUMBER 5 MAY, 1951

Investigation of Turbulent Flames*

BÉLA KARLOVITZ,† D. W. DENNISTON, JR.,† AND F. E. WELLS†
Central Experiment Station, Bureau of Mines, Pittsburgh, Pennsylvania
(Received October 2, 1950)

A new theory of turbulent burning velocity has been developed. Comparison of the predictions of the theory with turbulent burning-velocity measurements has led to recognition that the turbulent flame itself generates additional turbulence. A theory has been formulated to explain the production of turbulence by the turbulent flame, which permits calculation of the intensity of flame generated turbulence. A comparison of calculated maximum turbulence intensity values with the turbulence intensities that correspond to the measured turbulent burning-velocity data supports this theory.

INTRODUCTION

SINCE the earliest investigations of flames, it has been known that turbulence greatly influences flame propagation in explosive mixtures. However, the relation between the quantities which characterize turbulence and the turbulent burning velocity is still not clear.

The first of recent workers in this field, Damköhler,[1] recognized that the effect of turbulence on a flame differs radically according to whether the scale of turbulence is small or large as compared with the thickness of the combustion wave. According to Damköhler, fine-scale turbulence simply increases the transport phenomena within the flame front, thereby increasing the burning velocity. Large-scale turbulence leaves the structure of the combustion wave unaltered, but distorts or wrinkles the flame surface. The increased burning velocity is an effect of the increased flame surface.

Damköhler and later Shelkin[2] gave a fairly complete treatment for the case of fine-scale turbulence, and both developed burning-velocity formulas for the case of large-scale turbulence, starting from a somewhat specialized shape of the distorted flame front. According to these formulas, the burning velocity would increase almost linearly with the intensity of turbulence and be independent of the normal burning velocity at high turbulence intensities.

Bollinger and Williams[3] carried out a number of turbulent burning-velocity measurements to test the theories of Damköhler and Shelkin. Their findings do not agree with the predictions of the theories. In particular, they found that the normal burning velocity retained a controlling influence even at high turbulence intensities.

In order to clear up the existing confusion and to gain an understanding of the fundamental phenomena involved in turbulent flame propagation, a study of turbulent flames was initiated in the laboratories of the Bureau of Mines. In the course of this work, a new theory of turbulent burning velocity was developed for the case of large-scale turbulence, and turbulent burning-velocity measurements were carried out.[4] Comparison of the predictions of the theory with the measured burning-velocity data led to the recognition that the turbulent flame itself generates additional turbulence. A mechanism was recognized whereby the flame could generate turbulence, permitting calculation of the intensity of the flame-generated turbulence. The available experimental data appear to substantiate this theory. Further measurements are in progress for an extended experimental test.

THEORY OF TURBULENT BURNING VELOCITY FOR LARGE-SCALE TURBULENCE

In contrast to laminar flames, turbulent flames appear thick and diffuse to the eye (Fig. 1). The structure of such flames is illustrated by the instantaneous schlieren picture in Fig. 2. The rapid fluctuating motion of the thin, instantaneous flame front causes the typical diffuse

* This research is part of the work being done at the Bureau of Mines on Project NR 053 067, Contract NA onr 25-47, supported by the ONR and the Army Air Forces.

† Physicist, Physical Chemistry and Physics Section, Explosives Branch, Bureau of Mines, Pittsburgh, Pennsylvania.

[1] G. Damköhler, *Jahrbuch 1939 der deutschen Luftfahrtforschung*, p. 113; Z. Elektrochem. **46**, 601 (1940); English translation: NACA Tech. Memo. No. 1112, 1947.

[2] K. I. Shelkin, J. Tech. Phys. (U.S.S.R.) **13**, 520 (1943); English translation: NACA Tech. Memo. No. 1110, 1947.

[3] L. M. Bollinger and D. T. Williams, NACA Tech. Note No. 1707, 1948.

[4] B. Karlovitz, Phys. Rev. **77**, 574 (1950).

FIG. 1. Time exposure photograph of a turbulent natural gas-air flame. $Re=$ 10,000. Burner tube radius $R=15.8$ mm.

appearance of the turbulent flame. The instantaneous flame front is quite smooth in the neighborhood of the burner port, with wrinkles developing gradually as the distance from the port increases. The instantaneous flame front has a peculiar, nonsymmetrical character; it has sharp edges on the burned-gas side and rather smooth surface elements on the fresh-gas side.

Based on this structure of the turbulent flame, the mechanism of flame propagation in a turbulent explosive mixture may be pictured as follows: The fluctuating turbulent motion carries small portions of the flame front forward and backward at random, whereby the flame elements diffuse away from their original positions. In addition to this random motion, the flame moves at its normal burning velocity from one small gas volume to the next.

The mean displacement $\bar{X}$ produced by the turbulent motion is zero, because positive and negative displacements have equal probability. The root-mean-square

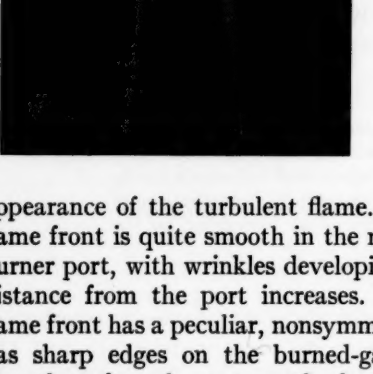

FIG. 2. Instantaneous schlieren photograph of a turbulent natural gas-air flame. $Re=$ 10,000. Burner tube radius $R=15.8$ mm.

value of the displacement can be calculated, according to G. I. Taylor,[5] as follows.

Let the turbulence be characterized by its *intensity* $u'=(\bar{u}^2)^{\frac{1}{2}}$, where u is the instantaneous value of the fluctuating velocity component perpendicular to the average turbulent flame front; by the *correlation coefficient* $R_t=\langle uu_t\rangle_{\text{Av}}/\bar{u}^2$, where u is the fluctuating velocity component at the arbitrary time t_0, u_t the fluctuating velocity component at the time t, measured from t_0; by the scale of turbulence

$$l_1=u'\int_0^\infty R_t dt;$$

and by a characteristic time

$$T_0=\int_0^\infty R_t dt.$$

The variation of $\bar{X}^2$ with time is given by the equation

$$\frac{d}{dt}\bar{X}^2=2\bar{u}^2\int_0^t R_t dt. \tag{1}$$

For time intervals t, which are small compared with the characteristic time $T_0(t/T_0\ll 1)$, $R_t\approx 1$ during the entire time interval t and the root-mean-square displacement is

$$(\bar{X}^2)^{\frac{1}{2}}=u't. \tag{2}$$

For time intervals t, which are very large by comparison with $T_0(t/T_0\gg 1)$, $\int_0^t R_t dt$ equals a definite limiting value T_0, and the root-mean-square displacement is

$$(\bar{X}^2)^{\frac{1}{2}}=(2l_1u't)^{\frac{1}{2}}. \tag{3}$$

For time intervals t of the order of $T_0(t\approx T_0)$, the displacement depends on the shape of the correlation curve $R(t)$. Assuming a correlation function of the form $R(t)=\exp(-t/T_0)$, the root-mean-square displacement is

$$(\bar{X}^2)^{\frac{1}{2}}=(2l_1u't)^{\frac{1}{2}}\{1-T_0/t[1-\exp(-t/T_0)]\}^{\frac{1}{2}}. \tag{4}$$

The essential new element in the case of flame propagation beyond simple diffusion is propagation of the flame from one small gas volume to the next due to its normal burning velocity. The average time interval during which a flame element is bound to a volume of gas is assumed to be

$$t_1=l_1/S_u, \tag{5}$$

where S_u is the normal burning velocity or the burning velocity increased by the effect of fine-scale turbulence if the latter has any appreciable effect.

The average velocity of the displacement of the flame front by large-scale turbulence is therefore

$$S_t=(\bar{X}^2)^{\frac{1}{2}}/t_1. \tag{6}$$

[5] G. I. Taylor, Proc. London Math. Soc. **A20**, 196 (1921). H. L. Dryden, Quart. Appl. Math. Vol. I, No. 1, p. 37 (1943).

In the case of weak turbulence, as compared with normal burning velocity, where $u'/S_u=t_1/T_0\ll 1$, the turbulent burning velocity is

$$S_t=(\bar{X}^2)^{\frac{1}{2}}/t_1=u't_1/t_1=u'. \tag{7}$$

For very strong turbulence, when $u'/S_u=t_1/T_0\gg 1$, the turbulent burning velocity is

$$S_t=\frac{(\bar{X}^2)^{\frac{1}{2}}}{t_1}=\frac{(2l_1u't_1)^{\frac{1}{2}}}{t_1}=(2S_uu')^{\frac{1}{2}}. \tag{8}$$

For intermediate values of u'/S_u,

$$S_t=(2S_uu')^{\frac{1}{2}}\{1-S/u'[1-\exp(-u'/S_u)]\}^{\frac{1}{2}}. \tag{9}$$

The diffusion caused by the turbulent motion proceeds forward and backward with equal velocity. It broadens the distribution of an assembly but does not produce a net motion of the entire assembly. In contrast, stationary turbulent flames move forward with a constant velocity and maintain a constant width. The reason for this behavior is shown in Fig. 3. Starting from an arbitrary wavy flame front which is thought to be produced by turbulent fluctuations, the position that the flame front would assume by normal propagation is shown for subsequent short time intervals, while the turbulent motion is thought to be absent. Portions of the flame front soon intersect each other, thus producing the characteristic shape of the instantaneous flame front. Sharp edges appear on the burned-gas side and slightly curved surface elements on the fresh-gas side. Because of their oblique positions the back portions of the flame move forward with increased velocity. The increased velocity compensates for backward diffusion and causes the entire flame to move forward.

Adjacent points of the flame front are moved apart by turbulent diffusion, turbulence constantly tending to increase the area of the flame front. As can be seen from Fig. 3, normal flame propagation tends to reduce the area of the flame front. The area of the instantaneous flame front per unit area of the smooth average turbulent flame front is determined by the balance of these two opposing effects. In the steady state the increased undulated flame-front area is just sufficient to burn all the mixture that flows across the turbulent flame.

To obtain the total turbulent burning velocity S_T, the normal burning velocity S_u has to be added to the velocity S_t produced by the turbulent diffusion:

$$S_T=S_u+S_t. \tag{10}$$

The relation between the intensity of turbulence and the total turbulent burning velocity is shown in Fig. 4, in nondimensional representation. The diagram is valid for any fuel and mixture ratio. The two limiting cases of very weak and very strong turbulence are also shown in the diagram.

According to this theoretical result, the effect of turbulence should be independent of the scale of the turbulence; the total turbulent burning velocity should increase at first linearly, but later more slowly with the turbulence intensity; the normal burning velocity S_u should remain the most important controlling factor even at very high intensity turbulence.

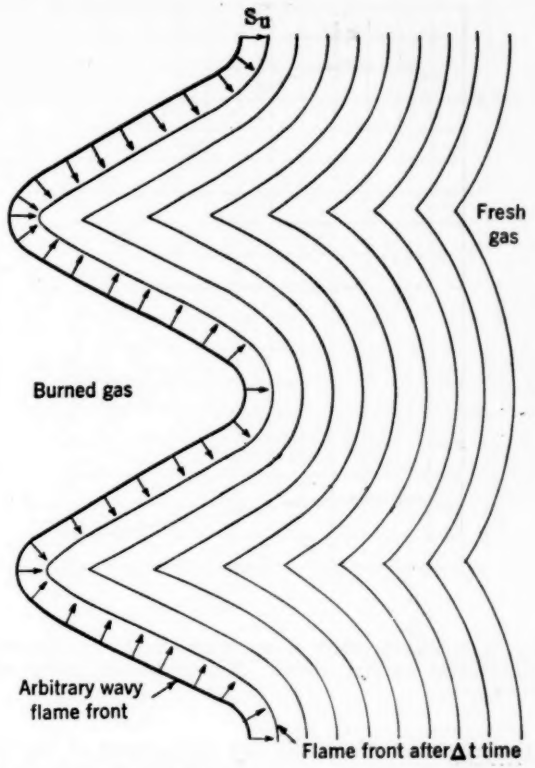

FIG. 3. The effect of normal flame propagation on the development of the turbulent flame front.

EXPERIMENTAL RESULTS

Experimental flames for burning-velocity measurements were produced at the top of long vertical burner tubes of radius $R=15.8$ mm. Measurements on burner tubes of other diameters are in progress. The turbulence

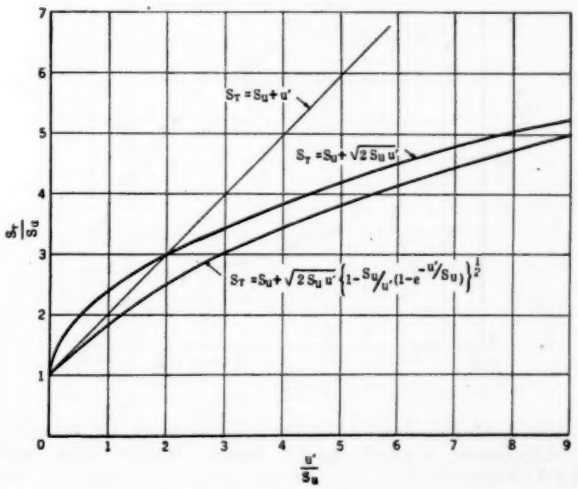

FIG. 4. Total turbulent burning velocity in function of turbulence intensity. Theoretical curve.

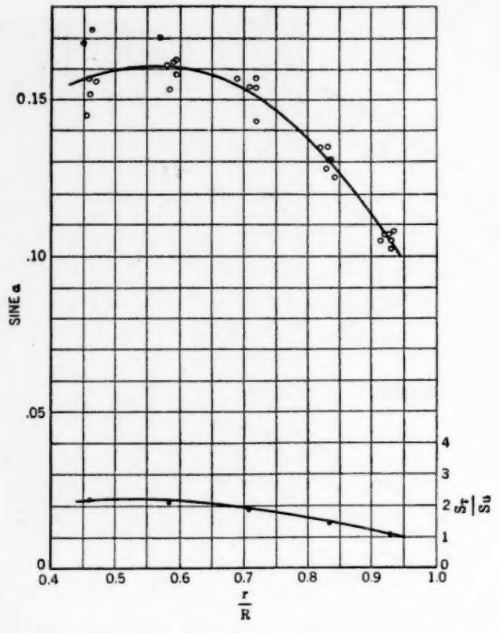

FIG. 5. Measured values of sine α and S_T/S_u for $Re=10{,}000$. Stoichiometric natural gas-air flames. Burner tube radius $R=15.8$ mm.

of the approach flow was the turbulence of the fully developed pipe flow. No grids or other turbulence-producing elements were used. The flames were enveloped by a coaxial air flow of comparable velocity to eliminate mixing with the surrounding quiescent air. Stoichiometric natural gas-air mixtures with a normal burning velocity of $S_u=40.6$ cm/sec and stoichiometric acetylene-air mixtures with $S_u=175$ cm/sec were used.[6]

The flow velocity and the turbulence intensity vary along the radius and height in the flame; therefore, local

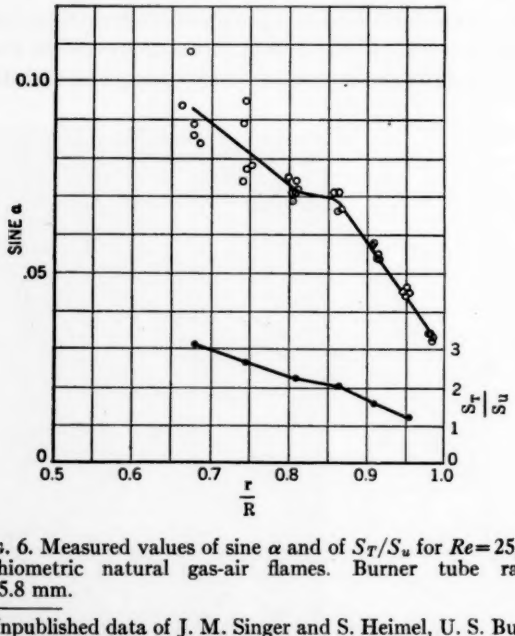

FIG. 6. Measured values of sine α and of S_T/S_u for $Re=25{,}000$. Stoichiometric natural gas-air flames. Burner tube radius $R=15.8$ mm.

[6] Unpublished data of J. M. Singer and S. Heimel, U. S. Bureau of Mines, Pittsburgh, Pennsylvania.

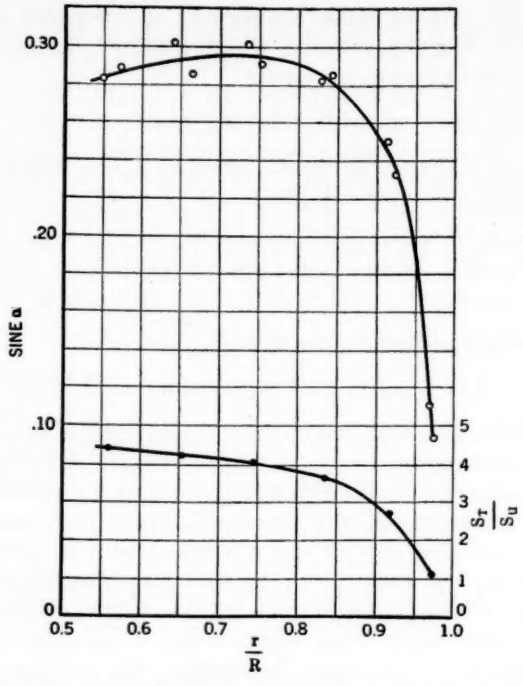

FIG. 7. Measured values of sine α and of S_T/S_u for $Re=25{,}000$. Stoichiometric acetylene-air flames. Burner tube radius $R=15.8$ mm.

measurements of the turbulent burning velocity are necessary to permit comparison of experimental data with the predictions of the theory. The local turbulent burning velocity was measured by the angle method, using the relation $S_T=U$ sine α, where U is the local mean flow velocity, and α the angle included by the average turbulent flame front and the approach flow velocity. The diffuse turbulent flame has no definite boundaries to represent the average turbulent flame front; therefore, the most probable position of the instantaneous flame front, which is marked with good approximation by the maximum brightness of the flame,

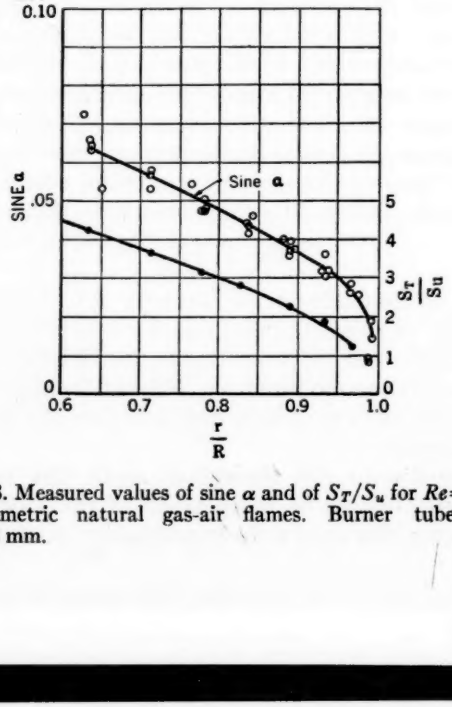

FIG. 8. Measured values of sine α and of S_T/S_u for $Re=50{,}000$. Stoichiometric natural gas-air flames. Burner tube radius $R=15.8$ mm.

was taken to represent the average turbulent flame front. The location of the maximum brightness was measured on long-time (≈1 min) exposure flame negatives with a spectroscopic densitometer.

Figures 5 to 9 show the measured values of sine α and of S_T/S_u in function of the radius for stoichiometric natural gas-air, and acetylene-air flames with the Reynolds number of the approach flow varying from 10,000 to 50,000.

The radial turbulence intensity data of the approach flow were obtained from turbulence measurements on an air jet issuing from a pipe into a coaxial air flow; the experiments were carried out under Dr. Kennedy F. Rubert's supervision by the Langley Field Laboratory of the National Advisory Committee for Aeronautics.[7]

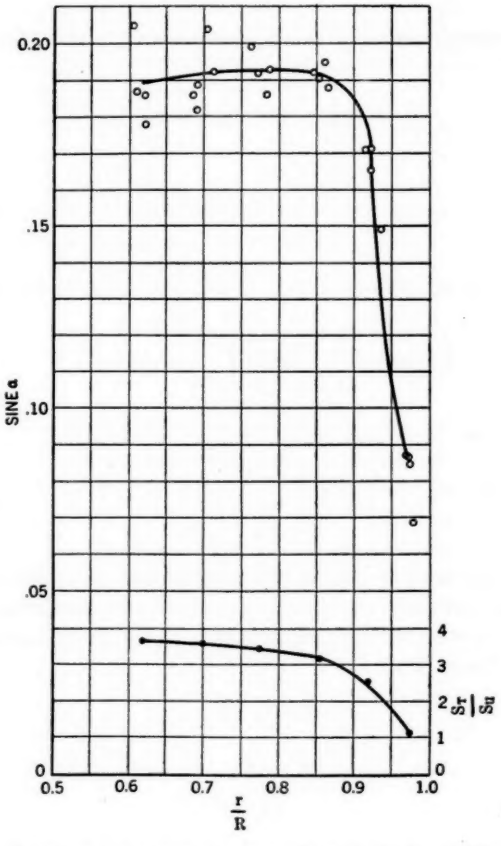

FIG. 9. Measured values of sine α and of S_T/S_u for $Re=50{,}000$. Stoichiometric acetylene-air flames. Burner tube radius $R=15.8$ mm.

The measured burning-velocity data are, in general, higher than the values calculated from the above theory. To obtain a closer comparison, a calculation was made of the turbulence intensity which would be required by the theory to fit the measured turbulent burning-velocity data. These turbulence intensity values are shown in Figs. 10 to 12, together with the radial turbulence intensity of the approach flow. The turbulence intensity that corresponds to the measured turbulent burning velocity is nearly zero in the immediate vicinity of the tube wall, but increases rapidly

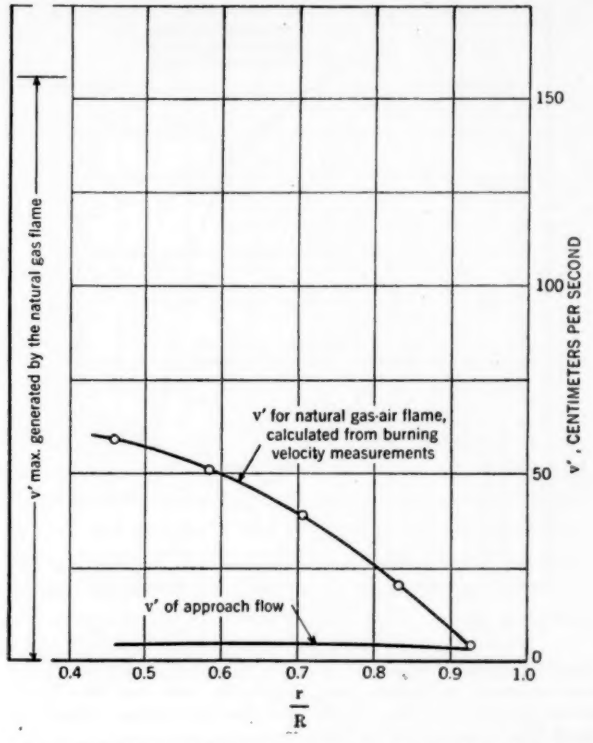

FIG. 10. Radial turbulence intensity v' calculated by the theory from measured turbulent burning-velocity data for $Re=10{,}000$. Natural gas-air flames. Mean approach flow velocity $U=490$ cm/sec.

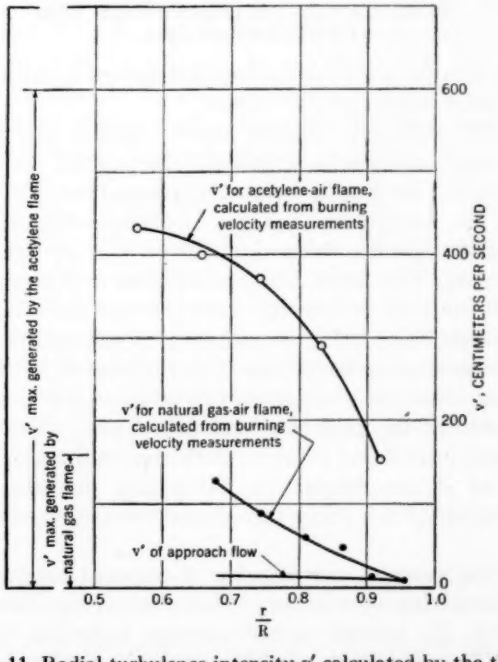

FIG. 11. Radial turbulence intensity v' calculated by the theory from measured turbulent burning-velocity data for $Re=25{,}000$ natural gas-air and $Re=25{,}000$ acetylene-air flames. Mean approach flow velocity $U=1225$ cm/sec.

[7] Unpublished data.

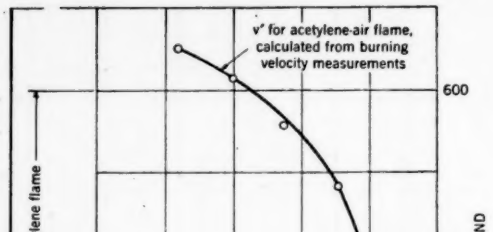

FIG. 12. Radial turbulence intensity v' calculated by the theory from measured turbulent burning-velocity data for $Re=50{,}000$ natural gas-air and $Re=50{,}000$ acetylene-air flames. Mean approach flow velocity $U=2450$ cm/sec.

with decreasing values of r/R (corresponding to increasing height in the flame) and soon reaches values many times greater than the approach flow. This result can be explained by assuming that additional turbulence is produced by the turbulent flame itself, which turbulence diffuses against the flow before the flame front.

TURBULENCE GENERATED BY THE TURBULENT FLAME

The process of turbulence production by the turbulent flame may be pictured as follows:

As the explosive mixture passes through the flame front with a velocity equal to the normal burning velocity S_u, its specific volume increases from V_1 to V_2 owing to heating of the gas. Correspondingly, the combustion gas leaves the flame front with the velocity $(V_2/V_1)S_u$. The flame front constitutes a flow source that introduces a velocity into the gas flow of the magnitude $(V_2-V_1)S_u/V_1$, which is always normal to the instantaneous flame front. In the case of a steady laminar flame, the direction of this additional velocity is constant. In the case of a turbulent flame, where the instantaneous flame front is undulated and small portions of it are subject to fluctuating motions, the orientation of this flame-introduced velocity fluctuates also.

On the average, this velocity of constant magnitude but fluctuating orientation will have an average forward velocity, $\bar{U}$, normal to the average turbulent flame front. The magnitude of this average forward velocity will be large for slightly turbulent flames and will decrease with increasing turbulence of the flame. After this average forward velocity is subtracted, the rest of the flame-introduced velocity components are distributed truly at random and constitute turbulence generated by the turbulent flame.

A schematic cross section of the turbulent flame front is given in Fig. 13. The undulated, fluctuating instantaneous flame front has on the average an area A per unit area of the average turbulent flame front. The forward velocity component of the flame-introduced velocity for the element dA is

$$\frac{V_2-V_1}{V_1}S_v\cos\varphi.$$

The average value of this forward velocity is

$$\bar{U}=\left[\frac{V_2-V_1}{V_1}S_u\cos\varphi\right]$$

$$=\frac{V_2-V_1}{V_1}S_u[\cos\varphi], \qquad (11)$$

where the square brackets [ ] denote average quantities.

$$[\cos\varphi]=\frac{1}{A}, \quad \text{since}\int_0^A\cos\varphi dA=1.$$

Therefore,

$$\bar{U}=\frac{V_2-V_1}{V_1}S_u\frac{1}{A}. \qquad (12)$$

The area ratio A equals the ratio of the turbulent and normal burning velocities, because the large-scale turbulence does not affect the structure of the instantaneous flame front. Thus,

$$A=S_T/S_u,$$

and

$$\bar{U}=\frac{V_2-V_1}{V_1}S_u\frac{S_u}{S_T}. \qquad (13)$$

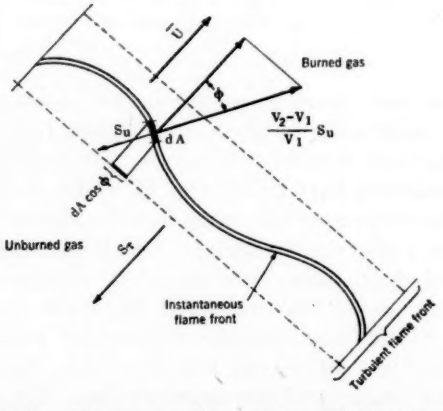

FIG. 13. Schematic cross section of the turbulent flame front, showing the various velocity vectors.

To calculate the intensity of the flame generated turbulence the amount of mechanical work developed by the gas as it moves across the pressure drop Δp of the instantaneous flame has to be determined first, because this work is the source of the additional turbulence energy. This expansion work can be calculated in the simplest way in a coordinate system in which the unburned gas is at rest. While the flame is moving with the velocity S_u into the unburned gas, the burned gas is accelerated by the pressure drop across the flame front to the velocity $(V_2-V_1)S_u/V_1$, as shown in Fig. 14. The expansion work of the gas $\int_{p_1}^{p_2} V dp$ appears as the kinetic energy of the burned gas $1/2g[(V_2-V_1)S_u/V_1]^2$; therefore, the expansion work can be calculated without the knowledge of the functional relationship between V and p in the flame front.

Part of this expansion work, corresponding to the mean forward velocity $\bar{U}$, is added to the energy of the mean flow; the remaining part provides energy for the flame generated turbulence. Therefore, the total intensity of the flame generated turbulence may be calculated from the energy equation:

$$\bar{u}^2+\bar{v}^2+\bar{w}^2=\left(\frac{V_2-V_1}{V_1}S_u\right)^2-\left(\frac{V_2-V_1}{V_1}S_u\frac{S_u}{S_T}\right)^2, \quad (14)$$

where $\bar{u}^2$, $\bar{v}^2$, and $\bar{w}^2$ are the mean square values of the flame generated turbulent velocity components. In the case of a laminar flame, $S_T/S_u=1$, and no turbulence is generated by the flame. With increasing values of S_T/S_u, that is, as the flame becomes more turbulent, the flame generated turbulence approaches an upper limit:

$$\bar{u}^2+\bar{v}^2+\bar{w}^2=\left(\frac{V_2-V_1}{V_1}S_u\right)^2, \quad (15)$$

or if uniform energy distribution is assumed among the three components,

$$u'=v'=w'=\frac{1}{\sqrt{3}}\left(\frac{V_2-V_1}{V_1}\right)S_u. \quad (16)$$

In Figs. 10–12, this maximal value of the flame generated turbulence is indicated on the left side. At lower Reynolds' numbers of the flow, the turbulence intensity which corresponds to the measured burning velocity is smaller than this maximal value. At

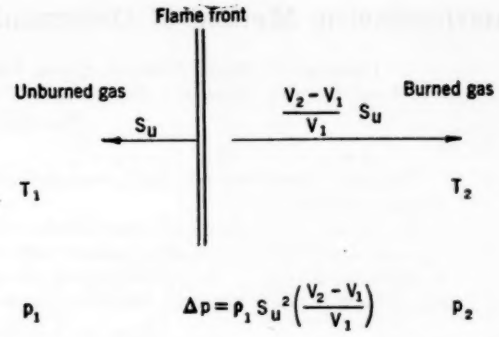

FIG. 14. Schematic representation of the motion of the flame front and of the burned gas relative to the unburned gas.

$Re=50{,}000$ (Fig. 12), the turbulence intensity in the flame approaches this maximal value for both the natural gas and the acetylene flame. This seems to indicate the correctness of the above theories of turbulent burning velocity and of flame generated turbulence. Further measurements at higher Reynolds' numbers and with burner tubes of different diameters are in progress for an extended test of the theories.

CONCLUSIONS

The theoretical formula of turbulent burning velocity shows that large-scale turbulence may increase the burning velocity several fold, but its effectiveness diminishes with increasing intensity; in addition, the normal burning velocity remains a more important factor than turbulence, even at very high turbulence intensity.

Even at moderate turbulence intensity of the approach flow, the flame generated turbulence is more important than the turbulence of the approach flow, although some turbulence in the approach flow is necessary for the flame to generate turbulence. For flame generated turbulence, the normal burning velocity remains as before the most significant factor.

ACKNOWLEDGMENTS

This study of turbulent flames was initiated by Drs. Bernard Lewis and Guenther von Elbe, who also gave much advice and encouragement in the course of this work. The authors wish to thank the National Advisory Committee for Aeronautics for permission to use the results of the turbulence measurements, made under Dr. Kennedy F. Rubert's supervision at Langley Field, before publication.

An Interferometric Method of Determining Diffusion Coefficients in Gaseous Systems*

CHARLES A. BOYD, NORMAN STEIN, VIRGINIA STEINGRIMSSON, AND WILLIAM F. RUMPEL
Naval Research Laboratory, Department of Chemistry, University of Wisconsin, Madison, Wisconsin
(Received February 2, 1951)

This paper describes a new type of experimental method for accurately measuring diffusion coefficients in gaseous systems.

The change of composition in the diffusion cell is followed by measuring the change in refractive index with an interferometer. Results obtained using this method compare favorably with some values reported in the earlier literature. In addition, values are reported for new systems not studied previously. A comparison is made between measured values and those calculated from viscosity data.

I. INTRODUCTION

THE process of gaseous diffusion and its temperature dependence are of great importance in the field of chemistry because they depend entirely upon the forces between the unlike molecules of the diffusing gases and are not masked by collisions between like molecules. In the case of spherical nonpolar molecules, kinetic theory has been developed to the point where the energy of interaction between unlike molecules can be readily obtained from an interpretation of the experimental coefficients of diffusion. In the case of more complicated molecules possessing dipoles, hydrogen bonds, geometrical assymetries, etc., it is expected that the theory will soon be developed to the point where at least semiquantitative interpretation can be made of the intermolecular forces. However, at the present time there is a lack of accurate measurements of the coefficients of diffusion of gases. The majority of the measurements available in the literature were obtained more than thirty years ago with methods which are not capable of yielding results of high precision. In the present work we have developed an interferometric method for measuring coefficients of diffusion to an accuracy of approximately one part in 500. Experimental results are given for nine pairs of gases at one atmosphere pressure and 25°C.

The general theory relating transport phenomena and intermolecular forces was first developed by Chapman, Enskog, and other workers. Chapman and Cowling[1] have expressed these results in a form involving certain "collision integrals" which depend upon the exact form of the molecular interaction. Hirschfelder, Bird, and Spotz[2] have evaluated these collision integrals in terms of the Lennard-Jones expression for the potential energy of interaction for spherical nonpolar molecules:

$$E(r)=4\epsilon[-(r/r_0)^6+(r/r_0)^{12}]. \quad (1)$$

The coefficients of diffusion are then expressed in terms of the temperature and the so-called force constants, ϵ/k and r_0. These force constants can be determined by experimental measurements of one transport property at two temperatures and can be used in predicting the other transport properties or the equation of state of the system.

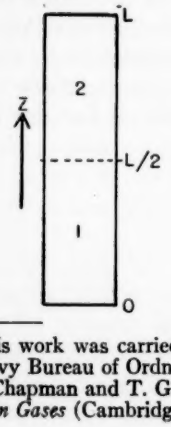

FIG. 1. Schematic representation of one-dimensional diffusion.

II. THEORETICAL DEVELOPMENT

Diffusion is the transport of molecules of a particular type between spatial regions of a system containing two or more chemical species. Diffusion may be due to gradients of concentration, temperature, or pressure or to the presence of external forces. In the present treatment we are concerned only with diffusion in binary mixtures due to concentration gradients.

Consider a one-dimensional problem in which the concentrations of the two chemical species vary along the Z coordinate. Such a situation is represented schematically in Fig. 1. Here, a long vessel of constant cross-sectional area and shape is divided by some means into two symmetrical compartments. One compartment is filled with gas 1 and the other with gas 2 at the same pressure and temperature. If the dividing partition represented by the dotted line is removed in such a fashion as not to give rise to any flow, a system of one-dimensional diffusion is established and molecules of 1 and 2 will intermix, finally resulting in a solution of constant composition.

This process can be represented by a partial differential equation:†

$$\partial X_1/\partial t = D(\partial^2 X_1/\partial Z^2), \quad (2)$$

* This work was carried out under Contract NOrd 9938 with the Navy Bureau of Ordnance.

[1] S. Chapman and T. G. Cowling, *Mathematical Theory of Non-Uniform Gases* (Cambridge University Press, London, 1939).

[2] Hirschfelder, Bird, and Spotz, J. Chem. Phys. **16**, 968 (1948); Chem. Revs. **44**, 205 (1949); Trans. Am. Soc. Mech. Engrs. **71**, 921 (1949).

† The derivation of this equation, as well as the solution for different types of boundary conditions, can be found in any elementary text on the subject.

where X_1 = mole fraction of component 1, D = the diffusion coefficient, and Z = the coordinate along which the diffusion is occurring.

Using the proper boundary conditions corresponding to the experimental details a solution can be obtained in terms of a fourier series:

$$X_1=\tfrac{1}{2}+\sum_{n=1}^{\infty}\left[\frac{\sin(n\pi/2)}{(n\pi/2)}\right]\exp\left(-\frac{n^2\pi^2Dt}{L^2}\right)\cos\left(\frac{n\pi Z}{L}\right). \quad (3)$$

Equation (3) relates the concentration, X_1, to the time, t, and the position Z inside the cell in terms of the diffusion coefficient, D, and the cell dimension, L. Thus, in principle, one can determine a value of D by measuring the concentration at some position in a diffusion cell at a series of times.

In practice, the summation in Eq. (3) can be simplified by choosing the proper experimental conditions. First, if the position is chosen such that Z is equal to $L/6$, it is seen that terms for $n=3, 9, 12 \cdots$ are zero. Further, if the value of t is sufficiently large, terms for values of n above 3 are unimportant. This critical time depends upon the dimensions of the diffusion cell and the value of D as well as the value of Z. Under these conditions, Eq. (3) simplifies to the first term of the series:

$$X_1=(1/2)+(2/\pi)[\exp(-\pi^2Dt/L^2)]\cos(\pi/6). \quad (4)$$

This may be rearranged to give

$$D=[L^2/(\pi^2t)]\ln\left[\frac{(2/\pi)[\cos(\pi/6)]}{X_1-\frac{1}{2}}\right], \quad (5)$$

which is the form used to calculate the value of the diffusion coefficient from our experimental data. Equation (3) was derived by assuming that the diffusion coefficient is constant and independent of concentration. In reality this is only approximately true; and, consequently, the value of D calculated from this equation represents a peculiar type of average value and depends very weakly on the geometry of the diffusion cell used in making the measurements. This type of diffusion coefficient corresponds to the so-called integral diffusion coefficient sometimes used in diffusion studies in solutions.

III. EXPERIMENTAL APPARATUS

The one-dimensional diffusion represented in Fig. 1 is achieved experimentally in the cell illustrated in Fig. 2. This cell is composed of two symmetrical halves of rectangular cross section 12.699 cm by 2.223 cm and having a total length of 38.121±0.002 cm. The rectangular cross section is necessary, since a sufficiently long optical path through the cell is needed to obtain the required accuracy in refractive index measurement, whereas, it is also necessary to have the cells slide only a short distan ceover one another to create the initial interface at the start of a diffusion run. The two half-cells can be slid together or apart by means of two sliding plates which slip over one another at the interface similar to the Tselius electrophoresis cell. The sliding faces of these plates were ground and hand-lapped against a third plate to insure flatness. It has been found that when the cell is assembled with a thin layer of silicone grease between the plates, it can be evacuated and filled without leakage. This cell is constructed from cold-rolled steel plates $\frac{7}{16}$ inch thick. The sliding plates were made from $\frac{3}{4}$-inch plates of $12\frac{1}{2}$ percent chromium tool steel. All parts were given special heat treatment to relieve stresses in the material before assembly to prevent subsequent warping.

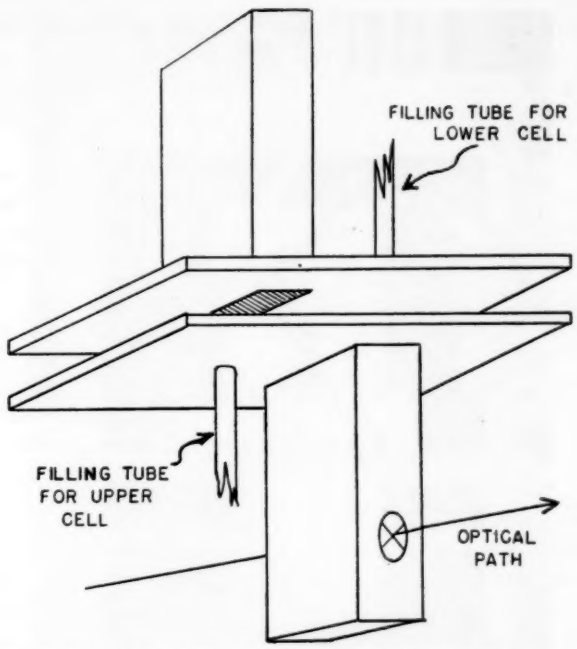

FIG. 2. Schematic drawing of the one-dimensional diffusion cell.

A pair of plate glass windows $\frac{3}{4}$ inch in diameter are located opposite to one another in the narrow walls of the bottom cell. These provide an optical path through the cell for purposes of measuring the refractive index of the diffusing gas. The exact location of the point which is one-sixth of the total cell length up from the bottom is determined by a set of cross hairs on the front window.

Figure 3 shows the diffusion cell mounted in the thermostat. The tubes connecting the walls of the thermostatic bath with the windows in the cell provide a convection free tunnel for the light beam from the interferometer as it goes through the test section. This is necessary in order to minimize spurious fringe shifts occurring during a diffusion run due to convection currents outside the cell.

The refractive index of the gas mixture in the cell is measured by means of an optical interferometer of the Mach-Zehnder type. A schematic sketch of the optical system with the cell in position is shown in Fig. 4. Light from a sodium lamp is collimated and passed through

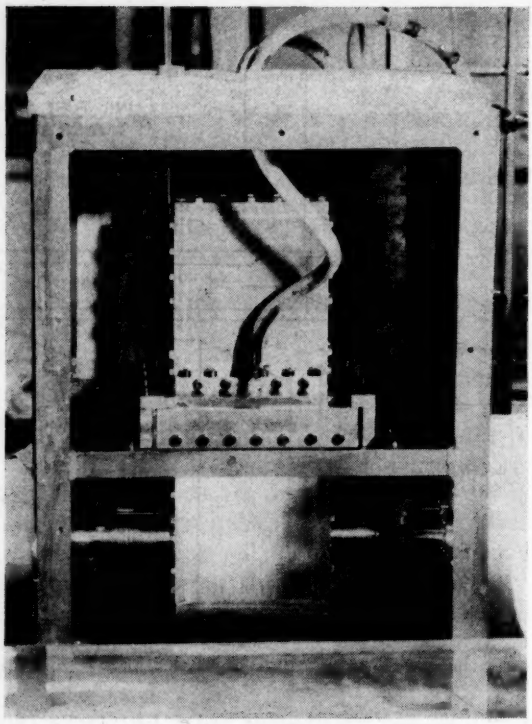

FIG. 3. Diffusion cell mounted in thermostat.

the beam splitting mirror I. The two beams so produced are reflected by means of mirrors II and III to a second partially-silvered mirror IV and by proper adjustment are brought into vertical interference. The emerging beam with its vertical interference bands is observed by means of a telescope and is recorded photographically.

The theory of the Mach-Zehnder interferometer is discussed in detail elsewhere,[3] and it is necessary at this point only to state that the fringes produced are virtual and are adjusted so as to be in the same plane as the cross hairs on the diffusion cell window. This makes it possible to measure the refractive index change in the cell at a known position.

Since small variations in room temperature or barometric pressure may produce unequal changes in optical

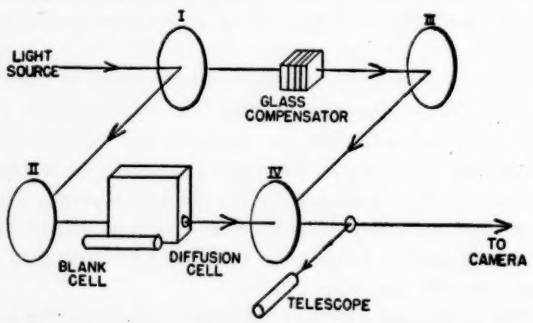

FIG. 4. Optical system with diffusion cell in place. Mirrors I and IV—Partially silvered. Mirrors II and III—Full silvered.

[3] E. H. Winkler, "Analytical studies of the Mach-Zehnder interferometer," Naval Ordnance Laboratory Report 1077 (1947).

density in the two arms of the interferometer during the course of a diffusion run, it is necessary to provide a blank cell of the same path length as the test cell, but having a constant index of refraction, in order to make the appropriate blank corrections. The glass compensator in the opposite arm from the test section compensates the extreme changes in optical density produced by the windows in the test section.

To make a diffusion study, the cell is first slid apart, the two halves are evacuated and flushed several times, and filled with the gases which are to be studied. The heavier gas is put in the bottom cell to prevent gravitational mixing. After the two half-cells have been equilibrated to temperature and pressure, they are slid together and the diffusion starts. When the cells are half-way closed a micro-switch activates the camera shutter and a picture is taken of the timer and the zero fringe position, thus giving a record of the start of the experiment. It has also been found necessary to take a second photograph of the fringes immediately after the cell is closed because of the fact that small irreversible fringe shifts occur on closing. If this second picture is taken within four seconds of the start of the experiment, no detectable fringe shift due to diffusion will have occurred.

Integral fringe shifts are counted visually by means of the reading telescope, but simultaneous photographs of the timer and fringes are taken at arbitrary fringe shifts to allow an accurate determination of the fringe shift at a measured time. It is estimated that fringe shifts can be determined in this fashion to ± 0.03 fringe.

IV. REDUCTION OF DATA

The primary quantity measured by the interferometer during the course of the diffusion is the change of refractive index of the gases. This is related to the observed fringe shift by means of the expression:

$$s=(l/\lambda)(n_m-n_0), \tag{6}$$

where s=fringe shift in terms of number of fringes, l=optical path length in test cell, λ=wavelength of light used, n_0=initial refractive index, and n_m=refractive index of gas mixture. This equation can be rewritten for ease of substitution later on as

$$s=(l/\lambda)[(n_m-1)-(n_0-1)]. \tag{7}$$

The refractive index of a substance is related to the molar refractivity through the Lorentz-Lorenz relation:

$$N=(M/\rho)[(n^2-1)/(n^2+2)], \tag{8}$$

where N=the molar refractivity, n=the refractive index, M=the molecular weight of the gas, and ρ=the density. In the case of gases n is very closely approximated by unity and so this expression can be rewritten to a very close approximation as

$$N=[(2M)/(3\rho)](n-1). \tag{9}$$

Further, it is reasonable to assume that for gases at

pressures close to atmospheric, the molar refractivity is an additive property and consequently for a binary mixture,

$$N_m = X_1 N_1 + (1-X_1)N_2. \quad (10)$$

Therefore, where X_1 = mole fraction component 1, the relation between the molar refractivity and the refractive index of a mixture will be given by

$$[X_1N_1+(1-X_1)N_2] = [2/(3\rho)][X_1M_1+(1-X_1)M_2](n_m-1), \quad (11)$$

where subscripts 1 and 2 refer to the two components and m refers to the mixture. The density term appearing in these expressions can be obtained to a sufficient degree of accuracy from the virial equation of state using the second virial coefficient,

$$(PV)/(RT) = 1+(B_m/V), \quad (12)$$

where p = pressure, T = temperature, R = gas constant, B_m = second virial coefficient, V = molar volume, and

$$\rho = M/V. \quad (13)$$

These equations are combined and the resulting expression rearranged to give:

$$X_1 = \left(\frac{1}{N_1+N_2}\right)\left\{\left[\frac{2\lambda S}{3l}+\frac{N_1}{(RT/P)+B_1}\right] \times\left[\left(\frac{RT}{P}\right)+B_m\right]-N_2\right\}. \quad (14)$$

This is the working equation which is used to calculate the concentration from the interferometer readings.

The second virial coefficients for the pure components, and the mixtures are calculated at the run temperature according to the methods developed by Hirschfelder, Bird, and Spotz,[2] which can be summarized as follows:

For a pure component we have

$$B_i = b_{0i}F(kT/\epsilon_i), \quad (15)$$

$$b_{0i} = (2Nr_{0i}^3)/3. \quad (16)$$

The function $F(kT/\epsilon)$ has been tabulated.[2]

For a mixture we have

$$B_m = B_1X_1^2+2B_{12}X_1X_2+B_2X_2^2, \quad (17)$$

where B_{12} is estimated by assuming the force constants between unlike molecules are of the form:

$$\epsilon_{12} = (\epsilon_1\epsilon_2)^{\frac{1}{2}}, \quad (18)$$

$$r_{012} = (r_{01}+r_{02})/2. \quad (19)$$

In order to obtain a value of the second virial coefficient, B_m, to be used in Eq. (16), it is necessary to proceed in the following way. First, estimate X_1 from Eq. (14) assuming B_m is zero. Then substitute this value of X_1 into Eq. (17), to get an expression for B_m, which can then be used in Eq. (14) to obtain a better value of X_1. The value of X_1 thus obtained from Eq. (14) can be substituted along with the corresponding value of time into Eq. (5) in order to obtain a value of the diffusion coefficient.

It is sometimes necessary to make small adjustments to the value of the diffusion coefficients so obtained in order to correct for small variations in temperature or pressure. This adjustment is made according to the formula

$$D_{760\text{ mm},25^\circ\text{C}} = D_{T,P}\frac{(298.16)^{\frac{3}{2}}PW'(kT/\epsilon_{12})}{T^{\frac{3}{2}}(760)W'[R(298)/\epsilon_{12}]}, \quad (20)$$

where $W'(kT/\epsilon)$ is a tabulated function appearing in the previous reference.[2]

V. EXPERIMENTAL RESULTS

A. Preliminary Experiments

Before the diffusion cell described in the previous sections was constructed, preliminary experiments were carried out in order to test the feasibility of this method. In particular, considerable attention was paid to the possibility of convection currents being set up in the diffusing system because of the fact that the two half-cells are slid across each other in order to establish the initial diffusion interface. This was investigated by constructing a test cell from Lucite similar to the cell described previously but having flat windows running the entire length of the cell rather than at one position. This made possible the observation of the gases near the interface. This cell could not be made leakproof, but this was relatively unimportant for the purpose for which it was intended.

The half-cells were filled with CO_2 and H_2 gases and the halves slid together. The behavior of the system was followed by observing the gradients of the refractive index with an optical schlieren apparatus which was being used at the time for studies of turbulence in gas streams.

Although the speed of closing the cell was varied over a wide range, no evidences of convection were observed by this method. There was a slight deviation of the initial interface away from horizontal which became more pronounced as the cell was closed more slowly. This is unquestionably due to the fact that one side of the diffusion boundary is established before the other. As the diffusion proceeded this initial deviation soon disappeared because of diffusion. Runs with this test cell were also observed with the optical interferometer and no irregular fringe shifts were observed.

The results of these tests coupled with the fact that later results obtained with the regular diffusion cell were very reproducible show that convection and initial mixing at the boundary are relatively unimportant.

B. Final Results

A comparison of the values of the diffusion coefficient obtained in separate runs on the same pair of gases is

TABLE I. Comparison of diffusion coefficient determined for the same gases in different runs, $H_2-C_2H_6$.

Fringe number	Mole fraction C_2H_6	D_{12} Run No. 3	D_{12} Run No. 6
23	0.80	0.540	0.540
32	0.72	0.541	0.540
35	0.70	0.540	0.539
40	0.66	0.538	0.538

made in Table I. The column labeled as approximate concentration of ethane refers to the concentration of ethane at the point in the cell where the fringe shift was measured.

It is seen that for comparable fringe shifts the values of D are in good agreement between the two runs. It is interesting to note that in both runs there is a slight trend in the calculated diffusion coefficient toward lower values as the run proceeds.

This trend is real and has been observed in a large number of cases. It is believed that this is a manifestation of the fact that the diffusion coefficient is not a constant but has a weak concentration dependence. It should be emphasized that the values of D in Table I are not those corresponding directly to the particular composition given in the second column.

Table II shows a comparison of diffusion coefficients determined by the present method with values determined by other workers for the same systems.

In general, the agreement between the two sets of values is reasonably good. Only in the case of H_2-CO_2 is there any appreciable discrepancy, and it is interesting to note that the value obtained by the present method is bracketed by the results of the previous investigations. The present reported value is an average of 20 determinations made during 3 runs, all of which were within 0.13 percent of the average value.

Table III is a summary of the diffusion coefficients which have been measured by the present method. Also included in this table are values of diffusion coefficients for these systems estimated by the methods of Hirschfelder, Bird, and Spotz.

The force constants for the interaction between the unlike molecules which are necessary for these calculations were not experimentally available. Therefore, it was necessary to estimate them by using the averaging methods described in the Hirschfelder, Bird, and Spotz reference. Force constants for the like molecules used in the averaging were obtained from viscosity data unless otherwise noted.

TABLE II. Comparison of diffusion coefficients determined by the present method with earlier results. $P=1$ atmos.

System	T(°C)	D_{12} (this work)	D_{12} (other work)
H_2-CO_2	20	0.629	0.622[a] 0.639[b] 0.60[c]
N_2-CO_2	20	0.160	0.163[b] 0.16[c]
H_2-CH_4	25	0.726	0.729[d]
$H_2-C_2H_6$	25	0.537	0.535[d]

[a] A. Lonius, Ann. 29, 664 (1909).
[b] L. E. Boardman and N. E. Wild, Proc. Roy. Soc. (London) A162, 511 (1937).
[c] L. Waldman, Naturwissenschaften 32, 223 (1944).
[d] V. Obermayer, Sitzb. Akad. Wiss. Wien, 81, 1102 (1880).

The agreement between the measured values and the calculated values are good, considering the assumptions that the molecular interaction can be described in terms of a Lennard-Jones potential, and that the force constants can be estimated in the above manner. The fact that good agreement is obtained for systems involving ethane or butane must mean that at these temperatures, owing to rotation, these molecules are effectively spherically symmetrical in their interaction with other molecules.

It is also interesting to note the difference in diffusion coefficients for iso-butane and for normal butane into nitrogen as given in Table III, the value for iso-butane being approximately seven percent lower than that for normal butane. As might be expected from structural considerations, this difference may be interpreted as meaning that the collision diameter for iso-butane is slightly larger than that for normal butane.

TABLE III. Comparison of experimental diffusion coefficients and calculated values. $P=1$ atmos. $T=25$°C.

System	D_{12} (Measured)	D_{12} (Calculated)[a]
H_2-CO_2	0.646	0.631
N_2-CO_2	0.165	0.152
H_2-SF_6[b,c]	0.418	0.464
H_2-CH_4	0.726	0.705
$H_2-C_2H_6$	0.537	0.556
$N_2-C_2H_6$	0.148	0.139
$N_2-C_2H_4$	0.163	0.156
$N_2-n\ C_4H_{10}$	0.0960	0.0986
N_2-iso C_4H_{10}	0.0908	0.0961

[a] Hirschfelder, Bird, and Spotz, Chem. Revs. 44, 205 (1949).
[b] Force constants for SF_6 estimated from critical data.
[c] Supplied by the Pennsylvania Salt Manufacturing Company.

VI. SUMMARY

A method is described for the determination of diffusion coefficients in gaseous systems using an interferometric method for obtaining the gas composition at a known position in the cell during the course of the diffusion.

Good agreement is observed between values obtained by the present method and other methods previously used. The present method has the additional advantage that it makes possible several determinations of the diffusion coefficient during the course of a diffusion run.

Good agreement is also observed between values of diffusion coefficients obtained for various systems and those estimated by the methods of Hirschfelder, Bird, and Spotz, by assuming the Lennard-Jones form of the

potential energy and using force constants between unlike molecules taken to be averages of the force constants between like molecules evaluated from viscosity data.

Future work will include a study of the variation of the diffusion coefficient with temperature, which will lead directly to the determination of the force constants for interaction between unlike molecules.

The authors gratefully acknowledge the interest and assistance of Professor Joseph O. Hirschfelder in this work. They would also like to acknowledge the work of Mr. Lloyd E. Lincoln, in the construction of the cell.

THE JOURNAL OF CHEMICAL PHYSICS VOLUME 19, NUMBER 5 MAY, 1951

Tripyramidal Bond Orbitals

GEORGE H. DUFFEY
Chemistry Department, South Dakota State College, Brookings, South Dakota
(Received January 29, 1951)

Three nine-bond arrangements which are not forbidden in *spd* hybridization are described. Of these, the tripyramidal arrangement is discussed in detail since it seems most favorable sterically. In this arrangement there are two types of orbitals, six trigonal prism orbitals and three equatorial orbitals. When the average orbital strength is greatest, it equals 2.983. Some light is thrown on the following structures: TaF_7^{-2}, OsF_8, and conjectural OsF_9^-.

IN being readily hydrolyzed, OsF_8 behaves[1] as a coordinatively unsaturated compound. With alkali fluorides, OsF_8 reacts yielding apparently either OsF_9^- or OsF_{10}^{-2}. Furthermore, in solution thorium acetylacetonate, ThA_4, tends[1] to polymerize. It forms with ammonia the compound $(ThA_4)_2 \cdot NH_3$. Also, $M_6[Th(CO_3)_5]$aq. and $M_6[Ce(CO_3)_5]$aq. may be prepared.[1] Thus, in some complexes of osmium, thorium, and cerium, the central atom seems to have a coordination number greater than eight.

One might rule out the OsF_{10}^{-2}, but not the OsF_9^-, structure for the following reasons. When the central atom has no unshared electrons in the valence shells (as here), its maximum covalence is nine in the usual *spd* hybridization. In osmium complexes, one would not expect arrangements forbidden in *spd* hybridization, since the available *f* orbitals are relatively unstable. Note that in either thorium or cerium, *f* orbitals are readily available and may be used to give a structure with coordination number ten.

It seems of interest to consider likely arrangements for OsF_9^-. At the same time, some light will be thrown on 7-covalent and 8-covalent structures.

Using the method of Van Vleck[2] and Kimball,[3,4] one can show that at least three arrangements of nine bonds about a central atom are allowed in *spd* hybridization. The first arrangement is obtained when an atom is added near the middle of each four-sided face of the TaF_7^{-2} structure[5] in such a way that the C_{2v} symmetry is kept. Since the related polyhedron can be constructed from three pyramids of suitable shapes, the bases of the pyramids forming the sides of a truncated trigonal prism, this arrangement is here named an irregular tripyramidal arrangement. The bond orbitals yield a reducible representation which may be broken down as follows:

$$\sigma = 4A_1 + A_2 + 2B_1 + 2B_2. \quad (1)$$

To get the second arrangement, one may let the first assume the symmetry C_{4v}; or one may spread a square face of the tetragonal antiprism structure and, keeping the C_{4v} symmetry, add the ninth atom above this face. Now

$$\sigma = 3A_1 + B_1 + B_2 + 2E. \quad (2)$$

The third arrangement, described in Table I, is obtained from the first when each pyramid is made rectangular, right, and equivalent. This arrangement is here named the tripyramidal arrangement. It has the symmetry D_{3h} and

$$\sigma = 2A_1' + A_2'' + 2E' + E''. \quad (3)$$

In each arrangement all the irreducible representations needed are available[3] in *spd* hybridization.

TABLE I. Angular coordinates of the maxima in the bond orbitals in the tripyramidal arrangement.

Bond orbital number	ϑ	φ
1	ϑ_1	0°
2	ϑ_1	120°
3	ϑ_1	240°
4	$180°-\vartheta_1$	0°
5	$180°-\vartheta_1$	120°
6	$180°-\vartheta_1$	240°
7	90°	60°
8	90°	180°
9	90°	300°

[1] N. V. Sidgwick, *The Chemical Elements and Their Compounds* (Oxford University Press, London, 1950), Vols. I and II.
[2] J. H. Van Vleck, J. Chem. Phys. **3**, 803 (1935).
[3] G. E. Kimball, J. Chem. Phys. **8**, 188 (1940).
[4] Eyring, Walter, and Kimball, *Quantum Chemistry* (John Wiley and Sons, Inc., New York, 1944).
[5] J. L. Hoard, J. Am. Chem. Soc. **61**, 1252 (1939).

TABLE II. Properties of some tripyramidal bond orbitals.

Function maximized	m[a]	n[a]	S_1[b]	ϑ_1[c]	S_7[d]
$6S_1+3S_7$	0.5846	0.6583	2.984	44°36′	2.982
$6S_1+2S_7$	0.5897	0.6846	2.985	44°54′	2.978
$6S_1+S_7$	0.5959	0.7310	2.987	45°29′	2.971
S_1	0.5972	0.8464	2.989	47°16′	2.940

[a] The trigonal prism orbitals have the over-all composition $s^n p^{1+2m} d^{5-n-2m}$.
[b] Maximum value of a trigonal prism orbital.
[c] Acute angle between the z axis and the maximum in a trigonal prism orbital. See Table I.
[d] Maximum value of an equatorial orbital.

From a steric standpoint the tripyramidal arrangement seems to be favorable.[6] It has two groups of bonds: the six bonds leading to the basal corners of the pyramids and the three bonds leading to the vertexes. The former may be called trigonal prism bonds, the latter equatorial bonds. The trigonal prism bonds may be formed from the bond orbitals $\psi_1, \cdots \psi_6$, described in an earlier[7] discussion. The equatorial bonds may be formed from the following bond orbitals, which are combinations of ψ_7, ψ_8, and ψ_9 of the earlier[7] discussion:

$$\phi_7=(1/\sqrt{3})\psi_7+[1/(6)^{\frac{1}{2}}]\psi_8+(1/\sqrt{2})\psi_9, \quad (4)$$

$$\phi_8=(1/\sqrt{3})\psi_7-(\sqrt{2}/\sqrt{3})\psi_8, \quad (5)$$

$$\phi_9=(1/\sqrt{3})\psi_7+[1/(6)^{\frac{1}{2}}]\psi_8-(1/\sqrt{2})\psi_9. \quad (6)$$

Now S_1 is the maximum value of ψ_1, and S_7 is the maximum value of ϕ_7. The angle ϑ_1 is the acute angle between the z axis and the maximum in a trigonal prism orbital (approximately the angle between the z axis and a trigonal prism bond). The over-all composition of the trigonal prism orbitals is $s^n p^{1+2m} d^{5-n-2m}$; the over-all composition of the equatorial orbitals $s^{1-n} p^{2-2m} d^{n+2m}$.

As a rough indication of bond energy, the author uses Pauling's index in the form of Eq. (13) of "Hexacovalent bond orbitals III."[8] Assume the sum of the R's (the ionic resonance energy) over all bonds is not changed appreciably when the parameters α and β are changed. Likewise, assume the sum of the W's (the energy required to excite the valence electrons to give the molecular valence state of the central atom) over all bonds is constant. The first assumption seems reasonable when the attached atoms are all alike. The second assumption seems reasonable for molecules or ions of type AB_9 where the bond orbitals of A have constant over-all composition (here sp^3d^5). In types AB_8 and AB_7 the bond orbitals of A do not have a fixed over-all composition, and one would not expect the sum of the W's to be constant as the parameters vary, except when the s, p, and d orbitals are of equal stability.

Thus, in molecules or ions of type AB_9 the values of the parameters giving the largest sum of the bond energies are found by maximizing $6S_1+3S_7$. The results are given in the first row of Table II.

The tripyramidal structure for OsF_9^- uses one $6s$, three $6p$, and five $5d$ orbitals of the osmium atom, the nine orbitals most readily available for hybridization. No unshared electrons would have to be promoted. The structure seems favorable enough stericly. The average strength (average maximum value) of the best tripyramidal orbitals equals 2.983 (nearly as great as the maximum for an spd orbital, 3.000). Hence, if OsF_9^- exists, it may have the tripyramidal arrangement.

Molecules or ions of types AB_8 and AB_7 can have incomplete irregular tripyramidal arrangements. Calculations on these arrangements would be long drawn-out. However, these structures may not be far from (regular) tripyramidal structures where one and two equatorial bonds, respectively, are missing. On the latter structures the calculations are carried out with the assumptions noted before. The results for AB_8 are given in the second row of Table II; those for AB_7 in the third row. The over-all compositions of the bond orbitals are $s^{0.895}p^{2.726}d^{4.379}$ and $s^{0.821}p^{2.461}d^{3.718}$, respectively.

If OsF_9^- has the tripyramidal arrangement, OsF_8 probably has either the tetragonal antiprism[9] arrangement or the incomplete irregular tripyramidal arrangement. Either structure could readily add a fluoride ion to give the tripyramidal arrangement. The dodecahedral[10] arrangement of OsF_8 could probably pick up an ion less readily, inasmuch as in the unperturbed state this arrangement must have a highly scattered unoccupied ninth orbital (ψ_9).

One might expect OsF_8 and TaF_8^{-3} to have the same structure, both molecules being isoelectronic. In both osmium and tantalum the $6p$ orbitals are more unstable than the $6s$ or $5d$ orbitals, and here there are no unshared electrons in the valence shells. Strong incomplete (AB_8) tripyramidal bond orbitals can be set up containing less than three p orbitals. See the second row of Table II. Three p orbitals are needed in the tetragonal antiprism arrangement. Hence, one might expect that OsF_8 and TaF_8^{-3} would have the incomplete irregular tripyramidal arrangement. However, the antiprism arrangement has been reported for TaF_8^{-3}.[11]

For TaF_7^{-2} and NbF_7^{-2} strong incomplete tripyramidal bond orbitals can be set up containing less of the unstable p orbitals than the pentagonal bipyramidal[12] orbitals contain. See the third row of Table II. It is not surprising that these ions have[5] incomplete irregular tripyramidal structures.

[6] L. Pauling, *The Nature of the Chemical Bond* (Cornell University Press, Ithaca, New York, 1940), p. 382.
[7] G. H. Duffey, J. Chem. Phys. **17**, 1328 (1949).
[8] G. H. Duffey, J. Chem. Phys. **18**, 510 (1950).
[9] G. H. Duffey, J. Chem. Phys. **18**, 746 (1950).
[10] G. H. Duffey, J. Chem. Phys. **18**, 1444 (1950).
[11] See reference 5b (Hoard) of Marchi, Fernelius, and McReynolds, J. Am. Chem. Soc. **65**, 329 (1943).
[12] G. H. Duffey, J. Chem. Phys. **18**, 943 (1950).

Solutions of the Fermi-Thomas-Dirac Equation

N. METROPOLIS AND J. R. REITZ
Los Alamos Scientific Laboratory, Los Alamos, New Mexico

(Received February 12, 1951)

Solutions of the Fermi-Thomas-Dirac equation are given for 24 different elements. Both neutral atom and positive ion solutions are given. These results were obtained by evaluating the series expansion for the FTD function at small distances from the origin and by numerical integration of the differential equation at larger distances. The numerical solutions were done on the ENIAC.

I. INTRODUCTION

SOLUTIONS of the Fermi-Thomas-Dirac (abbreviated FTD) equation have been given by a number of investigators for several different elements.[1] However, only a few elements have been treated thus far, and in some of these instances more solutions might be desired. Recently, one of the authors[2] has computed wave functions of electrons in various atomic fields. As a starting point for these calculations, the potential field of each atom was needed; this was obtained from the FTD model of the atom.

The FTD equation was solved numerically for each case on the ENIAC, the electronic computer at Aberdeen Proving Ground, Maryland. Since the computational routine was quite simple, the procedure was repeated approximately every fourth Z value throughout the periodic table, and solutions corresponding to about seven different atomic radii were obtained for each element. The purpose of the present paper is to make these solutions readily available for use in physical, chemical, and astrophysical problems.

II. DISCUSSION

The FTD equation

$$d^2\psi/dx^2=x(\epsilon+\psi^{\frac{1}{2}}/x^{\frac{1}{2}})^3 \tag{1}$$

with $\epsilon=(3/32\pi^2)^{\frac{1}{3}}Z^{-\frac{1}{3}}=0.211783Z^{-\frac{1}{3}}$ results from Poisson's equation for the electrostatic potential when the following substitutions are made:

$$\begin{aligned} eV_0&=E_0+2me^4/h^2-Ze^2\psi/\mu x,\\ r\ (\text{the radial coordinate})&=\mu x, \end{aligned} \tag{2}$$

with $\mu=a_0(9\pi^2/128Z)^{\frac{1}{3}}=0.88534a_0Z^{-\frac{1}{3}}$, $E_0=$maximum Fermi energy in the atom, $a_0=$Bohr radius. Of course, the charge density in Poisson's equation is first expressed statistically as a function of potential V_0.

The procedure and notation used here are the same as those of Feynman, Metropolis, and Teller.[1] Initial values of ψ can be obtained from the series expansion about the origin,

$$\psi=1+a_2x+a_3x^{\frac{3}{2}}+a_4x^2+\cdots, \tag{3}$$

the coefficients of which have been given to a_9.[3]

As before, the more convenient independent variable w was introduced, where w is defined by $x=w^2/2$. The ENIAC procedure consisted of evaluating the expansion at intervals of $\Delta w=0.04$ up to $w=0.48$, at which point direct numerical integration of the differential equation was automatically begun. In practice, a choice of a_2 (the initial slope) is made by setting a group of manual switches; the ENIAC then computes the coefficients $a_3, a_4, \cdots a_8$. This procedure is adequate for five-decimal digit accuracy.

For each element, several different initial slopes were chosen, and the equation was integrated until the boundary condition was satisfied. Neutral atom solutions correspond to the condition that the electric field vanishes at the boundary, or from Eq. (2),

$$(d\psi/dx)_{x=x_0}=(\psi/x)_{x=x_0}. \tag{4}$$

This condition is met at a different atomic radius, x_0, for each different initial slope, and thus we obtain solutions corresponding to atoms of various sizes.

If the initial slope is chosen too steep, the function ψ will become zero before Eq. (4) is satisfied. But the charge density ρ is proportional to $(\epsilon+\psi^{\frac{1}{2}}/x^{\frac{1}{2}})^3$, and thus ψ cannot go negative or ρ will become complex. The solution must be cut off at x_i, the radius at which $\psi=0$, and this value x_i is the ionic radius. These solutions represent positive ions. It should be noted that in the FTD model, in contrast to the Fermi-Thomas model, the electron density jumps discontinuously from

[1] Feynman, Metropolis, and Teller, Phys. Rev. **75**, 1561 (1949); J. C. Slater and H. M. Krutter, Phys. Rev. **47**, 559 (1935); H. Jensen, Z. Physik **111**, 373 (1938); K. Umeda, J. Faculty Sci., Hokkaido Imp. Univ., Series III **5**, 171 (1942). Jensen's solutions for the noble gases have also been given by P. Gombás, *Die Statistische Theorie des Atoms und Ihre Anwendungen* (Springer-Verlag, Wien, 1949).

[2] J. R. Reitz, Phys. Rev. **77**, 10 (1950).

[3] See reference 1, Table IV. N. March (private communication) has pointed out that the last coefficient a_9, as given by Feynman, Metropolis, and Teller (reference 1, Table IV) is incorrect. His value, which has been verified by us, is

$$a_9=\frac{14}{45}\epsilon^3-\frac{1}{42}a_2^2\epsilon^2+\frac{41}{210}a_2\epsilon-\frac{1}{252}a_2^3+\frac{2}{27}.$$

In addition, he has computed

$$a_{10}=\frac{17}{200}\epsilon^4+\frac{137}{1400}a_2\epsilon^2+\frac{5}{28}\epsilon+\frac{1}{175}a_2^2;$$

and we have further derived

$$a_{11}=\frac{\epsilon^5}{99}+\frac{37}{3465}\epsilon^3a_2+\frac{15397}{83160}\epsilon^2+\frac{1}{132}a_2^3\epsilon^2+\frac{83}{9240}a_2^2\epsilon+\frac{31}{1485}a_2+\frac{1}{1056}a_2^4.$$

TABLE I. Solutions of the Fermi-Thomas-Dirac equation ($Z=6$).

w	Case 1 2ψ	Case 2 2ψ	Case 3 2ψ	Case 4 2ψ	Case 5 2ψ	Case 6 2ψ
0.08	1.98969	1.98969	1.98969	1.98969	1.98969	1.98970
0.16	1.96070	1.96070	1.96070	1.96072	1.96073	1.96074
0.24	1.91588	1.91589	1.91590	1.91593	1.91596	1.91599
0.32	1.85800	1.85802	1.85803	1.85808	1.85814	1.85819
0.40	1.78965	1.78968	1.78969	1.78977	1.78986	1.78994
0.48	1.71320	1.71325	1.71327	1.71339	1.71351	1.71362
0.56	1.63084	1.63090	1.63093	1.63109	1.63125	1.63141
0.64	1.54447	1.54456	1.54460	1.54481	1.54502	1.54524
0.72	1.45579	1.45590	1.45595	1.45622	1.45650	1.45677
0.80	1.36622	1.36636	1.36642	1.36677	1.36711	1.36745
0.88	1.27698	1.27715	1.27723	1.27766	1.27808	1.27850
0.96	1.18906	1.18927	1.18938	1.18989	1.19041	1.19093
1.04	1.10328	1.10353	1.10366	1.10428	1.10491	1.10553
1.12	1.02027	1.02057	1.02072	1.02147	1.02222	1.02297
1.20	0.94051	0.94087	0.94105	0.94194	0.94283	0.94372
1.28	0.86435	0.86477	0.86499	0.86604	0.86709	0.86815
1.36	0.79202	0.79252	0.79277	0.79401	0.79526	0.79651
1.44	0.72367	0.72426	0.72455	0.72601	0.72748	0.72895
1.52	0.65936	0.66004	0.66040	0.66211	0.66383	0.66555
1.60	0.59908	0.59989	0.60030	0.60230	0.60432	0.60633
1.68	0.54279	0.54373	0.54421	0.54655	0.54891	0.55127
1.76	0.49038	0.49147	0.49204	0.49477	0.49752	0.50028
1.84	0.44173	0.44300	0.44366	0.44685	0.45006	0.45328
1.92	0.39668	0.39817	0.39894	0.40266	0.40640	0.41015
2.00	0.35509	0.35681	0.35771	0.36204	0.36640	0.37078
2.08	0.31674	0.31876	0.31980	0.32485	0.32993	0.33503
2.16	0.28147	0.28383	0.28504	0.29092	0.29684	0.30278
2.24	0.24909	0.25184	0.25324	0.26010	0.26700	0.27392
2.32	0.21942	0.22261	0.22425	0.23224	0.24028	0.24835
2.40	0.19225	0.19597	0.19788	0.20719	0.21656	0.22597
2.48	0.16741	0.17175	0.17397	0.18483	0.19575	0.20673
2.56	0.14472	0.14977	0.15237	0.16503	0.17778	0.19059
2.64	0.12400	0.12989	0.13292	0.14769	0.16257	0.17755
2.72	0.10507	0.11194	0.11548	0.13273	0.15013	0.16765
2.80	0.08777	0.09580	0.09992	0.12008	0.14044	0.16097
2.88	0.07193	0.08131	0.08613	0.10973	0.13358	0.15766
2.96	0.05738	0.06835	0.07400	0.10164	0.12964	0.15794
3.04	0.04394	0.05680	0.06343	0.09587	0.12879	0.16213
3.12	0.03146	0.04655	0.05433	0.09248	0.13127	0.17065
3.20	0.01974	0.03749	0.04665	0.09160	0.13743	
3.28	0.00858	0.02952	0.04032	0.09342		
3.36	−0.00226	0.02253	0.03531	0.09820		
3.44	−0.01311	0.01645	0.03161			
3.52		0.01116	0.02924			
3.60		0.00658	0.02824			
3.68		0.00261	0.02869			
3.76		−0.00088				
3.84		−0.00409				

$Z=6$	$-a_2$	w_0	w_i	Z_i
Case 1	1.6863		3.3432	0.6766
Case 2	1.6861		3.7392	0.2382
Case 3	1.6860	3.6806		
Case 4	1.6855	3.3149		
Case 5	1.6850	3.1736		
Case 6	1.6845	3.0819		

TABLE II. Solutions of the FTD equation ($Z=10$).

w	Case 1 2ψ	Case 2 2ψ	Case 3 2ψ	Case 4 2ψ	Case 5 2ψ	Case 6 2ψ
0.08	1.98985	1.98987	1.98987	1.98987	1.98987	1.98987
0.16	1.96136	1.96141	1.96141	1.96142	1.96143	1.96144
0.24	1.91735	1.91747	1.91748	1.91750	1.91752	1.91753
0.32	1.86056	1.86077	1.86078	1.86082	1.86085	1.86087
0.40	1.79354	1.79387	1.78202	1.79395	1.79399	1.79403
0.48	1.71864	1.71911	1.71913	1.71922	1.71929	1.71934
0.56	1.63797	1.63861	1.63865	1.63877	1.63887	1.63894
0.64	1.55342	1.55427	1.55431	1.55448	1.55461	1.55469
0.72	1.46661	1.46770	1.46776	1.46797	1.46814	1.46825

TABLE II.—*Continued.*

w	Case 1 2ψ	Case 2 2ψ	Case 3 2ψ	Case 4 2ψ	Case 5 2ψ	Case 6 2ψ
0.80	1.37894	1.38031	1.38038	1.38065	1.38086	1.38099
0.88	1.29157	1.29326	1.29335	1.29369	1.29394	1.29411
0.96	1.20547	1.20753	1.20763	1.20805	1.20836	1.20856
1.04	1.12139	1.12389	1.12401	1.12451	1.12488	1.12513
1.12	1.03995	1.04294	1.04309	1.04368	1.04413	1.04443
1.20	0.96159	0.96514	0.96532	0.96603	0.96656	0.96692
1.28	0.88663	0.89084	0.89105	0.89189	0.89252	0.89294
1.36	0.81529	0.82024	0.82049	0.82148	0.82222	0.82271
1.44	0.74766	0.75348	0.75377	0.75494	0.75581	0.75639
1.52	0.68381	0.69062	0.69096	0.69233	0.69335	0.69403
1.60	0.62369	0.63165	0.63205	0.63365	0.63484	0.63563
1.68	0.56723	0.57652	0.57699	0.57884	0.58024	0.58117
1.76	0.51431	0.52513	0.52567	0.52784	0.52946	0.53054
1.84	0.46476	0.47736	0.47799	0.48051	0.48240	0.48366
1.92	0.41842	0.43307	0.43380	0.43673	0.43892	0.44039
2.00	0.37508	0.39209	0.39294	0.39635	0.39890	0.40060
2.08	0.33453	0.35427	0.35526	0.35921	0.36217	0.36415
2.16	0.29652	0.31942	0.32057	0.32516	0.32859	0.33089
2.24	0.26083	0.28737	0.28871	0.29403	0.29802	0.30069
2.32	0.22719	0.25796	0.25951	0.26569	0.27031	0.27340
2.40	0.19537	0.23101	0.23281	0.23997	0.24533	0.24892
2.48	0.16509	0.20636	0.20844	0.21674	0.22296	0.22712
2.56	0.13607	0.18385	0.18626	0.19588	0.20309	0.20792
2.64	0.10805	0.16332	0.16612	0.17728	0.18564	0.19124
2.72	0.08071	0.14465	0.14789	0.16082	0.17052	0.17703
2.80	0.05376	0.12768	0.13143	0.14643	0.15769	0.16525
2.88	0.02688	0.11230	0.11665	0.13405	0.14712	0.15590
2.96	−0.00027	0.09838	0.10343	0.12362	0.13881	0.14902
3.04	−0.02807	0.08582	0.09167	0.11512	0.13278	0.14466
3.12		0.07451	0.08130	0.10855	0.12910	0.14295
3.20		0.06435	0.07224	0.10393	0.12789	0.14405
3.28		0.05526	0.06443	0.10133	0.12930	0.14820
3.36		0.04716	0.05782	0.10085	0.13355	0.15570
3.44		0.03997	0.05239	0.10263		
3.52		0.03363	0.04811	0.10688		
3.60		0.02807	0.04498			
3.68		0.02323	0.04302			
3.76		0.01907	0.04228			
3.84		0.01554	0.04284			
3.92		0.01261	0.04479			
4.00		0.01025				
4.08		0.00843				
4.16		0.00714				
4.24		0.00638				
4.32		0.00617				
4.40		0.00654				

$Z=10$	$-a_2$	w_0	w_i	Z_i
Case 1	1.6600		2.9592	2.535
Case 2	1.6580	4.3413		
Case 3	1.6579	3.8713		
Case 4	1.6575	3.4979		
Case 5	1.6572	3.3755		
Case 6	1.6570	3.3153		

TABLE III. Solutions of the FTD equation ($Z=14$).

w	Case 1 2ψ	Case 2 2ψ	Case 3 2ψ	Case 4 2ψ	Case 5 2ψ	Case 6 2ψ
0.08	1.98995	1.98996	1.98996	1.98997	1.98998	1.98998
0.16	1.96174	1.96177	1.96179	1.96182	1.96184	1.96187
0.24	1.91820	1.91826	1.91830	1.91837	1.91843	1.91849
0.32	1.86204	1.86214	1.86222	1.86234	1.86245	1.86255
0.40	1.79579	1.79595	1.79608	1.79628	1.79644	1.79660
0.48	1.72179	1.72203	1.72221	1.72250	1.72273	1.72296
0.56	1.64214	1.64246	1.64272	1.64311	1.64343	1.64375
0.64	1.55869	1.55912	1.55946	1.55997	1.56039	1.56082
0.72	1.47306	1.47360	1.47404	1.47469	1.47524	1.47578
0.80	1.38660	1.38729	1.38784	1.38866	1.38934	1.39003
0.88	1.30049	1.30133	1.30201	1.30303	1.30387	1.30472
0.96	1.21565	1.21669	1.21751	1.21875	1.21978	1.22081

TABLE III.—*Continued.*

w	Case 1 2ψ	Case 2 2ψ	Case 3 2ψ	Case 4 2ψ	Case 5 2ψ	Case 6 2ψ
1.04	1.13286	1.13410	1.13510	1.13659	1.13784	1.13908
1.12	1.05269	1.05418	1.05537	1.05716	1.05865	1.06014
1.20	0.97560	0.97737	0.97879	0.98091	0.98269	0.98446
1.28	0.90189	0.90399	0.90567	0.90818	0.91028	0.91238
1.36	0.83179	0.83426	0.83624	0.83920	0.84167	0.84414
1.44	0.76540	0.76830	0.77062	0.77410	0.77700	0.77990
1.52	0.70278	0.70617	0.70889	0.71296	0.71636	0.71975
1.60	0.64390	0.64786	0.65103	0.65579	0.65976	0.66372
1.68	0.58869	0.59331	0.59701	0.60256	0.60718	0.61181
1.76	0.53706	0.54244	0.54674	0.55319	0.55858	0.56396
1.84	0.48885	0.49510	0.50010	0.50761	0.51387	0.52013
1.92	0.44392	0.45118	0.45699	0.46571	0.47298	0.48026
2.00	0.40209	0.41051	0.41724	0.42736	0.43580	0.44425
2.08	0.36316	0.37292	0.38073	0.39247	0.40226	0.41207
2.16	0.32694	0.33825	0.34730	0.36090	0.37226	0.38363
2.24	0.29324	0.30633	0.31681	0.33257	0.34573	0.35892
2.32	0.26185	0.27699	0.28912	0.30737	0.32263	0.33792
2.40	0.23256	0.25007	0.26410	0.28523	0.30291	0.32064
2.48	0.20516	0.22540	0.24163	0.26610	0.28658	0.30715
2.56	0.17946	0.20283	0.22161	0.24993	0.27367	0.29753
2.64	0.15523	0.18223	0.20394	0.23673	0.26425	0.29195
2.72	0.13229	0.16345	0.18854	0.22652	0.25844	0.29064
2.80	0.11041	0.14636	0.17537	0.21936	0.25643	0.29387
2.88	0.08939	0.13085	0.16439	0.21538	0.25846	0.30207
2.96	0.06901	0.11680	0.15558	0.21473	0.26486	0.31575
3.04	0.04905	0.10412	0.14898	0.21765	0.27608	
3.12	0.02929	0.09270	0.14461	0.22445		
3.20	0.00947	0.08247	0.14257	0.23553		
3.28	−0.01064	0.07335	0.14299			
3.36	−0.03122	0.06526	0.14604			
3.44		0.05816	0.15197			
3.52		0.05198				
3.60		0.04670				
3.68		0.04228				
3.76		0.03869				
3.84		0.03593				
3.92		0.03400				
4.00		0.03293				
4.08		0.03273				
4.16		0.03349				

$Z=14$	$-a_2$	w_0	w_i	Z_i
Case 1	1.6450		3.2379	2.846
Case 2	1.6440	4.1630		
Case 3	1.6432	3.4290		
Case 4	1.6420	3.1702		
Case 5	1.6410	3.0513		
Case 6	1.6400	2.9658		

TABLE IV. Solutions of the FTD equation ($Z=16$).

w	Case 1 2ψ	Case 2 2ψ	Case 3 2ψ
0.08	1.98999	1.98999	1.98999
0.16	1.96188	1.96189	1.96190
0.24	1.91851	1.91854	1.91856
0.32	1.86259	1.86263	1.86268
0.40	1.79664	1.79670	1.79678
0.48	1.72298	1.72308	1.72320
0.56	1.64372	1.64385	1.64401
0.64	1.56070	1.56087	1.56108
0.72	1.47552	1.47574	1.47601
0.80	1.38956	1.38983	1.39017
0.88	1.30395	1.30429	1.30471
0.96	1.21964	1.22006	1.22057
1.04	1.13739	1.13789	1.13851
1.12	1.05779	1.05838	1.05913
1.20	0.98127	0.98198	0.98286
1.28	0.90816	0.90900	0.91005
1.36	0.83867	0.83966	0.84089
1.44	0.77293	0.77409	0.77554
1.52	0.71098	0.71234	0.71403
1.60	0.65281	0.65440	0.65637
1.68	0.59837	0.60022	0.60252

TABLE IV.—*Continued.*

w	Case 1 2ψ	Case 2 2ψ	Case 3 2ψ
1.76	0.54756	0.54971	0.55239
1.84	0.50026	0.50275	0.50587
1.92	0.45632	0.45922	0.46284
2.00	0.41558	0.41895	0.42314
2.08	0.37789	0.38179	0.38665
2.16	0.34306	0.34758	0.35321
2.24	0.31093	0.31615	0.32267
2.32	0.28132	0.28736	0.29490
2.40	0.25406	0.26105	0.26976
2.48	0.22900	0.23707	0.24714
2.56	0.20596	0.21528	0.22693
2.64	0.18480	0.19557	0.20902
2.72	0.16538	0.17780	0.19334
2.80	0.14755	0.16189	0.17984
2.88	0.13119	0.14773	0.16846
2.96	0.11616	0.13524	0.15919
3.04	0.10236	0.12436	0.15204
3.12	0.08966	0.11504	0.14704
3.20	0.07796	0.10724	0.14425
3.28	0.06715	0.10094	0.14378
3.36	0.05715	0.09614	0.14579
3.44	0.04784	0.09286	0.15046
3.52	0.03915	0.09116	0.15808
3.60	0.03096	0.09109	
3.68	0.02320	0.09278	
3.76	0.01576	0.09636	
3.84	0.00855		
3.92	0.00145		
4.00	−0.00566		

$Z=16$	$-a_2$	w_0	w_i	Z_i
Case 1	1.6394		3.9364	1.396
Case 2	1.6390	3.7400		
Case 3	1.6385	3.4649		

TABLE V. Solutions of the FTD equation ($Z=18$).

w	Case 1 2ψ	Case 2 2ψ	Case 3 2ψ	Case 4 2ψ	Case 5 2ψ
0.08	1.99001	1.99001	1.99001	1.99001	1.99002
0.16	1.96197	1.96198	1.96199	1.96199	1.96202
0.24	1.91870	1.91873	1.91875	1.91876	1.91882
0.32	1.86292	1.86297	1.86300	1.86302	1.86312
0.40	1.79714	1.79722	1.79727	1.79730	1.79746
0.48	1.72368	1.72380	1.72387	1.72392	1.72415
0.56	1.64464	1.64480	1.64489	1.64496	1.64528
0.64	1.56184	1.56206	1.56218	1.56227	1.56269
0.72	1.47690	1.47717	1.47734	1.47745	1.47799
0.80	1.39117	1.39151	1.39172	1.39186	1.39254
0.88	1.30579	1.30622	1.30647	1.30664	1.30748
0.96	1.22170	1.22222	1.22253	1.22273	1.22377
1.04	1.13965	1.14027	1.14064	1.14089	1.14214
1.12	1.06022	1.06096	1.06141	1.06171	1.06320
1.20	0.98385	0.98473	0.98526	0.98562	0.98739
1.28	0.91085	0.91190	0.91253	0.91295	0.91504
1.36	0.84144	0.84267	0.84341	0.84391	0.84637
1.44	0.77573	0.77718	0.77804	0.77862	0.78152
1.52	0.71376	0.71546	0.71647	0.71715	0.72054
1.60	0.65553	0.65751	0.65869	0.65948	0.66343
1.68	0.60096	0.60326	0.60464	0.60557	0.61017
1.76	0.54996	0.55264	0.55424	0.55532	0.56067
1.84	0.50239	0.50551	0.50737	0.50862	0.51484
1.92	0.45812	0.46173	0.46388	0.46534	0.47256
2.00	0.41696	0.42114	0.42364	0.42533	0.43370
2.08	0.37874	0.38359	0.38648	0.38844	0.39814
2.16	0.34329	0.34890	0.35225	0.35451	0.36574
2.24	0.31041	0.31689	0.32077	0.32338	0.33638
2.32	0.27992	0.28741	0.29189	0.29491	0.30994
2.40	0.25163	0.26029	0.26547	0.26896	0.28633
2.48	0.22537	0.23536	0.24134	0.24537	0.26544
2.56	0.20095	0.21247	0.21937	0.22403	0.24721
2.64	0.17819	0.19148	0.19944	0.20481	0.23159
2.72	0.15692	0.17224	0.18142	0.18761	0.21855
2.80	0.13697	0.15462	0.16520	0.17235	0.20808

TABLE V.—*Continued.*

w	Case 1 2ψ	Case 2 2ψ	Case 3 2ψ	Case 4 2ψ	Case 5 2ψ
2.88	0.11818	0.13849	0.15069	0.15893	0.20021
2.96	0.10036	0.12374	0.13780	0.14731	0.19500
3.04	0.08337	0.11026	0.12646	0.13742	0.19256
3.12	0.06702	0.09793	0.11660	0.12925	0.19304
3.20	0.05116	0.08668	0.10819	0.12279	0.19663
3.28	0.03561	0.07640	0.10118	0.11803	0.20363
3.36	0.02019	0.06701	0.09557	0.11503	0.21438
3.44	0.00472	0.05843	0.09136	0.11385	
3.52	−0.01098	0.05059	0.08856	0.11459	
3.60	−0.02703	0.04341	0.08723	0.11738	
3.68		0.03683	0.08743	0.12242	
3.76		0.03079	0.08927		
3.84		0.02521	0.09289		
3.92		0.02005			
4.00		0.01524			
4.08		0.01072			
4.16		0.00643			
4.24		0.00230			
4.32		−0.00175			
4.40		−0.00581			

$Z=18$	$-a_2$	w_0	w_i	Z_i
Case 1	1.6360		3.4642	3.047
Case 2	1.6355		4.2855	0.9757
Case 3	1.6352	3.8094		
Case 4	1.6350	3.6481		
Case 5	1.6340	3.3045		

TABLE VI. Solutions of the FTD equation ($Z=22$).

w	Case 1 2ψ	Case 2 2ψ	Case 3 2ψ	Case 4 2ψ	Case 5 2ψ
0.08	1.99005	1.99005	1.99005	1.99005	1.99006
0.16	1.96212	1.96213	1.96213	1.96214	1.96217
0.24	1.91904	1.91906	1.91907	1.91910	1.91916
0.32	1.86351	1.86354	1.86356	1.86361	1.86371
0.40	1.79804	1.79808	1.79812	1.79820	1.79836
0.48	1.72494	1.72501	1.72506	1.72517	1.72541
0.56	1.64629	1.64639	1.64645	1.64661	1.64694
0.64	1.56393	1.56406	1.56414	1.56436	1.56478
0.72	1.47944	1.47961	1.47972	1.47999	1.48053
0.80	1.39419	1.39439	1.39453	1.39487	1.39555
0.88	1.30929	1.30954	1.30971	1.31013	1.31098
0.96	1.22567	1.22598	1.22619	1.22671	1.22774
1.04	1.14409	1.14447	1.14471	1.14534	1.14658
1.12	1.06512	1.06557	1.06587	1.06662	1.06810
1.20	0.98920	0.98973	0.99009	0.99097	0.99274
1.28	0.91664	0.91727	0.91768	0.91873	0.92082
1.36	0.84763	0.84837	0.84886	0.85010	0.85256
1.44	0.78231	0.78318	0.78375	0.78521	0.78809
1.52	0.72071	0.72173	0.72240	0.72410	0.72747
1.60	0.66282	0.66401	0.66479	0.66677	0.67071
1.68	0.60858	0.60996	0.61087	0.61318	0.61776
1.76	0.55788	0.55948	0.56054	0.56323	0.56856
1.84	0.51060	0.51246	0.51369	0.51681	0.52300
1.92	0.46659	0.46875	0.47018	0.47379	0.48097
2.00	0.42569	0.42819	0.42984	0.43403	0.44234
2.08	0.38772	0.39061	0.39253	0.39737	0.40700
2.16	0.35251	0.35586	0.35807	0.36367	0.37481
2.24	0.31987	0.32374	0.32630	0.33277	0.34565
2.32	0.28963	0.29410	0.29705	0.30453	0.31941
2.40	0.26160	0.26676	0.27017	0.27880	0.29599
2.48	0.23561	0.24156	0.24549	0.25545	0.27530
2.56	0.21149	0.21834	0.22288	0.23437	0.25727
2.64	0.18907	0.19696	0.20219	0.21543	0.24185
2.72	0.16818	0.17726	0.18328	0.19854	0.22903
2.80	0.14866	0.15911	0.16604	0.18362	0.21879
2.88	0.13036	0.14238	0.15035	0.17059	0.21118
2.96	0.11313	0.12694	0.13610	0.15941	0.20624
3.04	0.09681	0.11267	0.12320	0.15003	0.20411
3.12	0.08125	0.09945	0.11156	0.14245	0.20491
3.20	0.06630	0.08718	0.10109	0.13665	0.20887

TABLE VI.—*Continued.*

w	Case 1 2ψ	Case 2 2ψ	Case 3 2ψ	Case 4 2ψ	Case 5 2ψ
3.28	0.05182	0.07575	0.09173	0.13268	0.21626
3.36	0.03765	0.06507	0.08341	0.13058	0.22744
3.44	0.02365	0.05502	0.07608	0.13045	
3.52	0.00964	0.04553	0.06970	0.13240	
3.60	−0.00451	0.03648	0.06422	0.13659	
3.68	−0.01895	0.02778	0.05963	0.14325	
3.76		0.01934	0.05589		
3.84		0.01106	0.05302		
3.92		0.00283	0.05101		
4.00		−0.00546	0.04988		
4.08		−0.01389	0.04967		
4.16			0.05044		
4.24			0.05224		

$Z=22$	$-a_2$	w_0	w_i	Z_i
Case 1	1.6300		3.5746	3.490
Case 2	1.6297		3.9475	2.245
Case 3	1.6295	4.2112		
Case 4	1.6290	3.6226		
Case 5	1.6280	3.3088		

TABLE VII. Solutions of the FTD equation ($Z=26$).

w	Case 1 2ψ	Case 2 2ψ	Case 3 2ψ	Case 4 2ψ	Case 5 2ψ
0.08	1.99007	1.99007	1.99008	1.99011	1.99012
0.16	1.96222	1.96223	1.96225	1.96237	1.96240
0.24	1.91926	1.91929	1.91932	1.91961	1.91967
0.32	1.86389	1.86395	1.86400	1.86451	1.86461
0.40	1.79863	1.79871	1.79879	1.79960	1.79976
0.48	1.72577	1.72588	1.72600	1.72717	1.72740
0.56	1.64738	1.64754	1.64770	1.64931	1.64963
0.64	1.56529	1.56550	1.56572	1.56784	1.56826
0.72	1.48109	1.48136	1.48164	1.48436	1.48490
0.80	1.39612	1.39646	1.39680	1.40023	1.40091
0.88	1.31151	1.31193	1.31235	1.31658	1.31742
0.96	1.22817	1.22868	1.22920	1.23435	1.23538
1.04	1.14685	1.14747	1.14809	1.15431	1.15555
1.12	1.06812	1.06886	1.06961	1.07705	1.07853
1.20	0.99241	0.99329	0.99418	1.00302	1.00479
1.28	0.92003	0.92107	0.92212	0.93257	0.93466
1.36	0.85118	0.85240	0.85363	0.86594	0.86840
1.44	0.78596	0.78740	0.78885	0.80328	0.80617
1.52	0.72443	0.72612	0.72780	0.74468	0.74806
1.60	0.66656	0.66853	0.67049	0.69019	0.69413
1.68	0.61228	0.61457	0.61686	0.63980	0.64439
1.76	0.56150	0.56416	0.56682	0.59349	0.59882
1.84	0.51407	0.51716	0.52025	0.55121	0.55741
1.92	0.46985	0.47343	0.47701	0.51292	0.52011
2.00	0.42866	0.43281	0.43696	0.47857	0.48690
2.08	0.39033	0.39513	0.39993	0.44810	0.45776
2.16	0.35467	0.36021	0.36577	0.42150	0.43269
2.24	0.32150	0.32789	0.33431	0.39876	0.41171
2.32	0.29061	0.29799	0.30539	0.37989	0.39489
2.40	0.26182	0.27033	0.27887	0.36495	0.38232
2.48	0.23495	0.24475	0.25459	0.35405	0.37415
2.56	0.20980	0.22109	0.23242	0.34731	0.37061
2.64	0.18619	0.19918	0.21222	0.34497	0.37198
2.72	0.16394	0.17887	0.19388	0.34728	0.37864
2.80	0.14286	0.16001	0.17728	0.35464	0.39109
2.88	0.12278	0.14247	0.16232	0.36751	0.40995
2.96	0.10352	0.12611	0.14891	0.38653	
3.04	0.08490	0.11078	0.13696		
3.12	0.06674	0.09637	0.12642		
3.20	0.04886	0.08275	0.11723		
3.28	0.03108	0.06979	0.10933		
3.36	0.01322	0.05737	0.10271		
3.44	−0.00490	0.04537	0.09733		
3.52	−0.02344	0.03366	0.09320		
3.60		0.02212	0.09033		
3.68		0.01063	0.08876		
3.76		−0.00093	0.08852		
3.84		−0.01271	0.08971		
3.92			0.09242		

TABLE VII.—*Continued.*

$Z=26$	$-a_2$	w_0	w_i	Z_i
Case 1	1.6260		3.4184	5.059
Case 2	1.6255		3.7536	3.551

TABLE VII.—*Continued.*

$Z=26$	$-a_2$	w_0	w_i	Z_i
Case 3	1.6250	3.9326		
Case 4	1.6200	2.9410		
Case 5	1.6190	2.8851		

TABLE VIII. Solutions of the FTD equation ($Z=29$).

w	Case 1 2ψ	Case 2 2ψ	Case 3 2ψ	Case 4 2ψ	Case 5 2ψ	Case 6 2ψ	Case 7 2ψ	Case 8 2ψ	Case 9 2ψ
0.08	1.98998	1.99008	1.99009	1.99009	1.99009	1.99009	1.99009	1.99010	1.99010
0.16	1.96186	1.96225	1.96230	1.96230	1.96231	1.96231	1.96231	1.96233	1.96235
0.24	1.91845	1.91932	1.91943	1.91945	1.91946	1.91946	1.91946	1.91952	1.91955
0.32	1.86244	1.86398	1.86419	1.86422	1.86424	1.86424	1.86425	1.86434	1.86440
0.40	1.79634	1.79876	1.79908	1.79913	1.79916	1.79916	1.79917	1.79932	1.79940
0.48	1.72243	1.72593	1.72640	1.72647	1.72651	1.72652	1.72653	1.72675	1.72687
0.56	1.64276	1.64758	1.64822	1.64832	1.64837	1.64838	1.64840	1.64870	1.64887
0.64	1.55915	1.56552	1.56637	1.56649	1.56656	1.56658	1.56660	1.56700	1.56721
0.72	1.47315	1.48132	1.48241	1.48257	1.48266	1.48268	1.48271	1.48323	1.48350
0.80	1.38606	1.39633	1.39770	1.39790	1.39802	1.39804	1.39807	1.39872	1.39906
0.88	1.29898	1.31166	1.31335	1.31360	1.31375	1.31377	1.31381	1.31462	1.31504
0.96	1.21278	1.22823	1.23029	1.23060	1.23078	1.23081	1.23086	1.23184	1.23235
1.04	1.12813	1.14677	1.14926	1.14963	1.14984	1.14988	1.14994	1.15112	1.15175
1.12	1.04555	1.06785	1.07082	1.07127	1.07152	1.07157	1.07164	1.07305	1.07380
1.20	0.96538	0.99188	0.99542	0.99594	0.99625	0.99630	0.99639	0.99807	0.99895
1.28	0.88784	0.91916	0.92334	0.92397	0.92432	0.92439	0.92449	0.92647	0.92752
1.36	0.81304	0.84989	0.85481	0.85554	0.85596	0.85603	0.85615	0.85849	0.85972
1.44	0.74096	0.78415	0.78992	0.79078	0.79127	0.79136	0.79150	0.79424	0.79569
1.52	0.67150	0.72199	0.72873	0.72974	0.73031	0.73041	0.73058	0.73375	0.73547
1.60	0.60450	0.66335	0.67122	0.67239	0.67306	0.67316	0.67337	0.67712	0.67908
1.68	0.53972	0.60817	0.61732	0.61869	0.61947	0.61918	0.61983	0.62419	0.62648
1.76	0.47685	0.55631	0.56694	0.56853	0.56944	0.56960	0.56986	0.57492	0.57758
1.84	0.41553	0.50762	0.51996	0.52180	0.52286	0.52304	0.52334	0.52922	0.53230
1.92	0.35538	0.46192	0.47622	0.47835	0.47957	0.47979	0.48014	0.48695	0.49053
2.00	0.29594	0.41901	0.43556	0.43803	0.43945	0.43969	0.44010	0.44798	0.45213
2.08	0.23674	0.37869	0.39781	0.40068	0.40231	0.40260	0.40307	0.41219	0.41698
2.16	0.17728	0.34072	0.36281	0.36612	0.36800	0.36834	0.36888	0.37942	0.38496
2.24	0.11704	0.30487	0.33037	0.33419	0.33636	0.33675	0.33737	0.34955	0.35595
2.32	0.05549	0.27092	0.30031	0.30471	0.30723	0.30767	0.30839	0.32245	0.32984
2.40	−0.00784	0.23860	0.27246	0.27754	0.28044	0.28095	0.28178	0.29800	0.30653
2.48		0.20769	0.24665	0.25250	0.25584	0.25643	0.25739	0.27608	0.28592
2.56		0.17792	0.22272	0.22945	0.23330	0.23397	0.23508	0.25662	0.26797
2.64		0.14904	0.20049	0.20824	0.21267	0.21344	0.21472	0.23952	0.25261
2.72		0.12078	0.17982	0.18872	0.19382	0.19471	0.19618	0.22474	0.23982
2.80		0.09289	0.16055	0.17078	0.17663	0.17766	0.17934	0.21222	0.22960
2.88		0.06509	0.14252	0.15427	0.16100	0.16218	0.16412	0.20195	0.22198
2.96		0.03712	0.12561	0.13909	0.14682	0.14817	0.15040	0.19392	0.21703
3.04		0.00872	0.10967	0.12512	0.13399	0.13554	0.13810	0.18818	0.21483
3.12		−0.02033	0.09455	0.11226	0.12244	0.12422	0.12716	0.18478	0.21555
3.20			0.08014	0.10042	0.11209	0.11413	0.11750	0.18383	0.21937
3.28			0.06628	0.08949	0.10286	0.10521	0.10907	0.18545	0.22656
3.36			0.05285	0.07939	0.09472	0.09741	0.10184	0.18984	0.23746
3.44			0.03972	0.07004	0.08760	0.09069	0.09578	0.19724	
3.52			0.02676	0.06136	0.08148	0.08502	0.09085		
3.60			0.01381	0.05327	0.07631	0.08038	0.08707		
3.68			0.00076	0.04571	0.07209	0.07676	0.08444		
3.76			−0.00000	0.03860	0.06881	0.07416	0.08300		
3.84				0.03188	0.06648	0.07262	0.08278		
3.92				0.02548	0.06510	0.07216	0.08385		
4.00				0.01933	0.06473	0.07285	0.08631		
4.08				0.01337	0.06540	0.07475			
4.16				0.00752	0.06719	0.07797			
4.24				0.00172					
43.2				−0.00412					

$Z=29$	$-a_2$	w_0	w_i	Z_i
Case 1	1.6400		2.3902	13.89
Case 2	1.6250		3.0642	8.030
Case 3	1.6230		3.6847	4.397
Case 4	1.6227		4.2637	2.250
Case 5	1.62253	4.1739		
Case 6	1.6225	4.1037		
Case 7	1.62245	4.0141		
Case 8	1.6215	3.4439		
Case 9	1.6210	3.3257		

TABLE IX. Solutions of the FTD equation ($Z=33$).

w	Case 1 2ψ	Case 2 2ψ	Case 3 2ψ	Case 4 2ψ	Case 5 2ψ	Case 6 2ψ	Case 7 2ψ	Case 8 2ψ
0.08	1.99010	1.99011	1.99011	1.99011	1.99011	1.99011	1.99012	1.99012
0.16	1.96235	1.96237	1.96238	1.96239	1.96239	1.96239	1.96240	1.96242
0.24	1.91954	1.91960	1.91962	1.91963	1.91964	1.91965	1.91966	1.91972
0.32	1.86438	1.86448	1.86452	1.86454	1.86456	1.86457	1.86459	1.86469
0.40	1.79937	1.79953	1.79958	1.79961	1.79964	1.79966	1.79969	1.79985
0.48	1.72680	1.72703	1.72710	1.72715	1.72720	1.72722	1.72727	1.72750
0.56	1.64874	1.64906	1.64915	1.64922	1.64928	1.64931	1.64938	1.64970
0.64	1.56699	1.56742	1.56755	1.56763	1.56772	1.56776	1.56784	1.56827
0.72	1.48315	1.48370	1.48386	1.48397	1.48408	1.48413	1.48424	1.48478
0.80	1.39854	1.39923	1.39943	1.39957	1.39971	1.39977	1.39991	1.40059
0.88	1.31429	1.31513	1.31538	1.31555	1.31572	1.31581	1.31598	1.31682
0.96	1.23130	1.23233	1.23263	1.23284	1.23305	1.23315	1.23336	1.23439
1.04	1.15030	1.15155	1.15192	1.15217	1.15242	1.15254	1.15279	1.15403
1.12	1.07188	1.07336	1.07381	1.07411	1.07441	1.07455	1.07485	1.07634
1.20	0.99644	0.99821	0.99873	0.99909	0.99944	0.99962	0.99997	1.00174
1.28	0.92429	0.92638	0.92700	0.92742	0.92784	0.92805	0.92847	0.93055
1.36	0.85563	0.85808	0.85882	0.85931	0.85981	0.86005	0.86054	0.86300
1.44	0.79056	0.79344	0.79430	0.79488	0.79546	0.79575	0.79632	0.79920
1.52	0.72912	0.73249	0.73349	0.73417	0.73485	0.73519	0.73586	0.73922
1.60	0.67128	0.67521	0.67638	0.67717	0.67796	0.67836	0.67914	0.68306
1.68	0.61697	0.62155	0.62291	0.62383	0.62475	0.62521	0.62612	0.63069
1.76	0.56609	0.57141	0.57299	0.57406	0.57513	0.57567	0.57672	0.58203
1.84	0.51850	0.52466	0.52650	0.52774	0.52898	0.52960	0.53083	0.53699
1.92	0.47403	0.48117	0.48330	0.48474	0.48618	0.48689	0.48832	0.49545
2.00	0.43250	0.44077	0.44323	0.44490	0.44657	0.44740	0.44904	0.45730
2.08	0.39375	0.40331	0.40615	0.40808	0.41001	0.41096	0.41287	0.42242
2.16	0.35756	0.36860	0.37188	0.37411	0.37634	0.37744	0.37965	0.39069
2.24	0.32373	0.33647	0.34026	0.34284	0.34541	0.34669	0.34923	0.31698
2.32	0.29208	0.30677	0.31114	0.31411	0.31707	0.31855	0.32148	0.33620
2.40	0.26239	0.27931	0.28435	0.28777	0.29119	0.29289	0.29628	0.31325
2.48	0.23446	0.25394	0.25974	0.26368	0.26762	0.26958	0.27348	0.29305
2.56	0.20810	0.23049	0.23717	0.24171	0.24624	0.24850	0.25299	0.27555
2.64	0.18308	0.20882	0.21649	0.22172	0.22694	0.22954	0.23471	0.26070
2.72	0.15923	0.18877	0.19760	0.20361	0.20961	0.21260	0.21855	0.24849
2.80	0.13632	0.17022	0.18035	0.18726	0.19416	0.19759	0.20444	0.23892
2.88	0.11417	0.15301	0.16464	0.17258	0.18051	0.18446	0.19233	0.23205
2.96	0.09256	0.13703	0.15037	0.15949	0.16860	0.17314	0.18219	0.22794
3.04	0.07130	0.12215	0.13745	0.14791	0.15838	0.16359	0.17401	0.22672
3.12	0.05018	0.10825	0.12579	0.13779	0.14981	0.15580	0.16778	0.22855
3.20	0.02899	0.09523	0.11531	0.12907	0.14288	0.14977	0.16354	0.23367
3.28	0.00755	0.08296	0.10595	0.12173	0.13759	0.14551	0.16135	0.24235
3.36	−0.01434	0.07135	0.09765	0.11575	0.13395	0.14306	0.16131	0.25497
3.44	−0.03675	0.06028	0.09035	0.11111	0.13203	0.14251	0.16354	
3.52		0.04966	0.08403	0.10783	0.13189	0.14396	0.16821	
3.60		0.03938	0.07865	0.10595	0.13363	0.14755	0.17556	
3.68		0.02934	0.07419	0.10552	0.13739	0.15345		
3.76		0.01944	0.07063	0.10660	0.14335			
3.84		0.00958	0.06798	0.10932				
3.92		−0.00034	0.06625	0.11380				
4.00		−0.01045	0.06547					
			0.06567					
			0.06691					
			0.06928					

$Z=33$	$-a_2$	w_0	w_i	Z_i
Case 1	1.6210		3.3078	7.441
Case 2	1.6200		3.9172	4.039
Case 3	1.6197	4.2079		
Case 4	1.6195	3.8850		
Case 5	1.6193	3.7223		
Case 6	1.6192	3.6636		
Case 7	1.6190	3.5711		
Case 8	1.6180	3.3059		

TABLE X. Solutions of the FTD equation ($Z=37$).

w	Case 1 2ψ	Case 2 2ψ	Case 3 2ψ	Case 4 2ψ	Case 5 2ψ	Case 6 2ψ	Case 7 2ψ
0.08	1.99012	1.99012	1.99012	1.99013	1.99013	1.99013	1.99014
0.16	1.96241	1.96242	1.96243	1.96244	1.96244	1.96245	1.96247
0.24	1.91968	1.91971	1.91974	1.91974	1.91976	1.91977	1.91983
0.32	1.86463	1.86468	1.86472	1.86473	1.86476	1.86478	1.86488
0.40	1.79974	1.79983	1.79989	1.79991	1.79995	1.79999	1.80015
0.48	1.72733	1.72744	1.72754	1.72756	1.72763	1.72768	1.72791
0.56	1.64943	1.64959	1.64972	1.64975	1.64985	1.64991	1.65024
0.64	1.56788	1.56809	1.56826	1.56830	1.56843	1.56851	1.56894
0.72	1.48423	1.48450	1.48472	1.48477	1.48494	1.48505	1.48559
0.80	1.39983	1.40017	1.40044	1.40051	1.40072	1.40085	1.40154
0.88	1.31578	1.31620	1.31654	1.31663	1.31688	1.31705	1.31790
0.96	1.23301	1.23352	1.23394	1.23404	1.23435	1.23455	1.23558
1.04	1.15224	1.15286	1.15335	1.15348	1.15385	1.15410	1.15534
1.12	1.07403	1.07477	1.07536	1.07551	1.07596	1.07626	1.07774
1.20	0.99881	0.99969	1.00040	1.00057	1.00111	1.00146	1.00322
1.28	0.92688	0.92792	0.92876	0.92896	0.92959	0.93001	0.93210
1.36	0.85843	0.85966	0.86064	0.86089	0.86163	0.86212	0.86458
1.44	0.79358	0.79502	0.79617	0.79646	0.79733	0.79790	0.80078
1.52	0.73236	0.73404	0.73539	0.73573	0.73674	0.73741	0.74078
1.60	0.67475	0.67671	0.67828	0.67867	0.67985	0.68064	0.68456
1.68	0.62067	0.62295	0.62477	0.62523	0.62661	0.62752	0.63209
1.76	0.57002	0.57267	0.57479	0.57532	0.57692	0.57798	0.58329
1.84	0.52267	0.52574	0.52820	0.52882	0.53067	0.53190	0.53806
1.92	0.47845	0.48202	0.48486	0.48558	0.48773	0.48915	0.49629
2.00	0.43721	0.44133	0.44462	0.44545	0.44794	0.44958	0.45784
2.08	0.39874	0.40350	0.40731	0.40827	0.41114	0.41305	0.42260
2.16	0.36287	0.36837	0.37277	0.37387	0.37720	0.37939	0.39043
2.24	0.32941	0.33575	0.34082	0.34210	0.34593	0.34847	0.36121
2.32	0.29815	0.30546	0.31130	0.31277	0.31719	0.32012	0.33482
2.40	0.26890	0.27731	0.28405	0.28574	0.29084	0.29421	0.31115
2.48	0.24146	0.25115	0.25890	0.26085	0.26671	0.27060	0.29012
2.56	0.21565	0.22679	0.23570	0.23795	0.24469	0.24916	0.27165
2.64	0.19127	0.20406	0.21431	0.21689	0.22464	0.22978	0.25567
2.72	0.16814	0.18281	0.19457	0.19754	0.20645	0.21236	0.24215
2.80	0.14605	0.16287	0.17637	0.17978	0.19001	0.19680	0.23108
2.88	0.12483	0.14409	0.15957	0.16348	0.17523	0.18303	0.22245
2.96	0.10428	0.12631	0.14405	0.14853	0.16201	0.17096	0.21631
3.04	0.08421	0.10939	0.12969	0.13483	0.15029	0.16057	0.21273
3.12	0.06445	0.09318	0.11640	0.12228	0.14000	0.15179	0.21182
3.20	0.04479	0.07753	0.10406	0.11079	0.13109	0.14463	0.21373
3.28	0.02506	0.06229	0.09258	0.10027	0.12353	0.13906	0.21866
3.36	0.00507	0.04732	0.08187	0.09066	0.11730	0.13512	0.22688
3.44	−0.01533	0.03248	0.07183	0.08188	0.11237	0.13283	
3.52	−0.03622	0.01762	0.06238	0.07386	0.10877	0.13226	
3.60		0.00260	0.05345	0.06654	0.10651	0.13350	
3.68		−0.01269	0.04494	0.05987	0.10563	0.13668	
3.76		−0.02832	0.03677	0.05379	0.10621	0.14195	
3.84			0.02888	0.04827	0.10833		
3.92			0.02118	0.04326	0.11211		
4.00			0.01359	0.03871			
4.08			0.00604	0.03460			
4.16			−0.00156	0.03089			
4.24			−0.00929	0.02756			
4.32				0.02458			
4.40				0.02192			
4.48				0.01957			
4.56				0.01751			
4.64				0.01572			
4.72				0.01419			
4.80				0.01292			
4.88				0.01189			
4.96				0.01111			
5.04				0.01057			
5.12				0.01028			
5.20				0.01024			
5.28				0.01047			

$Z=37$	$-a_2$	w_0	w_i	Z_i
Case 1	1.6185		3.3800	7.930
Case 2	1.6180		3.6137	6.350
Case 3	1.6176		4.1436	3.658
Case 4	1.6175	5.2637		
Case 5	1.6172	3.9154		
Case 6	1.6170	3.7465		
Case 7	1.6160	3.3793		

TABLE XI. Solutions of the FTD equation ($Z=41$).

w	Case 1 2ψ	Case 2 2ψ	Case 3 2ψ	Case 4 2ψ	Case 5 2ψ	Case 6 2ψ
0.08	1.99013	1.99013	1.99014	1.99014	1.99014	1.99014
0.16	1.96247	1.96247	1.96248	1.96248	1.96249	1.96251
0.24	1.91981	1.91982	1.91984	1.91985	1.91985	1.91991
0.32	1.86485	1.86486	1.86490	1.86492	1.86493	1.86503
0.40	1.80009	1.80011	1.80016	1.80019	1.80021	1.80037
0.48	1.72782	1.72784	1.72791	1.72796	1.72798	1.72821
0.56	1.65008	1.65011	1.65021	1.65028	1.65031	1.65063
0.64	1.56870	1.56875	1.56887	1.56896	1.56900	1.56943
0.72	1.48525	1.48530	1.48546	1.48557	1.48563	1.48617
0.80	1.40104	1.40111	1.40132	1.40146	1.40152	1.40221
0.88	1.31721	1.31730	1.31755	1.31772	1.31780	1.31865
0.96	1.23466	1.23476	1.23507	1.23528	1.23538	1.23641
1.04	1.15411	1.15424	1.15461	1.15486	1.15498	1.15623
1.12	1.07614	1.07629	1.07673	1.07703	1.07718	1.07867
1.20	1.00116	1.00134	1.00187	1.00222	1.00240	1.00417
1.28	0.92948	0.92969	0.93032	0.93073	0.93095	0.93304
1.36	0.86130	0.86154	0.86228	0.86277	0.86302	0.86548
1.44	0.79672	0.79701	0.79787	0.79845	0.79874	0.80162
1.52	0.73579	0.73612	0.73713	0.73780	0.73814	0.74151
1.60	0.67847	0.67887	0.68004	0.68083	0.68122	0.68515
1.68	0.62472	0.62518	0.62655	0.62746	0.62792	0.63249
1.76	0.57442	0.57495	0.57654	0.57760	0.57814	0.58345
1.84	0.52745	0.52807	0.52991	0.53114	0.53176	0.53792
1.92	0.48366	0.48437	0.48650	0.48793	0.48864	0.49578
2.00	0.44288	0.44369	0.44617	0.44781	0.44864	0.45690
2.08	0.40493	0.40588	0.40873	0.41063	0.41159	0.42114
2.16	0.36964	0.37073	0.37403	0.37622	0.37733	0.38836
2.24	0.33682	0.33808	0.34189	0.34442	0.34569	0.35842
2.32	0.30630	0.30775	0.31213	0.31505	0.31652	0.33119
2.40	0.27788	0.27955	0.28460	0.28796	0.28965	0.30656
2.48	0.25139	0.25331	0.25912	0.26299	0.26494	0.28440
2.56	0.22665	0.22886	0.23554	0.23999	0.24223	0.26463
2.64	0.20349	0.20603	0.21370	0.21882	0.22139	0.24715

TABLE XI.—*Continued.*

w	Case 1 2ψ	Case 2 2ψ	Case 3 2ψ	Case 4 2ψ	Case 5 2ψ	Case 6 2ψ
2.72	0.18174	0.18465	0.19346	0.19933	0.20229	0.23190
2.80	0.16123	0.16457	0.17467	0.18141	0.18480	0.21883
2.88	0.14180	0.14562	0.15720	0.16492	0.16882	0.20790
2.96	0.12329	0.12766	0.14091	0.14976	0.15423	0.19911
3.04	0.10554	0.11053	0.12569	0.13582	0.14093	0.19246
3.12	0.08838	0.09408	0.11141	0.12300	0.12885	0.18799
3.20	0.07167	0.07817	0.09794	0.11120	0.11790	0.18578
3.28	0.05525	0.06265	0.08519	0.10034	0.10799	0.18593
3.36	0.03896	0.04737	0.07304	0.09033	0.09908	0.18857
3.44	0.02264	0.03218	0.06138	0.08110	0.09110	0.19391
3.52	0.00616	0.01695	0.05010	0.07258	0.08399	0.20219
3.60	−0.01063	0.00154	0.03910	0.06469	0.07773	
3.68	−0.02780	−0.01418	0.02827	0.05738	0.07226	
3.76			0.01751	0.05059	0.06756	
3.84			0.00670	0.04426	0.06361	
3.92			−0.00423	0.03833	0.06039	
4.00			−0.01539	0.03275	0.05791	
4.08				0.02748	0.05616	
4.16				0.02245	0.05516	
4.24				0.01764	0.05493	
4.32				0.01298	0.05552	
4.40				0.00842	0.05697	
4.48				0.00392		
4.56				−0.00056		
4.64				−0.00511		

$Z=41$	$-a_2$	w_0	w_i	Z_i
Case 1	1.6162		3.5495	7.616
Case 2	1.6161		3.6079	7.205
Case 3	1.6158		3.8892	5.464
Case 4	1.6156		4.5499	2.627
Case 5	1.6155	4.4149		
Case 6	1.6145	3.5020		

TABLE XII. Solutions of the FTD equation ($Z=45$).

w	Case 1 2ψ	Case 2 2ψ	Case 3 2ψ	Case 4 2ψ	Case 5 2ψ	Case 6 2ψ	Case 7 2ψ
0.08	1.99015	1.99015	1.99015	1.99015	1.99015	1.99015	1.99016
0.16	1.96252	1.96252	1.96252	1.96253	1.96253	1.96255	1.96258
0.24	1.91993	1.91993	1.91994	1.91994	1.91995	1.92000	1.92005
0.32	1.86505	1.86506	1.86507	1.86508	1.86509	1.86517	1.86528
0.40	1.80039	1.80041	1.80043	1.80044	1.80046	1.80059	1.80075
0.48	1.72824	1.72827	1.72829	1.72831	1.72834	1.72852	1.72876
0.56	1.65065	1.65068	1.65071	1.65075	1.65078	1.65104	1.65136
0.64	1.56943	1.56947	1.56951	1.56955	1.56960	1.56993	1.57036
0.72	1.48614	1.48619	1.48624	1.48630	1.48635	1.48679	1.48733
0.80	1.40211	1.40218	1.40225	1.40232	1.40239	1.40293	1.40362
0.88	1.31847	1.31855	1.31863	1.31872	1.31880	1.31948	1.32033
0.96	1.23611	1.23621	1.23631	1.23642	1.23652	1.23734	1.23837
1.04	1.15577	1.15589	1.15601	1.15614	1.15626	1.15726	1.15850
1.12	1.07800	1.07815	1.07830	1.07845	1.07860	1.07979	1.08127
1.20	1.00325	1.00342	1.00360	1.00377	1.00395	1.00536	1.00713
1.28	0.93180	0.93200	0.93221	0.93242	0.93263	0.93430	0.93639
1.36	0.86385	0.86410	0.86434	0.86459	0.86483	0.86679	0.86925
1.44	0.79952	0.79981	0.80009	0.80038	0.80067	0.80297	0.80585
1.52	0.73885	0.73919	0.73952	0.73986	0.74020	0.74289	0.74625
1.60	0.68183	0.68222	0.68260	0.68300	0.68340	0.68653	0.69046
1.68	0.62838	0.62884	0.62928	0.62975	0.63021	0.63385	0.63842
1.76	0.57842	0.57895	0.57946	0.58000	0.58054	0.58477	0.59008
1.84	0.53181	0.53242	0.53302	0.53365	0.53427	0.53917	0.54533
1.92	0.48841	0.48913	0.48982	0.49055	0.49126	0.49694	0.50408
2.00	0.44808	0.44890	0.44970	0.45054	0.45137	0.45794	0.46620
2.08	0.41063	0.41158	0.41251	0.41348	0.41443	0.42203	0.43157
2.16	0.37589	0.37699	0.37806	0.37918	0.38029	0.38906	0.40008
2.24	0.34371	0.34498	0.34621	0.34750	0.34878	0.35890	0.37162
2.32	0.31389	0.31535	0.31678	0.31826	0.31973	0.33140	0.34607
2.40	0.28628	0.28796	0.28960	0.29131	0.29301	0.30644	0.32335
2.48	0.26071	0.26264	0.26453	0.26650	0.26844	0.28392	0.30340
2.56	0.23701	0.23924	0.24140	0.24367	0.24591	0.26370	0.28614
2.64	0.21504	0.21759	0.22008	0.22269	0.22526	0.24572	0.27154

TABLE XII.—*Continued.*

w	Case 1 2ψ	Case 2 2ψ	Case 3 2ψ	Case 4 2ψ	Case 5 2ψ	Case 6 2ψ	Case 7 2ψ
2.72	0.19464	0.19757	0.20043	0.20342	0.20637	0.22988	0.25960
2.80	0.17567	0.17903	0.18230	0.18573	0.18912	0.21613	0.25032
2.88	0.15799	0.16184	0.16559	0.16952	0.17341	0.20442	0.24375
2.96	0.14146	0.14587	0.15017	0.15468	0.15913	0.19472	0.23998
3.04	0.12597	0.13101	0.13593	0.14109	0.14619	0.18702	0.23911
3.12	0.11137	0.11714	0.12277	0.12868	0.13451	0.18135	0.24133
3.20	0.09757	0.10416	0.11059	0.11734	0.12402	0.17774	0.24686
3.28	0.08443	0.09195	0.09929	0.10701	0.11464	0.17627	0.25599
3.36	0.07184	0.08041	0.08879	0.09760	0.10633	0.17704	0.26910
3.44	0.05970	0.06946	0.07901	0.08907	0.09904	0.18019	
3.52	0.04788	0.05898	0.06986	0.08133	0.09273	0.18591	
3.60	0.03627	0.04889	0.06127	0.07435	0.08736	0.19445	
3.68	0.02478	0.03909	0.05317	0.06807	0.08293		
3.76	0.01328	0.02949	0.04548	0.06245	0.07941		
3.84	0.00167	0.02000	0.03814	0.05746	0.07682		
3.92	−0.01014	0.01052	0.03109	0.05306	0.07516		
4.00	−0.01613	0.00097	0.02424	0.04922	0.07446		
4.08		−0.00873	0.01754	0.04594	0.07476		
4.16		−0.01365	0.01093	0.04318	0.07612		
4.24			0.00432	0.04094	0.07862		
4.32			−0.00233	0.03922			
4.40			−0.00910	0.03802			
4.48				0.03735			
4.56				0.03723			
4.64				0.03768			
4.72				0.03874			

$Z=45$	$-a_2$	w_0	w_i	Z_i
Case 1	1.6142		3.8514	6.353
Case 2	1.6141		4.0081	5.431
Case 3	1.6140		4.2921	4.027
Case 4	1.6139	4.7113		
Case 5	1.6138	4.2307		
Case 6	1.6130	3.5598		
Case 7	1.6120	3.3099		

TABLE XIII. Solutions of the FTD equation ($Z=49$).

w	Case 1 2ψ	Case 2 2ψ	Case 3 2ψ	Case 4 2ψ	Case 5 2ψ	Case 6 2ψ
0.08	1.99016	1.99016	1.99016	1.99016	1.99016	1.99017
0.16	1.96256	1.96256	1.96256	1.96256	1.96257	1.96260
0.24	1.92001	1.92002	1.92003	1.92003	1.92005	1.92011
0.32	1.86520	1.86522	1.86522	1.86523	1.86527	1.86537
0.40	1.80062	1.80065	1.80066	1.80067	1.80073	1.80089
0.48	1.72856	1.72860	1.72862	1.72863	1.72872	1.72896
0.56	1.65107	1.65113	1.65115	1.65116	1.65129	1.65161
0.64	1.56995	1.57004	1.57006	1.57008	1.57025	1.57067
0.72	1.48678	1.48689	1.48692	1.48694	1.48716	1.48771
0.80	1.40288	1.40302	1.40305	1.40308	1.40336	1.40404
0.88	1.31936	1.31953	1.31957	1.31961	1.31995	1.32079
0.96	1.23713	1.23733	1.23738	1.23744	1.23785	1.23888
1.04	1.15691	1.15716	1.15722	1.15728	1.15778	1.15902
1.12	1.07928	1.07957	1.07965	1.07972	1.08032	1.08180
1.20	1.00465	1.00500	1.00509	1.00517	1.00588	1.00765
1.28	0.93332	0.93374	0.93384	0.93394	0.93478	0.93687
1.36	0.86550	0.86599	0.86611	0.86623	0.86721	0.86967
1.44	0.80129	0.80187	0.80201	0.80215	0.80330	0.80618
1.52	0.74074	0.74142	0.74158	0.74175	0.74310	0.74646
1.60	0.68383	0.68462	0.68482	0.68501	0.68658	0.69050
1.68	0.63051	0.63142	0.63165	0.63187	0.63370	0.63826
1.76	0.58066	0.58172	0.58199	0.58225	0.58437	0.58967
1.84	0.53418	0.53541	0.53572	0.53602	0.53848	0.54462
1.92	0.49091	0.49234	0.49269	0.49304	0.49589	0.50300
2.00	0.45070	0.45236	0.45277	0.45317	0.45646	0.46469
2.08	0.41339	0.41530	0.41578	0.41624	0.42005	0.42956
2.16	0.37881	0.38101	0.38156	0.38210	0.38649	0.39747
2.24	0.34679	0.34933	0.34996	0.35058	0.35564	0.36831
2.32	0.31715	0.32008	0.32080	0.32151	0.32736	0.34196
2.40	0.28973	0.29310	0.29394	0.29476	0.30149	0.31831
2.48	0.26438	0.26825	0.26922	0.27016	0.27790	0.29728
2.56	0.24093	0.24538	0.24649	0.24757	0.25647	0.27877
2.64	0.21923	0.22434	0.22561	0.22686	0.23709	0.26273
2.72	0.19913	0.20501	0.20647	0.20790	0.21965	0.24913
2.80	0.18051	0.18725	0.18892	0.19056	0.20405	0.23793

w	Case 1 2ψ	Case 2 2ψ	Case 3 2ψ	Case 4 2ψ	Case 5 2ψ	Case 6 2ψ
2.88	0.16323	0.17095	0.17287	0.17475	0.19022	0.22916
2.96	0.14716	0.15600	0.15820	0.16035	0.17810	0.22282
3.04	0.13218	0.14230	0.14481	0.14728	0.16762	0.21900
3.12	0.11818	0.12975	0.13263	0.13545	0.15874	0.21779
3.20	0.10505	0.11826	0.12155	0.12478	0.15146	0.21933
3.28	0.09267	0.10776	0.11152	0.11521	0.14576	0.22381
3.36	0.08095	0.09816	0.10246	0.10667	0.14165	0.23147
3.44	0.06978	0.08941	0.09431	0.09912	0.13916	0.24265
3.52	0.05907	0.08143	0.08702	0.09252	0.13836	
3.60	0.04873	0.07417	0.08055	0.08683	0.13932	
3.68	0.03865	0.06758	0.07486	0.08202	0.14217	
3.76	0.02874	0.06162	0.06991	0.07808	0.14704	
3.84	0.01891	0.05623	0.06568	0.07500		
3.92	0.00907	0.05139	0.06216	0.07279		
4.00	−0.00087	0.04706	0.05933	0.07146		
4.08	−0.01100	0.04321	0.05718	0.07104		
4.16		0.03982	0.05574	0.07157		
4.24		0.03686	0.05500	0.07311		
4.32		0.03433	0.05501	0.07572		
4.40		0.03220	0.05579			
4.48		0.03047	0.05739			
4.56		0.02914				
4.64		0.02820				
4.72		0.02768				
4.80		0.02756				
4.88		0.02789				
4.96		0.02868				

$Z=49$	$-a_2$	w_0	w_i	Z_i
Case 1	1.6127		3.9930	6.122
Case 2	1.6125	4.9415		
Case 3	1.61245	4.4805		
Case 4	1.6124	4.2919		
Case 5	1.6120	3.7717		
Case 6	1.6110	3.3990		

TABLE XIV. Solutions of the FTD equation ($Z=53$).

w	Case 1 2ψ	Case 2 2ψ	Case 3 2ψ	Case 4 2ψ	Case 5 2ψ	Case 6 2ψ	Case 7 2ψ	Case 8 2ψ
0.08	1.99016	1.99016	1.99016	1.99016	1.99016	1.99017	1.99017	1.99018
0.16	1.96258	1.96258	1.96258	1.96258	1.96259	1.96259	1.96260	1.96264
0.24	1.92005	1.92006	1.92007	1.92007	1.92008	1.92010	1.92011	1.92019
0.32	1.86527	1.86529	1.86530	1.86531	1.86532	1.86535	1.86537	1.86552
0.40	1.80073	1.80075	1.80077	1.80078	1.80080	1.80085	1.80088	1.80112
0.48	1.72871	1.72874	1.72876	1.72878	1.72881	1.72888	1.72892	1.72928
0.56	1.65127	1.65130	1.65133	1.65136	1.65140	1.65149	1.65156	1.65204
0.64	1.57020	1.57024	1.57028	1.57032	1.57037	1.57049	1.57058	1.57122
0.72	1.48707	1.48712	1.48717	1.48723	1.48728	1.48745	1.48756	1.48837
0.80	1.40320	1.40327	1.40334	1.40340	1.40347	1.40368	1.40381	1.40484
0.88	1.31971	1.31979	1.31987	1.31996	1.32004	1.32030	1.32047	1.32173
0.96	1.23749	1.23759	1.23770	1.23780	1.23790	1.23821	1.23842	1.23996
1.04	1.15728	1.15740	1.15753	1.15765	1.15778	1.15815	1.15840	1.16026
1.12	1.07963	1.07978	1.07993	1.08008	1.08023	1.08067	1.08097	1.08320
1.20	1.00497	1.00514	1.00532	1.00550	1.00568	1.00621	1.00656	1.00920
1.28	0.93359	0.93380	0.93401	0.93422	0.93442	0.93505	0.93547	0.93859
1.36	0.86569	0.86593	0.86618	0.86642	0.86667	0.86741	0.86790	0.87157
1.44	0.80137	0.80166	0.80195	0.80224	0.80252	0.80339	0.80396	0.80827
1.52	0.74068	0.74101	0.74135	0.74169	0.74203	0.74304	0.74371	0.74874
1.60	0.68359	0.68398	0.68438	0.68477	0.68516	0.68634	0.68712	0.69299
1.68	0.63004	0.63050	0.63096	0.63142	0.63187	0.63324	0.63415	0.64098
1.76	0.57993	0.58046	0.58099	0.58153	0.58205	0.58364	0.58470	0.59263
1.84	0.53313	0.53374	0.53435	0.53497	0.53559	0.53743	0.53865	0.54785
1.92	0.48948	0.49018	0.49090	0.49162	0.49233	0.49445	0.49587	0.50653
2.00	0.44882	0.44964	0.45047	0.45129	0.45212	0.45458	0.45622	0.46854
2.08	0.41099	0.41193	0.41288	0.41384	0.41479	0.41764	0.41953	0.43377
2.16	0.37579	0.37688	0.37798	0.37909	0.38018	0.38346	0.38565	0.40210
2.24	0.34306	0.34431	0.34558	0.34685	0.34812	0.35190	0.35443	0.37339
2.32	0.31260	0.31404	0.31551	0.31697	0.31843	0.32279	0.32570	0.34756
2.40	0.28424	0.28590	0.28759	0.28927	0.29095	0.29597	0.29931	0.32450
2.48	0.25780	0.25971	0.26165	0.26359	0.26551	0.27128	0.27513	0.30413
2.56	0.23310	0.23530	0.23752	0.23975	0.24196	0.24860	0.25302	0.28638
2.64	0.20998	0.21250	0.21505	0.21761	0.22015	0.22777	0.23285	0.27121
2.72	0.18827	0.19115	0.19408	0.19701	0.19993	0.20867	0.21450	0.25860
2.80	0.16779	0.17110	0.17446	0.17781	0.18116	0.19118	0.19787	0.24854
2.88	0.14840	0.15219	0.15603	0.15987	0.16370	0.17518	0.18285	0.24106
2.96	0.12993	0.13426	0.13865	0.14305	0.14743	0.16057	0.16937	0.23622
3.04	0.11224	0.11718	0.12219	0.12722	0.13223	0.14726	0.15733	0.23412
3.12	0.09516	0.10079	0.10651	0.11225	0.11797	0.13516	0.14668	0.23489
3.20	0.07854	0.08496	0.09148	0.09802	0.10454	0.12418	0.13736	0.23872
3.28	0.06224	0.06953	0.07695	0.08440	0.09184	0.11425	0.12933	0.24586
3.36	0.04610	0.05438	0.06281	0.07129	0.07975	0.10532	0.12255	0.25661
3.44	0.02997	0.03936	0.04893	0.05855	0.06818	0.09731	0.11701	
3.52	0.01373	0.02433	0.03516	0.04608	0.05701	0.09019	0.11269	
3.60	−0.00277	0.00917	0.02140	0.03375	0.04616	0.08391	0.10962	
3.68	−0.01964	−0.00625	0.00752	0.02147	0.03551	0.07844	0.10781	
3.76		−0.02200	−0.00659	0.00911	0.02497	0.07374	0.10730	
3.84			−0.02101	−0.00342	0.01445	0.06980	0.10816	
3.92				−0.01621	0.00384	0.06661	0.11047	
4.00					−0.00693	0.06415	0.11435	
4.08					−0.01792	0.06245		
4.16						0.06150		
4.24						0.06134		
4.32						0.06201		
4.40						0.06355		
4.48						0.06604		

$Z=53$	$-a_2$	w_0	w_i	Z_i
Case 1	1.6119		3.5866	9.873
Case 2	1.6118		3.6477	9.336
Case 3	1.6117		3.7228	8.710
Case 4	1.6116		3.8182	7.964
Case 5	1.6115		3.9487	7.028
Case 6	1.6112	4.4266		
Case 7	1.6110	3.9929		
Case 8	1.6095	3.3492		

TABLE XV. Solutions of the FTD equation ($Z=57$).

w	Case 1 2ψ	Case 2 2ψ	Case 3 2ψ	Case 4 2ψ	Case 5 2ψ	Case 6 2ψ	Case 7 2ψ
0.08	1.99016	1.99017	1.99017	1.99017	1.99017	1.99023	1.99024
0.16	1.96257	1.96260	1.96262	1.96262	1.96263	1.96287	1.96288
0.24	1.92005	1.92011	1.92015	1.92016	1.92016	1.92071	1.92074
0.32	1.86526	1.86536	1.86544	1.86545	1.86546	1.86644	1.86649
0.40	1.80070	1.80087	1.80100	1.80101	1.80103	1.80256	1.80264
0.48	1.72866	1.72890	1.72908	1.72911	1.72913	1.73135	1.73147
0.56	1.65119	1.65151	1.65176	1.65180	1.65183	1.65488	1.65504
0.64	1.57007	1.57050	1.57083	1.57088	1.57092	1.57495	1.57516
0.72	1.48688	1.48742	1.48786	1.48791	1.48797	1.49314	1.49341
0.80	1.40293	1.40361	1.40416	1.40423	1.40430	1.41080	1.41114
0.88	1.31933	1.32018	1.32085	1.32094	1.32102	1.32905	1.32947
0.96	1.23698	1.23801	1.23884	1.23894	1.23904	1.24883	1.24934
1.04	1.15661	1.15785	1.15884	1.15896	1.15909	1.17089	1.17151
1.12	1.07875	1.08023	1.08142	1.08157	1.08172	1.09584	1.09658
1.20	1.00383	1.00560	1.00701	1.00719	1.00736	1.02413	1.02501
1.28	0.93215	0.93423	0.93590	0.93611	0.93632	0.95613	0.95718
1.36	0.86388	0.86633	0.86830	0.86854	0.86879	0.89210	0.89332
1.44	0.79913	0.80200	0.80431	0.80459	0.80488	0.83221	0.83365
1.52	0.73793	0.74128	0.74397	0.74431	0.74465	0.77658	0.77826
1.60	0.68024	0.68415	0.68728	0.68767	0.68807	0.72531	0.72727
1.68	0.62598	0.63053	0.63418	0.63463	0.63509	0.67842	0.68070
1.76	0.57504	0.58032	0.58456	0.58509	0.58562	0.63595	0.63861
1.84	0.52728	0.53340	0.53831	0.53892	0.53954	0.59793	0.60101
1.92	0.48252	0.48960	0.49529	0.49599	0.49671	0.56437	0.56794
2.00	0.44058	0.44877	0.45534	0.45616	0.45698	0.53530	0.53944
2.08	0.40127	0.41072	0.41831	0.41925	0.42021	0.51079	0.51559
2.16	0.36437	0.37527	0.38403	0.38512	0.38622	0.49092	0.49647
2.24	0.32967	0.34223	0.35234	0.35359	0.35486	0.47582	0.48224
2.32	0.29697	0.31143	0.32306	0.32451	0.32597	0.46566	0.47309
2.40	0.26604	0.28267	0.29605	0.29772	0.29940	0.46068	0.46929
2.48	0.23667	0.25576	0.27115	0.27307	0.27500	0.46120	0.47118
2.56	0.20862	0.23053	0.24821	0.25041	0.25263	0.46763	0.47920
2.64	0.18168	0.20680	0.22708	0.22961	0.23216	0.48049	0.49393
2.72	0.15563	0.18439	0.20764	0.21054	0.21347	0.50046	0.51609
2.80	0.13024	0.16312	0.18976	0.19309	0.19645	0.52838	0.54659
2.88	0.10529	0.14283	0.17332	0.17713	0.18098		
2.96	0.08055	0.12334	0.15821	0.16257	0.16698		
3.04	0.05580	0.10449	0.14431	0.14930	0.15435		
3.12	0.03082	0.08611	0.13155	0.13725	0.14303		
3.20	0.00541	0.06803	0.11982	0.12634	0.13294		
3.28	−0.02059	0.05010	0.10904	0.11649	0.12403		
3.36	−0.04723	0.03214	0.09914	0.10763	0.11625		
3.44		0.01401	0.09003	0.09973	0.10957		
3.52		−0.00444	0.08167	0.09272	0.10396		
3.60		−0.02330	0.07397	0.08657	0.09939		
3.68			0.06690	0.08124	0.09587		
3.76			0.06038	0.07671	0.09341		
3.84			0.05438	0.07297	0.09203		
3.92			0.04885	0.07000	0.09176		
4.00			0.04374	0.06781	0.09266		
4.08			0.03902	0.06640	0.09479		
4.16			0.03465	0.06579	0.09827		
4.24			0.03059	0.06602			
4.32			0.02681	0.06714			
4.40			0.02328	0.06920			
4.48			0.01997				
4.56			0.01685				
4.64			0.01389				
4.72			0.01107				
4.80			0.00836				
4.88			0.00573				
4.96			0.00316				
5.04			0.00061				
5.12			−0.00195				

$Z=57$	$-a_1$	w_0	w_i	Z_i
Case 1	1.6120		3.2168	14.80
Case 2	1.6110		3.5009	11.57
Case 3	1.6102		5.0591	2.303
Case 4	1.6101	4.3965		
Case 5	1.6100	4.1360		
Case 6	1.6005	2.7795		
Case 7	1.6000	2.7599		

TABLE XVI. Solutions of the FTD equation ($Z=61$).

w	Case 1 2ψ	Case 2 2ψ	Case 3 2ψ	Case 4 2ψ	Case 5 2ψ	Case 6 2ψ	Case 7 2ψ	Case 8 2ψ	Case 9 2ψ	Case 10 2ψ
0.08	1.99017	1.99018	1.99018	1.99018	1.99018	1.99018	1.99019	1.99019	1.99020	1.99023
0.16	1.96262	1.96264	1.96265	1.96265	1.96266	1.96267	1.96268	1.96270	1.96273	1.96286
0.24	1.92016	1.92020	1.92021	1.92022	1.92024	1.92027	1.92028	1.92033	1.92039	1.92068
0.32	1.86546	1.86552	1.86554	1.86556	1.86559	1.86564	1.86567	1.86577	1.86587	1.86639
0.40	1.80102	1.80111	1.80114	1.80118	1.80123	1.80131	1.80134	1.80150	1.80166	1.80247
0.48	1.72911	1.72925	1.72929	1.72934	1.72941	1.72953	1.72958	1.72981	1.73004	1.73121
0.56	1.65178	1.65198	1.65204	1.65210	1.65220	1.65236	1.65243	1.65275	1.65307	1.65467
0.64	1.57085	1.57110	1.57118	1.57127	1.57140	1.57161	1.57169	1.57212	1.57254	1.57466
0.72	1.48785	1.48818	1.48829	1.48839	1.48856	1.48883	1.48894	1.48948	1.49003	1.49275
0.80	1.40412	1.40453	1.40467	1.40481	1.40501	1.40535	1.40549	1.40617	1.40686	1.41028
0.88	1.32077	1.32127	1.32144	1.32161	1.32186	1.32229	1.32246	1.32330	1.32414	1.32837
0.96	1.23868	1.23930	1.23951	1.23971	1.24002	1.24054	1.24074	1.24177	1.24280	1.24795
1.04	1.15860	1.15934	1.15959	1.15984	1.16021	1.16084	1.16108	1.16232	1.16357	1.16978
1.12	1.08107	1.08196	1.08226	1.08255	1.08300	1.08374	1.08404	1.08552	1.08701	1.09444
1.20	1.00651	1.00757	1.00792	1.00828	1.00881	1.00969	1.01004	1.01180	1.01357	1.02240
1.28	0.93522	0.93647	0.93689	0.93731	0.93794	0.93898	0.93939	0.94148	0.94356	0.95399
1.36	0.86740	0.86887	0.86936	0.86985	0.87059	0.87181	0.87230	0.87475	0.87721	0.88948
1.44	0.80314	0.80486	0.80544	0.80602	0.80688	0.80832	0.80889	0.81176	0.81464	0.82902
1.52	0.74249	0.74450	0.74518	0.74585	0.74686	0.74854	0.74921	0.75257	0.75593	0.77274
1.60	0.68542	0.68777	0.68855	0.68934	0.69052	0.69247	0.69325	0.69717	0.70108	0.72068
1.68	0.63187	0.63460	0.63551	0.63642	0.63780	0.64007	0.64098	0.64553	0.65009	0.67289
1.76	0.58173	0.58490	0.58596	0.58702	0.58861	0.59125	0.59230	0.59759	0.60288	0.62938
1.84	0.53487	0.53854	0.53977	0.54100	0.54284	0.54590	0.54713	0.55326	0.55939	0.59013
1.92	0.49114	0.49539	0.49681	0.49823	0.50037	0.50391	0.50533	0.51243	0.51953	0.55514
2.00	0.45037	0.45528	0.45693	0.45857	0.46104	0.46514	0.46677	0.47499	0.48321	0.52443
2.08	0.41238	0.41806	0.41996	0.42185	0.42471	0.42944	0.43133	0.44082	0.45032	0.49801
2.16	0.37700	0.38355	0.38574	0.38793	0.39122	0.39669	0.39887	0.40982	0.42080	0.47593
2.24	0.34404	0.35158	0.35411	0.35663	0.36043	0.36673	0.36925	0.38189	0.39455	0.45825
2.32	0.31331	0.32200	0.32491	0.32781	0.33219	0.33945	0.34235	0.35692	0.37153	0.44511
2.40	0.28463	0.29462	0.29797	0.30132	0.30636	0.31471	0.31805	0.33484	0.35168	0.43666
2.48	0.25782	0.26930	0.27315	0.27700	0.28279	0.29240	0.29625	0.31558	0.33498	0.43315
2.56	0.23269	0.24587	0.25030	0.25472	0.26138	0.27243	0.27685	0.29910	0.32146	0.43487
2.64	0.20906	0.22420	0.22927	0.23435	0.24200	0.25470	0.25978	0.28538	0.31113	0.44222
2.72	0.18678	0.20412	0.20994	0.21577	0.22455	0.23913	0.24497	0.27442	0.30408	0.45572
2.80	0.16565	0.18551	0.19219	0.19886	0.20893	0.22568	0.23239	0.26625	0.30043	0.47601
2.88	0.14552	0.16824	0.17588	0.18353	0.19508	0.21430	0.22200	0.26095	0.30034	0.50392
2.96	0.12621	0.15218	0.16093	0.16969	0.18291	0.20496	0.21381	0.25861	0.30404	
3.04	0.10756	0.13721	0.14721	0.15724	0.17239	0.19768	0.20784	0.25938	0.31183	
3.12	0.08942	0.12323	0.13465	0.14612	0.16346	0.19246	0.20414	0.26348	0.32408	
3.20	0.07161	0.11011	0.12316	0.13626	0.15611	0.18937	0.20278	0.27116	0.34130	
3.28	0.05397	0.09777	0.11265	0.12761	0.15032	0.18848	0.20390	0.28277		
3.36	0.03635	0.08609	0.10305	0.12013	0.14612	0.18991	0.20765			
3.44	0.01860	0.07497	0.09429	0.11379	0.14352	0.19380	0.21423			
3.52	0.00057	0.06434	0.08632	0.10856	0.14258	0.20037	0.22393			
3.60	−0.01785	0.05408	0.07907	0.10444	0.14338	0.20987				
3.68	−0.03669	0.04412	0.07251	0.10144	0.14602					
3.76		0.03436	0.06657	0.09956	0.15065					
3.84		0.02471	0.06123	0.09884	0.15745					
3.92		0.01508	0.05645	0.09934						
4.00		0.00540	0.05219	0.10112						
4.08		−0.00442	0.04844	0.10427						
4.16		−0.01443	0.04517							
4.24			0.04235							
4.32			0.03999							
4.40			0.03807							
4.48			0.03659							
4.56			0.03554							
4.64			0.03494							
4.72			0.03480							
4.80			0.03514							
4.88			0.03599							

$Z=61$	$-a_2$	w_0	w_i	Z_i
Case 1	1.6100		3.5225	12.24
Case 2	1.6094		4.0442	7.579
Case 3	1.6092	4.8898		
Case 4	1.6090	4.0916		
Case 5	1.6087	3.7877		
Case 6	1.6082	3.5517		
Case 7	1.6080	3.4895		
Case 8	1.6070	3.2812		
Case 9	1.6060	3.1532		
Case 10	1.6010	2.8360		

TABLE XVII. Solutions of the FTD equation ($Z=65$).

w	Case 1 2ψ	Case 2 2ψ	Case 3 2ψ	Case 4 2ψ	Case 5 2ψ	Case 6 2ψ
0.08	1.99011	1.99018	1.99018	1.99019	1.99019	1.99021
0.16	1.96237	1.96265	1.96266	1.96268	1.96270	1.96275
0.24	1.91958	1.92022	1.92025	1.92028	1.92033	1.92045
0.32	1.86443	1.86556	1.86561	1.86566	1.86576	1.86597
0.40	1.79939	1.80117	1.80125	1.80133	1.80149	1.80181
0.48	1.72675	1.72932	1.72944	1.72955	1.72979	1.73026
0.56	1.64853	1.65206	1.65223	1.65239	1.65271	1.65335
0.64	1.56654	1.57120	1.57141	1.57163	1.57205	1.57290
0.72	1.48230	1.48829	1.48856	1.48883	1.48938	1.49047
0.80	1.39712	1.40465	1.40499	1.40533	1.40601	1.40738
0.88	1.31209	1.32138	1.32180	1.32223	1.32307	1.32476
0.96	1.22807	1.23939	1.23991	1.24042	1.24145	1.24351
1.04	1.14574	1.15940	1.16002	1.16064	1.16189	1.16437
1.12	1.06564	1.08197	1.08271	1.08345	1.08494	1.08791
1.20	0.98811	1.00751	1.00839	1.00928	1.01104	1.01457
1.28	0.91341	0.93632	0.93737	0.93841	0.94050	0.94466
1.36	0.84165	0.86860	0.86983	0.87106	0.87351	0.87841
1.44	0.77288	0.80446	0.80589	0.80733	0.81021	0.81595
1.52	0.70703	0.74392	0.74560	0.74728	0.75064	0.75735
1.60	0.64400	0.68697	0.68893	0.69089	0.69480	0.70263
1.68	0.58359	0.63354	0.63582	0.63810	0.64265	0.65175
1.76	0.52558	0.58353	0.58618	0.58882	0.59411	0.60468
1.84	0.46969	0.53682	0.53988	0.54294	0.54907	0.56133
1.92	0.41562	0.49324	0.49678	0.50033	0.50743	0.52162
2.00	0.36302	0.45264	0.45674	0.46084	0.46904	0.48546
2.08	0.31152	0.41484	0.41958	0.42431	0.43379	0.45276
2.16	0.26072	0.37967	0.38513	0.39059	0.40153	0.42344
2.24	0.21021	0.34694	0.35323	0.35953	0.37214	0.39742
2.32	0.15956	0.31647	0.32372	0.33097	0.34550	0.37465
2.40	0.10834	0.28809	0.29642	0.30477	0.32150	0.35508
2.48	0.05611	0.26160	0.27119	0.28078	0.30002	0.33871
2.56	0.00250	0.23685	0.24785	0.25887	0.28100	0.32555
2.64	−0.05277	0.21366	0.22628	0.23893	0.26436	0.31565
2.72	−0.10974	0.19185	0.20632	0.22083	0.25004	0.30908
2.80		0.17127	0.18784	0.20448	0.23801	0.30597
2.88		0.15176	0.17072	0.18977	0.22825	0.30651
2.96		0.13316	0.15483	0.17664	0.22078	0.31093
3.04		0.11532	0.14005	0.16501	0.21564	0.31955
3.12		0.09807	0.12628	0.15481	0.21289	0.33277
3.20		0.08127	0.11341	0.14601	0.21263	0.35111
3.28		0.06478	0.10135	0.13857	0.21500	
3.36		0.04844	0.08999	0.13246	0.22021	
3.44		0.03210	0.07924	0.12769	0.22848	
3.52		0.01564	0.06901	0.12426		
3.60		−0.00108	0.05922	0.12219		
3.68		−0.01817	0.04978	0.12153		
3.76			0.04061	0.12235		
3.84			0.03163	0.12473		
3.92			0.02275	0.12879		
4.00			0.01390			
4.08			0.00499			
4.16			−0.00403			
4.24			−0.01322			

$Z=65$	$-a_2$	w_0	w_i	Z_i
Case 1	1.6200		2.5637	28.38
Case 2	1.6090		3.5948	12.33
Case 3	1.6085		4.1245	7.570
Case 4	1.6080	3.9338		
Case 5	1.6070	3.4580		
Case 6	1.6050	3.1425		

TABLE XVIII. Solutions of the FTD equation ($Z=69$).

w	Case 1 2ψ	Case 2 2ψ	Case 3 2ψ	Case 4 2ψ	Case 5 2ψ	Case 6 2ψ
0.08	1.99018	1.99019	1.99019	1.99019	1.99020	1.99021
0.16	1.96265	1.96268	1.96269	1.96270	1.96273	1.96275
0.24	1.92022	1.92027	1.92030	1.92033	1.92039	1.92045
0.32	1.86555	1.86566	1.86571	1.86576	1.86586	1.86597
0.40	1.80116	1.80132	1.8014υ	1.80148	1.80164	1.80180
0.48	1.72930	1.72953	1.72965	1.72977	1.73000	1.73024
0.56	1.65203	1.65235	1.65251	1.65267	1.65299	1.65331
0.64	1.57114	1.57157	1.57178	1.57199	1.57241	1.57284
0.72	1.48819	1.48874	1.48901	1.48928	1.48983	1.49037
0.80	1.40450	1.40519	1.40553	1.40587	1.40656	1.40724
0.88	1.32117	1.32202	1.32244	1.32286	1.32371	1.32455
0.96	1.23910	1.24013	1.24064	1.24116	1.24219	1.24322
1.04	1.15901	1.16025	1.16087	1.16149	1.16273	1.16397
1.12	1.08144	1.08293	1.08367	1.08441	1.08590	1.08738
1.20	1.00682	1.00859	1.00947	1.01035	1.01211	1.01388
1.28	0.93544	0.93753	0.93856	0.93961	0.94169	0.94378
1.36	0.86748	0.86994	0.87116	0.87239	0.87484	0.87729
1.44	0.80305	0.80593	0.80736	0.80880	0.81167	0.81455
1.52	0.74218	0.74554	0.74721	0.74890	0.75225	0.75561
1.60	0.68484	0.68875	0.69070	0.69267	0.69657	0.70049
1.68	0.63095	0.63550	0.63776	0.64005	0.64460	0.64915
1.76	0.58040	0.58569	0.58831	0.59097	0.59625	0.60153
1.84	0.53305	0.53918	0.54223	0.54530	0.55142	0.55755
1.92	0.48875	0.49584	0.49936	0.50293	0.51001	0.51711
2.00	0.44731	0.45550	0.45958	0.46369	0.47188	0.48009
2.08	0.40854	0.41800	0.42270	0.42746	0.43692	0.44640
2.16	0.37225	0.38316	0.38858	0.39407	0.40499	0.41594
2.24	0.33823	0.35081	0.35706	0.36338	0.37597	0.38860
2.32	0.30629	0.32076	0.32796	0.33525	0.34975	0.36431
2.40	0.27622	0.29286	0.30114	0.30952	0.32622	0.34299
2.48	0.24781	0.26692	0.27644	0.28608	0.30529	0.32461
2.56	0.22086	0.24279	0.25372	0.26479	0.28689	0.30912
2.64	0.19516	0.22030	0.23284	0.24556	0.27095	0.29653
2.72	0.17051	0.19930	0.21367	0.22826	0.25743	0.28686
2.80	0.14670	0.17963	0.19609	0.21283	0.24632	0.28017
2.88	0.12354	0.16115	0.18000	0.19917	0.23762	0.27657
2.96	0.10081	0.14372	0.16527	0.18723	0.23136	0.27618
3.04	0.07832	0.12720	0.15182	0.17696	0.22761	0.27921
3.12	0.05587	0.11145	0.13956	0.16832	0.22645	0.28592
3.20	0.03325	0.09634	0.12840	0.16129	0.22803	0.29662
3.28	0.01030	0.08175	0.11827	0.15588	0.23254	0.31176
3.36	−0.01315	0.06754	0.10911	0.15209	0.24021	
3.44	−0.03716	0.05360	0.10085	0.14998	0.25135	
3.52		0.03978	0.09345	0.14959		
3.60		0.02598	0.08685	0.15103		
3.68		0.01207	0.08103	0.15440		
3.76		−0.00204	0.07593	0.15986		
3.84		−0.01645	0.07155			
3.92			0.06786			
4.00			0.06485			
4.08			0.06251			
4.16			0.06084			
4.24			0.05987			
4.32			0.05960			
4.40			0.06006			
4.48			0.06131			
4.56			0.06340			

$Z=69$	$-a_2$	w_0	w_i	Z_i
Case 1	1.6090		3.3154	16.75
Case 2	1.6080		3.7485	11.49
Case 3	1.6075	4.5316		
Case 4	1.6070	3.7682		
Case 5	1.6060	3.4096		
Case 6	1.6050	3.2373		

$1/3\pi^5 a_0^3$ to zero at the ionic radius, x_i. It can be readily shown that the ionic charge, Z_i, which is presented by the ion at distances greater than x_i is

$$Z_i = -Zx_i(d\psi/dx)_{x=x_i}. \tag{5}$$

The accompanying Tables I–XXIV give the function ψ (actually 2ψ is tabulated) *versus* the independent variable w for various elements and various initial slopes. The function is given to five decimals and at an interval $\Delta w=0.08$. Quadratic interpolation is sufficient to obtain intermediate values.

TABLE XIX. Solutions of the FTD equation ($Z=73$).

w	Case 1 2ψ	Case 2 2ψ	Case 3 2ψ	Case 4 2ψ	Case 5 2ψ	Case 6 2ψ	Case 7 2ψ
0.08	1.99019	1.99019	1.99019	1.99020	1.99020	1.99020	1.99021
0.16	1.96268	1.96270	1.96271	1.96271	1.96273	1.96274	1.96278
0.24	1.92027	1.92033	1.92035	1.92036	1.92039	1.92042	1.92050
0.32	1.86565	1.86576	1.86579	1.86581	1.86586	1.86591	1.86607
0.40	1.80131	1.80147	1.80152	1.80155	1.80163	1.80171	1.80196
0.48	1.72952	1.72975	1.72982	1.72987	1.72998	1.73010	1.73045
0.56	1.65232	1.65264	1.65274	1.65280	1.65296	1.65312	1.65360
0.64	1.57151	1.57194	1.57206	1.57215	1.57236	1.57257	1.57321
0.72	1.48865	1.48920	1.48936	1.48947	1.48974	1.49001	1.49083
0.80	1.40506	1.40574	1.40595	1.40608	1.40643	1.40677	1.40779
0.88	1.32183	1.32267	1.32293	1.32310	1.32352	1.32394	1.32521
0.96	1.23987	1.24090	1.24121	1.24141	1.24193	1.24244	1.24399
1.04	1.15989	1.16113	1.16150	1.16175	1.16237	1.16299	1.16486
1.12	1.08245	1.08393	1.08438	1.08468	1.08542	1.08616	1.08839
1.20	1.00796	1.00973	1.01026	1.01061	1.01149	1.01237	1.01502
1.28	0.93672	0.93881	0.93943	0.93985	0.94089	0.94193	0.94506
1.36	0.86892	0.87137	0.87211	0.87259	0.87382	0.87504	0.87872
1.44	0.80466	0.80753	0.80839	0.80896	0.81040	0.81183	0.81614
1.52	0.74396	0.74732	0.74833	0.74899	0.75067	0.75235	0.75739
1.60	0.68682	0.69073	0.69190	0.69268	0.69464	0.69659	0.70246
1.68	0.63315	0.63769	0.63906	0.63996	0.64224	0.64451	0.65134
1.76	0.58284	0.58812	0.58971	0.59076	0.59340	0.59604	0.60396
1.84	0.53577	0.54188	0.54372	0.54494	0.54800	0.55106	0.56025
1.92	0.49177	0.49884	0.50097	0.50238	0.50592	0.50946	0.52010
2.00	0.45066	0.45884	0.46130	0.46293	0.46703	0.47112	0.48343
2.08	0.41228	0.42172	0.42456	0.42644	0.43117	0.43590	0.45012
2.16	0.37643	0.38731	0.39059	0.39276	0.39822	0.40368	0.42009
2.24	0.34291	0.35545	0.35923	0.36173	0.36802	0.37431	0.39324
2.32	0.31152	0.32596	0.33031	0.33319	0.34044	0.34769	0.36951
2.40	0.28209	0.29869	0.30370	0.30701	0.31534	0.32369	0.34883
2.48	0.25440	0.27347	0.27923	0.28303	0.29262	0.30223	0.33117
2.56	0.22827	0.25015	0.25677	0.26114	0.27216	0.28320	0.31651
2.64	0.20350	0.22859	0.23618	0.24120	0.25386	0.26655	0.30487
2.72	0.17990	0.20865	0.21735	0.22311	0.23763	0.25221	0.29630
2.80	0.15729	0.19019	0.20016	0.20676	0.22342	0.24015	0.29087
2.88	0.13548	0.17307	0.18449	0.19205	0.21115	0.23036	0.28871
2.96	0.11427	0.15720	0.17026	0.17891	0.20081	0.22285	0.29000
3.04	0.09349	0.14244	0.15737	0.16727	0.19235	0.21765	0.29496
3.12	0.07295	0.12869	0.14574	0.15707	0.18579	0.21483	0.30391
3.20	0.05246	0.11584	0.13531	0.14825	0.18115	0.21449	0.31722
3.28	0.03186	0.10380	0.12601	0.14080	0.17847	0.21676	
3.36	0.01097	0.09247	0.11778	0.13468	0.17782	0.22184	
3.44	−0.01034	0.08176	0.11059	0.12988	0.17931	0.22995	
3.52	−0.03217	0.07158	0.10440	0.12643	0.18308	0.24142	
3.60		0.06185	0.09918	0.12433	0.18932		
3.68		0.05248	0.09492	0.12364	0.19825		
3.76		0.04340	0.09161	0.12441			
3.84		0.03452	0.08926	0.12674			
3.92		0.02576	0.08789	0.13075			
4.00		0.01705	0.08751	0.13657			
4.08		0.00831	0.08819				
4.16		−0.00051	0.08998				
4.24		−0.00951	0.09296				

$Z=73$	$-a_2$	w_0	w_i	Z_i
Case 1	1.6080		3.4014	16.55
Case 2	1.6070		4.1553	8.437
Case 3	1.6067	4.2330		
Case 4	1.6065	3.9405		
Case 5	1.6060	3.6268		
Case 6	1.6055	3.4638		
Case 7	1.6040	3.2032		

For each neutral atom tabulation a w_0 value is given, defined by $x_0=w_0^2/2$, and for each ion a w_i is given. The w_0 and w_i values are obtained by linear interpolation; a small inaccuracy results in the fourth decimal digit. From these values the radius of the atom or ion can be obtained. In addition, Z_i is given for ions.

III. ACKNOWLEDGMENTS

The authors would like to express their thanks to the staff of the Ballistics Research Laboratory, Aberdeen Proving Ground, Maryland, for the use of the ENIAC and for their kind cooperation in carrying out the computations; and to Miss Lois Cook and Mr. John B. Jackson for assistance in checking the tables.

TABLE XX. Solutions of the FTD equation ($Z=77$).

w	Case 1 2ψ	Case 2 2ψ	Case 3 2ψ	Case 4 2ψ	Case 5 2ψ	Case 6 2ψ	Case 7 2ψ	Case 8 2ψ	Case 9 2ψ	Case 10 2ψ
0.08	1.99019	1.99019	1.99019	1.99020	1.99020	1.99020	1.99020	1.99021	1.99021	1.99022
0.16	1.96268	1.96270	1.96271	1.96271	1.96272	1.96273	1.96274	1.96275	1.96278	1.96280
0.24	1.92027	1.92033	1.92035	1.92036	1.92038	1.92039	1.92042	1.92044	1.92050	1.92056
0.32	1.86565	1.86575	1.86578	1.86580	1.86584	1.86586	1.86591	1.86596	1.86606	1.86616
0.40	1.80130	1.80146	1.80151	1.80154	1.80159	1.80162	1.80171	1.80179	1.80195	1.80211
0.48	1.72950	1.72973	1.72980	1.72985	1.72992	1.72997	1.73008	1.73020	1.73044	1.73067
0.56	1.65229	1.65261	1.65271	1.65277	1.65287	1.65293	1.65309	1.65325	1.65357	1.65389
0.64	1.57146	1.57189	1.57201	1.57210	1.57223	1.57231	1.57252	1.57273	1.57316	1.57358
0.72	1.48857	1.48912	1.48928	1.48939	1.48955	1.48966	1.48993	1.49021	1.49075	1.49130
0.80	1.40494	1.40562	1.40583	1.40597	1.40617	1.40631	1.40665	1.40699	1.40767	1.40836
0.88	1.32166	1.32250	1.32276	1.32293	1.32318	1.32335	1.32377	1.32419	1.32504	1.32588
0.96	1.23963	1.24066	1.24097	1.24117	1.24148	1.24169	1.24220	1.24272	1.24375	1.24478
1.04	1.15956	1.16081	1.16117	1.16143	1.16180	1.16205	1.16266	1.16329	1.16453	1.16577
1.12	1.08201	1.08350	1.08394	1.08424	1.08469	1.08498	1.08572	1.08647	1.08795	1.08944
1.20	1.00739	1.00916	1.00968	1.01004	1.01057	1.01092	1.01180	1.01269	1.01445	1.01622
1.28	0.93599	0.93808	0.93870	0.93912	0.93975	0.94016	0.94120	0.94225	0.94433	0.94642
1.36	0.86799	0.87045	0.87117	0.87167	0.87241	0.87290	0.87412	0.87535	0.87780	0.88025
1.44	0.80350	0.80637	0.80722	0.80781	0.80867	0.80924	0.81067	0.81212	0.81499	0.81786
1.52	0.74253	0.74589	0.74688	0.74757	0.74857	0.74924	0.75091	0.75260	0.75595	0.75931
1.60	0.68506	0.68897	0.69013	0.69093	0.69210	0.69288	0.69483	0.69680	0.70070	0.70462
1.68	0.63101	0.63556	0.63691	0.63783	0.63920	0.64010	0.64236	0.64466	0.64920	0.65376
1.76	0.58026	0.58554	0.58710	0.58818	0.58976	0.59082	0.59344	0.59610	0.60138	0.60667
1.84	0.53267	0.53879	0.54060	0.54185	0.54368	0.54490	0.54794	0.55103	0.55714	0.56327
1.92	0.48807	0.49515	0.49724	0.49869	0.50081	0.50222	0.50574	0.50931	0.51640	0.52349
2.00	0.44628	0.45446	0.45688	0.45855	0.46101	0.46263	0.46670	0.47083	0.47902	0.48723
2.08	0.40709	0.41654	0.41933	0.42126	0.42410	0.42598	0.43067	0.43544	0.44491	0.45439
2.16	0.37032	0.38121	0.38443	0.38666	0.38993	0.39210	0.39751	0.40302	0.41394	0.42489
2.24	0.33575	0.34829	0.35199	0.35456	0.35833	0.36083	0.36707	0.37342	0.38602	0.39865
2.32	0.30316	0.31759	0.32185	0.32481	0.32915	0.33203	0.33921	0.34653	0.36104	0.37560
2.40	0.27234	0.28893	0.29383	0.29723	0.30222	0.30553	0.31379	0.32222	0.33893	0.35571
2.48	0.24308	0.26212	0.26775	0.27166	0.27740	0.28120	0.29069	0.30039	0.31962	0.33895
2.56	0.21516	0.23699	0.24345	0.24793	0.25453	0.25889	0126980	0.28095	0.30307	0.32533
2.64	0.18835	0.21336	0.22076	0.22591	0.23347	0.23848	0.25100	0.26381	0.28925	0.31487
2.72	0.16244	0.19105	0.19953	0.20543	0.21410	0.21985	0.23421	0.24892	0.27817	0.30766
2.80	0.13721	0.16990	0.17960	0.18636	0.19629	0.20287	0.21934	0.23623	0.26984	0.30380
2.88	0.11245	0.14975	0.16083	0.16856	0.17992	0.18746	0.20633	0.22570	0.26433	0.30345
2.96	0.08792	0.13041	0.14306	0.15189	0.16488	0.17351	0.19513	0.21735	0.26175	0.30683
3.04	0.06343	0.11174	0.12616	0.13624	0.15108	0.16094	0.18569	0.21118	0.26223	0.31422
3.12	0.03875	0.09357	0.10999	0.12148	0.13841	0.14969	0.17801	0.20724	0.26596	0.32598
3.20	0.01368	0.07574	0.09440	0.10749	0.12680	0.13967	0.17207	0.20560	0.27320	0.34260
3.28	−0.01192	0.05809	0.07927	0.09415	0.11616	0.13085	0.16791	0.20638	0.28427	
3.36	−0.03817	0.04047	0.06447	0.08137	0.10641	0.12317	0.16555	0.20972		
3.44		0.02272	0.04985	0.06901	0.09749	0.11660	0.16508	0.21582		
3.52		0.00472	0.03530	0.05699	0.08934	0.11111	0.16657	0.22493		
3.60		−0.01365	0.02069	0.04519	0.08190	0.10669	0.17017			
3.68		−0.03244	0.00590	0.03352	0.07511	0.10335	0.17605			
3.76			−0.00915	0.02186	0.06894	0.10109				
3.84			−0.02454	0.01012	0.06333	0.09993				
3.92				−0.00178	0.05826	0.09992				
4.00				−0.01392	0.05368	0.10111				
4.08					0.04956	0.10358				
4.16					0.04589	0.10743				
4.24					0.04264					
4.32					0.03978					
4.40					0.03730					
4.48					0.03520					
4.56					0.03346					
4.64					0.03208					
4.72					0.03105					
4.80					0.03038					
4.88					0.03009					
4.96					0.03017					
5.04					0.03066					
5.12					0.03156					

$Z=77$	$-a_2$	w_0	w_4	Z_i
Case 1	1.6080		3.2430	20.01
Case 2	1.6070		3.5407	15.58
Case 3	1.6067		3.7115	13.43
Case 4	1.6065		3.9081	11.27
Case 5	1.6062	5.0931		
Case 6	1.6060	4.1340		
Case 7	1.6055	3.6995		
Case 8	1.6050	3.5066		
Case 9	1.6040	3.2950		
Case 10	1.6030	3.1648		

TABLE XXI. Solutions of the FTD equation ($Z=81$).

w	Case 1 2ψ	Case 2 2ψ	Case 3 2ψ	Case 4 2ψ	Case 5 2ψ	Case 6 2ψ	Case 7 2ψ	Case 8 2ψ
0.08	1.99019	1.99020	1.99020	1.99020	1.99020	1.99021	1.99021	1.99022
0.16	1.96268	1.96273	1.96273	1.96274	1.96274	1.96275	1.96278	1.96280
0.24	1.92027	1.92039	1.92040	1.92042	1.92043	1.92044	1.92050	1.92056
0.32	1.86565	1.86585	1.86587	1.86590	1.86593	1.86596	1.86606	1.86616
0.40	1.80129	1.80162	1.80165	1.80170	1.80173	1.80178	1.80194	1.80210
0.48	1.72949	1.72995	1.73000	1.73007	1.73012	1.73019	1.73042	1.73065
0.56	1.65226	1.65290	1.65297	1.65306	1.65313	1.65322	1.65355	1.65387
0.64	1.57142	1.57226	1.57235	1.57248	1.57256	1.57269	1.57311	1.57354
0.72	1.48850	1.48959	1.48970	1.48986	1.48997	1.49013	1.49068	1.49122
0.80	1.40483	1.40620	1.40633	1.40654	1.40668	1.40688	1.40756	1.40825
0.88	1.32150	1.32319	1.32336	1.32361	1.32378	1.32403	1.32488	1.32572
0.96	1.23941	1.24147	1.24167	1.24198	1.24219	1.24249	1.24352	1.24455
1.04	1.15926	1.16174	1.16199	1.16236	1.16261	1.16299	1.16423	1.16547
1.12	1.08161	1.08458	1.08488	1.08532	1.08562	1.08607	1.08755	1.08904
1.20	1.00687	1.01040	1.01075	1.01128	1.01163	1.01216	1.01392	1.01569
1.28	0.93532	0.93948	0.93990	0.94052	0.94094	0.94157	0.94365	0.94573
1.36	0.86714	0.87204	0.87253	0.87326	0.87375	0.87449	0.87694	0.87939
1.44	0.80243	0.80817	0.80874	0.80960	0.81018	0.81104	0.81391	0.81678
1.52	0.74120	0.74791	0.74858	0.74959	0.75026	0.75127	0.75462	0.75798
1.60	0.68343	0.69125	0.69203	0.69320	0.69399	0.69516	0.69907	0.70298
1.68	0.62903	0.63812	0.63903	0.64039	0.64130	0.64267	0.64721	0.65176
1.76	0.57787	0.58842	0.58948	0.59105	0.59211	0.59370	0.59897	0.60425
1.84	0.52980	0.54203	0.54325	0.54508	0.54630	0.54814	0.55425	0.56037
1.92	0.48465	0.49879	0.50021	0.50232	0.50374	0.50587	0.51294	0.52003
2.00	0.44221	0.45856	0.46019	0.46264	0.46428	0.46674	0.47492	0.48311
2.08	0.40229	0.42116	0.42305	0.42587	0.42777	0.43060	0.44005	0.44951
2.16	0.36467	0.38643	0.38860	0.39186	0.39404	0.39731	0.40821	0.41914
2.24	0.32913	0.35418	0.35668	0.36043	0.36295	0.36672	0.37929	0.39189
2.32	0.29543	0.32424	0.32712	0.33144	0.33435	0.33868	0.35316	0.36768
2.40	0.26334	0.29645	0.29977	0.30473	0.30807	0.31306	0.32972	0.34645
2.48	0.23263	0.27064	0.27444	0.28015	0.28399	0.28973	0.30889	0.32815
2.56	0.20305	0.24664	0.25101	0.25756	0.26197	0.26856	0.29059	0.31275
2.64	0.17438	0.22429	0.22930	0.23682	0.24188	0.24945	0.27476	0.30025
2.72	0.14636	0.20345	0.20919	0.21781	0.22361	0.23229	0.26136	0.29067
2.80	0.11875	0.18396	0.19053	0.20041	0.20706	0.21701	0.25038	0.28409
2.88	0.09131	0.16569	0.17320	0.18450	0.19212	0.20352	0.24181	0.28058
2.96	0.06380	0.14848	0.15707	0.17000	0.17871	0.19177	0.23570	0.28031
3.04	0.03599	0.13222	0.14202	0.15679	0.16676	0.18171	0.23211	0.28345
3.12	0.00767	0.11677	0.12795	0.14481	0.15620	0.17330	0.23114	0.29027
3.20	−0.02134	0.10200	0.11474	0.13397	0.14698	0.16655	0.23292	0.30110
3.28	−0.05109	0.08779	0.10228	0.12421	0.13906	0.16144	0.23765	0.31636
3.36		0.07402	0.09049	0.11546	0.13241	0.15801	0.24557	
3.44		0.06056	0.07925	0.10768	0.12702	0.15629	0.25699	
3.52		0.04731	0.06849	0.10081	0.12288	0.15635		
3.60		0.03413	0.05811	0.09483	0.11999	0.15830		
3.68		0.02093	0.04801	0.08970	0.11839	0.16226		
3.76		0.00760	0.03811	0.08540	0.11813	0.16840		
3.84		−0.00596	0.02833	0.08193	0.11926			
3.92		−0.01981	0.01858	0.07927	0.12188			
4.00			0.00877	0.07743	0.12610			
4.08			−0.00115	0.07644				
4.16			−0.01127	0.07630				
4.24				0.07708				
4.32				0.07882				
4.40				0.08159				

$Z=81$	$-a_2$	w_0	w_i	Z_i
Case 1	1.6080		3.1413	22.94
Case 2	1.6060		3.8050	13.08
Case 3	1.6058		4.0707	10.30
Case 4	1.6055	4.3733		
Case 5	1.6053	3.9987		
Case 6	1.6050	3.7549		
Case 7	1.6040	3.4091		
Case 8	1.6030	3.2392		

TABLE XXII. Solutions of the FTD equation ($Z=84$).

w	Case 1 2ψ	Case 2 2ψ	Case 3 2ψ	Case 4 2ψ	Case 5 2ψ	Case 6 2ψ	Case 7 2ψ	Case 8 2ψ	Case 9 2ψ
0.08	1.99020	1.99020	1.99020	1.99020	1.99020	1.99020	1.99020	1.99020	1.99021
0.16	1.96273	1.96274	1.96274	1.96275	1.96275	1.96275	1.96275	1.96275	1.96275
0.24	1.92039	1.92041	1.92043	1.92043	1.92043	1.92043	1.92043	1.92044	1.92044
0.32	1.86585	1.86589	1.86592	1.86593	1.86594	1.86594	1.86594	1.86594	1.86595
0.40	1.80161	1.80168	1.80173	1.80174	1.80174	1.80175	1.80175	1.80176	1.80177
0.48	1.72994	1.73004	1.73011	1.73013	1.73013	1.73014	1.73014	1.73015	1.73018
0.56	1.65288	1.65301	1.65311	1.65314	1.65315	1.65315	1.65316	1.65317	1.65321
0.64	1.57223	1.57240	1.57253	1.57257	1.57258	1.57258	1.57259	1.57261	1.57266
0.72	1.48954	1.48976	1.48992	1.48997	1.48999	1.48999	1.49000	1.49003	1.49008
0.80	1.40612	1.40639	1.40660	1.40667	1.40668	1.40669	1.40670	1.40674	1.40681
0.88	1.32308	1.32342	1.32367	1.32376	1.32377	1.32378	1.32380	1.32384	1.32392
0.96	1.24131	1.24172	1.24203	1.24213	1.24216	1.24217	1.24219	1.24224	1.24234
1.04	1.16153	1.16203	1.16240	1.16253	1.16255	1.16256	1.16259	1.16265	1.16278
1.12	1.08430	1.08490	1.08534	1.08549	1.08552	1.08553	1.08556	1.08564	1.08579
1.20	1.01003	1.01074	1.01126	1.01144	1.01148	1.01150	1.01153	1.01162	1.01179
1.28	0.93901	0.93985	0.94047	0.94068	0.94073	0.94074	0.94079	0.94089	0.94110
1.36	0.87144	0.87243	0.87316	0.87341	0.87346	0.87348	0.87353	0.87365	0.87389
1.44	0.80742	0.80858	0.80943	0.80972	0.80978	0.80981	0.80987	0.81001	0.81030
1.52	0.74699	0.74834	0.74934	0.74968	0.74975	0.74978	0.74985	0.75001	0.75035
1.60	0.69012	0.69169	0.69285	0.69325	0.69333	0.69337	0.69345	0.69364	0.69403
1.68	0.63674	0.63857	0.63992	0.64038	0.64048	0.64052	0.64061	0.64083	0.64129
1.76	0.58676	0.58887	0.59045	0.59098	0.59109	0.59114	0.59125	0.59150	0.59203
1.84	0.54003	0.54248	0.54430	0.54493	0.54505	0.54511	0.54523	0.54553	0.54614
1.92	0.49641	0.49925	0.50136	0.50207	0.50222	0.50228	0.50243	0.50278	0.50348
2.00	0.45573	0.45901	0.46145	0.46228	0.46244	0.46252	0.46269	0.46309	0.46390
2.08	0.41781	0.42160	0.42441	0.42537	0.42556	0.42565	0.42585	0.42631	0.42725
2.16	0.38248	0.38685	0.39010	0.39120	0.39142	0.39152	0.39175	0.39228	0.39337
2.24	0.34955	0.35459	0.35832	0.35960	0.35985	0.35996	0.36022	0.36084	0.36209
2.32	0.31883	0.32463	0.32893	0.33039	0.33069	0.33082	0.33112	0.33183	0.33327
2.40	0.29015	0.29681	0.30175	0.30344	0.30378	0.30393	0.30427	0.30509	0.30675
2.48	0.26331	0.27096	0.27664	0.27858	0.27896	0.27914	0.27953	0.28047	0.28238
2.56	0.23814	0.24692	0.25343	0.25566	0.25611	0.25631	0.25676	0.25783	0.26003
2.64	0.21446	0.22452	0.23200	0.23455	0.23506	0.23529	0.23581	0.23705	0.23956
2.72	0.19210	0.20362	0.21219	0.21512	0.21570	0.21597	0.21656	0.21798	0.22086
2.80	0.17088	0.18407	0.19388	0.19723	0.19790	0.19820	0.19889	0.20050	0.20381
2.88	0.15065	0.16572	0.17694	0.18078	0.18154	0.18189	0.18267	0.18452	0.18830
2.96	0.13124	0.14844	0.16125	0.16564	0.16652	0.16691	0.16781	0.16993	0.17425
3.04	0.11247	0.13208	0.14671	0.15173	0.15272	0.15318	0.15420	0.15662	0.16157
3.12	0.09419	0.11652	0.13320	0.13893	0.14007	0.14059	0.14176	0.14452	0.15017
3.20	0.07625	0.10163	0.12064	0.12717	0.12847	0.12907	0.13040	0.13355	0.14000
3.28	0.05848	0.08729	0.10892	0.11636	0.11785	0.11852	0.12004	0.12364	0.13100
3.36	0.04072	0.07336	0.09795	0.10643	0.10812	0.10889	0.11062	0.11472	0.12312
3.44	0.02284	0.05974	0.08765	0.09730	0.09923	0.10010	0.10207	0.10675	0.11632
3.52	0.00468	0.04630	0.07795	0.08891	0.09110	0.09210	0.09434	0.09967	0.11057
3.60	−0.01384	0.03292	0.06875	0.08120	0.08370	0.08483	0.08738	0.09344	0.10586
3.68		0.01950	0.05999	0.07412	0.07695	0.07824	0.08114	0.08803	0.10218
3.76		0.00592	0.05159	0.06761	0.07083	0.07229	0.07558	0.08342	0.09953
3.84		−0.00790	0.04348	0.06162	0.06528	0.06693	0.07067	0.07958	0.09793
3.92			0.03559	0.05613	0.06027	0.06215	0.06639	0.07651	0.09742
4.00			0.02785	0.05107	0.05577	0.05790	0.06271	0.07421	0.09803
4.08			0.02021	0.04642	0.05174	0.05416	0.05962	0.07269	0.09983
4.16			0.01258	0.04215	0.04817	0.05091	0.05711	0.07196	0.10292
4.24			0.00492	0.03822	0.04504	0.04814	0.05517	0.07204	
4.32			−0.00284	0.03461	0.04232	0.04583	0.05380	0.07299	
4.40			−0.01075	0.03129	0.04000	0.04398	0.05302	0.07485	
4.48				0.02823	0.03808	0.04259	0.05285	0.07770	
4.56				0.02541	0.03655	0.04165	0.05330		
4.64				0.02281	0.03541	0.04119	0.05441		
4.72				0.02042	0.03466	0.04120	0.05623		
4.80				0.01821	0.03430	0.04173			
4.88				0.01617	0.03436	0.04279			
4.96				0.01429	0.03486				
5.04				0.01254	0.03581				
5.12				0.01092					
5.20				0.00941					
5.28				0.00800					
5.36				0.00668					
5.44				0.00544					
5.52				0.00426					
5.60				0.00314					
5.68				0.00205					
5.76				0.00100					
5.84				−0.00002					

$Z=84$	$-a_2$	w_0	w_i	Z_i
Case 1	1.6060		3.5404	17.13
Case 2	1.6056		3.7944	13.75
Case 3	1.6053		4.2908	8.770
Case 4	1.6052		5.8380	1.576
Case 5	1.60518	5.0304		
Case 6	1.60517	4.8885		
Case 7	1.60515	4.6875		
Case 8	1.6051	4.4315		
Case 9	1.6050	4.1721		

TABLE XXIII. Solutions of the FTD equations ($Z=88$).

w	Case 1 2ψ	Case 2 2ψ	Case 3 2ψ	Case 4 2ψ	Case 5 2ψ	Case 6 2ψ	Case 7 2ψ	Case 8 2ψ	Case 9 2ψ
0.08	1.99020	1.99021	1.99021	1.99021	1.99021	1.99021	1.99021	1.99021	1.99021
0.16	1.96274	1.96275	1.96276	1.96276	1.96276	1.96276	1.96276	1.96276	1.96278
0.24	1.92042	1.92044	1.92045	1.92046	1.92046	1.92046	1.92047	1.92047	1.92050
0.32	1.86591	1.86595	1.86597	1.86598	1.86598	1.86599	1.86599	1.86600	1.86605
0.40	1.80170	1.80177	1.80180	1.80182	1.80182	1.80182	1.80183	1.80185	1.80193
0.48	1.73007	1.73016	1.73021	1.73023	1.73024	1.73025	1.73026	1.73028	1.73040
0.56	1.65305	1.65318	1.65325	1.65328	1.65328	1.65329	1.65331	1.65334	1.65350
0.64	1.57245	1.57262	1.57270	1.57274	1.57275	1.57277	1.57279	1.57283	1.57304
0.72	1.48980	1.49002	1.49013	1.49018	1.49019	1.49021	1.49024	1.49029	1.49056
0.80	1.40644	1.40671	1.40685	1.40692	1.40693	1.40695	1.40698	1.40705	1.40739
0.88	1.32345	1.32379	1.32396	1.32404	1.32406	1.32408	1.32413	1.32421	1.32463
0.96	1.24174	1.24215	1.24236	1.24246	1.24248	1.24251	1.24256	1.24266	1.24318
1.04	1.16202	1.16251	1.16276	1.16289	1.16291	1.16295	1.16301	1.16313	1.16376
1.12	1.08484	1.08544	1.08574	1.08589	1.08591	1.08596	1.08603	1.08618	1.08692
1.20	1.01063	1.01134	1.01169	1.01187	1.01191	1.01196	1.01205	1.01222	1.01310
1.28	0.93968	0.94052	0.94093	0.94114	0.94118	0.94125	0.94135	0.94156	0.94260
1.36	0.87217	0.87316	0.87365	0.87389	0.87394	0.87401	0.87414	0.87438	0.87560
1.44	0.80822	0.80937	0.80995	0.81024	0.81029	0.81038	0.81052	0.81081	0.81224
1.52	0.74786	0.74920	0.74987	0.75021	0.75027	0.75038	0.75054	0.75088	0.75255
1.60	0.69106	0.69263	0.69341	0.69380	0.69387	0.69399	0.69419	0.69458	0.69653
1.68	0.63776	0.63958	0.64049	0.64095	0.64103	0.64117	0.64140	0.64185	0.64412
1.76	0.58786	0.58997	0.59103	0.59156	0.59166	0.59182	0.59208	0.59261	0.59524
1.84	0.54122	0.54367	0.54489	0.54550	0.54562	0.54581	0.54611	0.54672	0.54978
1.92	0.49769	0.50053	0.50195	0.50265	0.50279	0.50300	0.50336	0.50406	0.50760
2.00	0.45712	0.46040	0.46203	0.46285	0.46301	0.46325	0.46367	0.46448	0.46857
2.08	0.41932	0.42311	0.42500	0.42594	0.42612	0.42640	0.42688	0.42782	0.43254
2.16	0.38412	0.38848	0.39066	0.39175	0.39196	0.39229	0.39284	0.39392	0.39936
2.24	0.35134	0.35636	0.35887	0.36013	0.36036	0.36074	0.36138	0.36263	0.36889
2.32	0.32079	0.32657	0.32946	0.33090	0.33117	0.33161	0.33234	0.33378	0.34099
2.40	0.29228	0.29893	0.30225	0.30391	0.30423	0.30473	0.30557	0.30722	0.31552
2.48	0.26565	0.27329	0.27710	0.27901	0.27937	0.27995	0.28091	0.28282	0.29236
2.56	0.24072	0.24948	0.25386	0.25605	0.25646	0.25712	0.25823	0.26042	0.27137
2.64	0.21731	0.22735	0.23237	0.23489	0.23536	0.23612	0.23739	0.23990	0.25247
2.72	0.19525	0.20675	0.21250	0.21539	0.21593	0.21680	0.21826	0.22113	0.23555
2.80	0.17438	0.18753	0.19412	0.19743	0.19805	0.19904	0.20071	0.20400	0.22054
2.88	0.15453	0.16957	0.17710	0.18089	0.18160	0.18273	0.18465	0.18841	0.20735
2.96	0.13555	0.15272	0.16133	0.16565	0.16646	0.16776	0.16995	0.17426	0.19595
3.04	0.11728	0.13686	0.14668	0.15163	0.15255	0.15404	0.15654	0.16146	0.18628
3.12	0.09957	0.12186	0.13307	0.13870	0.13976	0.14146	0.14431	0.14994	0.17832
3.20	0.08225	0.10760	0.12037	0.12680	0.12801	0.12994	0.13320	0.13963	0.17208
3.28	0.06518	0.09397	0.10850	0.11583	0.11721	0.11941	0.12313	0.13046	0.16755
3.36	0.04821	0.08085	0.09737	0.10571	0.10728	0.10979	0.11403	0.12238	0.16478
3.44	0.03119	0.06813	0.08689	0.09638	0.09816	0.10102	0.10585	0.11537	0.16383
3.52	0.01400	0.05570	0.07698	0.08776	0.08979	0.09303	0.09853	0.10938	0.16477
3.60	−0.00350	0.04346	0.06755	0.07979	0.08209	0.08578	0.09203	0.10439	0.16772
3.68	−0.02139	0.03128	0.05853	0.07241	0.07503	0.07922	0.08633	0.10039	0.17284
3.76		0.01909	0.04984	0.06557	0.06854	0.07330	0.08137	0.09737	0.18031
3.84		0.00676	0.04140	0.05921	0.06258	0.06798	0.07715	0.09536	
3.92		−0.00576	0.03316	0.05329	0.05711	0.06323	0.07365	0.09437	
4.00		−0.01855	0.02503	0.04776	0.05209	0.05903	0.07085	0.09444	
4.08			0.01694	0.04259	0.04748	0.05534	0.06877	0.09563	
4.16			0.00884	0.03772	0.04326	0.05216	0.06739	0.09799	
4.24			0.00064	0.03313	0.03938	0.04946	0.06675	0.10164	
4.32			−0.00768	0.02877	0.03583	0.04723	0.06686		
4.40			−0.01616	0.02461	0.03258	0.04548	0.06777		
4.48				0.02062	0.02960	0.04419	0.06951		
4.56				0.01675	0.02688	0.04338	0.07217		
4.64				0.01299	0.02439	0.04305			
4.72				0.00929	0.02212	0.04323			
4.80				0.00562	0.02006	0.04394			
4.88				0.00195	0.01818	0.04521			
4.96				−0.00174	0.01647				
5.04				−0.00549	0.01493				
5.12					0.01355				
5.20					0.01230				
5.28					0.01119				
5.36					0.01022				
5.44					0.00936				
5.52					0.00862				
5.60					0.00800				
5.68					0.00748				
5.76					0.00708				
5.84					0.00679				
5.92					0.00660				
6.00					0.00653				
6.08					0.00658				
6.16					0.00675				

$Z=88$	$-a_2$	w_0	w_i	Z_i
Case 1	1.6054		3.5841	17.36
Case 2	1.6050		3.8834	13.40
Case 3	1.6048		4.2463	9.654
Case 4	1.6047		4.9224	5.008
Case 5	1.60468	6.1224		
Case 6	1.60465	4.8680		
Case 7	1.6046	4.5063		
Case 8	1.6045	4.2098		
Case 9	1.6040	3.7237		

TABLE XXIV. Solutions of FTD equation ($Z=92$).

w	Case 1 2ψ	Case 2 2ψ	Case 3 2ψ	Case 4 2ψ	Case 5 2ψ	Case 6 2ψ	Case 7 2ψ	Case 8 2ψ
0.08	1.99021	1.99021	1.99021	1.99021	1.99021	1.99021	1.99021	1.99021
0.16	1.96275	1.96276	1.96277	1.96277	1.96277	1.96277	1.96277	1.96278
0.24	1.92045	1.92047	1.92048	1.92049	1.92049	1.92049	1.92049	1.92050
0.32	1.86596	1.86600	1.86601	1.86603	1.86603	1.86603	1.86604	1.86605
0.40	1.80177	1.80184	1.80186	1.80189	1.80189	1.80190	1.80191	1.80192
0.48	1.73017	1.73027	1.73029	1.73034	1.73034	1.73035	1.73036	1.73039
0.56	1.65319	1.65332	1.65335	1.65342	1.65342	1.65343	1.65345	1.65348
0.64	1.57261	1.57279	1.57283	1.57292	1.57292	1.57293	1.57296	1.57300
0.72	1.49001	1.49023	1.49029	1.49040	1.49040	1.49041	1.49045	1.49051
0.80	1.40668	1.40696	1.40703	1.40717	1.40718	1.40719	1.40724	1.40731
0.88	1.32373	1.32408	1.32417	1.32434	1.32434	1.32436	1.32442	1.32450
0.96	1.24206	1.24249	1.24259	1.24280	1.24281	1.24283	1.24290	1.24300
1.04	1.16237	1.16289	1.16302	1.16327	1.16328	1.16330	1.16339	1.16351
1.12	1.08524	1.08586	1.08601	1.08630	1.08632	1.08635	1.08645	1.08660
1.20	1.01106	1.01180	1.01198	1.01233	1.01235	1.01238	1.01251	1.01268
1.28	0.94014	0.94102	0.94122	0.94164	0.94166	0.94170	0.94185	0.94206
1.36	0.87267	0.87370	0.87394	0.87443	0.87445	0.87450	0.87467	0.87492
1.44	0.80875	0.80995	0.81024	0.81081	0.81084	0.81090	0.81110	0.81138
1.52	0.74841	0.74982	0.75015	0.75082	0.75085	0.75092	0.75116	0.75149
1.60	0.69164	0.69328	0.69367	0.69445	0.69449	0.69457	0.69484	0.69523
1.68	0.63837	0.64027	0.64072	0.64163	0.64167	0.64177	0.64208	0.64254
1.76	0.58848	0.59069	0.59122	0.59228	0.59232	0.59243	0.59280	0.59332
1.84	0.54187	0.54442	0.54504	0.54626	0.54632	0.54644	0.54687	0.54747
1.92	0.49836	0.50132	0.50203	0.50344	0.50351	0.50365	0.50415	0.50485
2.00	0.45780	0.46122	0.46205	0.46368	0.46375	0.46392	0.46449	0.46530
2.08	0.42002	0.42397	0.42492	0.42680	0.42689	0.42708	0.42774	0.42868
2.16	0.38484	0.38939	0.39048	0.39265	0.39276	0.39297	0.39373	0.39481
2.24	0.35206	0.35731	0.35857	0.36107	0.36119	0.36144	0.36231	0.36356
2.32	0.32152	0.32755	0.32900	0.33188	0.33202	0.33231	0.33332	0.33475
2.40	0.29303	0.29996	0.30163	0.30494	0.30510	0.30543	0.30659	0.30824
2.48	0.26641	0.27437	0.27629	0.28009	0.28027	0.28065	0.28199	0.28388
2.56	0.24149	0.25062	0.25282	0.25719	0.25740	0.25783	0.25936	0.26154
2.64	0.21808	0.22856	0.23108	0.23609	0.23633	0.23682	0.23858	0.24108
2.72	0.19604	0.20803	0.21092	0.21666	0.21693	0.21750	0.21952	0.22238
2.80	0.17518	0.18890	0.19221	0.19878	0.19909	0.19974	0.20205	0.20533
2.88	0.15535	0.17103	0.17481	0.18232	0.18268	0.18343	0.18607	0.18983
2.96	0.13638	0.15428	0.15860	0.16719	0.16760	0.16846	0.17148	0.17577
3.04	0.11813	0.13854	0.14347	0.15328	0.15375	0.15473	0.15818	0.16309
3.12	0.10043	0.12368	0.12930	0.14049	0.14103	0.14214	0.14608	0.15169
3.20	0.08314	0.10957	0.11597	0.12873	0.12935	0.13062	0.13511	0.14151
3.28	0.06609	0.09611	0.10340	0.11793	0.11863	0.12008	0.12520	0.13251
3.36	0.04916	0.08319	0.09147	0.10800	0.10880	0.11045	0.11629	0.12462
3.44	0.03218	0.07069	0.08008	0.09888	0.09979	0.10167	0.10832	0.11781
3.52	0.01503	0.05851	0.06915	0.09050	0.09154	0.09368	0.10124	0.11206
3.60	−0.00242	0.04654	0.05859	0.08280	0.08398	0.08641	0.09502	0.10734
3.68		0.03468	0.04829	0.07574	0.07708	0.07984	0.08963	0.10364
3.76		0.02283	0.03818	0.06925	0.07077	0.07390	0.08503	0.10099
3.84		0.01089	0.02816	0.06329	0.06502	0.06857	0.08121	0.09937
3.92		−0.00121	0.01816	0.05783	0.05978	0.06382	0.07816	0.09884
4.00			0.00808	0.05281	0.05502	0.05960	0.07588	0.09944
4.08			−0.00213	0.04821	0.05072	0.05590	0.07438	0.10122
4.16				0.04400	0.04683	0.05270	0.07368	0.10427
4.24				0.04013	0.04334	0.04998	0.07381	
4.32				0.03660	0.04022	0.04774	0.07479	
4.40				0.03336	0.03746	0.04596	0.07670	
4.48				0.03041	0.03503	0.04466	0.07960	
4.56				0.02771	0.03293	0.04382		
4.64				0.02525	0.03115	0.04347		
4.72				0.02302	0.02968	0.04362		
4.80				0.02100	0.02851	0.04430		
4.88				0.01917	0.02764	0.04553		
4.96				0.01752	0.02708			
5.04				0.01605	0.02684			
5.12				0.01474	0.02692			
5.20				0.01358	0.02734			
5.28				0.01257	0.02813			
5.36				0.01171				
5.44				0.01098				
5.52				0.01039				
5.60				0.00994				
5.68				0.00962				
5.76				0.00944				
5.84				0.00940				
5.92				0.00951				
6.00				0.00977				

$Z=92$	$-a_2$	w_0	w_i	Z_i
Case 1	1.60492		3.5889	18.15
Case 2	1.6045		3.9120	13.73
Case 3	1.6044		4.0634	12.00
Case 4	1.6042	5.9577		
Case 5	1.60419	5.2540		
Case 6	1.60417	4.8749		
Case 7	1.6041	4.4328		
Case 8	1.6040	4.1773		

A New Type of Short Wavelength Absorption Band in Alkali Halides Containing Color Centers

CHARLES J. DELBECQ, PETER PRINGSHEIM, AND PHILIP YUSTER
Argonne National Laboratory, Chicago, Illinois

(Received January 29, 1951)

Photo-chemically and additively colored potassium iodide crystals exhibit absorption bands in the ultraviolet which do not have the characteristic properties of V-bands. An interpretation of the origin of these bands is proposed.

INTRODUCTION

IRRADIATION of a potassium iodide crystal at room temperature with soft x-rays produces, along with the usual F-band, a relatively sharp band in the ultraviolet region of the spectrum. This ultraviolet band has its peak near 235 mμ when the absorption spectrum of the irradiated crystal is measured at room temperature.[1,2] An additional weak and poorly defined band stretches from about 280 to 380 mμ and thus covers the same spectral region as the bands observed by Mollwo[3] in potassium iodide crystals containing an excess of iodine. According to Seitz,[4] the band found by Mollwo should be a V-band characteristic of potassium iodide. However, the nature of this band is still quite uncertain and shall not be treated in the present paper. On the other hand, the band at 235 mμ, which will be called the β-band, has a property characteristic of V-bands in that it is bleached simultaneously with the F-band when the crystal is exposed to F-light. Nevertheless, the experiments described in this paper seem to prove that the β-band is of another type.

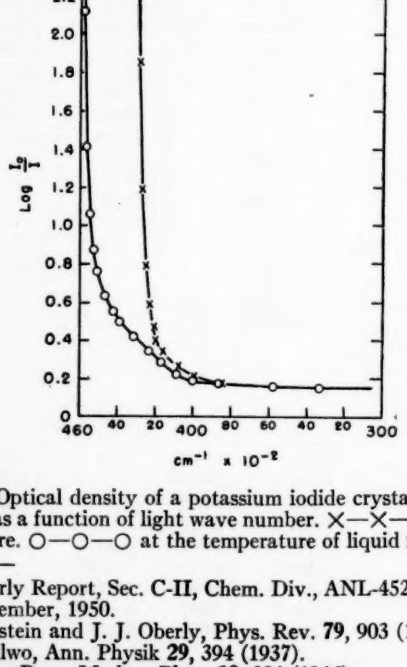

FIG. 1. Optical density of a potassium iodide crystal measured *versus* air as a function of light wave number. ×—×—× at room temperature. ○—○—○ at the temperature of liquid nitrogen.

EXPERIMENTAL METHODS

The material used in our investigations consisted, in part, of crystals grown in our laboratory by means of the Kyropoulos method* from Baker and Adamson reagent grade potassium iodide and, in part, of potassium iodide crystals obtained from the Harshaw Chemical Company. In our experiments we found no appreciable difference in the behavior of the two kinds of crystals.

Color centers were produced in the crystals in two different ways—photo-chemically and additively. The photo-chemical coloration was obtained by exposure to x-rays (50 kv, 45 ma, W target) transmitted through a beryllium window. Additively colored potassium iodide crystals were prepared by heating rectangular blocks of potassium iodide, 12 mm×8 mm×4 mm, for three hours at 500°C in an atmosphere of sodium vapor in an evacuated Pyrex tube. Subsequently, the Pyrex tube was quenched in a stream of cold air. After the outermost parts of the potassium iodide block had been removed, plates from 0.5 to 1 mm thick were cleaved from the interior and were used in our measurements.

As mentioned previously by Smakula[5] and shown in Fig. 1, the first fundamental absorption band of potassium iodide, which at room temperature has its peak at 220 mμ, has a long wavelength tail which extends well beyond 240 mμ. At the temperature of liquid nitrogen, the peak of the fundamental band is shifted to 211 mμ,[6] and the long wavelength tail is also displaced toward shorter wavelength (Fig. 1). In a potassium iodide crystal containing color centers, the β-band, which appears at 235 mμ when measured at room temperature, is shifted to 226 mμ when measured at liquid nitrogen temperature. The tail of the fundamental band and the β-band are better separated at low temperatures, and, therefore, all measurements of absorption spectra mentioned in the following paragraphs were performed at liquid nitrogen temperature using a

[1] Quarterly Report, Sec. C-II, Chem. Div., ANL-4526, Sec. 1.7, April-September, 1950.
[2] E. Burstein and J. J. Oberly, Phys. Rev. **79**, 903 (1950).
[3] E. Mollwo, Ann. Physik **29**, 394 (1937).
[4] F. Seitz, Revs. Modern Phys. **18**, 384 (1946).

* We want to express our thanks to Ruth Casler Voreck who helped us greatly by growing and cleaving the crystals.
[5] A. Smakula, Z. Physik **63**, 762 (1930).
[6] H. Fesefeld, Z. Physik **64**, 626 (1930).

Beckman spectrophotometer in combination with the Dewar tube, which has been described in a preceding paper.[7]

In the apparatus which was used for these experiments, the comparison blank could only be maintained at room temperature. From Fig. 1 it is obvious that total absorption would take place in the comparison blank at approximately 233 mμ, and, consequently, in order to take advantage of the fact that the tail of the fundamental band shifts toward shorter wavelengths at liquid nitrogen temperature, measurements were made using air as blank. Using air as blank also has the advantage that the slit of the spectrophotometer need not be opened as wide as would be necessary for directly comparing the colored plate with a blank which itself has a great absorbing power in the spectral region under consideration. Even without any absorbing medium in the light path, the slit width must be made fairly large for light of wavelengths below 230 mμ. By observing, at a constant wavelength, the change in the measured absorption which is caused by a change in the slit width, it was ascertained that, in a range of very steeply rising absorption, the use of a wide slit can appreciably affect the result. All measurements on photo-chemically colored crystals were therefore made *versus* air, first with the fresh sample and then with the same sample after irradiation; the absorption coefficients were determined as the differences between the two measurements. The same method could not be applied to additively colored samples; in this case a blank was cleaved from a block before the block was heated in a sodium vapor atmosphere, and the thickness of the plate cleaved from the large colored block was made as nearly equal to that of the blank as possible. The points for the absorption curves of additively colored crystals were obtained by subtracting the readings of the blank *versus* air from those of the colored crystal *versus* air. Such absorption curves can be in error, because it was found that blanks selected from the same lot grown in our laboratory or obtained from Harshaw sometimes varied appreciably in their absorption coefficients near the tail of the fundamental band.

Even at liquid nitrogen temperature the β-band is superimposed upon the steeply rising long wavelength branch of the fundamental band, and, therefore, the final absorption values may be in error for both photochemically colored and additively colored crystals since they are obtained as relatively small differences of two large numbers (absorptions in the colored sample and in the blank). Because of the above facts these data for the absorption in the ultraviolet are somewhat less accurate than those obtained in other spectral regions such as the visible, but they are quite reliable in their general trend.

[7] Casler, Pringsheim, and Yuster, J. Chem. Phys. **18**, 887 (1950).

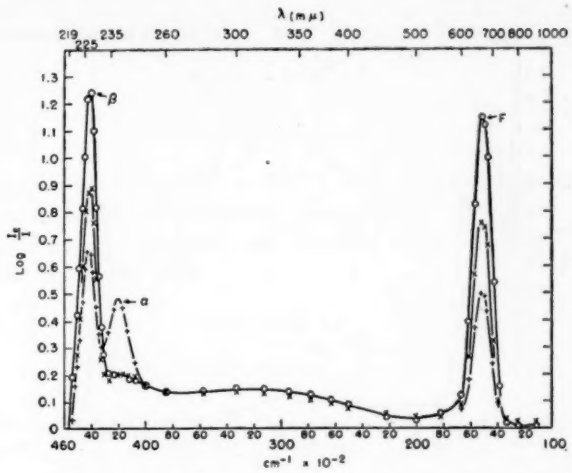

FIG. 2. Changes in the absorption in a potassium iodide crystal due to treatment as indicated (all measurements made at liquid nitrogen temperature). ○—○—○ 20-minutes exposure to soft x-rays at room temperature. ×—×—× 75 hours in dark at room temperature. +—+—+ 35 minutes bleach with *F*-light at liquid nitrogen temperature.

EXPERIMENTAL RESULTS

When a potassium iodide crystal is exposed for 20 minutes at room temperature to soft x-rays, it exhibits *F*- and β-bands of about the same height and half-width (Fig. 2). After standing in the dark for 75 hours, both bands have dropped by about the same amount. If subsequently the crystal is irradiated at liquid nitrogen temperature with *F*-light, both bands drop again, and simultaneously a new band with peak at 238 mμ appears. This new band, which will be called the α-band, is still fairly stable at dry ice temperature but vanishes very soon when the crystal is warmed up to room temperature.

If a potassium iodide crystal is exposed to x-rays at dry ice temperature or at the temperature of liquid nitrogen, the α-band is formed simultaneously with the *F*- and β-bands.† After *F*-light irradiation at liquid nitrogen temperature, the α-band is greatly enhanced, while the *F*-band and the β-band drop by similar amounts (Fig. 3). Figure 3 differs from Fig. 2 in that the short wavelength branch of the β-band drops to zero at 220 mμ in the latter, while in the former there is a steep rise below 222 mμ which is further increased when the crystal is exposed to *F*-light. The *F*-, α-, and β-bands vanish completely when the crystal in which the color centers were produced at low temperature is warmed up to room temperature, while in the crystal x-rayed at room temperature the *F*- and β-bands persist through long periods of time (Fig. 2). This behavior is in agreement with the experience obtained with other alkali halides: color centers produced at low temperatures are always less stable than those produced at

† After irradiating potassium iodide with x-rays at the temperature of liquid nitrogen, Burstein and Oberly (reference 2) observed an absorption band near 2300A which is apparently identical with our α-band.

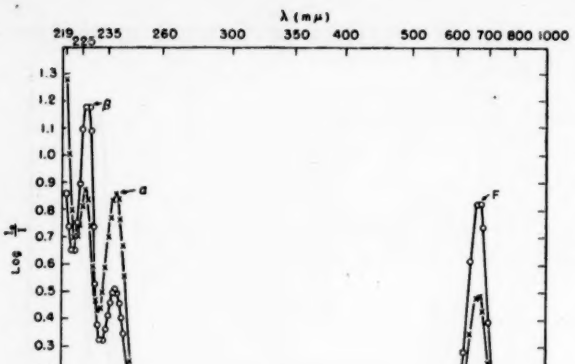

FIG. 3. Changes in the absorption in a potassium iodide crystal due to treatment as indicated (all measurements made at liquid nitrogen temperature). O—O—O 2 minutes exposure to soft x-rays at dry ice temperature. ×—×—× 15 minutes bleach with light of $\lambda > 580$ mμ at liquid nitrogen temperature.

higher temperatures, supposedly because of the different nature of the V-centers formed preferentially at various temperatures.

Figure 4 represents the behavior of an additively colored potassium iodide crystal which is quite analogous to that of samples photo-chemically colored at room temperature. The β-band, as well as the F-band, is present in the spectrum of the freshly colored crystal, while the α-band is absent. By irradiation with F-light at liquid nitrogen temperature, the intensities of the F-band and the β-band are decreased, and the α-band appears. Simultaneously, the absorption on the long wavelength side of the F-band increases appreciably, owing to the formation of F'-centers. This phenomenon can be seen to a much lesser degree in Fig. 2 and even less distinctly in Fig. 3. Positive holes are present in the photo-chemically colored crystals of Figs. 2 and 3,

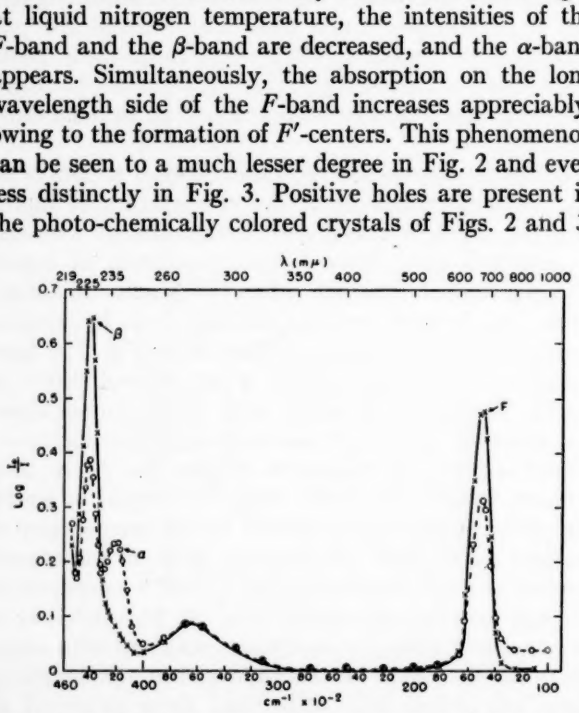

FIG. 4. Changes in the absorption in a potassium iodide crystal due to treatment as indicated (all measurements made at liquid nitrogen temperature). ×—×—× additively colored in sodium vapor. O—O—O bleached with F-light at liquid nitrogen temperature.

and most of the drop in F-band intensity is due to real, nonreversible bleaching caused by recombination of F-center electrons with positive holes. In the additively colored crystal no positive holes are present, and the bleaching in the F- and β-bands, accompanied by the formation of F'-centers, is reversible. If, after bleaching an additively colored crystal at liquid nitrogen temperature with F-light, such a crystal is exposed to light of wavelengths longer than 760 mμ, which is absorbed by F'-centers, the F'-band and the α-band drop, while the F-band and the β-band are enhanced. When the crystal is warmed up to room temperature, it is completely restored to its initial state with only the F- and β-bands present in its absorption spectrum. The low wide band with peak at 275 mμ (36400 cm^{-1}), which may originate from some unknown impurity, is not affected by the various treatments mentioned in this paragraph.

DISCUSSION OF RESULTS

The mere fact that the F-band and the β-band appear in additively colored crystals with about the same relative intensity as in photo-chemically colored samples proves that the β-band cannot be ascribed to V-centers —positive holes stabilized somewhere in the crystal lattice. In addition to the observations described above, which prove that the β-band cannot be ascribed to V-centers, such an assumption seems to be contradicted also by the following discussion. One might perhaps admit that, while some of the electrons ejected from F-centers by light absorption recombine with V-centers (β-centers), others are captured elsewhere forming new electron surplus centers (α-centers). It is highly improbable, however, that electrons ejected from F'-centers should contribute to weakening the α-band if one does not assume that the existence of this band is directly coupled with the existence of F'-centers. Yet Figs. 2 and 3 prove that this coupling does not exist; they show high α-band intensities and very low F'-bands.

The observations regarding the new bands, which have been termed α and β in order to differentiate them from the well-known electron surplus bands (F, F', M, etc.) and electron deficiency bands (V), can be interpreted by another hypothesis. It may be emphasized once more that the bands α and β are superimposed on the steep slope of the tail of the first fundamental absorption band which is supposedly due to perturbations caused by the various lattice defects. The presence of certain well-defined singularities in sufficient numbers, such as negative ion vacancies or F-centers, may affect the first fundamental frequency of the crystal in such a way that new well-defined absorption bands corresponding to perturbed transitions of the valency electrons of the adjacent halide ions appear superimposed on the tail of the fundamental absorption band. According to this hypothesis, the β-band is due to the presence of F-centers, and the α-band to the

presence of isolated negative ion vacancies. The latter are assumed to be quite unstable at room temperature, having a high probability of combining with positive ion vacancies to form doublets, quartets, etc., and it is supposed that under these conditions they produce no new selective absorption bands in the spectral region accessible to the Beckman spectrophotometer. At liquid nitrogen temperature, on the other hand, the mobility of the ion vacancies is so low that a negative ion vacancy, once formed by the ejection of an electron from an F-center, does not vanish again without an external cause. If the above assumptions are correct, the following should hold true: (1) the ratio of the areas under the F- and β-bands should be a constant; (2) at temperatures at which single negative ion vacancies are stable, the disappearance of F-centers caused by bleaching with F-light should be followed by the appearance of α-centers.

Since the areas covered by the F- and β-bands and the changes in these areas during experiments are of the same order of magnitude, it follows that (1) is valid. The comparison of the areas under the F- and α-bands is not quite so simple. Representing the areas under the F- and α-bands by (F) and (α), and the number of negative ion vacancies by (v^-), our hypothesis asserts that

$$(\alpha)=k(v^-),$$

where k is a constant. When an additively colored crystal is bleached at liquid nitrogen temperature with F-light, F'-centers are formed, and, therefore, one negative ion vacancy is formed for every two F-centers destroyed. When, on the other hand, the F-band of a photo-chemically colored crystal is bleached at liquid nitrogen temperature with F-light, all of the electrons released from the F-centers may be captured by V-centers; in this case one negative ion vacancy is formed for each F-center destroyed. Then the relation between the decrease in area under the F-band and the increase in the number of negative ion vacancies is for the two cases given by

$$\Delta(F)_a=2k'\Delta(v^-)_a,$$

and

$$\Delta(F)_p=k'\Delta(v^-)_p,$$

where the subscripts a and p refer to additive and photo-chemical coloration, respectively, and k' is a constant. Rearranging and dividing these two expressions gives the ratio

$$\frac{\Delta(F)_a/\Delta(v^-)_a}{\Delta(F)_p/\Delta(v^-)_p}=2.$$

Experimentally, the ratio is found to be between 1.5 and 2, and this can be interpreted as indicating that, even in photo-chemically colored crystals, the fraction of the F-centers which, by bleaching, is converted into F'-centers is not quite negligible.

It does not seem that the appearance of bands of the type described in this paper is restricted to potassium iodide (see also reference 2). The peak of the first fundamental absorption band of potassium bromide at room temperature lies at 188 mμ, and its tail can be followed up to about 220 mμ; at liquid nitrogen temperature the latter is shifted toward shorter wavelengths by about 10 mμ.[4] After irradiation with x-rays at room temperature, the intensity of the absorption in the region below 215 mμ is enhanced: this may be ascribed to the formation of a β-band. By irradiation with F-light at room temperature this absorption is decreased and simultaneously a drop in the F-band is noticed. At the temperature of liquid nitrogen the β-band is shifted beyond the accessible spectral range of the Beckman spectrophotometer, but if the crystal is exposed to F-light at liquid nitrogen temperature, the absorption in the region below 210 mμ is increased, corresponding to the formation of an α-band.

We expect to continue the measurements on potassium bromide and other halide crystals soon with an instrument that is capable of measurements below 2000A.

The Concentration Dependence of the Viscosity of Solutions of Macromolecules

JACOB RISEMAN
International Resistance Company, Philadelphia, Pennsylvania

AND

ROBERT ULLMAN*
Department of Mathematics, Polytechnic Institute of Brooklyn, Brooklyn, New York

(Received January 2, 1951)

The theory of the concentration dependence of the viscosities of solutions is developed for the dumbbell, rigid rod, and flexible chain macromolecules. Both the intramolecular hydrodynamic interactions between the monomer units of the same molecule and the intermolecular interactions between monomer units of different molecules are considered. The methods of Riseman and Kirkwood are applied throughout. The numerical result of the calculation for the dumbbell shaped molecule is compared with that obtained by Simha.

INTRODUCTION

THE use of viscosity measurements as a means of obtaining information about the molecular structure and properties of macromolecules in solution has resulted in a number of theories which have attempted to interpret this phenomenon. In general, these theories have restricted themselves to a concentration range such that the over-all influence of the solute particles on the original solvent viscosity is a linear superposition of the effect of each individual particle. That is, each particle is to be treated separately, as in the case of the infinitely dilute solution. In order to consider solutions of finite concentration, we must account for the hydrodynamic interactions of the particle. Guth and Simha,[1,2] using the results of Smoluchowski,[3] considered solutions of spherical and dumbbell-shaped particles, respectively, and calculated the first interaction coefficient, which appears in the viscosity equation as a term quadratic in concentration.

In considering the question of hydrodynamic interaction, it is worth while recalling that the reason for the failure of the Staudinger law to relate quantitatively the intrinsic viscosity of a flexible macromolecule with the first power of the molecular weight is essentially due to a neglect of the hydrodynamic interactions of the monomeric units of the polymer chain. Thus, not only must a theory of the concentration dependence of viscosity, but also that of intrinsic viscosity, take into consideration the existence of hydrodynamic interactions. In the latter case these interactions occur only between parts of the same molecule, whereas in the former interactions between the parts of different molecules must also be included. Conversely, one would expect that any formal method which permitted proper account to be taken of intramolecular interactions should, at least, in principle, be capable of handling intermolecular interactions. Aside from the added complexity that the latter situation introduces, a fundamental difference occurs in the calculation of average values. For a single macromolecule, one would be interested, for this purpose, in the spatial distribution of the monomeric elements of the chain, whereas for a system of macromolecules in solution, distribution functions of higher order relating to the simultaneous positions of elements of more than a single chain would be required. In particular, under a condition of high dilution, the radial distribution of the centers of mass becomes important. Kirkwood and Riseman,[4–6] in a series of papers have demonstrated a method of accounting for the intramolecular hydrodynamic interactions by utilizing a formula due to Oseen.[7,8] In accordance with what has been discussed above, we shall utilize this method to account for the hydrodynamic interactions between molecules (or their monomer units) responsible for the dependence of viscosity on concentration.

It has been empirically suggested that the viscosity of a polymer solution could be represented by a power series in concentration,[9] such that

$$\eta=\eta_0[1+[\eta]c+k'[\eta]^2c^2+\cdots], \qquad (1)$$

where η is the solution viscosity, η_0 the solvent viscosity, $[\eta]$ the intrinsic viscosity ($\lim_{c\to 0}(\eta-\eta_0)/\eta_0 c=[\eta]$), c the concentration in g/100 ml, and k' a factor supposedly independent of molecular weight, but possibly dependent on the nature of the solute-solvent system. Various other forms have also been proposed[10–12] to

* Submitted in partial fulfillment of the requirements for the Doctor of Philosophy in chemistry at the Polytechnic Institute of Brooklyn.

[1] E. Guth and R. Simha, Kolloid-Z. **74**, 266 (1936).
[2] R. Simha, J. Research Natl. Bur. Standards **42**, 409 (1949).
[3] M. Smoluchowski, Bull. Acad. Sci. Cracovie **1A**, 28 (1911).
[4] J. G. Kirkwood and J. Riseman, J. Chem. Phys. **16**, 565 (1948).
[5] J. Riseman and J. G. Kirkwood, J. Chem. Phys. **17**, 442 (1949).
[6] J. Riseman and J. G. Kirkwood, J. Chem. Phys. **18**, 512 (1950).
[7] Carl W. Oseen, Hydrodynamik (Akademische Verlagsgesellschaft, Leipzig, 1927).
[8] J. M. Burgers, *Second Report on Viscosity and Plasticity* (Noord-Hollandsche Uitgeversmaatschappij, Amsterdam, 1938), Chapter III, N.V.
[9] M. L. Huggins, J. Am. Chem. Soc. **64**, 2716 (1942).
[10] W. Phillipoff and K. Hess, Z. physik. Chem. **B31**, 237 (1936).
[11] H. Fikentscher and H. Mark, Kolloid-Z. **49**, 135 (1929).
[12] F. Eirich, Repts. Prog. Phys. **7**, 329 (1940).

represent the course of the behavior of viscosity with concentration.

We shall show in this paper, that subject to certain approximations Eq. (1) does indeed represent the behavior of the viscosity of a solution with concentration. Also, since the results of Smoluchowski have been used previously in treating this problem, we shall show that the latter are essentially a first-order approximation of those obtained here. Accordingly, the Smoluchowski equation, the modified form used by Simha, and a generalization of that equation will be derived. In so far as we shall have occasion to make use of the intrinsic viscosity results for a dumbbell-shaped particle, we shall also derive that expression, in which the mutual hydrodynamic interactions between the parts of the same molecule will be taken into account. The symbols and terminology used here are similar, for the most part, to those used in the previous papers[4–6] mentioned, and the reader is referred to those papers for additional details.

SMOLUCHOWSKI'S RESULTS AND THE INTRINSIC VISCOSITY OF A DUMBBELL-SHAPED PARTICLE

Smoluchowski considered the effect of a second particle on the velocity distribution around a spherical particle with translational motion in a viscous fluid, originally described[13] by Stokes. In particular, he obtained the result that the familiar frictional resistance, as given by Stokes had to be modified such that the resistance was no longer in the direction of motion, and furthermore depended inversely on distance of separation of the two particles. If the velocities of the two particles are the same, it becomes clear that the frictional coefficient loses its scalar character, and becomes a tensor quantity. In the same way, we shall show that in the more general case, where the velocities are not similar, a tensor frictional resistance constant can be defined.

The velocity field in the neighborhood of an arbitrary point in a fluid in which a set of particles exerting forces on the fluid are present, can be described, as has already been discussed,[4] by means of a formula due to Oseen.[7,8] Thus, if a particle labeled l, at distance $\mathbf{R}_l$ from the point under consideration, exerts a force $\mathbf{F}_l$ on the fluid, the velocity at this point is given by

$$\begin{aligned} \mathbf{v}&=\mathbf{v}^0-\zeta\textstyle\sum_l \mathbf{T}(\mathbf{R}_l)\cdot\mathbf{w}_l,\\ \mathbf{F}_l&=-\zeta\mathbf{w}_l,\\ \mathbf{w}_l&=\mathbf{v}_l-\mathbf{u}_l,\\ \mathbf{T}(\mathbf{R}_l)&=(1/8\pi\eta_0 R_l)\{\mathbf{I}+\mathbf{R}_l\mathbf{R}_l/R_l^2\}, \end{aligned} \tag{2}$$

where ζ is a scalar friction constant, $\mathbf{v}_l$ the velocity the fluid would possess at the point of location of particle l if that particle were not present, $\mathbf{u}_l$ the velocity with which particle l is moving, $\mathbf{v}^0$ and $\mathbf{v}$ the original and perturbed fluid velocities, respectively, at the point in question, and η_0 the fluid viscosity. The relative velocities $\mathbf{w}_l$, are in turn obtained from the set of equations (2), written alternatively as

$$\begin{aligned} \mathbf{w}_l&=\mathbf{w}_l{}^0-\zeta\textstyle\sum_{s\neq l}\mathbf{T}_{ls}\cdot\mathbf{w}_s,\\ \mathbf{F}_l&=-\zeta\mathbf{w}_l{}^0-\zeta\textstyle\sum_{s\neq l}\mathbf{T}_{ls}\cdot\mathbf{F}_s,\\ \mathbf{w}_l{}^0&=\mathbf{v}_l{}^0-\mathbf{u}_l,\\ \mathbf{T}_{ls}&=(1/8\pi\eta_0 R_{ls})\{\mathbf{I}+\mathbf{R}_{ls}\mathbf{R}_{ls}/R_{ls}^2\}. \end{aligned} \tag{3}$$

Equations (2) and (3) suffice to describe the hydrodynamic behavior of the system and form the basis of our future considerations.

Let us consider first the case treated by Smoluchowski, in which only 2 spherical particles labeled 1 and 2 are present: ζ is then equal to $6\pi\eta_0 a$ (Stokes' result), and the sum in Eq. (3) reduces to a single term. $\mathbf{w}_l$ is set equal to $\mathbf{w}_1{}^0$ and $\mathbf{w}_2{}^0$, respectively; and as a first approximation the 2 members of the set of equations (3) are solved by a method of iteration. Setting $\mathbf{F}_1$ and $\mathbf{F}_2$ equal to $\mathbf{F}_1{}^0$ and $\mathbf{F}_2{}^0$, respectively, makes Eqs. (2) and (3) yield

$$\begin{aligned} \mathbf{F}_1&=-\zeta\{\mathbf{w}_1{}^0+\mathbf{T}_{12}\cdot\mathbf{F}_2\},\\ \mathbf{F}_2{}^0&=-\zeta\mathbf{w}_2{}^0. \end{aligned} \tag{4}$$

If $\mathbf{w}_1{}^0$ were equal to $\mathbf{w}_2{}^0$, Eqs. (4) would be Smoluchowski's results. As written, these equations are a slightly modified form of the Smoluchowski equations mentioned by Simha.[2] Written out explicity, Eqs. (4) become

$$\begin{aligned} \mathbf{F}_1=-6\pi\eta_0 a\{&\mathbf{w}_1{}^0-(3a/4R_{12})\mathbf{w}_2{}^0\\ &-(3a/4R_{12}{}^3)\mathbf{R}_{12}(\mathbf{R}_{12}\cdot\mathbf{w}_2{}^0)\}. \end{aligned} \tag{4a}$$

With $\mathbf{w}_1{}^0$ equal to $\mathbf{w}_2{}^0$ Eqs. (4) can be rewritten

$$\begin{aligned} \mathbf{F}_1&=-\mathbf{Z}\cdot\mathbf{w}_1{}^0,\\ \mathbf{Z}&=\zeta\{\mathbf{I}-\zeta\mathbf{T}_{12}\},\\ \zeta&=6\pi\eta_0 a, \end{aligned} \tag{4b}$$

which defines the tensor frictional coefficient $\mathbf{Z}$ and results, as seen in Eq. (4a), in a frictional resistance not in the same direction as the motion. With $\mathbf{w}_1{}^0$ unequal to $\mathbf{w}_2{}^0$, the tensor frictional coefficient itself becomes a quantity dependent on the motion of both particles:

$$\begin{aligned} \mathbf{F}_1&=\zeta\{\mathbf{I}-\mathbf{S}\}\cdot\mathbf{w}_1{}^0,\\ \mathbf{S}&=\zeta(\mathbf{T}_{12}\cdot\mathbf{w}_2{}^0)\mathbf{w}_1{}^0/\mathbf{w}_1{}^0\cdot\mathbf{w}_1{}^0. \end{aligned} \tag{4c}$$

The above considerations lend themselves to an interesting interpretation of the effect of additional particles on the frictional coefficient, namely, the phenomenon of concentration dependence. Working from Eq. (4), we may consider the frictional coefficient as immediately dependent only upon the nature of the particle and the fluid with which it is in contact; the proper frictional resistance is obtained by the use of the correct value of the relative velocity, since the bracketed quantity in Eq. (4) is just the relative velocity at the point of location of particle 1. On the other hand, if the velocity is taken as the original velocity $\mathbf{w}_1{}^0$, one obtains, as seen from Eqs. (4b) or (4c), a tensor fric-

[13] Horace Lamb, *Hydrodynamics* (Dover Publications, New York, 1945), p. 602.

tional coefficient which is dependent upon interparticle distance, and therefore upon concentration as well. Consequently, we note that the effect of concentration can be placed either in the velocity term, since each particle will join in influencing the velocity distribution, or placed in a "concentration dependent" frictional coefficient.

For a single spherical particle ($\zeta=6\pi\eta_0 a$), Eq. (2) leads to the Stokes' velocity distribution. A pair of spherical particles and the same approximations that led to Eqs. (4) result in a velocity distribution very similar to the original equations of Smoluchowski,[3] and is essentially that used by Simha.[2] Thus approximating $\mathbf{w}_s$ by $\mathbf{w}_s^0$ in Eq. (3), and substituting into Eq. (2) gives the velocity as

$$\mathbf{v}=\mathbf{v}^0-\zeta\{\mathbf{T}(\mathbf{R}_1)\cdot\mathbf{w}_1^0-\zeta\mathbf{T}(\mathbf{R}_1)\cdot\mathbf{T}_{12}\cdot\mathbf{w}_2^0+\mathbf{T}(\mathbf{R}_2)\cdot\mathbf{w}_2^0-\zeta\mathbf{T}(\mathbf{R}_2)\cdot\mathbf{T}_{12}\cdot\mathbf{w}_1^0\}. \quad (5)$$

From the linear nature of this result, the velocity distribution at any arbitrary point may be regarded as a superposition of the effects at that point produced by each of these particles, and may be written after setting $\mathbf{v}_0$ equal to zero as

$$\mathbf{v}(1)=-\zeta\{\mathbf{T}(\mathbf{R}_1)\cdot\mathbf{w}_1^0-\zeta\mathbf{T}(\mathbf{R}_1)\cdot\mathbf{T}_{12}\cdot\mathbf{w}_2^0\}, \quad (5a)$$

where $\mathbf{v}(1)$ is the effect of the particle designated as 1 on the velocity at an arbitrary point in solution.

For a pair of particles, the two equations to which Eq. (3) reduced can be solved exactly. This result, if substituted in Eq. (2), would yield a velocity distribution of a higher degree of accuracy than the approximate methods outlined above. As can easily be verified by substitution, the solutions of Eq. (3) are

$$\mathbf{w}_1=\frac{\mathbf{w}_1^0-\zeta B\mathbf{w}_2^0-\zeta B\mathbf{e}_{12}(\mathbf{e}_{12}\cdot\mathbf{w}_2^0)}{1-\zeta^2B^2}-\frac{\zeta^2B^2\mathbf{e}_{12}}{(1-4\zeta^2B^2)(1-\zeta^2B^2)}\{\mathbf{e}_{12}\cdot\mathbf{w}_2^0-2\zeta B(\mathbf{e}_{12}\cdot\mathbf{w}_2^0)\},$$

$$B=1/8\pi\eta_0|R_{12}|, \quad (6)$$

$$\mathbf{e}_{12}=\mathbf{R}_{12}/|R_{12}|.$$

Multiplication by ζ yields the corresponding frictional resistance. If the second term, which is of the order of $\{1/R_{12}^2\}$ is dropped, and the denominator of the first term expanded to the same order, we obtain, with ζ set equal to $6\pi\eta_0 a$, the modified Smoluchowski result Eq. (4a).

If the two particles under consideration are joined so that they form a single dumbbell-shaped particle, the intrinsic viscosity is readily calculated. Referring to some earlier papers,[4,6] we have the intrinsic viscosity given by

$$[\eta]=A\zeta G/100M\eta_0,$$
$$G=-(1/\zeta\dot{\epsilon})\langle(\mathbf{R}_{01}\cdot\mathbf{e}_y)(\mathbf{F}_1\cdot\mathbf{e}_x)+(\mathbf{R}_{02}\cdot\mathbf{e}_y)(\mathbf{F}_2\cdot\mathbf{e}_x)\rangle_{Av}, \quad (7)$$
$$\mathbf{v}_l^0=\dot{\epsilon}(\mathbf{R}_{0l}\cdot\mathbf{e}_y)\mathbf{e}_x,$$

where M and A are the molecular weight and Avogadro's number, respectively. $\mathbf{R}_{0l}$ is the distance from the center of mass to element l, $\dot{\epsilon}$ is the velocity gradient, $\mathbf{e}_x$, $\mathbf{e}_y$, $\mathbf{e}_z$ are unit vectors defining a right-handed coordinate system with the origin located at the center of mass.

If overwhelming brownian movement is assumed, $\mathbf{u}_l$ may be set equal to zero.[6] The segments of the dumbbell are chosen to be spheres with frictional coefficient $\zeta=6\pi\eta_0 a$. Using Eqs. (3), (6), and (7) and averaging over all orientations of the dumbbell gives the result

$$(\eta-\eta_0)/\eta_0=\left\{\frac{3L^2}{2a^2(1-3a/8L)}+\frac{9L}{80a(1-3a/8L)(1-3a/4L)}\right\}c, \quad (8)$$

where c is the volume fraction of dumbbell particles in solution, a is the radius of the element at the end of the dumbbell, and $2L$ the length of the dumbbell. Expanding the denominators, we have for the intrinsic viscosity

$$[\eta]=\frac{\pi aL^2A}{25M}\left\{1+\frac{9}{20}\frac{a}{L}+\frac{9a^2}{40L^2}+\cdots\right\}. \quad (8a)$$

The difference between the result for the intrinsic viscosity in Eq. (8a) and the coefficient of c in Eq. (8) arises in the conversion of concentration units from volume fraction to grams per 100 ml.

This result, it should be mentioned, explicitly accounts for the higher dynamic coupling between the parts of the dumbbell. With Smoluchowski's results, only the first interaction coefficient $1+9a/20L$ [Eq. (8a)] was previously obtained.

THE CONCENTRATION DEPENDENCE OF VISCOSITY

From what has been mentioned earlier, a system of forces acting on a fluid will perturb the original flow pattern of the fluid. Furthermore, because of the linear nature of our equations, the net effect at any chosen point will be the linear superposition of the action of each of these forces. Consequently, attention is to be focused on the perturbing effect due to a single member of the force system, remembering, however, that the nature and magnitude of this force is itself dependent on the presence and distribution of the other members of the system. For a solution of high polymer molecules, the forces exerted on the fluid are those due to the frictional resistance of the monomeric elements which make up the chains. Since it is necessary to account for intermolecular as well as intramolecular efforts, a somewhat lengthy notation will be necessary. Greek letters used as superscripts will designate the different molecules, and italic letters as subscripts will designate the chain elements. Thus, the vector distance between the lth element of molecule α and the jth element of molecule β will be represented by $\mathbf{R}_{lj}^{\alpha\beta}$. Consider now

the perturbed velocity $\mathbf{v}'(\alpha)$ at some large distance, from the center of mass of molecule α. From Eq. (2) the perturbed velocity is written

$$\mathbf{v}'(\alpha)=\frac{1}{8\pi\eta_0}\sum_{l=-n}^{n}\left\{\frac{\mathbf{I}}{|\mathbf{R}_0{}^{\alpha}-\mathbf{R}_{0l}{}^{\alpha}|}+\frac{(\mathbf{R}_0{}^{\alpha}-\mathbf{R}_{0l}{}^{\alpha})(\mathbf{R}_0{}^{\alpha}-\mathbf{R}_{0l}{}^{\alpha})}{|\mathbf{R}_0{}^{\alpha}-\mathbf{R}_{0l}{}^{\alpha}|^3}\right\}\cdot\mathbf{F}_l{}^{\alpha}, \quad (9)$$

where the forces $\mathbf{F}_l{}^{\alpha}$ are themselves determined by the presence of all other molecules β, as well as the other elements of the molecule α. By a slight extension of the method of Burgers,[8] used in previous papers[4,6] to which the reader is referred, it is readily found that the reduction in velocity gradient due to the presence of N macromolecules per ml leads to a formula for the viscosity of the solution:

$$\eta=\eta_0\Big/\left(1+\frac{N}{\dot{\epsilon}\eta_0}\sum_{l=-n}^{n}\langle(\mathbf{R}_{0l}\cdot\mathbf{e}_y)(\mathbf{F}_l\cdot\mathbf{e}_x)\rangle_{Av}\right). \quad (10)$$

The superscript α has been omitted, since all the molecules are similar, and $\mathbf{F}_l$ itself is a concentration dependent term. $\dot{\epsilon}$, as before, is the velocity gradient, and the average is taken over the distribution of distances between hydrodynamically effective elements, as well as over all configurations of the molecule, which configuration may differ from the case of the isolated molecule leading to the expression for the intrinsic viscosity. The crux of the problem is to evaluate the average quantities shown in Eq. (10). For this purpose, three different molecular models have been chosen, the dumbbell, the rigid rod, and a centrosymmetric flexible molecule. The calculation shall be restricted to solutions sufficiently dilute so that the configurational distributions of each of the molecules is essentially unaffected by the presence of other molecules. These restrictions are introduced in order to obtain numerical results, and as can be seen, would be unnecessary were the necessary molecular distribution functions known.

The force exerted on the fluid by the lth element of the αth molecule can be written according to Eq. (3) as

$$\mathbf{F}_l{}^{\alpha}=-\zeta\mathbf{w}_l{}^{0\alpha}-\zeta\sum_{\substack{s=-n\\ s\neq l}}^{n}\mathbf{T}_{ls}{}^{\alpha\alpha}\cdot\mathbf{F}_s{}^{\alpha}-\zeta\sum_{\substack{\beta=1\\ \beta\neq\alpha}}^{N}\mathbf{T}_{lk}{}^{\alpha\beta}\cdot\mathbf{F}_k{}^{\beta}, \quad (11)$$

with the term $-\zeta\sum_{s\neq l}\mathbf{T}_{ls}\cdot\mathbf{F}_s$ in Eq. (3) now split into two parts. The first part [the second term on the right of Eq. (11)] includes all the perturbations on $\mathbf{F}_l{}^{\alpha}$ by other elements of the same molecular chain, while the final term in Eq. (11) represents the perturbation by all the elements on all the other chains. If the final term in Eq. (11) were dropped, it could be inferred that the concentration of the solution is so dilute that the intermolecular interactions are vanishingly small. That problem (intrinsic viscosity theory) has already been solved for the flexible and rod-type molecules by Kirkwood and Riseman[4,6] and for the dumbbell molecule by Simha,[2] and in the previous section of this paper. The final term in Eq. (11) is the significant term in this theory. The concentration effect is dependent upon the hydrodynamic interactions between the elements of different molecules, which interactions are all included in this final term.

In the calculation of the perturbed force, the corresponding Oseen tensor is expanded in power of $1/R_{00}{}^{\alpha\beta}$, where $R_{00}{}^{\alpha\beta}$ is the distance between the centers of mass of the αth and βth molecules. It is assumed that the average distribution of the molecular centers and the average distribution of the chain elements of a given molecule about its center are independent, and the computation of average configurations both inter- and intramolecular are performed in this way. The averages computed with respect to the intermolecular distribution are expressed explicitly as a function of concentration and the intramolecular distances. By substitution of the results in Eqs. (11) and (10), the velocity is obtained as a function of concentration. The details of the computation differ considerably for the different molecular types. In the case of the dumbbell molecule, the sum in Eq. (10) is evaluated directly, while in the cases of the rigid rod and flexible macromolecules, the sum is replaced by an integral, and the integral equation then solved as indicated in references 4 and 6.

From Eq. (2)

$$\mathbf{T}_{lk}{}^{\alpha\beta}=\frac{1}{8\pi\eta_0}\left\{\frac{\mathbf{I}}{|\mathbf{R}_{00}{}^{\alpha\beta}-\mathbf{R}_{0l}{}^{\alpha}+\mathbf{R}_{0k}{}^{\beta}|}+\frac{(\mathbf{R}_{00}{}^{\alpha\beta}-\mathbf{R}_{0l}{}^{\alpha}+\mathbf{R}_{0k}{}^{\beta})(\mathbf{R}_{00}{}^{\alpha\beta}-\mathbf{R}_{0l}{}^{\alpha}+\mathbf{R}_{0k}{}^{\beta})}{|\mathbf{R}_{00}{}^{\alpha\beta}-\mathbf{R}_{0l}{}^{\alpha}+\mathbf{R}_{0k}{}^{\beta}|^3}\right\}. \quad (12)$$

The unperturbed velocity of the fluid will be taken as a simple shear $\mathbf{v}^0=\dot{\epsilon}(\mathbf{R}\cdot\mathbf{e}_y)\mathbf{e}_x$. Since the molecular models with which we deal in this paper are all centrosymmetric, $\mathbf{R}_{0k}=-\mathbf{R}_{0-k}$, $\mathbf{F}_k=-\mathbf{F}_{-k}$, and the average of the difference between two Oseen tensors $\langle\mathbf{T}_{l-k}{}^{\alpha\beta}-\mathbf{T}_{lk}{}^{\alpha\beta}\rangle_{Av}$ will be used for the calculation of the intermolecular perturbations. Expanding $\mathbf{T}_{l-k}{}^{\alpha\beta}-\mathbf{T}_{lk}{}^{\alpha\beta}$ in powers of $1/R_{00}{}^{\alpha\beta}$ up to powers of $O(1/R_{00}{}^{\alpha\beta})^3$, the sum over all β—molecules is replaced by an integral over the volume. The integral, $\int(\mathbf{T}_{l-k}{}^{\alpha\beta}-\mathbf{T}_{lk}{}^{\alpha\beta})\rho_{00}{}^{\alpha\beta}dv$ cannot be determined unless the molecular distribution function $\rho_{00}{}^{\alpha\beta}$ is known. Since this function is not known, it is taken to be uniform, a reasonable approximation for the dilute solutions considered here. The integral is evaluated by conversion to a surface integral, and the average obtained is given by

$$\langle\mathbf{T}_{l-k}{}^{\alpha\beta}-\mathbf{T}_{lk}{}^{\alpha\beta}\rangle_{Av}=(2/15)[-4(\mathbf{R}_{0l}{}^{\alpha}\cdot\mathbf{R}_{0k}{}^{\beta})\mathbf{I}+\mathbf{R}_{0k}{}^{\beta}\mathbf{R}_{0l}{}^{\alpha}+\mathbf{R}_{0l}{}^{\alpha}\mathbf{R}_{0k}{}^{\beta}]. \quad (13)$$

Combining Eqs. (13) and (11), the force exerted on the fluid by the lth element of the αth molecule is found to be

$$\mathbf{F}_l^\alpha = -\zeta \mathbf{w}_l^{0\alpha} - \zeta \sum_{\substack{s=-n \\ s\neq l}}^{n} \mathbf{T}_{ls}^{\alpha\alpha} \cdot \mathbf{F}_s^\alpha - \frac{N}{15\eta_0}\Big[\sum_{k=-n}^{n} 4(\mathbf{R}_{0l}^\alpha \cdot \mathbf{R}_{0k}^\beta)\mathbf{I} - \mathbf{R}_{0k}^\beta \mathbf{R}_{0l}^\alpha - \mathbf{R}_{0l}^\alpha \mathbf{R}_{0k}^\beta\Big] \cdot \mathbf{F}_k^\beta. \quad (14)$$

N is the number of molecules per unit volume in the fluid, and $\mathbf{F}_l^\alpha$ is therefore a function of concentration. This dependence on concentration arises naturally in accounting for the hydrodynamic forces between chain elements on different molecules.

From Eq. (14), $\mathbf{F}_l^\alpha$ may be written as $\mathbf{A}+(\mathbf{F}_k^\beta \cdot \mathbf{B})\mathbf{D}c$, where $\mathbf{A}$, $\mathbf{B}$, and $\mathbf{D}$ are vectors which do not depend upon the solution concentration, and c is the concentration in arbitrary units. $\mathbf{F}_k^\beta$ is a vector of the same form as $\mathbf{F}_l^\alpha$. By iteration it is easy to see that

$$\mathbf{F}_l^\alpha = \sum_{n=0}^{\alpha} \mathbf{A}_n c^n,$$

and Eq. (10) may be written as

$$\eta = \eta_0/(1+\sum_{n=1}^{\infty} a_n c^n) = \eta_0[1+\sum_{n=0}^{\infty} k_n c^n], \quad (15)$$

where the constants k_n are derived from the constants a_n by a multinomial expansion. It is significant that the manner in which η the coefficient of viscosity of the solution varies with concentration is not hypothesized, but is derived directly from Eqs. (2) and (10). In order to calculate the coefficient of viscosity by means of Eqs. (11) and (14), it is necessary to express the quantity $\mathbf{F}_k^\beta$ in terms of the intramolecular distances, and the constants of the physical system. In this paper the chief consideration is the computation of the coefficient of c^2 in the expansion

$$\eta = \eta_0[1+\sum_{n=1}^{\infty} k_n c^n];$$

the terms in c^3 and higher will not be calculated here.

The force exerted by the kth element of the βth molecule as stated above, is a term which depends on concentration. The solution of Eqs. (14) and (10) is obtained by an iteration method, assuming at first, that $\mathbf{F}_k^\beta$ is not dependent upon concentration. In the following paragraph it will be shown that the concentration part of $\mathbf{F}_k^\beta$, when substituted in the power series expression for viscosity [Eq. (15)], contributes only to the coefficients of terms of the order of concentration cubed, and higher.

Equation (10) can be written as

$$\eta = \eta_0/(1+\langle P(\mathbf{F}_l^\alpha \cdot \mathbf{e}_x)\rangle_{Av} c), \quad (16)$$

where P is a quantity containing constants and intramolecular distances. If we use the fact that $\mathbf{F}_l^\alpha = \mathbf{A}+(\mathbf{F}_k^\beta \cdot \mathbf{B})\mathbf{D}c$ [see Eq. (14)], Eq. (16) becomes

$$\eta = \eta_0/(1+\langle P(\mathbf{A}\cdot\mathbf{e}_x)\rangle_{Av} c + \langle P(\mathbf{F}_k^\beta \cdot \mathbf{B})(\mathbf{D}\cdot\mathbf{e}_x)\rangle_{Av} c^2). \quad (17)$$

It is clear from Eq. (17) that $\mathbf{F}_k^\beta$ first appears as a coefficient of the concentration squared. If the intermolecular hydrodynamics perturbations on $\mathbf{F}_k^\beta$ were included, they would appear in a term proportional to concentration, and its over-all contribution to the viscosity would first appear in the coefficient of c^3. These and higher terms are not to be computed here, and therefore the omission of the concentration dependent part of F_k^β is valid in this calculation.

THE DUMBBELL MOLECULE

The concentration dependence of viscosity of a collection of dumbbell molecules is computed directly from Eqs. (10) and (14). Equation (10) becomes

$$\eta = \eta_0/(1+2N\langle(\mathbf{R}_{0l}\cdot\mathbf{e}_y)(\mathbf{F}_l\cdot\mathbf{e}_x)\rangle_{Av}/\dot{\epsilon}\eta_0). \quad (10a)$$

Substituting Eq. (14) in Eq. (10a), and averaging over all possible configurations of the αth and βth molecules, we obtain for the viscosity of a solution of dumbbell-shaped molecules

$$\eta = \eta_0 \Big/ \Big\{1-\Big(\frac{3L^2}{2a^2(1-3a/8L)} + \frac{9L}{80a(1-3a/8L)(1-3a/4L)}\Big)c + \Big(\frac{3L^4}{5a^4(1-3a/8L)^2} + \frac{27L^3}{400a^3(1-3a/8L)^2(1-3a/4L)} + \frac{81L^2}{16000a^2(1-3a/8L)^2(1-3a/4L)^2}\Big)c^2\Big\}. \quad (18)$$

The concentration c is expressed in terms of volume fraction ($c = 8\pi a^3 N/3$). In order to compare these results with those of Simha,[2] Eq. (18) is written as power series in concentration

$$\eta = \eta_0\Big[1+\Big(\frac{3L^2}{2a^2}+\frac{27L}{40a}+\cdots\Big)c + \Big(\frac{33L^4}{20a^3}+\frac{919L^3}{200a^3}+\cdots\Big)c^2\Big]. \quad (19)$$

The coefficient of c in Eq. (19) is the intrinsic viscosity, if concentration is expressed in units of grams of polymer per 100 ml of solution. When concentration is converted into appropriate units, Eq. (19) becomes

$$\eta = \eta_0[1+[\eta]c+(11/15)[\eta]^2(1+311a/225L)c^2]. \quad (20)$$

Simha's calculation[2] for the concentration dependence

of viscosity for a solution of dumbbell molecules yields

$$\eta=\eta_0[1+(3L^2/2a^2)c+(87L^4/50a^4)c^2], \quad (21a)$$

or

$$\eta=\eta_0[1+[\eta]c+(58/75)[\eta]^2c^2]. \quad (21b)$$

THE CENTROSYMMETRIC FLEXIBLE MOLECULE

Equations for the intrinsic viscosity of a solution of flexible random coil molecules has been derived by several authors.[4,14–17] The earlier equations[14–16] were derived from the laws governing viscous fluids, but neglected hydrodynamic interactions between the elements of a molecule. More recently, the papers of Debye and Bueche[17] and Kirkwood and Riseman[4] have considered the problem of intramolecular hydrodynamic interactions for the random coil molecule; but since they were interested only in the intrinsic viscosity, the interactions between monomer units on different molecules were ignored. The treatment here extends the calculation of Kirkwood and Riseman to include the interactions between the monomer elements on different molecules. However, in this paper the model of the flexible molecule is taken to be centrosymmetric. This restriction was not necessary in the derivation of the intrinsic viscosity formula, but is required for the numerical calculation of intermolecular effects.

The choice of a model with a center of symmetry to represent a physical flexible molecule is not realistic and prohibits the consideration of a large number of configurations which a real molecule possesses. The effect of this on the application of the theory to real flexible molecules has not been determined. The validity of the numerical results of the theory for an asymmetric flexible molecule is dependent upon the assumption that the configurations neglected in assuming the molecule to be centrosymmetric do not appreciably affect the average values computed here.

If the flexible molecule is assumed to be centrosymmetric, the force exerted on the fluid by the lth element of the αth molecule may be written [see Eq. (11) and (13)]

$$\mathbf{F}_l{}^\alpha=-\zeta\mathbf{w}_l{}^{0\alpha}-\zeta\sum_{\substack{s=-n\\ s\neq l}}^{n}\mathbf{T}_{ls}{}^{\alpha\alpha}\cdot\mathbf{F}_s{}^\alpha+\frac{\zeta N}{15\eta_0}\sum_{k=-n}^{n}\{4(\mathbf{R}_{0l}{}^\alpha\cdot\mathbf{R}_{0k}{}^\beta)\mathbf{I}-\mathbf{R}_{0k}{}^\beta\mathbf{R}_{0l}{}^\alpha-\mathbf{R}_{0l}{}^\alpha\mathbf{R}_{0k}{}^\beta\}\cdot\mathbf{F}_k{}^\beta. \quad (22)$$

It is convenient to consider the problem in two parts, keeping in mind that the final expression for viscosity is to be obtained by substitution in Eq. (10). The scalar product of $(\mathbf{R}_{0l'}\cdot\mathbf{e}_y)\mathbf{e}_x$ and $\mathbf{F}_l{}^{*\alpha}$ is formed, where $\mathbf{F}_l{}^{*\alpha}$ is the force exerted by the lth element of the αth molecule on the solution with the intermolecular forces [the terms multiplying N in Eq. (22)] neglected. This alone leads to the expression for intrinsic viscosity. $\mathbf{F}_l{}^{*\alpha}$ in this paper is the same as $\mathbf{F}_l$ in reference 4. The scalar product of $\mathbf{F}_l{}'^\alpha$ (the intermolecular perturbation) with $(\mathbf{R}_{0l'}\cdot\mathbf{e}_y)\mathbf{e}_x$ is also constructed.

Since $\mathbf{w}_l{}^0=\frac{1}{2}\dot\epsilon\{(\mathbf{R}_{0l}\cdot\mathbf{e}_y)\mathbf{e}_x+(\mathbf{R}_{0l}\cdot\mathbf{e}_x)\mathbf{e}_y\}$ (see reference 4), after we average over $\mathbf{T}_{ls}{}^{\alpha\alpha}$, Eq. (22) becomes

$$(\mathbf{R}_{0l'}{}^\alpha\cdot\mathbf{e}_y)(\mathbf{F}_l{}^{*\alpha}\cdot\mathbf{e}_x)=-\tfrac{1}{2}\zeta\dot\epsilon(\mathbf{R}_{0l'}{}^\alpha\cdot\mathbf{e}_y)(\mathbf{R}_{0l}{}^\alpha\cdot\mathbf{e}_y)-\frac{\zeta}{(6\pi^3)^{\frac{1}{2}}b\eta_0}\sum_{\substack{s=-n\\ s\neq l}}^{n}\frac{(\mathbf{R}_{0l'}{}^\alpha\cdot\mathbf{e}_y)(\mathbf{F}_s{}^{*\alpha}\cdot\mathbf{e}_x)}{|l-s|^{\frac{1}{2}}}, \quad (23)$$

$$(\mathbf{R}_{0l'}{}^\alpha\cdot\mathbf{e}_y)(\mathbf{F}_l{}'^\alpha\cdot\mathbf{e}_x)=-\left\{\frac{\zeta N}{15\eta_0}\sum_{k=-n}^{n}4(\mathbf{R}_{0k}{}^\beta\cdot\mathbf{e}_y)(\mathbf{F}_k{}^\beta\cdot\mathbf{e}_x)-(\mathbf{R}_{0k}{}^\beta\cdot\mathbf{e}_x)(\mathbf{F}_k{}^\beta\cdot\mathbf{e}_y)\right\}(\mathbf{R}_{0l'}{}^\alpha\cdot\mathbf{e}_y)(\mathbf{R}_{0l}{}^\alpha\cdot\mathbf{e}_y)-\frac{\zeta}{(6\pi^3)^{\frac{1}{2}}b\eta_0}\sum_{\substack{s=-n\\ s\neq l}}^{n}\frac{(\mathbf{R}_{0l'}{}^\alpha\cdot\mathbf{e}_y)(\mathbf{F}_s{}'^\alpha\cdot\mathbf{e}_x)}{|l-s|^{\frac{1}{2}}}. \quad (23a)$$

Because of the symmetry of $\mathbf{w}_l{}^0$ with respect to the x and y directions, we have

$$\langle(\mathbf{R}_{0k}{}^\beta\cdot\mathbf{e}_y)(\mathbf{F}_{0k}{}^\beta\cdot\mathbf{e}_x)\rangle_{Av}=\langle(\mathbf{R}_{0k}{}^\beta\cdot\mathbf{e}_x)(\mathbf{F}_k{}^\beta\cdot\mathbf{e}_y)\rangle_{Av}.$$

As in the case of the dumbbell molecule, the concentration dependent part of $\mathbf{F}_k{}^\beta$ does not contribute to the first interaction coefficient, and Eq. (23a) becomes

$$(\mathbf{R}_{0l'}{}^\alpha\cdot\mathbf{e}_y)(\mathbf{F}_l{}'^\alpha\cdot\mathbf{e}_x)=(20\zeta\dot\epsilon MN/A)[\eta](\mathbf{R}_{0l'}{}^\alpha\cdot\mathbf{e}_y)(\mathbf{R}_{0l}{}^\alpha\cdot\mathbf{e}_y)-\frac{\zeta}{(6\pi^3)^{\frac{1}{2}}b\eta_0}\sum_{\substack{s=+n\\ s\neq l}}^{n}\frac{(\mathbf{R}_{0l'}{}^\alpha\cdot\mathbf{e}_y)(\mathbf{F}_s{}^\alpha\cdot\mathbf{e}_x)}{|l-s|^{\frac{1}{2}}}. \quad (24)$$

It is apparent that Eq. (24) is of the same form as Eq. (23a) with the coefficient of the first term on the right changed. Therefore, the solution of Eq. (24) may be effected by the same method as was used in solving Eq. (23a). It is important to note that the coefficient of the inhomogeneous term is a constant times concentration in Eq. (24) and is not a function of concentration in Eq. (23a). This is according to expectation, since the intermolecular perturbations should vanish at low concentration, and the unperturbed hydrodynamic forces do not.

The formula for viscosity developed from the method of Burgers [Eq. (10)] can be expanded as a power series in concentration.

$$\eta=\eta_0\left[1-\frac{N}{\dot\epsilon\eta_0}\sum_{l=-n}^{n}\langle(\mathbf{R}_{0l}\cdot\mathbf{e}_y)(\mathbf{F}_l\cdot\mathbf{e}_x)\rangle_{Av}+\frac{N^2}{\epsilon^2\eta_0{}^2}\{\sum_{l=-n}^{n}\langle(\mathbf{R}_{0l}\cdot\mathbf{e}_y)(\mathbf{F}_l\cdot\mathbf{e}_x)\rangle_{Av}\}^2+\cdots\right]. \quad (25)$$

[14] W. Kuhn, Z. physik. Chem. **A161**, 1 (1932).
[15] M. L. Huggins, J. Phys. Chem. **43**, 439 (1939).
[16] H. A. Kramers, J. Chem. Phys. **14**, 415 (1946).
[17] P. Debye and F. Bueche, J. Chem. Phys. **16**, 573 (1948).

If $\mathbf{F}_l$ were replaced by $\mathbf{F}_l^*$, and concentration was expressed in grams per 100 ml, Eq. (25) could be written as

$$\eta=\eta_0[1+[\eta]c+[\eta]^2c^2], \tag{26}$$

in accordance with the definition of intrinsic viscosity. Equation (26) is not a correct expression for the concentration dependence of viscosity because the intermolecular interactions which appear naturally in the coefficient of c^2 are neglected.

Forming the scalar product of $(\mathbf{R}_{0l'}\cdot\mathbf{e}_y)\mathbf{e}_x$ with $\mathbf{F}_l$ [Eq. (23) is added to Eq. (24)],

$$(\mathbf{R}_{0l'}\cdot\mathbf{e}_y)(\mathbf{F}_l\cdot\mathbf{e}_x)$$
$$=-\tfrac{1}{2}\zeta\dot{\epsilon}\{1-(40MN/A)[\eta]\}(\mathbf{R}_{0l'}\cdot\mathbf{e}_y)(\mathbf{R}_{0l}\cdot\mathbf{e}_y)$$
$$-\frac{\zeta}{(6\pi^3)^{\frac{1}{2}}b\eta_0}\sum_{\substack{s=-n\\ s\neq l}}^{n}\frac{(\mathbf{R}_{0l'}\cdot\mathbf{e}_y)(\mathbf{F}_s\cdot\mathbf{e}_x)}{|l-s|^{\frac{1}{2}}} \tag{27}$$

and substituting the results in Eq. (25), we see equation for viscosity obtained by including the interactions between the monomer elements of the different molecules to be

$$\eta=\eta_0[1+[\eta](1-\tfrac{2}{5}[\eta]c)c+[\eta]^2c^2]$$
$$\eta=\eta_0[1+[\eta]c+\tfrac{3}{5}[\eta]^2c^2]. \tag{28}$$

This last is the formula for the concentration dependence of viscosity of the flexible chain molecule.

THE RIGID ROD MOLECULE

A hydrodynamic theory of intrinsic viscosity of solutions of rodlike macromolecules has been developed by Riseman and Kirkwood.[5]

This theory has been extended to include concentration effects in the manner indicated in the previous section. There are two important differences in detail. The original flow pattern about the rigid rod molecule is given by $\mathbf{w}_l^0=\dot{\epsilon}(\mathbf{R}_{0l}\cdot\mathbf{e}_y)\mathbf{e}_x$, and the term

$$\langle(\mathbf{R}_{0k}{}^{\beta}\cdot\mathbf{e}_x)(\mathbf{F}_k{}^{\beta}\cdot\mathbf{e}_y)\rangle_{\text{Av}}$$

vanishes when we average over-all positions of the βth molecule. The rest of the analysis is entirely analogous to that for the flexible molecule, and the coefficient of viscosity is found to be

$$\eta=\eta_0[1+[\eta]c+(11/15)[\eta]^2c^2]. \tag{29}$$

SUMMARY AND DISCUSSION OF RESULTS

The numerical results of this paper may be summarized by the formula $\eta=\eta_0[1+[\eta]c+k'[\eta]^2c^2]$, where k' is $(11/15)(1+311a/225L)$ for the dumbbell molecule, 11/15 for the rigid rod molecule, and $\frac{3}{5}$ for the centrosymmetric flexible molecule.

It is interesting to note that k' is dependent on the molecular dimensions for the dumbbell molecule, but is not for the rodlike and flexible molecules.

The explanation of this difference lies in the manner of averaging the Oseen tensor on a single molecule. In the expression for $\mathbf{F}_l{}^{\alpha}$ (the force exerted by the lth element of the αth molecule on the solution), the term

$$\sum_{\substack{s=-n\\ s\neq l}}^{n}\mathbf{T}_{ls}{}^{\alpha\alpha}\cdot\mathbf{F}_s{}^{\alpha}$$

appears. For the dumbbell molecule, this sum involves only a single term, and can be evaluated exactly. In the problem of the flexible and rod molecules, the sum is over $2n$ elements and cannot be evaluated directly. The assumption is made[5,7] that

$$\sum_{\substack{s=-n\\ s\neq l}}^{n}\mathbf{T}_{ls}{}^{\alpha\alpha}\cdot\mathbf{F}_s{}^{\alpha}=\sum_{\substack{s=-n\\ s\neq l}}^{n}\langle\mathbf{T}_{ls}{}^{\alpha\alpha}\rangle_{\text{Av}}\cdot\mathbf{F}_s{}^{\alpha}$$
$$=\sum_{\substack{s=-n\\ s\neq l}}^{n}f(l,s)\mathbf{F}_s{}^{\alpha}, \tag{30}$$

where $f(l, s)$ is a scalar function of l and s. This assumption, if applied to the dumbbell, has been shown by the authors in a separate calculation not included here to yield a value of k' which is independent of a and L.

Therefore, it may be concluded that the dependence of k' on molecular dimensions may be masked here by the method of averaging over the Oseen tensor. The exact nature of this dependence cannot be determined except by a rather dubious extrapolation from the results of the dumbbell molecule.

Light Scattering Studies on Coiling Polyelectrolytes*

F. T. WALL, J. W. DRENAN, M. R. HATFIELD,† AND C. L. PAINTER‡
Noyes Chemical Laboratory, University of Illinois, Urbana, Illinois

(Received December 12, 1950)

The molecular weight and size of polyacrylic acid in solution have been determined by measurement of light scattering. Use was made of Debye's 90° light scattering method employing two different wavelengths of light.

When the reciprocal specific scattering is plotted against concentration for homopolar polymers, a straight line is obtained which is readily extrapolated to zero concentration. Polyelectrolytes, however, are capable of ionizing in aqueous solution, thus becoming electrically charged by amounts depending upon the concentration. The electrostatic repulsion of the charges very probably affects the molecular size and gives rise to peculiar light scattering curves. By utilizing buffer solutions as solvents, the molecular size is held constant and the difficulties involved in the interpretation of scattering data are largely resolved.

The weight-average molecular weight of a certain sample of polyacrylic acid at *p*H values of 1.2, 3, 4, and 5 was found to be 206,000±10 percent. Molecular weight values at a particular *p*H using a specific buffer were reproducible to about ±3 percent. The remainder of the error was attributed to association of buffer ions with the charged polymer. The size of the particles in solution was found to be less than 550A in the low *p*H regions, with a definite tendency to increase at higher *p*H values. The slope of the straight line obtained when the reciprocal specific scattering was plotted against concentration was shown to be dependent upon *p*H. This dependence of slope may be related to particle size and shape.

In a non-ionizing solvent such as ethanol, the polymer exhibits scattering behavior typical of non-ionized polymers. The molecular weight of polyacrylic acid under these conditions was found to be 206,000, in agreement with values obtained in buffer solvents.

THE methods of Debye[1,2] for determination of molecular weights and sizes of high polymeric materials by light scattering have been used quite successfully by numerous investigators. The greater part of the work on polymers has been carried out on non-electrolytic substances, and relatively little information has appeared concerning light scattering measurements on polyelectrolytes. However, Doty and Steiner[3] as well as Edsall *et al.*[4] have done significant work on bovine serum albumin.§ Since polyelectrolytes are capable of ionizing in polar solvents, they exhibit many unusual properties by reason of their electrical charges, the magnitudes of which depend upon the extents of ionization. For example, changes in charge should result in size variations because of the electrostatic forces involved. Thus, while the light scattering techniques used for homopolar polymers can be applied to polyelectrolytes dissolved in suitable non-ionizing solvents, their use with aqueous solutions of coiling polyelectrolytes presents other problems because of the variability of molecular size.

The Debye turbidity equation has been used extensively and successfully for particles small in size compared with the wavelength of light used. This equation, which relates turbidity to molecular weight, is given by

$$(Hc/\tau)_0 = 1/M, \tag{1}$$

where H is a constant for a particular polymer solvent system. The subscript zero indicates that the numerical value of the expression used is that obtained by extrapolation to infinite dilution. Since the turbidity is related to scattering, the above expression can also be written

$$(Hc/\sigma)_0 = 16\pi/3M, \tag{2}$$

where σ is the fraction of the primary light scattered at 90°.

When the size of the molecules in solution is greater than about $\frac{1}{10}$ the wavelength of the incident light, the measured turbidity will be too small for use in the Debye equation. This is a result of destructive interference caused by path length differences. For these large molecules, several methods have been employed for correction of the Debye equation, the correction factor depending upon the dissymmetry of scattering.[2,5–7] Throughout this investigation a 90° scattering method was used which required the measurement of scattering for two or more wavelengths.[8] For such scattering the values of $(Hc/\sigma)_0$ will depend upon the wavelength of the light used, so that a turbidity correction factor must be introduced. This factor, (ϕ_λ) for a particular molecular model, can be expressed in terms of wavelength (λ), refractive index of solvent (μ_0), and the dimensions of the molecule (R). For our purposes, the ratio of ϕ values for two wavelengths has been calculated as a function of R for the random coil model. Particle size can then be determined by inverse use of a relationship which is defined in such a way that

$$(Hc/\sigma)_0^{\lambda_1}/(Hc/\sigma)_0^{\lambda_2} = \phi_{\lambda 1}/\phi_{\lambda 2}. \tag{3}$$

A value of unity for the ratio $\phi_{\lambda 1}/\phi_{\lambda 2}$ is, of course, indicative of small particles.

* This work was carried out in part under the sponsorship of the Office of Rubber Reserve, Reconstruction Finance Corporation.

† Present address: Minnesota Mining and Manufacturing Company, St. Paul, Minnesota.

‡ Present address: Procter and Gamble Company, Cincinnati, Ohio.

[1] P. Debye, J. Appl. Phys. **15**, 338 (1944).

[2] P. Debye, J. Phys. and Colloid Chem. **51**, 18 (1947).

[3] P. Doty and R. F. Steiner, J. Chem. Phys. **17**, 743 (1949).

[4] J. T. Edsall *et al.*, J. Am. Chem. Soc. **72**, 4641 (1950).

§ Recently, A. Katchalsky and H. Eisenberg, J. Polymer. Sci. VI, 145 (1951), have reported light scattering studies on polymethacrylic acid.

[5] R. S. Stein and P. Doty, J. Am. Chem. Soc. **68**, 159 (1946).

[6] Oster, Doty, and Zimm, J. Am. Chem. Soc. **69**, 1193 (1947).

[7] P. M. Doty, J. chim. phys. **44**, 76 (1947).

[8] The authors are indebted to Professor P. Debye for this particular light scattering method.

TABLE I. Polyacrylic acid. Various buffer solutions.

Buffer* or solvent	pH	$\left(\frac{c}{\sigma}\right)^0_B$	$\left(\frac{c}{\sigma}\right)^0_G$	$\left(\frac{Hc}{\sigma}\right)^0_0$ ×10⁶	$(\phi_B/\phi_G)_0$	M
A	1.2	13.01	34.02	79.06	0.987	210,600
B	3	12.43	34.56	74.89	0.975	223,700
B	3	12.20	32.54	76.41	0.970	219,300
D	3	13.69	36.25	78.61	0.961	213,100
C	4	15.15	39.56	93.94	0.990	178,200
C	4	16.14	40.15	89.12	1.041	188,000
G	4	13.45	35.36	82.13	0.998	204,000
G	4	14.06	37.10	86.00	0.995	194,800
E	5	15.03	37.95	76.53	1.054	218,900
F	5.6	13.98	32.81	56.87	1.134	294,600

* Buffer notation:
A—Hydrochloric acid (0.100 N).
B—Hydrochloric acid (0.02032 N)—potassium biphthalate (0.0500 M).
C—Potassium biphthalate (0.0500 M).
D—Citric acid (0.0794 M)—Disodium phosphate (0.0411 M).
E—Sodium hydroxide (0.0239 N)—Potassium biphthalate (0.0500 M).
F—Sodium hydroxide (0.0399 N)—Potassium biphthalate (0.0500 M).
G—Citric acid (0.0615 M)—Disodium phosphate (0.0771 M).

If $(Hc/\sigma)_0^\lambda$ is plotted against $(\mu_0/\lambda)^2$ and the resulting curve extrapolated to infinite wavelength, the intercept can be used in Eq. (2) to obtain the molecular weight.

EXPERIMENTAL

The light scattering instrument was designed and constructed in this laboratory and has been described in detail.[9] It consists of a constant mercury light source, lenses and diaphragms for suitable collimation of the primary light beam, and a photo-multiplier arrangement for detection and measurement of the scattered radiation. The instrument was set up to measure 90° scattering only.

The instrument was calibrated by means of a standard solution of polymer of known absolute turbidity. The standard used in this laboratory is a solution of polystyrene in toluene (0.5 g per 100 cc solution), the turbidity of which was determined by A. M. Bueche at Cornell University and independently in this laboratory.

Measurements of refractive indexes were made by a differential refractometer, which is similar in design to that described by P. P. Debye.[10] This instrument was calibrated by use of sucrose solutions, the refractive indexes of which are known to a high degree of accuracy.

The refractive index differences between polymer solutions and solvents were measured at a number of concentrations to establish the constancy of $(\mu-\mu_0/c)$; such constancy was assumed in the theoretical considerations. For the preparation of the polymeric acid, pure acrylic acid was mixed with toluene containing a small amount of benzoyl peroxide, and the resulting mixture flushed with nitrogen and then sealed. The polymerization required several days at room temperature. Elevated temperatures decrease the time necessary for polymerization but yield relatively low molecular weight products. The polymeric material was thoroughly washed with benzene and then dried. Further purification was brought about by extraction with benzene in a Soxhlet extractor.

All aqueous solutions were prepared with conductivity water (water doubly distilled in alkaline solution over potassium permanganate). Toluene was distilled over phosphorous pentoxide through a one-meter column packed with nichrome helices. All buffer solutions were prepared with reagent grade materials using formulas of Clark and Lubs and McIlvaine.[11] Solutions to be used in the light scattering instrument were filtered at least three times through a fine sintered glass filter.

RESULTS AND DISCUSSION

1. Water Solutions of Polyacrylic Acid

Light scattering measurements on polyacrylic acid in water solution made previously[9] yielded results which could not be interpreted by the same means used for non-electrolyte polymers. Scattering measurements for homopolar polymers (e.g., polystyrene) when plotted against concentration gave curves which were concave downward and very nearly linear at low concentrations. In the low concentration regions, plots of c/σ *vs* c for such polymers yield straight lines which can easily be extrapolated to infinite dilution.

The scattering curves for polyacrylic acid, however, are slightly concave upward in the low concentration regions, with a tendency to become straight lines at higher concentrations. This peculiarity is much more noticeable when c/σ is plotted against concentration (see Fig. 1). Extrapolation of such a curve is difficult, so the molecular weight obtained by this method is quite uncertain.

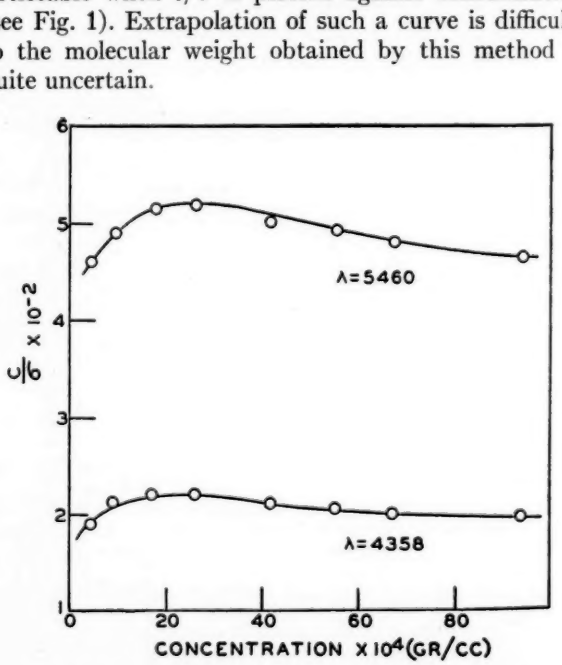

FIG. 1. Light scattering of aqueous polyacrylic acid solutions.

[9] C. L. Painter, "Molecular weight and particle size of polyelectrolytes by light scattering," Thesis, University of Illinois, Urbana, Illinois (1949).

[10] P. P. Debye, J. Appl. Phys. **17**, 392 (1946).

[11] See, for example, N. A. Lange and G. M. Forker, compilers, *Handbook of Chemistry* (Handbook Publishers, Inc., Sandusky, Ohio, 1944), sixth edition, pp. 1099–1102.

The explanation for this odd behavior of polyacrylic acid becomes apparent when the *p*H of this polymer in solution is examined. At low concentrations, even slight changes in the concentration markedly affect the *p*H. As the *p*H changes, the extent of ionization also changes, and the total charge on the polymer molecules is increased or decreased. The scattering is then affected not only by the explicit concentration changes, but also by changes in size resulting from the variability of charge. If the size could be held constant, polyacrylic acid should be expected to exhibit the same sort of scattering behavior as does polystyrene.

2. Buffer Solutions

The particle size in solution can be held constant by the utilization of a buffer solution, instead of water, as a "solvent." The ionization of the polyelectrolyte in low concentration regions is then fixed by the constant ionic environment.[4] The scattering curves for such solutions assume the shape of those obtained for homopolar polymers. A typical example of this behavior is shown in Fig. 2, which represents the scattering of polyacrylic acid in a solvent buffered at *p*H=4.

Light scattering runs were made on this polymeric material at several *p*H values using a variety of buffers. The results are tabulated in Table I. There are doubtless several factors contributing to the apparent variation of molecular weight values. First of all, the buffer ions may be associated with the polymer to varying degrees, causing a real change in molecular weight. Secondly, the refractive indexes can be affected by such association in a manner that would bring about apparent variations. In view of the fact that the values at a particular *p*H using a specific buffer are reproducible to about ±3 percent, some effects other than ordinary experimental error must be present.

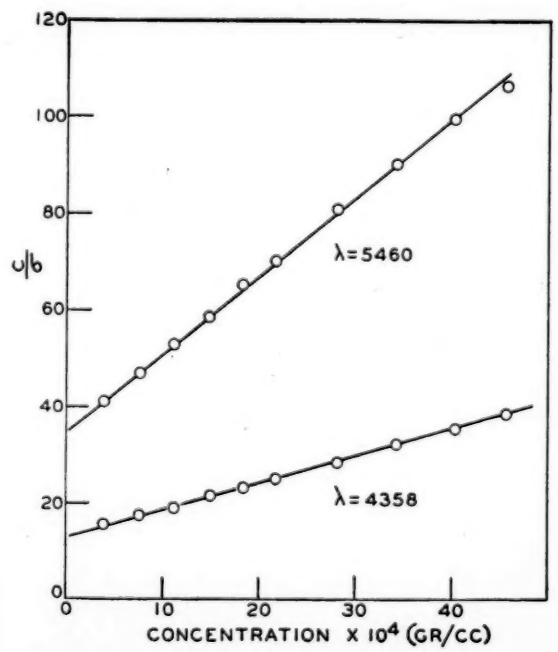

FIG. 2. Light scattering of polyacrylic acid in buffer solutions of *p*H=4.

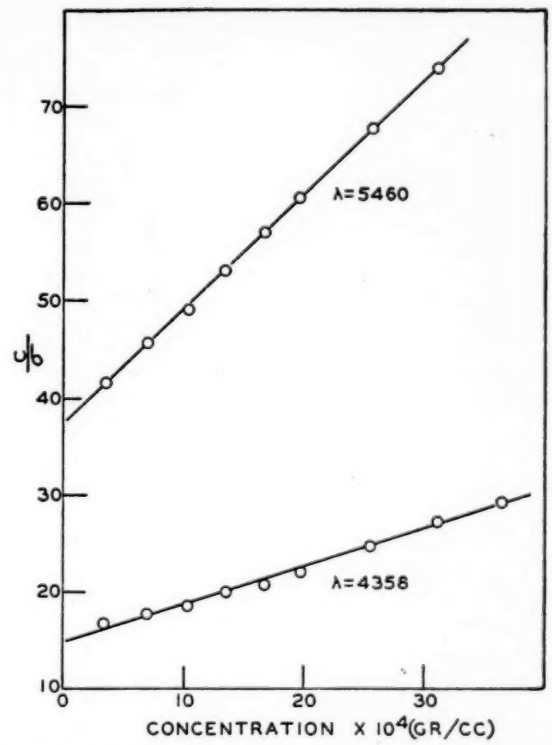

FIG. 3. Light scattering of polyacrylic acid in ethanol solution.

The molecular weight of 294,600 obtained at *p*H=5.6 is based on a very small number of experimental values and cannot be considered nearly as correct as the other values. Recent investigations[12] have indicated that plots of $(Hc/\sigma)_\lambda{}^0$ against $(\mu_0/\lambda)^2$ may not always result in straight lines; hence, measurements at more than two wavelengths are needed when large particles are considered, as in this instance.

The average molecular weight for polyacrylic acid under these conditions is 205,600±about 10 percent (excluding that at *p*H=5.6).

The indicated particle size in all cases except at *p*H=5.6 is small compared with the wavelength of the primary light within the experimental error. Although the value of ϕ_B/ϕ_G at 5.6 may be somewhat in error, it is probably an indication that the molecules do expand at higher *p*H values.

3. Alcohol Solutions of Polyacrylic Acid and Slopes of Scattering Curves

The light scattering of polyelectrolytes dissolved in non-ionizing solvents should resemble that of a typical non-electrolytic polymer. Although polyacrylic acid is practically insoluble in solvents such as toluene, benzene, etc., it is somewhat soluble in absolute ethanol. The scattering of such an alcohol solution was measured

[12] Private communication through the Office of Rubber Reserve.

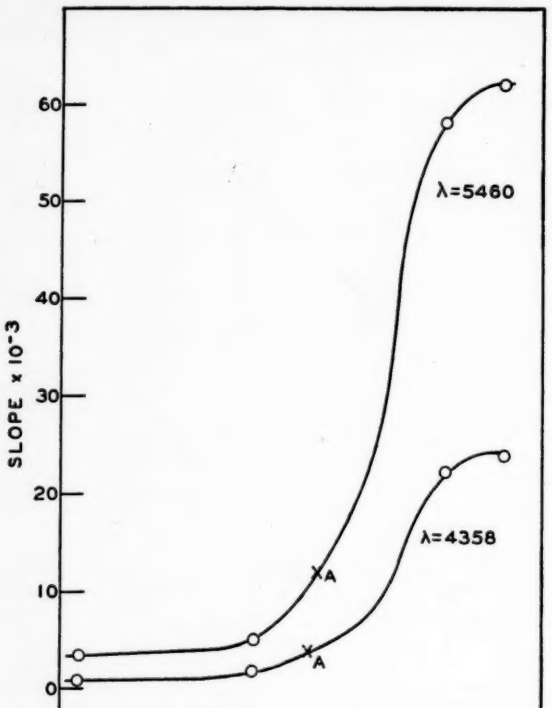

FIG. 4. Slope of light scattering curves (obtained from c/σ *vs* c) plotted against pH. X denoted ethyl alcohol solvent.

and plotted in Fig. 3. The molecular weight obtained by this experiment is 205,900, and the particle was again observed to be small compared with the wavelength of light used. Other nonpolar solvents in which polyacrylic acid is sufficiently soluble should yield light scattering results which are consistent with those obtained in alcohol. The slopes of the scattering curves (c/σ *vs* c), however, may be different, a particular slope being indicative of the relative "solvent power" of the solvent material.[2] A steep slope is generally associated with better solvent material; the turbidity, of course, increases more rapidly with concentration in poorer solvents.

This behavior of slope is also observed when buffer solutions are used as solvents. The values obtained for these slopes are reproducible to approximately ±8 percent. It appears that there is considerable dependence of slope upon pH. This relationship is illustrated in Fig. 4.

The sharp increase in slope which takes place at approximately pH=4 can be used as an indication of the trend of the scattering curves for water solutions in low concentrations. As the concentration decreases below the experimental limit of the light scattering instrument and approaches zero, the pH approaches that of water and the slopes of the scattering curves (c/σ) become extremely high.[3] In Fig. 1, for example, the curves must be nearly vertical at these concentrations.

Figure 4 serves to indicate the size and shape changes which occur as the pH is varied. For the concentration range of interest, the pH of a water solution of polyacrylic acid should be in the range 3 to 4, and the size and shape of the molecules appear to be substantially the same as if the polymer were not ionized. Solutions in nonpolar solvents, in which the solubility of the polymer is of the same order of magnitude as in water, should exhibit scattering slopes corresponding to those of aqueous solutions of pH 3 to 4. Ethanol is an example of such a solvent and is indicated by the point labeled A in Fig. 4.

This figure suggests that for pH values below 3, the shape of the molecule is very nearly that of a random coil, but at higher pH values the molecule expands because of its increased charges.

4. Theoretical Particle Sizes

For calculating theoretical particle sizes, the experimental molecular weight of polyacrylic acid will be taken as 206,000. The particle size for all pH values up through 4 is small (i.e., less than $\frac{1}{10}$ of the wavelength of the primary light). This means that the experimental particle size in this pH range at infinite dilution is less than 550A.

Use of the random coil model with the known single-bond carbon-carbon angle and distance yields a root-mean-square end-to-end distance R=164A for the molecule (free rotation). The rigid stick model predicts a chain length L=7170A. Since the experimental size is less than 550A, it is apparent that the linear coil is a better model for the polymer (under the conditions mentioned) than the rigid stick.

Electric Moments of Polar Polymers in Relation to Their Structure*

P. DEBYE AND F. BUECHE
Department of Chemistry, Cornell University, Ithaca, New York
(Received December 21, 1950)

From the observed angular dissymmetry of the light scattered by polymer solutions it has been possible to draw conclusions on the average size of the polymer coil. In general, the actual coil diameter found in this way is much larger than that calculated from a model with free rotation. (For polystyrene in benzene the factor is about 3.5.) This increase in size can satisfactorily be attributed to hindering of rotation around the chemical bonds. In order to obtain information about structural details of this hindered rotation, however, the size determination will have to be combined with evidence derived from other sources than light scattering. As such, the dipole moment, as derived from measurements of the dielectric constant of polymer solutions, obviously is a good choice. If a number of units are connected to each other in a chain, the contribution of the whole chain may be larger or smaller than would be the case if the units were free, depending on whether positions of parallelism or antiparallelism of the elementary electric moments are preponderant, taking the average over all the possible forms the coiling molecule can assume. A theory of this effect has been worked out, and experiments have been carried out. One of the examples is polyparachlorostyrene, for which the average contribution to the polarization of one chain element is substantially smaller in the polymer than that of the corresponding monomer.

VISCOSITY and light scattering measurements have shown that coiling chain polymer molecules occupy a volume much larger than is predicted by simple theories. The explanation for this which has often been given states that, owing to steric hindrances, the polymer chain cannot take on all configurations allowed by free rotation about the chain bonds. It is generally agreed that a very large part of this extra extension of the chain is due to hindering of rotation along the polymer chain.

The nature of this hindered rotation is now a dominant problem in polymer behavior. Unfortunately, viscosity and light scattering data can do little more than tell us that hindering exists. Infrared investigations have been made on very small molecules to solve just such problems as the one at hand, but the extension of this method to polymer molecules except in a few cases would seem to be excessively tedious if not impossible. We are therefore led to search for still another method for determining polymer behavior in solution-*a* method which will give a more detailed picture of the configurations assumed by the polymer molecule. Such a more detailed picture is provided by an analysis of the dipole moments of polar polymer molecules in solution.

To illustrate the sensitivity of the dipole moment of a polymer molecule to hindering of rotation, let us first consider a particularly simple type of polymer chain. It is one in which the valence bond angle is 180° and therefore the chain is a straight line of atoms. Consider further that dipole groups of moment μ come off the chain in some periodic fashion in a direction normal to the chain.

Now it is well known that a molecule's dipole contribution to the dielectric constant of a medium is proportional to μ^2. If our simple chain of N units is assumed to be completely stiff, then its contribution to the dielectric constant will either be zero or of the order of $(N\mu)^2$, depending upon whether the fixed dipoles on the stiff chain are so oriented that the dipoles cancel or add. This is to be compared with the value of $N\mu^2$ which would be true if the units of the chain were perfectly free to rotate. Therefore, since N is very large in practice, we see that the dipole moment contribution to the dielectric constant is extremely sensitive to the polymer configurations and to the hindering of internal polymer rotation.

Let us now proceed to an actual and general polymer molecule. It may be shown (see Appendix I) that for any polymer molecule, the average dipole contribution to the molecular polarization is equal to

$$\left\langle P \sum_{m=1}^{N_0} \sum_{n=1}^{N_0} (\mu_n f)(\mu_m f) \right\rangle_{\text{Av}} \frac{E}{3kT},$$

where μ_n is the vector magnitude of the nth dipole of the chain and f is a unit vector in the direction of the applied electric field E. The sums extend over all of the N_0 dipoles on the chain, and the average is to be taken over all of the possible chain configurations and orientations. P is the probability of occurrence of any particular chain configuration.

Therefore, we come to the result that the polymer molecule will act exactly like a single molecule of permanent moment $\bar{\mu}$ if we define $\bar{\mu}$ by the relation

$$\frac{\bar{\mu}^2}{3} = \left\langle P \sum_{m=1}^{N_0} \sum_{n=1}^{N_0} (\mu_n f)(\mu_m f) \right\rangle_{\text{Av}}.$$

We shall call $\bar{\mu}$ the average moment of the polymer molecule.

It is shown in Appendix II that in the case of a carbon-carbon chain with a dipole of moment μ coming off every other chain atom at an angle γ with the preceding $c-c$ chain bond and angle β with the following $c-c$ chain bond, the average turns out to be

$$\tfrac{1}{3}\mu^2 N_0[1+2p\cos\beta\cos\gamma/(1-p^2)],$$

* The work reported in this paper was done under a contract with the Reconstruction Finance Corporation, Office of Rubber Reserve.

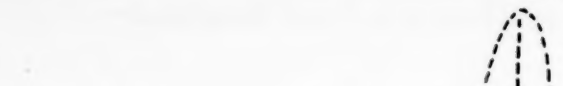

FIG. 1(a). A schematic diagram showing a series of four atoms along a polymer chain.

providing free rotation is assumed. By free rotation, we mean that each chain carbon rotates freely on the valence cone subject only to the restrictions that the $c-c$ bond distance and angle must be preserved. In the last expression, p is the cosine of the valence angle, i.e., $\frac{1}{3}$ for a $c-c$ chain.

For a molecule such as polyparachlorostyrene we have also that $\cos\beta=-\cos\gamma=p=\frac{1}{3}$. In that case, again assuming free rotation, we find the average dipole moment to be given by

$$\bar{\mu}^2=11N_0\mu^2/12,$$

where N_0 is the number of dipoles on the chain and μ is the moment of each of these dipoles.[1]

Therefore, we have obtained the result that if our assumption of free rotation were true, polyparachlorostyrene and similar polymers should have an average moment equal to $(0.92N_0)^{\frac{1}{2}}$ times the dipole moment of each chain unit. It is shown in Appendix IV that the quantity $\bar{\mu}^2/N_0$ is given by a single dipole moment measurement.

Since μ, the dipole moment of an individual chain group, is generally known, a check is easily obtained for our derived equation. Work in our laboratory (see Appendix IV) has shown that the theoretical factor 0.92 is too large. The correct factor as found experimentally is about 0.56 for p.p. chlorostyrene. The similar compound, polyvinylchloride is also found to give a low value for this factor, namely, about 0.75.[2]

We are therefore confronted with additional evidence that real polymer molecules do not possess complete freedom of internal rotation in dilute solution. It will be the purpose of the remaining sections of this paper

[1] R. M. Fuoss and J. G. Kirkwood, J. Am. Chem. Soc. **63**, 385 (1941), have derived an expression similar to this. However, owing to a mistake in their averaging process, the answers do not agree.

[2] R. M. Fuoss, J. Am. Chem. Soc. **63**, 2410 (1941), and also results obtained in our laboratory.

FIG. 1(b). An assumed potential for chain atom 4.

to show how these observed values of the average dipole moment may be combined with light scattering data in order to determine the nature and extent of the hindering of rotation in polymer molecules.[3]

Hindering of rotation must now be considered along with its consequences upon the calculation of the average dipole moment. To do this it becomes necessary to postulate a probable form of hindering to free rotation. This may be done as follows:

Let us consider any four adjacent chain atoms such as are shown schematically in Fig. 1(a). At any instant atoms 1, 2, and 3 define a plane. Consider now the possible movement of atom 4. If free rotation exists, this atom will be free to rotate on the dotted circle shown. We shall call this the valence circle.

In general, however, we have seen that atom 4 will be constrained in such a way that all positions of the valence circle are not equally probable. We can express this fact by stipulating that this atom experiences a certain potential at each point on this valence circle and, in general, the potential varies from point to point on the circle.

If θ is the angle of rotation of atom 4 out of the plane of atoms 1, 2, and 3 we can then say that this atom experiences a potential as a function of θ. The hindering to free rotation should then be expressible in terms of this potential, $V(\theta)$. For our calculations, it will be sufficient to approximate the actual potential by a deep rectangular potential well. An example of such an approximation is shown in Fig. 1(b).

Effectively then, we stipulate that there is a certain range of values of θ_4 in which atom 4 is free to rotate and that it is excluded from all other angles.

Such an approximation may seem at first thought to be quite a serious departure from reality. However, at a fixed temperature, it can be shown that any real potential may be represented to a fair accuracy by one or more such potential wells. This representation does, however, sacrifice an explicit temperature dependence of the dipole moment.

It may be easily seen that temperature effects will become apparent in the variation of the width of the

[3] This subject has been treated in another manner by W. Kuhn, Helv. Chim. Acta **31**, 1092 (1948). Unfortunately, his method of treatment does not lend itself well to the determination of the hindering process.

potential well. Since we shall express the width in terms of the so-called angle of free rotation, 2ϵ, we shall expect ϵ to vary with temperature. For example, if we were dealing with a simple potential such as is shown in Fig. 1(b), ϵ should increase with rising temperature. In what is to follow we shall assume ϵ and therefore the temperature to be constant.

Various hindering potentials have been used in the past to explain the size of molecules as found from light scattering and viscosity measurements. When any explicit form has been used, it has usually been similar to that shown in Fig. 1(b). Many others can be reduced to such a form. Furthermore, it is usually assumed that the center of this well is situated at such a position on the valence circle that its center coincides with $\theta=0$. That is to say, if the potential well were of near zero width, the chain would be nearly completely stiff and all its chain links would lie in a saw tooth arrangement in a single plane.

Owing to the wide use of such a model, we shall first calculate the dipole moment to be expected for poly-parachlorostyrene if its hindering were of this form. Such calculations have been made (see Appendix III) and the results are plotted in Fig. 2. On this graph we have plotted the ratio $\bar{\mu}^2/N_0\mu^2$ *vs* $\sin\epsilon/\epsilon$. For completely free rotation $\sin\epsilon/\epsilon$ is zero, and for a stiff chain it is unity.

For this calculation it has been assumed that the dipoles occur on alternate chain carbon atoms. These dipoles come off at the tetrahedral angle. But now it is possible to obtain two isomers because of the fact that the dipole group can occur on either one of two positions on the chain carbon.

Curve A in Fig. 2 is for the case where the dipoles appear on the same position on each chain unit. Curve B is for the case where the dipole position alternates. The latter structure probably applies in the case of polyvinyl chloride.[4] Although the structure of p.p.

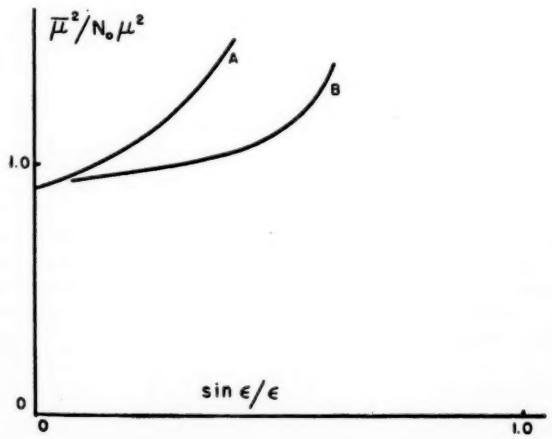

FIG. 2. The variation of dipole moment with degree of hindering for two normally planar molecular forms.

[4] C. W. Bunn, *Advances in Colloid Science* (Interscience Publishers, Inc., New York, 1946), Vol. 11.

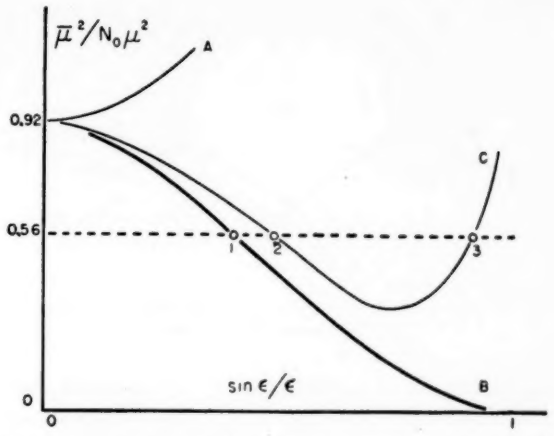

FIG. 3. Three typical curves showing the variation of dipole moment with degree of hindering.

chlorostyrene is not accurately known, it is probable that it is very much like polyvinyl chloride, and we shall assume this to be true.

In any event, both isomers are seen to give rise to curves which start out at $\bar{\mu}^2/N_0\mu^2$ values of 0.92 (i.e., the free rotation value) and rise rather rapidly as the chain becomes stiffer. Obviously, since the experimental value is 0.56, we see that it is impossible for this particular model for the hindering of free rotation in p.p. chlorostyrene to be correct. We must therefore conclude that symmetrical rotations of this type about a planar polymer configuration do not represent the true picture of this molecule.

We are, therefore, confronted with the problem of finding a potential for bond rotations which will give rise to an average dipole moment for the molecule equal to that observed. It need not be true that each chain bond experience the same potential as a function of θ; and, therefore, a large number of possible models exist. However, owing to obvious steric hindrances and with the known fact that the dipoles tend to cancel each other, this large number of possibilities may be reduced without actually calculating each one.

This process leaves a certain number of models as definite candidates for the true structures. It now becomes necessary to take definite models for the hindering and calculate how the dipole moment of our polymer molecule will depend upon the degree of stiffening of the chain for that particular model. In general, one obtains three different types of dependence. They are illustrated in Fig. 3.

Curve A is like the ones obtained previously for the traditional model. It starts at the free rotation value, 0.92, and rises more or less rapidly as the hindering increases. In such a model the dipoles do not oppose each other enough to reduce the value to the 0.56 found experimentally.

It is then logical to assume a model such that, if it were completely stiff, the dipoles exactly cancel each other. Such a model must obviously give a value of zero

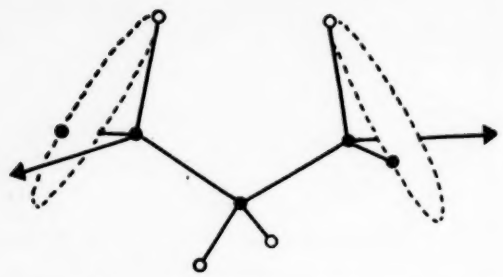

FIG. 4. A model which illustrates the probable zero configuration for polyparachlorostyrene.

when the chain is stiff. Curve B is typical of such a model. Since this curve passes through the experimental value, this model is a possible choice for the true polymer molecule.

A molecular configuration which has its dipoles nearly opposed when the chain is stiff gives rise to a curve such as curve C. The rapid rise near $\sin\epsilon/\epsilon=1$ is due to the fact that the stiff molecule must have a moment of $(N_0 f\mu)^2$, where f is the fraction of each dipole which remains uncompensated. It should be mentioned that this curve is extremely sensitive to small alterations in the assumed model. The position of the minimum rises very rapidly as the compensation of dipoles decreases.

We are therefore confronted with two possible types of models which are capable of giving the observed dipole moment. To proceed further we need the results of some other experiment. Fortunately, the size of the polymer molecule found from light scattering is sufficient to resolve the ambiguity.

For each of these models it is possible to calculate an expected size for the molecule. This may be done in a straightforward manner by simple modifications of known methods. These methods have been described elsewhere.[5] For each model we then obtain two values for $\sin\epsilon/\epsilon$, one which will explain the observed dipole moment and one which will explain the observed size.[6]

Points 1 and 2 of Fig. 3 are found to be at far lower values of $\sin\epsilon/\epsilon$ than is needed to explain the observed polymer size. Therefore, we are left with only one type of model which is capable of explaining both experimental facts. However, since this curve is so very sensitive to the particular model chosen for calculation, it is somewhat simpler to obtain the true value of $\sin\epsilon/\epsilon$ from the size of the molecule once the model has been approximately determined. This is true, since the size at a given $\sin\epsilon/\epsilon$ is relatively insensitive to the exact model chosen.

From such considerations we propose the following approximate picture of a polyparachlorostyrene molecule in solution.

If each chain link were at the center of the potential well in which it rotates, the chain would be rather extended and periodic in structure, repeating every four chain links. A typical segment of the chain may be illustrated schematically by use of Fig. 4. The actual model is thought to be a slight distortion of this form. Owing to the fact that the potential well has a definite width, the atoms rotate about this configuration through a certain free angle. This angle is about 65 degrees.

The model which we have postulated above is not the only one capable of satisfying the experimental facts. However, this model is probably the simplest reasonable one which is in agreement with experiment. The present method is very similar to x-ray crystal structure methods in that it is not capable of determining one and only one molecular model. Others may be possible. However, given any other postulated model, this method of attack can very easily determine if such a model is consistent with experimental facts.

APPENDIX I

The general equation for the dipole moment of a polymer molecule may be derived in a manner similar to that used in the case of simple dipoles. Consider a polymer molecule having N_0 dipoles of moment μ_n distributed along its length. If this molecule is placed in an electric field E, it will have a potential energy

$$-\sum_1^{N_0} V(\theta_n)-\sum_1^{N_0}\mu_n E,$$

where the added term in $V(\theta)$ is an internal potential due to steric and other factors. $V(\theta)$ is defined in the body of the paper.

If we now apply Boltzmann's distribution law, we find that the probability of finding our polymer molecule in any particular configuration is proportional to

$$\exp\Big[-\sum_1^{N_0}\frac{V(\theta_n)}{kT}-\sum_1^{N_0}\frac{\mu_n E}{kT}\Big].$$

However, since $\exp[-\Sigma V(\theta_n)/kT]$ is merely proportional to the probability of occurrence of any particular polymer configuration without an applied field we shall rewrite the above expression as

$$P(c)\exp[-\Sigma\mu_n E/kT].$$

The polymer will have a component of its moment along the direction of the applied field which is given by

$$\sum_1^{N_0}\mu_n f,$$

where f is a unit vector in the direction of the field. The product of this quantity with the probability function will give, upon integration over all possible chain configurations, the average contribution of a single polymer molecule to the polarization. This is, after the proper normalization,

$$\frac{\int\{P(c)\exp[x\Sigma\mu_n f]\}\Sigma\mu_n f d\tau}{\int\{P(c)\exp[x\Sigma\mu_n f]\}d\tau},$$

where x is E/kT and the integral is to be extended over all possible configurations.

This expression may be considerably simplified by expanding the exponential and dropping the higher terms so as to make the

[5] See, for example, a paper by W. J. Taylor, J. Chem. Phys. **16**, 257 (1948), which contains one method of calculation and gives references to others.

[6] We have found in our laboratory that polyparachlorostyrene molecules are about the same size as polystyrene molecules. Therefore, $R^2=25Na^2$. (A. M. Bueche, J. Am. Chem. Soc. **71**, 1452 (1949).)

average moment proportional to the electric field. Such an approximation is justified for all practical cases in which we can define a dielectric constant and no saturation effects are observable. The result for the average dipole polarization is $x\langle P\{\Sigma\mu_n f\}^2\rangle_{Av}$.

But this quantity is equal to $\bar{\mu}^2E/3kT$, where $\bar{\mu}$ is the average dipole moment of the whole polymer molecule. We therefore have finally for the average dipole moment of the polymer molecule

$$\bar{\mu}^2=3\left\langle P\left\{\sum_1^{N_0}\sum_1^{N_0}(\mu_n f)(\mu_m f)\right\}\right\rangle_{Av}.$$

APPENDIX II

To calculate the average dipole moment for a polymer molecule having free rotation we must evaluate $\langle\Sigma\Sigma(\mu_n f)(\mu_m f)\rangle_{Av}$. Now from a well-known geometrical relation we can obtain at once that

$$\cos(\mu_n,f)\cos(\mu_m,f)=\cos(\mu_n,\mu_m)\cos^2(\mu_n,f)+\sin(\mu_n,f)\cos(\mu_n,f)\sin(\mu_n,\mu_m)\cos\phi,$$

where ϕ is as shown in Fig. 5.

Since all directions of the field are equally probable, we obtain upon averaging that

$$\langle\cos(\mu_n,f)\cos(\mu_m,f)\rangle_{Av}=\tfrac{1}{3}\langle\cos(\mu_n,\mu_m)\rangle_{Av}.$$

The average for $\cos(\mu_n,\mu_m)$ may be easily found by a method similar to one first suggested by Eyring.[7]

If we consider the diagrams in Fig. 6, it is clear that we may write

$$\langle\cos(\mu_m,\mu_n)\rangle_{Av}=\langle\cos(a_k,\mu_m)\cos\beta+\sin(a_k\mu_m)\sin\beta\cos(\phi_k)\rangle_{Av}.$$

Now if free rotation exists, ϕ_k takes on all values from zero to 2π, and so the average of the second term is zero. We are then left with the relation

$$\langle\cos(\mu_n,\mu_m)\rangle_{Av}=\cos\beta\langle\cos(a_n,\mu_m)\rangle_{Av}.$$

The same process may be repeated again giving for the average

$$\cos\beta\cos\alpha\langle\cos(a_{n-1},\mu_m)\rangle_{Av}.$$

Finally, we obtain for the average

$$\cos\beta(\cos\alpha)^{(n-m-1)}\langle\cos(a_{m+1},\mu_m)\rangle_{Av},$$

and then

$$\langle\cos(\mu_n,\mu_m)\rangle_{Av}=\cos\beta\cos\gamma(\cos\alpha)^{n-m-1}.$$

In general, then if $K=(n-m)$ we obtain for $n\neq m$ the result

$$\langle\cos(\mu_n,\mu_m)\rangle_{Av}=\cos\beta\cos\gamma\cos^{k-1}\alpha.$$

If we use this fact, the series in the expression for the average dipole is readily evaluated. The result is

$$\bar{\mu}^2=\mu^2N_0[1+2p\cos\beta\cos\gamma/(1-p^2)],$$

where $p=\cos\alpha$. The approximation has been made that $p^N\ll1$. This is true in all practical cases.

APPENDIX III

To calculate the average dipole moment when hindering is present we proceed as in Appendix II down to the point where

$$\langle P(c)\cos(\mu_n,f)\cos(\mu_m,f)\rangle_{Av}=(1/3\mu^2)\langle P(c)\mu_n\mu_m\rangle_{Av}.$$

We now define unit vectors i_k, j_k, and h_k as shown in Fig. 6. We must therefore calculate $\langle P(c)i_ki_0\rangle_{Av}$. Now for the particular model under consideration it is clear that $P(c)$ is zero except for those values of θ_k which are inside the potential well. In these regions $P(c)$ will be unity. Therefore, because of the particular form assumed for the polymer molecule, it is true that as i_k rotates in its free angle, it will rotate in a symmetrical fashion so as to give an average value which is in the plane of h_k and h_{k-1}. It is therefore possible to express the average value of h_k and h_{k-1} and to write

$$\langle i_ki_0\rangle_{Av}=\langle Ah_ki_0+Bh_{k-1}i_0\rangle_{Av},$$

[7] H. Eyring, Phys. Rev. **39**, 746 (1932).

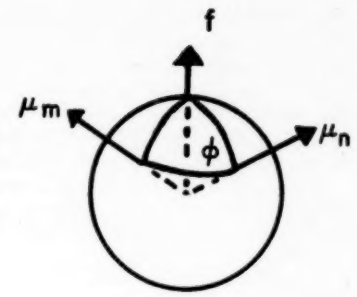

FIG. 5. A diagram illustrating the symbols used in the text.

where A and B are known constants which depend upon the function $\sin\epsilon/\epsilon$.

But the average of h_ki_0 can be related to the average of $h_{k-1}i_0$ and $h_{k-2}i_0$ in a similar manner. Therefore, we are able to arrive at a simple recurrence formula for the h_ki_0 and $h_{k-1}i_0$ averages. In this particular case this recurrence relation is sufficiently simple so that a compact closed form may be found quite readily for $\langle h_ki_0\rangle_{Av}$. After this is obtained, the result is substituted in the equation above, and all $\langle i_ki_0\rangle_{Av}$ are then determined. Using this relation, the series for $\bar{\mu}^2$ can then be summed. The above procedure was used to obtain the curves shown in Fig. 2.

More complicated potentials may be treated in the same manner. However, for twisted chain configurations it is often found that the recurrence relations become rather complicated. In such cases, the average is best found by reducing the recurrence relations down to a form such that each contains only the h's, i's, or j's along with i_0. The averages may then be calculated by numerical substitution in these relations. This latter procedure was followed in calculating the curves shown in Fig. 3.

APPENDIX IV

The experimental determination of the average dipole moment of poly p. chlorostyrene was done in the usual way by measuring

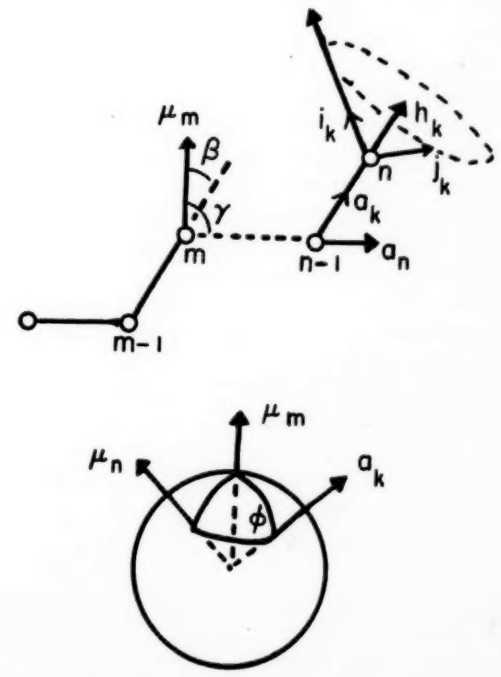

FIG. 6. Diagram showing the coordinates chosen for the calculations.

the dielectric constant of several concentrations of the polymer in benzene solutions. The cell was composed of three concentric metal cylinders enclosed in a glass tube. This cell has been used for a number of years in this laboratory for the determination of the dipole moments of low molecular weight compounds. Its capacitance was measured by the heterodyne beat method at a frequency of 1.5 Mc, which is well outside the dispersion range.

If M is the molecular weight of each chain unit, that is to say, the molecular weight of the polymer molecule is N_0M, then, providing N_0 is large compared with unity, it may be shown that

$$\bar{\mu}^2/N_0=(9kT/4\pi A)[P_\infty-M(n^2-1)/d_1(n^2+2)],$$

where A is Avogadro's number, n is the index of refraction of the solute, and P_∞ is the value at infinite dilution of

$$P=M\frac{100-x}{x}\left[\frac{\epsilon_{12}-1}{\epsilon_{12}+2}\frac{100}{(100-x)d_{12}}-\frac{\epsilon_0-1}{\epsilon_0+2}\frac{1}{d_0}\right].$$

In this expression, x is the weight percent of polymer, ϵ is the dielectric constant and d is the density. The subscripts 0, 1, and 12 refer to solvent, polymer, and solution, respectively.

Complete dielectric measurements were taken on two different batches of polymer. The average results obtained were $1.45D$ at 30°C and $1.46D$ at 50°C with an estimated error of about 1 percent.[8]

To find the quantity desired, $\bar{\mu}^2/N_0\mu^2$, we need yet the moment of the free chain unit. This was assumed to be the same as that for p-chlorotoluene, and a value of $1.93D$ was used. Although the values given in the literature do not agree too well with each other, this value was taken as an average of what appears to be the most reliable values. Assuming this value, we then obtain an experimental value of 0.56 for $\bar{\mu}^2/N_0\mu^2$.

[8] The monomer, parachlorostyrene, was kindly furnished by the Dow Chemical Company. Their analysis showed it to be 99.6 percent of the para isomer. The dipole values stated have been corrected for a small amount of chlorine lost during polymerization.

THE JOURNAL OF CHEMICAL PHYSICS VOLUME 19, NUMBER 5 MAY, 1951

The Vibrational Spectra of Molecules and Complex Ions in Crystals. V. Ammonia and Deutero-Ammonia*

F. P. READING AND D. F. HORNIG
Metcalf Research Laboratory, Brown University, Providence, Rhode Island
(Received November 20, 1950)

Infrared spectra of thin non-scattering films of NH_3 and ND_3 were obtained at −190°C. All four fundamentals of both compounds were observed with no evidence of inversion doubling of ν_2. The crystal spectrum of NH_3 suggests a frequency near 3450 cm^{-1} for ν_3 in the gas. The spectra are in agreement with a molecular crystal having the reported x-ray symmetry T^4. Two of the five torsional lattice vibrations were probably observed directly and one more strongly indicated in combination bands. A fourth lattice frequency of 53 cm^{-1} also occurs in combination bands. Since the coupling between the various internal vibrations and between the lattice and internal vibrations proved to be small, the potential function of the crystal was assumed to be separable into an internal and a lattice problem. A normal coordinate treatment of the internal vibrations fits all frequencies to better than one percent.

INTRODUCTION

AMMONIA is an example of a simple molecule which forms crystals of high symmetry in which the forces between the molecules are relatively large. It has been well studied in the gas phase; the additional features in the spectrum of the crystal arise from the effect of the crystalline field on the molecule and from coupling of the motions of the molecules. Since the intermolecular field arises largely from hydrogen bonding, these effects are of some interest in that they afford a tool for the more detailed study of the hydrogen bond. Furthermore, it has been reported that it is necessary to postulate dimerization of the molecules in the crystal in order to interpret the Raman spectrum.[1,2] It seems likely that the complications in the spectrum which this hypothesis was meant to explain are due instead to crystalline interaction and, indeed, it seems possible that a quantitative measure of such interaction may be obtained.

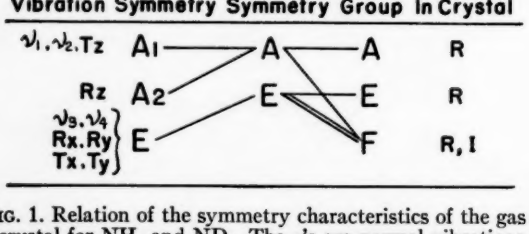

FIG. 1. Relation of the symmetry characteristics of the gas and the crystal for NH_3 and ND_3. The ν's are normal vibrations, the T's and R's translational and torsional lattice vibrations, and R and I indicate Raman and infrared activity, respectively.

The ammonia crystal has been reported by x-ray investigators to be cubic, having space group symmetry $T^4(P2_13)$, with four molecules per unit cell.[3,4] On the basis of present theory,[5,6] the spectrum of fundamental vibrations should be interpretable in detail, and it should be possible to determine whether the hydrogen atoms conform to the x-ray symmetry.

* This work was supported in part by ONR, under contract N6ori-88, Task Order I.

[1] G. B. B. M. Sutherland, Proc. Roy. Soc. (London) **141A**, 546 (1933).
[2] A. Dadieu and K. Kohlrausch, Naturwiss. **18**, 154 (1930).
[3] H. Mark and E. Pohland, Z. Krist. **61**, 532 (1925).
[4] J. de Smedt, Bull. classe. sci. Acad. roy. Belg. **11**, 655 (1925).
[5] D. F. Hornig, J. Chem. Phys. **16**, 1063 (1948).
[6] H. Winston and R. S. Halford, J. Chem. Phys. **17**, 607 (1949).

The relation between the symmetry species of the free molecule (C_{3v}), the symmetry about the center of gravity of each molecule in the crystal (C_3), and the symmetry of the entire unit cell† containing four molecules (T) is given in Fig. 1.‡ If the coupling between molecules is weak, it may be assumed that only vibrations of the same frequency in every molecule will couple; then Fig. 1 applies to the individual vibrations as well.

Only vibrations of species F may be active in the infrared spectrum of the crystal; consequently, vibrations of species A in the free molecule yield only one infrared active vibration in the crystal while each vibration of the doubly degenerate species E yields two infrared active vibrations. It should be noted that the appearance of doublets in this case is not owing to a removal of the degeneracy but to the fact that two different phases of coupling of the molecular motions give rise to infrared active fundamentals. All symmetry species may be active in the Raman spectrum so that vibrations of species A in the gas may give rise to two components in the Raman spectrum and vibrations of species E may give rise to three.

In addition to the internal vibrations of the molecules, the lattice vibrations, both motions of the center of gravity and torsional oscillations, may give rise to an infrared spectrum. Since the motions are strongly coupled, it is not strictly correct to separate the two categories, but it may be anticipated that the higher lattice frequencies are primarily torsions and the lower primarily translations. In particular, two infrared active vibrations may arise from the torsions about an axis perpendicular to the symmetry axis and one from the torsion about the symmetry axis. Similarly, there may be three infrared active vibrations arising from the translational motions; one of them, however, is the zero frequency limit of the acoustical branch of the lattice spectrum, so that only two may occur in the infrared spectrum.

EXPERIMENTAL METHOD

The ammonia and deutero-ammonia films were studied at -190°C, using the apparatus and techniques successfully employed by Hoffman in the study of crystalline HCN and BF_3.[7] The low temperature cell employed was a transmission type cell similar to that previously described[8] except that a side arm was attached to the outer jacket facing the cooling block. When gas was admitted through the side arm condensation took place, not only on the carrier plate but also on the surface of the cooling block and coolant reservoir. Using this procedure, it did not prove possible to obtain any information as to the thickness of the films obtained. This technique is extremely simple and convenient and makes it possible to adjust the film thickness readily. It is applicable to any material which has a sufficiently low vapor pressure at the temperature of liquid nitrogen and permits full recovery of the material when the cell is warmed.

Following the method of Hoffman, the NH_3 and ND_3 were admitted into the cell in small bursts through a stopcock connecting the cell with a storage bulb in which they were kept at a pressure of up to 20 cm Hg. The gas condensed on a one mm thick KBr (or KRS-5) plate held in the cooling block by a rectangular ring. If thermal contact of the plate to the block was maintained with a small amount of Apiezon "M" grease applied to the edge of the plate, the temperature of the center of the plate, measured with a thermocouple inserted into a small hole drilled into the KBr, was only 5°C above that of the copper block after ten minutes of cooling. The films obtained by this procedure were essentially non-scattering, except in the case of the thickest film studied, and it transmitted 90 percent of the radiation at 2500 cm^{-1}.

The NH_3 used was obtained from the Mathieson Alkali Company and was rated at 99.98 percent pure. No evidence of impurities was found in the spectra.

The ND_3 was prepared by passing D_2O vapor over two U-tubes filled with Mg_3N_2.[9] It was found necessary to space the Mg_3N_2 with plugs of glass wool to keep it from packing so tightly that the D_2O vapor could not flow through. The tube containing the D_2O and the U-tubes of Mg_3N_2 were separated by a U-tube filled with mercury, whose level was controlled by a leveling bulb. This enabled the D_2O to be stored for extended periods of time without being in contact with hydrogen containing greases. Before generation of the ND_3, the Mg_3N_2 was evacuated and heated to 350°C for two hours in order to remove traces of H_2O. The D_2O used§ was rated as 99.57 percent pure. The resultant ND_3 was found to be approximately 98 percent pure by comparing the relative intensities of ν_2 of ND_3 (815 cm^{-1}) and ND_2H (909 cm^{-1}).

The spectra were obtained with a double beam spectrophotometer[10] whose monochromator was taken from a Perkin-Elmer Model 12B spectrometer. CaF_2, NaCl, KBr, and KRS-5 prisms were utilized in these investigations.

The investigation in the KRS-5 region was complicated by the presence of a high percentage of stray light. In order to attenuate it, a stainless steel plate, roughened with aluminox grinding compound No. 120, was employed as the mirror before the entrance slit. This scattering filter reduced the stray light from 65 percent to 8 percent, at 450 cm^{-1} and from 87 percent to 31 percent at 310 cm^{-1} The reflectivity of this

† This is not the symmetry of the isolated unit cell but the effective symmetry in the crystal for active fundamental vibrations. Details are given in reference 5.

‡ In deriving Fig. 1, it is necessary to consider the separable degeneracy of species E encountered in C_3 and T individually.

[7] R. E. Hoffman, thesis, Brown University, 1949.

[8] E. L. Wagner and D. F. Hornig, J. Chem. Phys. **18**, 296 (1950).

[9] Smits, Muller, and Kröger, Z. physik. Chem. **B38**, 177 (1937).

§ Obtained from Norsk Hydro-Elektrisk Kvaelstofaktieselskab.

[10] Hornig, Hyde, and Adcock, J. Opt. Soc. Am. **40**, 497 (1950).

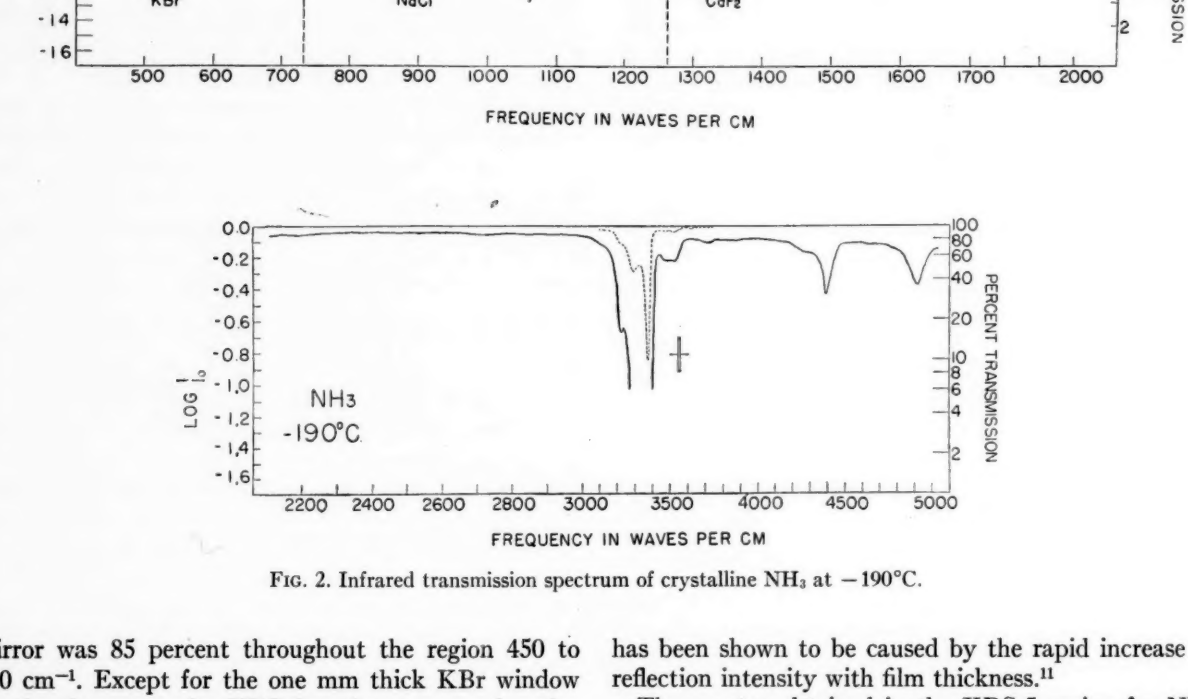

FIG. 2. Infrared transmission spectrum of crystalline NH_3 at $-190°C$.

mirror was 85 percent throughout the region 450 to 300 cm^{-1}. Except for the one mm thick KBr window on the thermocouple, KRS-5 optics were used exclusively in this region; under these conditions, spectra could be obtained to 300 cm^{-1}.

EXPERIMENTAL RESULTS

The spectra obtained for NH_3 and ND_3 at $-190°C$ from 500 cm^{-1} to 5000 cm^{-1} and 500 cm^{-1} to 3800 cm^{-1}, respectively, are shown in Figs. 2 and 3. These are experimental curves and have not been corrected for scattering nor has the noise level been appreciably smoothed. The solid line refers to a thick film, and the dotted line in regions of great absorption refers to a much thinner film. The absorption peak at 815 cm^{-1} in the thin ND_3 film shifts to a higher frequency in going to the thick film; we have studied a series of films of intermediate thickness and found that the frequency of the peak increases continuously to 820 cm^{-1} for a film with a peak absorption of 98 percent, although the line width remains approximately constant. The reason for this shift is not certain. Upon investigation of this phenomenon with a number of films of varying thickness and degree of scattering, the shift was found to depend only on the thickness. Consequently, it cannot result from an orientation effect which, of course, would be inconsistent with a cubic symmetry for the crystal. The shift resembles that of the ammonium salts which has been shown to be caused by the rapid increase of reflection intensity with film thickness.[11]

The spectra obtained in the KRS-5 region for NH_3 and ND_3 are shown in Figs. 4 and 5, respectively. Again these curves are experimental and no correction for stray light has been made, with the result that the bands are actually more intense than they appear to be in these figures. Curve A in Fig. 4 was obtained on the same thick film employed for Fig. 2. Comparing the relative intensities of the band at 527 cm^{-1} in curves A and B, it is seen that the band at 362 cm^{-1} is by far the most intense in the entire spectrum.

The band center of the ND_3 counterpart of this intense band lies, as may be seen in Fig. 5, below 300 cm^{-1}; and by comparison with the NH_3 curve, it is estimated to have its minimum at approximately 250 cm^{-1}.

FUNDAMENTAL FREQUENCIES IN THE CRYSTAL

The fundamental frequencies and relative integrated intensities found in the infrared spectrum of both NH_3 and ND_3 crystals, as well as the corresponding Raman bands for solid NH_3 as reported by Sutherland,[1] are shown in Table I. For comparison, the frequencies of the fundamentals in the gas[12] are also included. The error of the relative intensities is of the order of 10

[11] L. F. H. Bovey, J. Chem. Phys. **18**, 1684 (1950).

[12] See G. Herzberg, *Infrared and Raman Spectra of Polyatomic Molecules* (D. Van Nostrand Company, Inc., New York, 1945), p. 295.

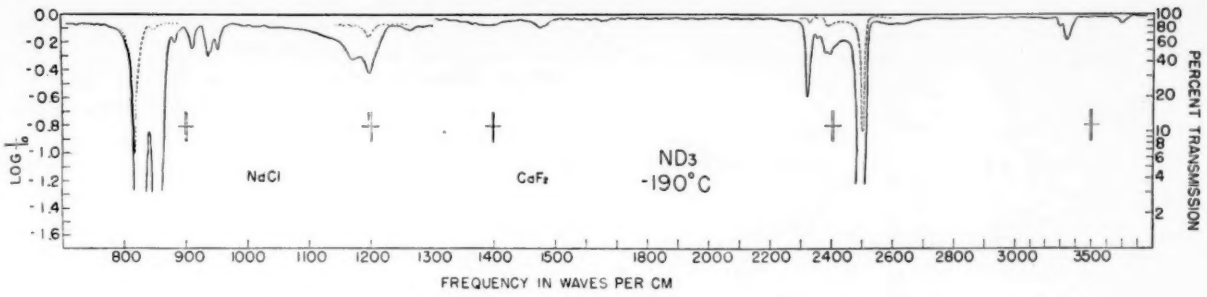

FIG. 3. Infrared transmission spectrum of crystalline NH_3 at $-190°C$.

percent. The average width at half-height of the resolved fundamentals is 22 cm^{-1} and none exceeds 35 cm^{-1}. It is, therefore, safe to conclude that the crystal is well ordered.[5,13]

The totally symmetric bending mode ν_2 occurs at 1060 cm^{-1} in NH_3 and 815 cm^{-1} in ND_3. This fundamental, which is split by 36 cm^{-1} in gaseous NH_3, has been observed in a number of films with no evidence of splitting and, consequently, of inversion doubling. This is to be expected, since hydrogen bonding certainly raises the potential barrier to the inversion by several kilocalories per mole.

The doubly degenerate bending vibration ν_4 occurs at 1646 cm^{-1} in NH_3 and 1196 cm^{-1} in ND_3. According to Fig. 1, it may have two components in the crystal. This may account for some of the absorption on the low frequency side of the observed peak in both NH_3 and ND_3, but absorption due to other causes, which will be discussed later, may also be expected in this region.

The only real question in the assignment concerns the hydrogen stretching vibrations, ν_1 and ν_3. The totally symmetric vibration ν_1 has been assigned to the shoulder at 3223 cm^{-1} in NH_3 and to the sharp peak at 2318 cm^{-1} in ND_3. The perpendicular stretching vibration ν_3 has been assigned to the very intense peaks at 3378 cm^{-1} and 2500 cm^{-1} in NH_3 and ND_3, respectively. If this assignment is correct, it is seen in Fig. 3 that ν_1 is only about $\frac{1}{10}$ as intense as ν_3 at 2500 cm^{-1}. Similarly, ν_1 in Fig. 2, although partially obscured, is not nearly as intense as ν_3. This assignment points to a complete reversal in the relative intensities of the two fundamentals in going from the gas to the crystal, since in the gas ν_1 is so intense that it completely obscures ν_3.[14] However, similarly great changes in relative intensity in going from the gas to the crystal have been observed before, for example, in HCN.[15]

The key to this assignment is the frequency 2318 cm^{-1} in ND_3 which is almost certainly a fundamental, both because of its sharpness and because no combination assignment fits it. Moreover, the corresponding line in NH_3 at 3223 cm^{-1} also appears to be sharp in the thick film and can be fitted only as $\nu_2+\nu_4+\nu_5$. It may be objected that the line at 2318 cm^{-1} appears to change intensity relative to its neighbor at 2390 cm^{-1} in going from thin to thick films, suggesting an impurity effect. However, in a number of films of varying thickness, the intensity ratio between it and the peak at 2500 cm^{-1} is constant so the variation must reside in the line at 2390 cm^{-1}. Undoubtedly the reason for this variation is that both of the partially deuterated ammonias also have lines in this vicinity. Since the lines at 2390 cm^{-1} and 3297 cm^{-1} in ND_3 and NH_3, respectively, fit their assignment to $2\nu_4$ and no satisfactory assignment based on their being fundamentals was possible, this alternative was eliminated.

The assignment of fundamental frequencies given in Table I yields the following values for the Teller-Redlich product ratios.‖

Species A:

$$\frac{\nu_1^H\nu_2^H}{\nu_1^D\nu_2^D}=\frac{3223\times1060}{2318\times815}=1.808 \text{ (harmonic value, 1.842).}$$

Species E:

$$\frac{\nu_3^H\nu_4^H}{\nu_3^D\nu_4^D}=\frac{3378\times1646}{2500\times1196}=1.860 \text{ (harmonic value, 1.871).}$$

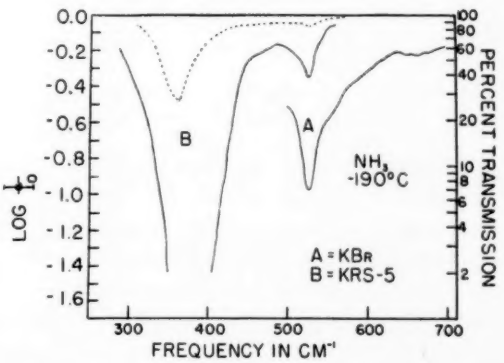

FIG. 4. Infrared transmission spectrum of crystalline NH_3 at $-190°C$ in KRS-5 region.

[13] D. F. Hornig, J. Chem. Phys. **17**, 1346 (1949).
[14] E. F. Barker, Phys. Rev. **55**, 657 (1939).
[15] R. E. Hoffman and D. F. Hornig, J. Chem. Phys. **17**, 1163 (1949).

‖ The moments of inertia used in calculating the harmonic values were those of the gas, taken from reference 25.

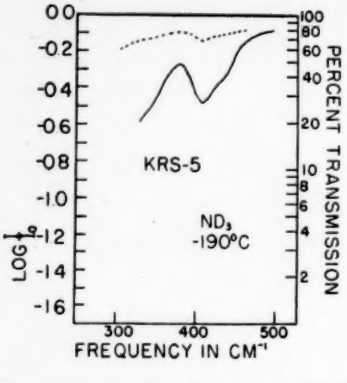

FIG. 5. Infrared transmission spectrum of spectrum of crystalline ND_3 at −190°C in KRS-5 region.

The agreement is as good as is usually obtained with deuterium substitution.

In order to consider the symmetry species separately, it is necessary to assume that the coupling between the molecules is weak so that there is no appreciable mixing of the A_1 and E vibrations (free molecule), which are both of species F in the crystal. It would be somewhat more rigorous to compare the product of all four vibrations of species F; this yields an experimental ratio of 3.363 compared to a theoretical ratio of 3.446. Rigorously it would be necessary to include the lattice frequencies of species F as well, but in this case it is probably safe to assume negligible interaction because of the wide frequency separation.

An alternate assignment in which the previous designations of ν_1 and ν_3 are interchanged was also considered. In this case, the Teller-Redlich product ratios would be:

$$\text{Species } A: \quad \frac{3378\times1060}{2500\times815}=1.757.$$

$$\text{Species } E: \quad \frac{3223\times1646}{2318\times1196}=1.914.$$

These ratios are not so far from the theoretical values as to rule out this possibility. Nevertheless, the ratio for species A is 5 percent low, somewhat more than might be expected, and the ratio for species E is 2 percent *high*, whereas anharmonicity usually produces a ratio lower than the harmonic value.

TABLE I. Fundamental frequencies of ammonia and deutero-ammonia.

Vibration	NH_3 frequencies (cm^{-1}) Crystal Infrared	Crystal Raman[a]	Gas Infrared	ND_3 frequencies Crystal Infrared	Gas Infrared
ν_1	3223(?)	3202(1)	3336	2318(1)	2419
ν_2	1060(12)	—	931.6 968.1	815(9)	748.6 749.0
ν_3	3378(10)	3369(4)	3414(?)	2500(12)	2555
ν_4	1646(1)	1585(0)	1627.5	1196(1)	1191
ν_5	527	—	—	406	—
$\nu_{5'}$	362	—	—	(250)[b]	—
$\nu_{5''}$	(250)[b]	—	—	(200)[b]	—
ν_6	(53)[b]	—	—	—	—

[a] See reference 1.
[b] Not directly observed. ν_5, $\nu_{5'}$, $\nu_{5''}$—Limiting perpendicular torsional oscillation in lattice; ν_6—Limiting parallel torsional oscillation in lattice or translational lattice vibration.

Other considerations also lead to the assignment given in Table I. Unless the crystalline field produces large interaction terms in a valence force potential function, ν_1 would remain lower in frequency than ν_3 in going from the gas to the crystal. Furthermore, in all cases of simple hydrogen bonded molecules which have been observed to date,[16] the frequency of hydrogen stretching vibrations decreases in passing from the gas to the crystal. If the alternate assignment were correct, however, ν_1 would increase in frequency by 42 cm^{-1}.

A knowledge of the polarization properties of the Raman spectrum in this region would assist in deciding the assignment; unfortunately, no polarization measurements on the crystal are yet available. However, the Raman spectrum of liquid ammonia[17,18] shows three lines, at 3220 cm^{-1}, 3300 cm^{-1}, and 3380 cm^{-1}, which have essentially the same frequencies as the lines observed in the infrared and Raman spectra of the crystal in the same region; it seems likely that the assignment in the liquid is the same as in the crystal. According to Bhagavantam, the line at 3220 cm^{-1} is strongly polarized, indicating an A type vibration, and that at 3380 cm^{-1} is only slightly polarized, indicating an E type vibration. These conclusions are in accord with the assignment arrived at here.

Although none of the four arguments presented are in themselves conclusive, they all point to the assignment of ν_3 to the higher of the frequencies in question and of ν_1 to the lower. This leads to the further conclusion that the relative intensities of the two vibrations in the infrared spectrum change enormously on crystallization.

Two Raman lines at 3202 cm^{-1} and 3369 cm^{-1} have been observed in the ammonia crystal in this region.[1] Since they apparently do not coincide with the infrared lines, they probably are the A component of ν_1 and the E component of ν_3 (under the unit cell group). It seems most likely then that the weak Raman line at 3202 cm^{-1} arises from ν_1 and that the strong line at 3369 cm^{-1} arises from ν_3, pointing to a reversal of the Raman intensities as well.

FREQUENCY OF ν_3 IN THE GAS

Since the fundamental frequencies in the crystal seem to be established, it may be possible to use them to help ascertain the frequency of the asymmetric stretching frequency ν_3 which is not certain in the gas. This frequency has been given as 3414 cm^{-1} by Barker[14] who considered the band at 2450 cm^{-1} to be $\nu_3-\nu_2$. However, this value is 85 cm^{-1} (2.5 percent) below that predicted by the Teller-Redlich product rule and the ND_3 frequencies, a greater deviation than might be expected

[16] D. F. Hornig, Trans. Faraday Soc., to be published.
[17] P. Daure, Trans. Faraday Soc. **25**, 825 (1929).
[18] S. Bhagavantam, Indian J. Phys. **5**, 54 (1930).

from the usual effect of anharmonicity. Consequently, Sutherland[19] chose the alternative value, 3450 cm^{-1}, taken from an absorption maximum which is not explained by the ν_1 band in this same region, which fits the product rule better.

The results of the crystalline investigation favor Sutherland's value. The shift in ν_3 for ND_3, where the gas frequency seems well established,[11] is -55 cm^{-1} or 2.2 percent. A proportionate shift in NH_3 would yield a frequency of 3452 cm^{-1} for ν_3 in the gas.

TORSIONAL VIBRATIONS

It seems highly probable that the two low-frequency peaks at 527 cm^{-1} and 362 cm^{-1} in NH_3 (Fig. 4) originate in the torsional oscillations perpendicular to the threefold axis. This motion, corresponding to the perpendicular rotation of the free molecule (Species E), may be expected to give two components in the crystal (Species F), which have been designated ν_5 and $\nu_{5'}$ in Table I. That they are so widely separated is a natural consequence of the fact that intermolecular coupling is a first order effect in lattice vibrations rather than a small perturbation, as in the case of the internal vibrations. A corresponding pair of lines occurs in ND_3 (Fig. 5), one at 406 cm^{-1}, and one at <300 cm^{-1}, which, from the shape of the high frequency side of the band, is estimated to be approximately at 250 cm^{-1}.

None of the three remaining infrared active fundamentals were observed directly, but the spectrum of NH_3 contains a series of sum and difference bands with a spacing of 53 cm^{-1} (Table II) which are centered about a frequency of 1048 cm^{-1}. This frequency must be the second, infrared inactive, component of ν_2 which is of species A in the crystal. The selection rules then require that the combining mode be of species F, identifying the frequency 53 cm^{-1} (ν_6) as one of the infrared active fundamentals. Preliminary observations of the Raman spectrum¶ of crystalline NH_3 confirm the deduction regarding the frequency 1048 cm^{-1} in that ν_2 has been resolved into two components at 1050 cm^{-1} and 1060 cm^{-1}.

The first component of a similar combination series in ND_3 is indicated by the band at 849 cm^{-1}. The band at 880 cm^{-1}, which at first sight appears to be the second component of the series, is probably an impurity, as will be discussed later. Furthermore, since no corresponding difference band was observed, it is not possible to place the inactive component of ν_2 (Species A) and, consequently, calculate the frequency of this lattice motion in ND_3.

Another torsional mode** is indicated by the bands at 1888 cm^{-1} in NH_3 and 1390 cm^{-1} in ND_3. These bands seem to require frequencies of about 250 cm^{-1} and 200 cm^{-1} in combination with the fundamentals at 1646 cm^{-1} and 1196 cm^{-1} in NH_3 and ND_3, respectively. This observation is substantiated by the fact that in the previously mentioned Raman spectrum of NH_3 a strong line was observed at 261 cm^{-1}. This vibration cannot yet be assigned; it may be the E type component of the perpendicular torsion, $\nu_{5''}$ (Table I), a component of the parallel torsion, or it may be the vibration ν_5 which was previously assigned to 527 cm^{-1}. In the latter case the absorption at 527 cm^{-1} would be ascribed to its first overtone.

TABLE II. Combination and overtone bands of crystalline NH_3 and ND_3.

NH_3 (cm^{-1}) obs	NH_3 (cm^{-1}) calc	ND_3 (cm^{-1}) obs	ND_3 (cm^{-1}) calc	Assignment
640–750	724	—	—	$2\nu_{5'}$
995	—	—	—	$\nu_2-\nu_6$
1100	—	849	—	$\nu_2+\nu_6$
1151	—	—	—	$\nu_2+2\nu_6$
1207	—	—	—	$\nu_2+3\nu_6$
1350–1600	—	1050–1180	—	ν_2+lattice modes
1600	1587	—	—	$\nu_2+\nu_5$
1888	—	1390	—	$\nu_2+\nu_{5''}$
3297	3292	2390	2392	$2\nu_4$
3450–3550	—	2550–2650	—	ν_1 or ν_3+lattice modes
4397	4438	3335	3315	$\nu_2+\nu_3$
4923	5024	3686	3696	$\nu_4+\nu_3$

COMBINATION AND OVERTONE BANDS

The combination and overtone bands observed are listed in Table II. They all differ from the characteristically sharp fundamentals in that they are broader and more diffuse, as is to be expected since the entire frequency branches arising from each of the combining fundamentals yield active combinations.[5,6]

The most interesting region of the spectrum is the broad region of tremendous integrated absorption intensity extending from 1350 cm^{-1} to 1650 cm^{-1} in the case of NH_3. It almost certainly arises in large part from the combination of the fundamental ν_2 at 1060 cm^{-1} with the torsional oscillations of the lattice. The complete frequency spectrum of these vibrations has not been calculated but it obviously extends from the vicinity of the limiting mode of this type at approximately 250 cm^{-1} ($\nu_{5''}$) to the vicinity of the limiting mode at 527 cm^{-1} (ν_5). It is not possible to discuss the details of this band without knowing the complete frequency distribution function of the torsional vibration branches, but it is probably significant that the regions of maximum absorption, 1422 cm^{-1} and 1587 cm^{-1}, are approximately coincident with the frequencies of combination with the observed limiting modes at 362 cm^{-1} and 527 cm^{-1}. This region is further complicated by the fact that the distribution $3\nu_5$ may be superimposed on it, as well as by the possibility that a second component of ν_4 may be contained in the shoulder between 1585 and 1640 cm^{-1}. The corre-

[19] G. B. B. M. Sutherland, Phys. Rev. **56**, 836 (1939).

¶ To be described in detail in another publication.

** Although it cannot be demonstrated that the vibrations discussed in this paragraph are torsions, the frequencies are all higher than expected for translations, so it is assumed that they are largely torsional motions.

TABLE IIIa. Force constants in the most general potential function for the internal vibrations of crystalline ammonia.

Symmetry		Valence force	
F_1	5.998 $\times 10^5$ dynes/cm	f_d	6.130 $\times 10^5$ dynes/cm
F_2	0.4852$\times 10^5$ dynes/cm	f_{dd}	−0.0712$\times 10^5$ dynes/cm
F_3	6.201 $\times 10^5$ dynes/cm	f_α	0.5835$\times 10^5$ dynes/cm
F_4	0.6377$\times 10^5$ dynes/cm	$f_{\alpha\alpha}$	−0.0492$\times 10^5$ dynes/cm
F_{12}	0.00 $\times 10^5$ dynes/cm	$f_{\alpha d}$	0.00 $\times 10^5$ dynes/cm
F_{34}	0.00 $\times 10^5$ dynes/cm	$f'_{\alpha d}$	0.00 $\times 10^5$ dynes/cm

TABLE IIIb. Comparison of calculated and observed frequencies using potential constants of Table IIIa.

	NH_3 freq. (cm^{-1})		ND_3 freq. (cm^{-1})	
	calc	obs	calc	obs
ν_1	3224	3223	2316	2318
ν_2	1069	1060	809	815
ν_3	3381	3378	2496	2500
ν_4	1649	1646	1194	1196

sponding region in ND_3 has only one clearly defined absorption maximum, while there are several in NH_3. This may possibly be due to the fact that $3\nu_5$ and $\nu_5+\nu_2$ fall some 50 cm^{-1} below ν_4 in NH_3, whereas in ND_3 they are slightly higher in frequency than ν_4.

The bands at 909, 1263, and 1475 cm^{-1} in ND_3 have been identified as partially deuterated ammonia bands by observing the spectrum of a two to one mixture of ND_3 and NH_3. This leaves only the bands at 880, 934, and 950 cm^{-1} in ND_3 to be accounted for, and from their varying relative intensity with respect to other bands in the spectra in going from one film to another, it seems highly probable that they are caused by some impurity. In two films they were absent altogether.

FORCE CONSTANTS IN THE AMMONIA CRYSTAL

Following the first paper in this series,[5] the potential function for the ammonia crystal may be written in the form

$$V=V_l+\sum_j V_j+V_{mm'}+V_{ml}, \tag{1}$$

where V_l includes only lattice coordinates (e.g., coordinates of the center of gravity and principal axes of each molecule), V_j includes the internal coordinates of the jth molecule, $V_{mm'}$ includes cross terms between the internal coordinates of different molecules, and V_{ml} represents cross terms between lattice and internal coordinates.

Because of the considerable frequency separation between lattice frequencies and internal frequencies, the effect of the term V_{ml} is probably small and in first approximation may be neglected. The small difference between the frequencies observed in the Raman and infrared spectra as well as the failure to find a second component of ν_3 and ν_4 suggest that the contribution of the coupling term $V_{mm'}$ is not great. In this case the potential function may be written in first approximation as

$$V=V_l+\sum_j V_j. \tag{2}$$

The problem of the lattice vibrations and the internal vibrations of the individual molecules now separates and the latter can be treated by the usual methods. The potential function V_j of each molecule differs from that of the free molecule only in that the crystalline field resulting from the equilibrium configuration of the crystal changes the effective valence force constants.

Since all four frequencies in both NH_3 and ND_3 were observed, it should be possible to evaluate the six force constants in the most general valence force potential function[20,21] given below:

$$2V=f_d\sum d_j^2+d_0^2f_\alpha\sum\alpha_{ij}^2+2f_{dd}\sum d_id_j+2d_0^2f_{\alpha\alpha}\sum\alpha_{ij}\alpha_{ik} +2d_0f'_{\alpha d}\sum\alpha_{ij}d_k+2d_0f_{\alpha d}\sum\alpha_{ij}d_i. \tag{3}$$

This potential function differs from that of the references cited in that it explicitly includes the factor of two in all cross terms whereas they include it in the interaction force constants. In Eq. (3), the equilibrium N−H distance is d_0 and the valence force constants are bond stretching (f_d), angle bending (f_α), bond-bond interaction (f_{dd}), angle-angle interaction ($f_{\alpha\alpha}$), bond adjacent angle interaction ($f_{\alpha d}$), and bond opposite angle interaction ($f'_{\alpha d}$).

Following the method of Wilson,[22] the changes in N−H bond lengths (d_j) and H−N−H bond angles (α_{ij}) were used as internal coordinates. Since the local symmetry about each molecule in the crystal is C_3, which contains two species, A and E, symmetry was used to factor the F and G matrices. The blocks of the factored F matrix are of the form given below, the latter block occurring twice.

$$\text{Species } A \quad \begin{vmatrix} F_1 & d_0F_{12} \\ d_0F_{12} & d_0^2F_2 \end{vmatrix} \qquad \text{Species } E \quad \begin{vmatrix} F_3 & d_0F_{34} \\ d_0F_{34} & d_0^2F_4 \end{vmatrix}.$$

The F's are the various symmetry force constants, given explicitly in terms of the valence force constants by the following relations:

$$\begin{aligned} F_1&=f_d+2f_{dd} & F_3&=f_d-f_{dd} \\ F_2&=f_\alpha+2f_{\alpha\alpha} & F_4&=f_\alpha-f_{\alpha\alpha} \\ F_{12}&=f'_{\alpha d}+2f_{\alpha d} & F_{34}&=f'_{\alpha d}-f_{\alpha d}. \end{aligned} \tag{4}$$

These symmetry force constants are like those used by Hemptinne and Delfosse,[20] except that their constants for Species E are twice those given above.

The G matrix elements were taken from those tabulated by Decius,[23] and the elements of the factored G-matrix contain the same linear combinations as the F matrix, Eq. (4).

[20] M. de Hemptinne and J. Delfosse, Ann. soc. sci. Bruxelles **56**, 373 (1936).
[21] J. Duchesne and I. Otellet, J. Chem. Phys. **17**, 1354 (1949).
[22] E. B. Wilson, Jr., J. Chem. Phys. **7**, 1047 (1939); **9**, 76 (1941).
[23] J. C. Decius, J. Chem. Phys. **16**, 1025 (1948).

There are eight possible sets of force constants which may be obtained for the general potential function; since all eight observed frequencies are needed to calculate the six force constants (one in each symmetry class is determined by the product rule and is independent of the specific potential function), no mathematical elimination is possible. The set which corresponds to normal coordinates in which the high frequencies are all N−H stretching frequencies and the low frequencies are bends is the only set which is physically reasonable and is given in Table IIIa. The frequencies calculated from this potential function are compared with those observed in Table IIIb. The discrepancy is less than 1 percent and is as good as the product rule in all cases.

It is of great interest that the best fit is obtained when the symmetry factored F matrix is diagonal. However, F_{12} and F_{34} cannot be determined with any precision, since they enter the equations for the frequencies either as squares or with very small coefficients. Conversely, the calculated frequencies are very insensitive to these constants. This is illustrated in Table IV by a set of force constants which are not quite a best fit (but which were obtained as a best fit in preliminary calculations) together with calculated and observed frequencies. Although the force constants are substantially different from those of Table IIIa, the maximum frequency deviation is still but 1.1 percent and the general fit is very nearly as good as with the force constants of Table IIIa. This same difficulty occurs, of course, in determining the potential function for gaseous ammonia.[20]

Because of the insensitivity to F_{12} and F_{34}, and because the best fit of the most general potential function was obtained when $F_{12}=F_{34}=0$, these constants were set equal to zero, and the four NH_3 frequencies were used to calculate the remaining four force constants. Four sets were obtained, one of them being the set of Table IIIa, but when they were used to calculate the four ND_3 frequencies, two of them, the expected number, gave a bad fit and were eliminated. The remaining set fitted almost as well as that of Table IIIa but was physically unreasonable, corresponding to the assignment of the high frequencies to bond bending coordinates and the low frequencies to bond stretching.

Two other more simplified potential functions were tried. The first included only the diagonal force constants f_d and f_α, and the second included f_d, f_α, and the off diagonal constant $f_{\alpha\alpha}$. In both cases the correlation between the observed and calculated frequencies was poor and their deviation greater than the deviation of the experimental from the theoretical product ratios.

TABLE IV. Comparison of calculated and observed frequencies using a slightly varied most general potential function.

Force constants ($\times 10^{-5}$ dyne/cm)		NH_3 freq. (cm^{-1}) calc	obs	ND_3 freq. (cm^{-1}) calc	obs
$F_1 = 5.911$	ν_1	3220	3223	2321	2318
$F_2 = 0.500$	ν_2	1069	1060	806	915
$F_3 = 6.075$	ν_3	3374	3378	2502	2500
$F_4 = 0.655$	ν_4	1654	1646	1192	1196
$F_{12} = -0.24$					
$F_{34} = 0.23$					

Until reliable values of all of the fundamental frequencies are available in gaseous ammonia, the potential function in the crystal cannot be compared in detail with that of the gas. Nevertheless, the effective N−H stretching force constant is certainly lowered about 5 percent, and the effective bending force constant is raised by approximately 40 percent.[24] This large apparent change is due chiefly to the failure to include the correction for the anharmonicity of ν_2 in the calculation of the gas force constants. Dennison[25] has calculated the harmonic value of ν_2 to be 1055 cm^{-1} in NH_3 and 803 cm^{-1} in ND_3. The bending force constants for the crystal are only about 5 percent higher than gas force constants calculated from these values. It is apparent then that the greatest effect of the crystalline field is to raise the barrier to inversion and largely eliminate the anharmonicity, a conclusion which agrees with that previously arrived at from the absence of any evidence of splitting of ν_2.

CONCLUSION

It appears then that the infrared spectra of crystalline NH_3 and ND_3 can be interpreted in terms of the motions of monomeric molecules, coupled weakly in a crystal lattice having the x-ray structure previously reported. There is no indication of the presence of dimers or higher polymers, except in the sense that any crystal is an infinite polymer.

[24] See reference 12, p. 177, for comparison with gas values.
[25] D. M. Dennison, Revs. Modern Phys. **12**, 175 (1940).

The Exchange of Water Between Hydrated Cations and Solvent

JOHN P. HUNT* AND HENRY TAUBE
George Herbert Jones Laboratory, University of Chicago, Chicago, Illinois
(Received October 16, 1950)

The rate of exchange of water between the hydrated forms of Al^{+++}, Cr^{+++}, Fe^{+++}, Ga^{+++}, and Th^{+4} and the solvent water has been measured in solutions of varying acidity. With the exception of chromic ion, and of ferric ion at low acidity, the exchange is complete in *ca* 3 min at 25°. For chromic ion, the half-time for exchange is independent of acidity over a wide range and is *ca* 40 hr at 1 *M* salt concentration. The coordination number of chromic ion for water over the entire acidity range is 6.0. The initial hold-back of oxygen by ferric ion at low acid is slight and is attributed to the presence of polynuclear hydrolyzed species. For all the cations, the distribution of oxygen isotopes in the final solution is noticeably different from random, the cations showing a greater affinity for H_2O^{18} over H_2O^{16}.

The rates of exchange are correlated with the electronic structure, which influences the energy required to form the transition state.

THIS paper presents and discusses the results of measurements of the rate at which water exchanges between dissolved (hydrated) cations and solvent water. Data of this type have significance in relation to a number of problems arising in solution chemistry and the chemistry of complex ions. In this introduction, a brief discussion is given of several important applications which can be made with the data under optimum circumstances. Not all of the applications have been fully realized, however, owing to the incompleteness of data of the type reported in this paper and of subsidiary data.

The exchange data can contribute directly to the problem of determining the stoichiometry of the complex constituted by dissolved cations and the molecules of water directly bound to them. This application rests on the reasonable presumption that water directly bound to the cation will exchange with water in the body of the solvent less rapidly than water held in succeeding layers. In principle at least, therefore, the exchange method offers a means of counting the directly bound water. An example of a successful application of this kind was described in a previous communication[1] in which some exchange results for Cr^{+++}aq were presented. The data obtained prove that a definite kinetic unit of formula $Cr(H_2O)_6^{+++}$ exists in aqueous solutions of chromic perchlorate.

Data on the rate of exchange of water between hydrated cations and solvent are of significance also in relation to the general problem concerned with the lability of complex ions and the factors influencing lability. Numerous observations have been made on the rates at which complex ions in water solution form, dissociate, or exchange groups. The exchange of water for water is a specially important case of reactions of this type, and it is of interest to discover whether this reaction shows the same general rate behavior as do the more definitely formulated reactions involving ligands other than solvent molecules. Furthermore, the data on the water exchange are of particular significance in attempting to arrive at an understanding of the factors which affect the lability of complex ions with respect to substitution. For the aquo ions, data exist from which the hydration energies can be calculated, and values for the hydrolysis constants of the aqueous cations are known. Both types of information are useful in reaching conclusions about the type of bond operative in the aquo complex ions, and the role that bond-type plays in determining the rate of substitution can be traced.

Although some kinetic data have been accumulated for reactions involving substitution in complex ions of coordination number six, little progress has been made in discovering the detailed mechanisms of the substitution reactions. The reactions which have been studied kinetically almost invariably involve water as reactant or product. Since water is also the solvent, the measurements have not specified the order of the reaction with respect to water. This hiatus leaves an important ambiguity about mechanism which, however, may be resolved by studies on the rate of exchange of water between complex ion and solvent. To illustrate: the reaction $Co(NH_3)_5H_2O^{+++}+Cl^-=Co(NH_3)_5Cl^{++}+H_2O$ has been found[2,3] to proceed by the rate law $k(Co(NH_3)_5H_2O^{+++})(Cl^-)$ in the forward direction, and by the rate law $k'(Co(NH_3)_5Cl^{++})$ in the reverse. Either mechanism (A) or (B) is consistent with these rate laws.

(A)

$$Co(NH_3)_5H_2O^{+++} \geq Co(NH_3)_5^{+++}+H_2O$$

(rapid equilibrium)

$$Co(NH_3)_5^{+++}+Cl^- \underset{k_1'}{\overset{k_1}{\rightleftarrows}} Co(NH_3)_5Cl^{++}$$

(rate determining)

(B)

$$Co(NH_3)_5H_2O^{+++}+Cl^- \underset{k_2'}{\overset{k_2}{\rightleftarrows}} Co(NH_3)_5Cl^{++}+H_2O.$$

* AEC predoctoral fellow, 1948–49.

[1] J. P. Hunt and H. Taube, J. Chem. Phys. **18**, 757 (1950).

[2] F. J. Garrick, Trans. Faraday Soc. **33**, 486 (1937).

[3] B. Adell, Z. anorg. u. allgem. Chem. **246**, 303 (1941).

According to mechanism (A), which is a dissociation mechanism, an intermediate of coordination number five is formed. Mechanism (B) is a substitution mechanism and implies an intermediate or activated complex of coordination number seven. Mechanism (A) requires that the *rate* of formation of the particular complex ion studied must always be less than the *rate* of exchange of water; mechanism (B) places no requirement on the relation of the rates for the two processes. The importance of water exchange studies in understanding systems of this type is evident.

EXPERIMENTAL METHODS

The procedure used in the exchange studies involves the following steps. Initially, a solution of precisely determined chemical composition, containing the metal salt and perchloric acid dissolved in water of ordinary isotopic composition, is mixed in a known amount with water enriched in O^{18}. Aliquots are withdrawn at measured intervals and subjected to vacuum distillation, thereby removing a part of the water rapidly. The samples of distillate water are equilibrated with carbon dioxide, and the isotopic composition of the carbon dioxide is determined by mass spectrometric analysis. From the mass ratio measurements, the isotopic composition of the distillate water after various time intervals can readily be calculated. From the chemical composition and the isotopic compositions of the ordinary and enriched samples, calculations can be made for the isotopic compositions expected in the solvent water, assuming various ways of distributing the water between hydrated cations and solvent.

A supply of water of ordinary isotopic composition was prepared by repeated distillation of ordinary water, and it was preserved in a Pyrex glass container. Water enriched in O^{18} was similarly treated and preserved. The solutions containing $Al^{+++}aq$, $Cr^{+++}aq$, $Fe^{+++}aq$, or $Ga^{+++}aq$ were prepared from samples of the corresponding perchlorates, specially prepared and purified. The compositions of the solid salts were established by analyzing for the metal ion and for perchlorate ion.[4] The solutions, as well as the solid salts, were analyzed. In both cases, the water content was established by difference. The compositions of the solid perchlorates are expressed by the following formulas:

$$Al(ClO_4)_{3.00}(H_2O)_{6.31}(HClO_4)_{0.30},$$
$$Fe(ClO_4)_3(H_2O)_{6.60}(HClO_4)_{0.35},$$
$$Ga(ClO_4)_{3.00}(H_2O)_{5.85}(HClO_4)_{0.28},$$
$$Cr(ClO_4)_{3.00}(H_2O)_{6.15}.$$

The aluminum, iron, and gallium perchlorates were crystallized from perchloric acid solution, chromium perchlorate from water. For the experiments with thorium ion, A. R. thorium nitrate was used without further purification, and only the composition of the solution was determined.

Some features of the isotope ratio measurements deserve mention. Except for some preliminary ones made with a Consolidated-Nier mass spectrometer,[5] the analyses were made with the high precision instrument constructed by H. C. Urey and co-workers. Relative values of isotope ratios are measured rather than absolute values, and, in reporting the results, the procedure was adopted of normalizing all readings by a factor so as to give a value of 2.000×10^{-3} for the ratio H_2O^{18}/H_2O^{16} in a standard of ordinary water. Precise relative values suffice for the applications which have been made of the results. It was found that the mass spectrometer did not give readings linear in isotopic composition over the range studied, *ca* 15 percent change. The deviation was never greater than 0.6 percent. Corrections were applied for the nonlinearity effect, based on an empirical calibration curve made using standards covering the range of ratios studied. The standards were made up from the reserve supplies of ordinary and enriched water. The isotopic ratio H_2O^{18}/H_2O^{16} of the normal water was taken as 2.000×10^{-3}. For the enriched water, this ratio was *ca* 7.5-fold greater, and it was measured by the analytical service of Consolidated Engineering Corporation. As has already been pointed out, the conclusions from the data are not sensitive to small variations in absolute enrichments, and, since in the analysis comparisons were made with empirical standards made up from the reserve supplies, they are not sensitive to small possible errors in measuring the relative abundances of O^{18} in the ordinary and enriched waters.

Certain symbols recur in the succeeding discussion, and for convenience in reference their meaning is defined here.

N_c^{∞} represents the value calculated for the mole fraction of H_2O^{18} *in the solvent water of the solution*, based on the proportions of light and enriched water, and their enrichment factors, assuming random mixing of the isotopes in all forms of water.

${}^nN_c$ represents the mole fraction of H_2O^{18} in the solvent water, calculated assuming that n molecules of water per cation are held back from exchanging on mixing.

N_{obs} represents the mole fraction of H_2O in a sample of water *distilled* from the solution, as determined by isotopic analysis. Right superscripts 0, t, and ∞ define the time after mixing.

R is the ratio $C^{12}O^{16}O^{18}/C^{12}O_2^{16}$ obtained from the mass spectrometer reading on normalization and after correcting for mass 45 and the nonlinearity effect.

Q is the mole ratio H_2O/CO_2 used in the equilibrations prior to mass ratio determinations.

[4] H. H. Willard, private communication. The method is a gravimetric one based on ϕ_4PClO_4. Details of the method are contained in the Ph.D. thesis "Water exchange between hydrated cations and solvent," J. P. Hunt, University of Chicago, Chicago, Illinois, 1950.

[5] Courtesy L. Friedman, Brookhaven National Laboratories.

TABLE I. Exchange of water with the container at 25° (volume of liquid, 10 cc).

Container	$t-t_0$ (days)	$N_{obs}\times10^3$
Pyrex	0.8	8.087
	16	8.097
	79	8.090
Kimble	0	8.404
	15	8.362

K is the equilibrium constant for the reaction

$$C^{12}O_2^{16}+H_2O^{18}=C^{12}O^{16}O^{18}+H_2O^{16},$$

and was calculated as 2.078 at 25°C based on data given by Urey.[6]

M is the molality of the species indicated, based on total water.

$t-t_0$ is the average elapsed time between mixing the solutions with the enriched water and the sampling by distillation.

N_{obs} is calculated from measured quantities using the relation

$$N_{obs}=[R/(K+R)]+[R/Q(1+R)]-R_0/Q.$$

R_0 is the ratio $CO^{16}O^{18}/CO_2^{16}$ in normal CO_2. The ratio Q was always greater than 50, and the maximum value of R is about 25×10^{-3}. It can be seen, therefore, that an error in determining relative values of R is directly reflected as the same fractional error (very nearly) in determining relative values of N_{obs}. The estimated error in relative values of R is ±0.2 percent. Q was measured to ±2 percent. At the minimum value of Q the maximum error is N_{obs} is contributed, and at maximum amounts to ±0.08 percent. Some error in N_{obs} was introduced because the CO_2+H_2O systems were not thermostatted during equilibration. From the maximum variation in room temperature and the temperature coefficient for K, the error from this source at maximum is ±0.1 percent. The reproducibility of the data support these estimates of error and show that, in the usual case, the relative values of N_{obs} are precise to within ±0.2 percent.

The values of N_e are also precise to within ±0.2 percent in the usual case. The greatest source of error in N_e arises in the determination of the mole fraction of ordinary water in the mixture. In the worst case, the analysis fixes the mole fraction to within ±0.3 percent.

The distillation method of sampling the solvent introduces a difficulty in the interpretation of the results. This separation method can reasonably be assumed to be free from any significant influence on the exchange phenomenon itself. The only change introduced by the distillation is an increase in the concentration of the solute by 30 percent at most. The results for the slow exchanges show that this change in concentration has no detectable effect on the observations; and furthermore, assuming reasonable kinetic behavior, it will be of no consequence in the rapid exchanges, which are completed by the time of the first sampling. The difficulty with the distillation method of sampling lies in the fact that the isotope ratio is determined on distillate water rather than solution water directly. Fractionation of the isotopes takes place during distillation, and for an equilibrium process the fractionation factor at 25° is 1.008.[7] The distillation process in these experiments was not conducted under equilibrium conditions, and it was necessary to make a special study of the fractionation produced by the distillation procedure under a variety of conditions. For removal of 0.22 of a sample of water, the ratio of the mole fraction of H_2O^{18} in the original water to that in the distillate was found to be 1.005. All distillations were carried out as reproducibly as possible, removing in every case *ca* 0.2 of the water in the solution. The effect exerted by salts on the fractionation by distillation is discussed in a later section of this paper.

Experiments were performed to test whether the data are affected by the exchange of ClO_4^- or the glass containers with the solvent. The results are reported in Tables I and II. They prove that neither of these possibilities for exchange influence the results, and they serve also to illustrate the reproducibility of certain of the steps in the procedure.

Since N_e^∞ represents the mole fraction of H_2O^{18} in the solvent water and N_{obs} that in the distillate, the ratio N_e^∞/N_{obs} is a measure of the fractionation on distillation from the salt solution, to be compared with 1.005 for pure water.

TABLE II. Exchange of ClO_4^- with solvent water. ($(NaClO_4)$, 4.5 M; $(HClO_4^-)$, 1.45 M. ClO_4^- of ordinary isotopic composition, solvent enriched in O^{18}; temperature, 25°.)

Container	$t-t_0$ (days)	$N_{obs}\times10^3$	N_e^∞/N_{obs} [a]
Pyrex	0.95	7.866	1.009
	9	7.857	1.010
	17	7.884	1.007
Paraffined pyrex	1.1	7.993	1.009
	17	8.004	1.008
	79	7.997	1.009

[a] Calculated for isotopic composition of water in solution assuming no exchange with ClO_4^- or container.

EXPERIMENTAL RESULTS

In Table III are presented the results of experiments with cations for which the exchange was observed to be complete within the time of the first sampling—*ca* 3 min. For the cations Al^{+++} and Ga^{+++}, both at low acidity and high acidity, and for Fe^{+++} at high acidity, the values of N_{obs} are independent of time and correspond closely (see factor N_e^∞/N_{obs}) to N_e^∞, the value calculated for random mixing in the solution. With Fe^{+++}, at lower acidity, a slight initial hold-back

[6] H. C. Urey, J. Chem. Soc. 562 (1947).

[7] E. H. Riesenfeld and T. L. Chang, Z. physik. Chem. **B33**, 127 (1936).

of water followed by a slow exchange, is observed. The solutions of Th^{+4} were studied at a single, rather low acidity. The data for Th^{+4} show that for this ion also exchange is complete by the time of the first sampling. An incidental conclusion which may be drawn from the data is that in one day NO_3^- does not exchange appreciably with water under the experimental conditions. In every case, the values of N_{obs} are far from those calculated for hold-back by each cation of 6 molecules of water (see values of ${}^6N_c$ in column 6).

For Cr^{+++}aq, the exchange of water with solvent was observed to proceed measurably slowly. The data relating to this exchange, published in an earlier communication, have been extended and are reported in full in Table IV.

TABLE III. Exchange data for Al^{+++}aq, Ga^{+++}aq, Fe^{+++}aq, Th^{+4}aq at 25°C.

Ion	M	MH^+	$t-t_0$ min 1	$N_{obs}\times10^3$	${}^6N_c\times10^3$	$N_c^\infty\times10^3$	N_c^∞/N_{obs}
Al^{+++}	1.106	0.336	4	6.107	6.744	6.179	1.012
			49	6.083			1.016
	0.9668	0.969	3	7.200	7.884	7.273	1.010
			10,000	7.199			1.010
			17,000	7.207			1.009
Ga^{+++}	1.046	0.295	2.5	6.101	6.739	6.203	1.016
			60	6.104			1.016
	1.241	1.199	2.5	4.477	4.938	4.549	1.016
	1.231	1.188	60	4.571	5.037	4.633	1.013
Fe^{+++}	1.082	0.385	4	6.210	6.738	6.185	0.996
			60	6.172			1.002
	1.154	1.177	3.5	5.791	6.413	5.863	1.012
	1.154	1.176	60	5.809	6.421	5.871	1.010
Th^{+4}	1.005	0.091	3	7.835		7.940	1.013
			1440	7.835			

DISCUSSION OF THE DATA

Equilibrium Aspects

The conclusion reached in an earlier communication that the coordination number of Cr^{+++} for water in aqueous solution is six is confirmed by the present data, which extend the acidity range investigated. The ratio ${}^6N_c/N_{obs}{}^0$, which compares the value calculated for the isotopic composition of the solvent water assuming hold-back per chromic ion of six molecules of water, with the isotopic composition of the distillate at zero time, has for experiments A, B, C, and D the values 1.006, 1.005, 1.013, and 1.006, respectively. The fractionation on distillation accounts for a ratio of 1.005. Within experimental error, the isotopic composition of the solvent water is that expected for hold-back by each chromic ion of six molecules of water. The high value of ${}^6N_c/N_{obs}{}^0$ in experiment C can be attributed to the high concentration of perchloric acid and the distillation fractionation produced by it. The ratio ${}^nN_c/N_{obs}{}^0$ is rather sensitive to the coordination number n. Thus, for experiment B, ${}^7N_c/N_{obs}{}^0$ is calculated to be 1.029—i.e., an increase in the assumed coordination number by one unit affects ${}^nN_c/N_{obs}{}^0$ by 24 parts per 1000. The precision of the data justifies the conclusion that the coordination number of chromic ion over the whole acidity range is 6.0±0.1.

The other ions studied—Al^{+++}, Fe^{+++}, Ga^{+++}, Th^{+4}, and, incidentally, H^+—exchange water so rapidly that the determination of coordination number by the present method was unsuccessful.

A second method of treating the data to obtain coordination numbers involves taking account of the total change in N_{obs} during the experiment, and the assumption that the distribution of the isotopes between solvent and hydrate water in the final solution is random. This method has advantages over the one previously discussed, since it is much less sensitive to errors in chemical analysis and is almost insensitive to the magnitude of the fractionation factor. It yields for the coordination number of chromic ion values slightly in excess of six. The coordination number is sufficiently well established as 6.0 by the previous method, and the deviation from six can be attributed to the failure of the assumption made in applying the second method. Since the value for n obtained by the second method is in excess of six, the conclusion follows that chromic ion displays a preference for H_2O^{18} over H_2O^{16} in extracting water molecules from the solvent to build the coordination sphere.

The chemical isotope-fractionation exerted by chromic ion, as well as the other cations studied, is demonstrated also by considering the data in another way. $N_c^\infty/N_{obs}^\infty$ compares the isotopic composition *of the solvent* water, as calculated for random mixing of the isotopes, with the isotopic composition of *distillate* obtained from the final equilibrium solution. The values of this ratio for experiments A, B, C, and D are 1.012, 1.011, 1.012, and 1.008, respectively. The fractionation is in excess of the value of 1.005 observed for pure water under the same conditions, and the direction of the change therefore shows that the salts reduce the activity of H_2O^{18} more than they do the activity of H_2O^{16}. In this connection, a comparison of the values of ${}^6N_c/N_{obs}{}^0$ for chromic perchlorate with the fractionation factor observed on distillation of water is significant.

TABLE IV. The exchange of H_2O between Cr^{+++}aq and solvent (temperature 25°±0.1; time in hr).

A		B[a]		C		D	
1.238 M $Cr(ClO_4)_3$		1.277 M $Cr(ClO_4)_3$ 0.109 M $HClO_4$		1.321 M $Cr(ClO_4)_3$ 1.310 M $HClO_4$		0.910 M $Cr(ClO_4)_3$ 0.0960 M $HClO_4$	
$t-t_0$	$N_{obs}\times10^3$	$t-t_0$	$N_{obs}\times10^3$	$t-t_0$	$N_{obs}\times10^3$	$t-t_0$	$N_{obs}\times10^3$
0.0[b]	8.296	0.0[b]	8.030	0.0[b]	7.995	0.00[b]	7.990
0.86	8.278	0.3	8.018	1.05	7.985	0.07	7.949
5.67	8.201	18.3	7.783	5.76	7.904	1.15	7.982
28.96	7.886	18.9	7.790	17.73	7.719	4.50	7.965
53.02	7.738	401.3	7.187	28.09	7.620	29.93	7.798
91.88	7.554	1176	7.154	51.49	7.433	48.71	7.701
483.6	7.406	∞[b]	7.154	99.43	7.261	481.6	7.397
				481.6	7.149	∞[b]	7.390
				∞[b]	7.149		
${}^6N_c/N_{obs}{}^0=1.006$		${}^6N_c/N_{obs}{}^0=1.005$		${}^6N_c/N_{obs}{}^0=1.013$		${}^6N_c/N_{obs}{}^0=1.006$	
$N_c^\infty/N_{obs}^\infty=1.012$		$N_c^\infty/N_{obs}^\infty=1.011$		$N_c^\infty/N_{obs}^\infty=1.012$		$N_c^\infty/N_{obs}^\infty=1.008$	

[a] The data as previously reported for experiment B were not normalized and differ slightly from the present ones in the values for $N_{obs}{}^0$ and $N_{obs}{}^\infty$. The value of $N_{obs}{}^\infty$ has now been improved by including additional analyses after longer time intervals.

[b] Values obtained by extrapolation. Since 1/2 time for exchange is *ca* 40 hr, values of N_{obs} after 400 hr represent essentially complete exchange.

The values of ${}^6N_c/N_{obs}{}^0$ are very close to 1.005, showing that $Cr(H_2O)_6^{+++}$ and ClO_4^- do not affect the relative activity of H_2O^{18} and H_2O^{16} enough to be detectable by the present measurements—i.e., the influence on the relative activities of H_2O^{18} and H_2O^{16} in the solvent by the hydrated cation and by the anion is very slight. The principal effect of salts in affecting the relative activities is, therefore, by operation of exchanges in the first sphere of hydration.

The data for chromium perchlorate have been treated taking into account the hydrate exchange equilibrium. Only two equilibria contribute appreciably to the overall effect:

$$Cr(H_2O)_6^{+++}+H_2O^{18} = Cr(H_2O)_5(H_2O^{18})^{+++}+H_2O, \quad K_1,$$

$$Cr(H_2O)_5(H_2O^{18})^{+++}+H_2O^{18} = Cr(H_2O)_4(H_2O^{18})_2^{+++}+H_2O, \quad K_2.$$

At the levels of enrichment with respect to O^{18} used in the experiments, species containing more than two molecules of H_2O^{18} per molecule of $Cr^{+++}aq$ are negligible. K_1 can be calculated from the data by applying the equation

$$K_1=\frac{(A-A_{aq})(1-N^\infty)/N^\infty}{\left(1+2K_2\frac{N^\infty}{1-N^\infty}\right)\left[m-\frac{(A-A_{aq})}{1+2K_2N^\infty/(1-N^\infty)}\right]}.$$

A is the total number of moles of H_2O^{18} in the system, A_{aq} is the number of moles of H_2O^{18} in the solvent (i.e., exclusive of that bound to Cr^{+++}) at equilibrium, and m is the total number of moles of Cr(111). N^∞ is $N_{obs}{}^\infty$ after correcting for the fractionation on distillation. For K_2, the statistical value of 2.5 was used. The calculation of K_1 is insensitive to the small deviation of K_2 from the statistical value due to isotope fractionation. It should be noted that activity coefficients will cancel to a good approximation in the isotope exchange equilibria. The values of K_1 calculated from the data are as follows.

	A	B	C	D
$K_1(\pm 0.13)$	6.28	6.28	6.10	6.10.

The mean value of 6.2 for K_1 seems reasonable in comparison with the value of 2.078 observed for K.

For the other cations as well, Fe^{+++} at low acid excepted, the values of $N_c{}^\infty/N_{obs}{}^\infty$ exceed the value of 1.005 observed for distillation fractionation from water. For these labile ions, trivalent ones as well as the tetravalent thorium ion, the effects attributable to isotope exchange fractionation are about the same in magnitude as for chromic ions. These exchange equilibria seem important enough to warrant further study. Such work is now in progress, and further discussion is deferred until extensive data of greater accuracy have been obtained.

The data for ferric ion at low acid show that there is a slight initial hold-back of oxygen by ferric ion and that a slow exchange of this hold-back continues. This effect can most reasonably be attributed to the existence in the system of condensed, hydrolyzed forms. Evidence for the formation of such species—soluble or colloidal—has been obtained in studies on solutions of ferric chloride; these studies have shown, furthermore, that the changes involving the formation of these species are slow.[8] Oxygen incorporated in the condensed forms as bridges between ferric ions can therefore be expected to exchange slowly and presumably accounts for the exchange effects. The ferric solutions were aged sufficiently long to permit the formation of condensed structures before the enriched water was added. From the work of Hall and Eyring,[9] a considerable fraction of the chromic ion in the experiment at low acid (experiment A) is also expected to be in condensed forms. Consistent with this, a distinct increase in acidity was observed during the experiment, presumably due to reactions of the type

$$2Cr(H_2O)_6^{+++}\rightarrow[(H_2O)_5CrOHCr(H_2O)_5]^{+5}+H^++H_2O.$$

The conclusions about coordination number are not affected, however, since they depend on observations at essentially $t=0$, before the condensed species have developed appreciably. At room temperatures, the rate of formation of the condensed species in chromic solutions is very slow. It is evident that the exchange method offers a useful tool in studying hydrous oxide systems.

Kinetic Aspects

The data show that $Al^{+++}aq$, $Fe^{+++}aq$, $Cr^{+++}aq$, and $Th^{+4}aq$ exchange water so rapidly that the rate of exchange cannot be measured by the method employed. Of the ions studied,[10] only for $Cr(H_2O)_6^{+++}$ is the rate slow enough to make a thorough kinetic investigation possible. Some quantitative features of the exchange data for $Cr(H_2O)_6^{+++}$ are brought out by Figs. 1 and 2, in which the values of $(N_{obs}{}^t-N_{obs}{}^\infty)$ for Experiments C and D are displayed as function of time on semilog plots. Within experimental error, the data conform to the rate law that the exchange is first order in $(N_{obs}{}^t-N_{obs}{}^\infty)$. The kinetic results of the four experiments are summarized in Table V.

Over a fairly wide range in acidity, from *ca* 10^{-2} *M* (experiment A) to *ca* 1.53 *M* (experiment C), the rate of exchange is independent of this parameter. This result is surprising in view of the fact that with Cl^- or CNS^- as the substituting groups the rate of substitution decreases as acidity increases. Not sufficient work has been done to establish the order of the reaction with respect to chromic ion. Column 5 presents the results obtained when the data are fitted to the following simple

[8] A. B. Lamb and A. G. Jacques, J. Am. Chem. Soc. **60**, 967, 1215 (1938).

[9] H. T. Hall and H. Eyring, J. Am. Chem. Soc. **72**, 782 (1950).

[10] $Co^{++}aq$, and $Co^{+++}aq$ in the presence of $Co^{++}aq$, have been observed to exchange rapidly with the solvent (Friedman, Taube, and Hunt, J. Chem. Phys. **18**, 759 (1950)).

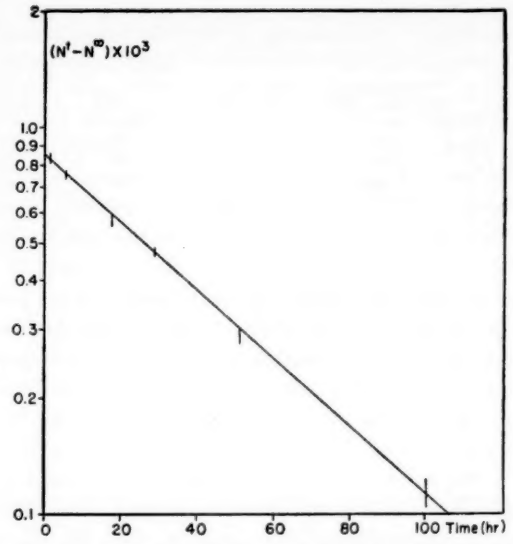

FIG. 1. Rate of exchange of $Cr(H_2O)_6^{+++}$ and solvent. 1.321 *M* $Cr(ClO_4)_3$, 1.310 *M* $HClO_4$; temperature, 25°.

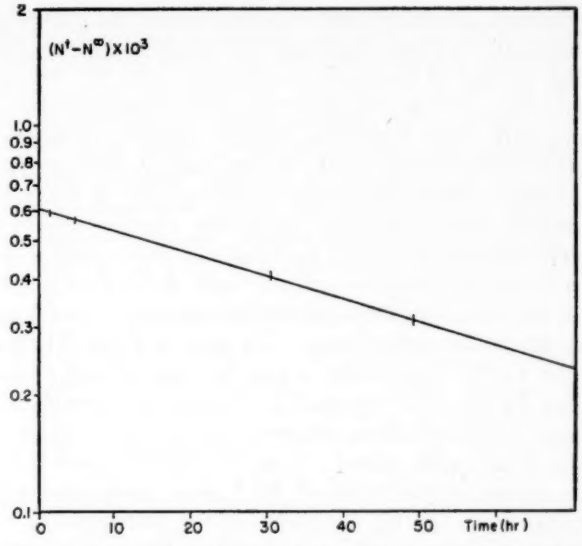

FIG. 2. Rate of exchange of $Cr(H_2O)_6^{+++}$ and solvent. 0.910 *M* $Cr(ClO_4)_3$, 0.906 *M* $HClO_4$; temperature, 25°.

mechanism:

$$Cr(H_2O)_6^{+++}+H_2O^{18}\underset{k_2'}{\overset{k_2}{\rightleftarrows}}Cr(H_2O)_5(H_2O^{18})^{+++}+H_2O.$$

The fact that the value of k_2 calculated is lower at lower concentrations would seem to indicate that the rate of exchange is higher than first order in the chromic salt and that the mechanism is more complex than the one indicated above. This conclusion is not considered as dependable, as yet, and further work on the kinetics of the exchange is in progress.

Examination of the literature shows that no conclusion about mechanism can be reached from existing data by comparing rates of complex ion formation with rate of water exchange. For chloride ion,[11] at any reasonable concentration, substitution of water by water would appear to be more rapid than water by chloride ion. Results for CNS^- and tartrate,[12,13] however, suggest that at sufficiently high concentrations of these ions, the rate of complex ion formation will exceed the rate of water exchange. Special experiments will need to be performed before definite conclusions can be reached.

The most striking feature of the observations made on the rates of water exchange is the great difference in the rate of exchange for $Cr(H_2O)_6^{+++}$, on the one hand, and the ions Al^{+++}aq, Fe^{+++}aq, Ga^{+++}aq, and Th^{+4}aq, on the other. The water exchange data are not singular in this respect. A similar difference in lability is noted when substitution reactions involving the formation or dissociation of complex ions are considered. Thus, a system containing $Cr(H_2O)_6^{+++}$, H^+, and F^- or Cl^-, requires days or weeks to reach equilibrium with respect to the formation of complex ions. However, with Fe^{+++} or Ga^{+++} in place of chromic ion, equilibrium is reached almost at once. Al^{+++} and Th^{+4} also appear to be very labile with respect to formation of complex ions in water solution. In the gross features, at least, the rates of water exchange resemble those involving substitution of other ligands, and if the coordination numbers for water of the aqueous cations were known, the water exchange reactions could presumably be formulated as definitely as complex ion formation reactions.

A discussion of the reasons underlying the difference in rates of substitution for the cations is carried forward most simply by considering first the series of ions of equal charge and similar radius: Al^{+++}, Cr^{+++}, Fe^{+++}, and Ga^{+++}. Data useful in the discussion following, and pertaining to these ions, are presented in Table VI.

From the data of Table VI it is evident that the unique rate behavior of Cr^{+++} cannot be attributed to a unique value of the ionic radius parameter. The data also show that a simple correlation between energy of interaction with the solvent and rate of exchange does not exist. Chromic ion does not have an unusually high hydration energy compared to the others, even after correction is made for the differences in ionic radii. A point of view which has frequently proved tempting is that a slow rate of substitution indicates a more covalent bond. An influence of bond type on rate of substitution cannot be denied; however, as the following discussion will show, there is no evidence that the bonds in the $Cr(111)-H_2O$ complex are more covalent than others of the ions, which are much more labile in substitution reactions.

Since Cr^{+++}, Fe^{+++}, and Ga^{+++} have nearly the same radii, the potential energies of the purely ionic states in the aquo complexes will be nearly the same. In view of this fact, it seems reasonable to suppose that a

[11] N. Bjerrum, Z. physik. Chem. **59**, 336 (1907).
[12] N. Bjerrum, Z. anorg. u. allgem. Chem. **118**, 131 (1921).
[13] J. P. Mathieu, Compt. rend. **193**, 1079 (1931).

relatively great covalent contribution to the energy of interaction for one of the ions will result in an unusually high energy of interaction of the ion with the solvent. The data of Table VI show that Cr^{+++} does not have a singularly high hydration energy. Another measure—other things being equal—of the quality of interaction between cations and water is the acidity of the aquo ions: it seems reasonable to suppose that for cations of equal charge and radius, a greater covalent contribution to the bond with water would result in a higher acidity for the aquo ion, since greater polarization of the water by the cation would ensue. The data of Table VI show that Cr^{+++} hydrolyzes somewhat less strongly than does Fe^{+++}. The remarkable feature of these data is that the four cations enhance the acidity of water to about the same extent—from $10^{-14}/55$ for pure water to values of the order of 10^{-4} when associated with metal ions. Lastly, the data on the stabilities of the halide complexes will be considered. It is notable that the stability of the complex CrF^{++} is within the same range as the stabilities of the Fe^{+++} and Ga^{+++}, and that the ratio of stabilities of the fluoride and chloride complexes for Cr^{+++} is about the same as it is for Fe^{+++}. An increase in stability of the chloride complex relative to the fluoride complex would be expected as the bonds become more covalent, owing to the greater polarizability of Cl^- relative to F^- (e.g., the iodide complex of Hg^{++} is more stable than is the chloride complex). From the evidence of the equilibrium data, the conclusion follows that the quality of the interaction with water is remarkably the same for all four cations, and there is no reasonable basis for classifying the chromic complexes as "covalent" and the others as "ionic."

Quite apart from the arguments presented in the previous paragraph, it is obvious that a simple relation between bond-type of the reactant complex ion and rate of substitution can hardly be expected, since the rate is determined by the difference in energy between the initial state and the activated state and not merely by the properties of the initial state. By adopting the more complete point of view and considering the influence on the energy of activation of changes in electronic structures of the complex ions, the present data, as well as other data on lability,[14] can be rationalized in a satisfactory manner without invoking extreme difference in bond-type for the reactant complexes.

For all complex ions containing central ions of sufficiently high charge, it is assumed that there is an important covalent contribution to the bonds. In the case of Cr^{+++} which has three unpaired d electrons, the orbital set d^2sp^3 is presumably used in forming bonds with the six associated groups. Thus, the five inner d orbitals for chromic ion are completely occupied, three by unpaired electrons and two by shared electron pairs. No vacant stable orbitals remain for interaction with an incoming substituting group. Any bond which a seventh group would make in forming the activated complex would require the promotion of inner d electrons or would be formed using less stable outer orbitals. In either event, the activation energy would be high as compared to the same process for V^{+++}, for example. V^{+++} has one less unpaired electron and therefore has a vacant inner d orbital. Less energy will be required to construct an intermediate complex with the incoming group, and a lower activation energy for the substitution reaction is expected. The lability of complexes of V(111) is known to be much greater than for Cr(111).[15]

The electron structures for Al^{+++}, Fe^{+++}, and Ga^{+++} in the aquo complex, and many other complexes differ in an important respect from that of Cr^{+++} and others of this type. For chromic ion, relatively stable inner d orbitals are hybridized with s and p orbitals of higher quantum number. With the former three ions, the inner orbitals are completely occupied[16] by unshared electrons. If d orbitals are included in octahedral hybridization, they are of the same principal quantum number as the s and p orbitals and are therefore relatively unstable. In comparison to Cr^{+++}, these ions more

TABLE V. Summary of rate data on exchange of H_2O with $Cr(H_2O)_6^{+++}$ (temperature 25°±0.1; k_2 defined in text).

No.	Molarity of $Cr(H_2O)_6(ClO_4)_3$	Molality of added $HClO_4$	$t_{\frac{1}{2}}$ (hr)	$k_2 \times 10^6$ mole^{-1} min^{-1}
A	1.042	0	36	4.28
B	1.058	0.127	40	3.91
C	1.046	1.524	34	4.67
D	0.778	0.107	50	2.91

TABLE VI. Some properties of trivalent cations.

Ion	Ion radius[a] (A°)	$-\Delta H$ hyd.[b] (kcal/mole)	K_{HOH}[c]	K_{HF}[d]	K_{Cl^-}[e]
Al	0.52	1109	1.4×10^{-5}	1570 at $\mu=0.5$	—
Cr	0.62	1048	1.5×10^{-4}	26.3 at $\mu=0.5$	0.3 at $\mu=0.3$
Fe	0.64	1038	6×10^{-3}	189 at $\mu=0.5$	5 at $\mu=0.3$
Ga	0.60	1115	2.5×10^{-3}	220 at $\mu=0.5$	<1 at $\mu=0.5$

[a] E. Kordes, Z. physik. Chem. **B48**, 91 (1940).

[b] Heat of hydration of gaseous ions. Necessary thermal data from *Tables of Selected Values of Chemical Thermodynamic Properties* (U. S. Bureau of Standards, Washington, D. C., 1947). $-\Delta H$ for Cl^- was taken as 88.7 kcal/mole (see Latimer, Pitzer, and Slansky, J. Chem. Phys. **7**, 108 (1939)).

[c] $K_{HOH}=(H^+)(MeOH^{++})/(Me^{+++})(H_2O)$. Data from *Oxidation Potentials* (W. M. Latimer, Prentice-Hall, Inc., New York, 1938).

[d] $K_{HF}=(H^+)(MeF^{++})/(Me^{+++})(HF)$. For information concerning Al^{+++}; C. Brosset, Separate (Stockholm), 1942; concerning Fe^{+++}, H. W. Dodgen and G. K. Rollefson, J. Am. Chem. Soc. **71**, 2600 (1949); concerning Cr^{+++} and Ga^{+++}, A. S. Wilson and H. Taube, to be published.

[e] $K_{Cl^-}=(MeCl^{++})/(Me^{+++})(Cl^-)$. For information concerning Cr^{+++}; N. Bjerrum, Z. physik. Chem. **59**, 336 (1907); concerning Fe^{+++}, E. Rabinowitch and W. H. Stockmayer, J. Am. Chem. Soc. **64**, 335 (1942); concerning Ga^{+++}, A. S. Wilson and H. Taube, to be published.

[14] A review of observations on the lability of complex ions and their interpretation is in preparation. H.T.

[15] This has been demonstrated by simple mixing experiments using F^-, CNS^-, pyrophosphate, citrate, and tartrate as associating groups.

[16] Magnetic data support the formulation of Fe^{+++}aq as having 5 unpaired d electrons (Werbel, Dibeler, and Vosburgh, J. Am. Chem. Soc. **65**, 2329 (1943). The electron structure of $Fe(CN)_6^{---}$, $Fe(O\ phen)_3^{+++}$, and a few other complexes, however, is of a different type.

readily assume configurations of lower coordination number, presumably because the increase in average stability of the orbitals as the configuration is stripped from sp^3d^2 to sp^3 helps compensate for the energy required. Thus, Al^{+++} and Fe^{+++} have coordination number 6 in the solid chlorides; however, an expenditure of energy of only 13.4 kcal per mole $AlCl_3$[17] and 16.5 kcal per mole $FeCl_3$[17] suffices to remove molecules of Me_2Cl_6 from the solid. The cations are tetracoordinated in the forms Me_2Cl_6. Solid $GaCl_3$ is also readily converted to Ga_2Cl_6. These considerations make it appear likely that exchange of groups attached to these ions would proceed by a dissociation mechanism of relatively low activation energy. A similar compensating factor when the coordination number for Cr^{+++} is reduced does not exist. No substance is known in which Cr(111) under relatively mild conditions has a coordination number less than 6, and for this ion, the dissociation mechanism can be expected to have a high activation energy. It is not possible, however, to estimate the relative activation energies of the "substitution" and "dissociation" mechanisms for chromic complexes, and therefore, it is not possible to predict with certainty which mechanism operates. The further experiments in progress on the kinetics of reactions with $Cr(H_2O)_6^{+++}$ will, it is hoped, yield an experimental answer.

[17] *Selected Values of Chemical Thermodynamic Properties* (U. S. Bureau of Standards, Washington, D. C., 1947).

ACKNOWLEDGMENTS

This work was supported by funds from the ONR under contract N6-ori-02026. The authors wish to express their appreciation to Dr. Samuel Epstein for help in isotope analyses, to Dr. Harold C. Urey for the use of his precise mass spectrometer, and to Dr. Lewis Friedman of the Brookhaven National Laboratories for making mass spectrometer analyses of preliminary samples.

THE JOURNAL OF CHEMICAL PHYSICS VOLUME 19, NUMBER 5 MAY, 1951

Macroscopic Space Charge in a Potassium Chloride Solution during Electrolysis

WILLIAM SCHRIEVER AND ELDON E. FERGUSON*
Physics Department, University of Oklahoma, Norman, Oklahoma
(Received December 4, 1950)

The macroscopic space charge and potential distributions were determined in a uniform column of 0.0024 *N* KCl solution during electrolysis by the methods used by Reed and Schriever. The platinum electrodes were 8×8 cm in area and spaced 40 cm apart; their constant potential difference was 8000 mv.

For the first time, all four space-charge regions were observed in one column of solution directly experimentally. The maximum negative space charge in the cathode region, 45×10^{-5} statcoulomb/cm³ at $x=0.6$ cm, and the maximum positive space charge in the anode region, 40×10^{-5} statcoulomb/cm³ at $x=37.7$ cm, both fell within the range of such space charges observed by Reed and Schriever.

The potential gradient between $x=10$ cm and $x=35$ cm had the constant value of 13.75 mv/mm. Thus, Ohm's law was obeyed in this region. The *mean* gradient in the first mm next to the cathode was 1130 mv/mm; that in the last mm next to the anode was 1200 mv/mm. The total fall of potential in these two one-mm layers was thus 29.1 percent of the total fall of potential between the electrodes. For $Zn(C_2H_3O_2)_2$ and $CuSO_4$ the falls in these two layers were respectively only 1 and 1.06 percent of the total; the greatest value observed by Reed and Schriever was 22.5 percent of the total for $NiSO_4$.

It is pointed out that the shapes of the potential distribution curves cannot be explained by phenomena which occur only at, and very near, the electrodes.

REED and Schriever[1] in 1949 reported the distributions of macroscopic space charges generated during the electrolysis of 0.0024 *N* solutions of $CuSO_4$, $CuCl_2$, $ZnSO_4$, $ZnCl_2$, $Zn(C_2H_3O_2)_2$, $NiSO_4$, $NiCl_2$, and $Al_2(SO_4)_3$. In each case, the electrodes were made of the same metal as the positive ion; the column of electrolyte was 8×8×40 cm; the electrodes were 8×8 cm in area and 40 cm apart; a constant potential difference of 8.000 v was maintained; and the current was allowed to pass for 15 minutes. Gordon[2] in a Letter to the Editor presented a number of criticisms of Reed and Schriever's results. Schriever[3] answered each of these criticisms and showed that the shapes of the potential distribution curves could not be explained by phenomena which occurred at or near the electrodes.

MacInnes, Shedlovsky, and Longworth[4] in a Letter to the Editor criticized Reed and Schriever's results. They reported some "admittedly relatively crude" experiments with a KCl solution. Schriever[5] answered these criticisms and also called attention to the work on KCl solution, which he and Ferguson had begun the preceding November but which was not yet complete in the anode half of the column.

* Submitted by E. E. Ferguson as a dissertation in partial fulfillment of the requirements for the MS degree in June, 1950.

[1] C. A. Reed and W. Schriever, J. Chem. Phys. **17**, 935–944 (1949).

[2] A. R. Gordon, J. Chem. Phys. **18**, 146 (1950).

[3] W. Schriever, J. Chem. Phys. **18**, 146–147 (1950).

[4] MacInnes, Shedlovsky, and Longworth, J. Chem. Phys. **18**, 233 (1950).

[5] W. Schriever, J. Chem. Phys. **18**, 763 (1950).

FIG. 1. Deviation-time curves for 16 positions along the column of a KCl solution and the resulting deviation-distance curve after the current had existed 15 minutes. Nine additional D, t curves for points near the electrodes were used in determining the D, x curve.

Murphy[6] described an apparatus and a method for the separation of electrolytes, which depend on gravity convection currents being set up by changes in concentration, and therefore in density, near the two electrodes due to electrolysis. He suggested that Reed and Schriever's conclusion may require modification in the light of his results. Dr. Murphy very kindly sent a copy of his manuscript to one of the writers (Schriever) who replied to the letter which accompanied it. Murphy's currents were 1500 times as great as those of Reed and Schriever; the currents per unit area of electrode were 1000 times as great; and the concentrations of his solutions were from 100 to 200 times as great. Schriever's reply to MacInnes, *et al.* (referred to earlier in this paper), concerning convection applies equally well to Murphy's suggested criticism. Thus, it appears reasonable to believe that such concentration changes as may have existed in Reed and Schriever's apparatus were too small to have caused appreciable convection during the short time that they existed.

[6] George W. Murphy, "The separation of simple electrolytes in solution by an electro-gravitational method," J. Electrochem. Soc., to be published.

THE PROBLEM AND PROCEDURE

Since solutions of potassium chloride are very widely used for standardizing conductivity cells, the space charge and the resulting electric field strength distributions along a uniform column of such a solution during electrolysis are of special interest. The measurements for making such determinations involved the use of electrodes which did not take part in the chemical reactions at their surfaces, since potassium could not be used. This was a significant departure from the conditions that existed during such determinations in the eight solutions which were reported in the first reference.

The apparatus and procedure were essentially the same as those described by Reed and Schriever.[1] The current electrodes were made by attaching with rubber cement pure platinum wrinkle-free sheets 0.003-inch thick to $\frac{1}{8}$-inch-thick plates of amphenol plastic. It was found necessary to coat the backs of the amphenol plates with the rubber cement in order to prevent their warping after immersion in the water solution. The probe electrode contained a No. 30 B. & S. gauge platinum wire.

The current electrodes were cleaned periodically by swabbing the platinum surfaces with dilute NaOH, rinsing with water, swabbing with dilute HNO_3, washing them thoroughly with water, and then immediately immersing them in the 0.0024 N KCl solution in the glass trough. After each 15-minute run, the solution was thoroughly stirred and the current electrode surfaces were thoroughly rubbed with a glass-wool swab. Gas bubbles were never visible during the regular 15-minute runs, but they did become visible after the current had passed 2 or 3 hours.

The values of the "chemical emf" (probe to current electrode) ranged from -157 to $+334$ mv. The variations of this emf during any series of runs did not exceed 100 mv and in almost all cases were considerably less. Reproducibility of data was found to depend neither on the magnitude of this emf nor on its rate of change. After the electrodes had been used for an hour or more this emf attained a rather steady value. It was also found that reproducibility of data was improved somewhat by passing the current through the solution for several hours after each cleaning of the electrodes, before the desired runs were made.

The electrometer was adjusted to a sensitivity of 2.06-mv/mm deflection. The probe correction was found to be 8 mv. The reference point for the "standard curve" method was at 10 cm from the cathode.

RESULTS

The data are depicted in Fig. 1 which is a reproduction of a drawing on a piece of profile paper measuring 17 by 22 inches. The deviation†-time (D, t) curves were run at 27 points, lying between 0.1 and 39.9 cm from the cathode. Since the standardization runs were at 10 cm from the cathode, a large number (57) of runs were made there. At the other 26 points, 83 runs were made; all except 6 of the curves were plotted from data which were the averages of from 2 to 9 runs. The distance of the point from the cathode is indicated on each of the 16 plotted curves. The temperature of the cabinet was maintained near 28°C.

Since the deviation-time curves are so nearly parallel to the time axis, only one deviation-distance curve was drawn; it is for a current duration of 15 minutes. This deviation-distance (D, x) curve is a straight line between $x=10$ and $x=35$ cm from cathode. Between $x=0.5$ and $x=10$ cm, this curve is concave upwards; between $x=35$ and $x=39.5$ cm, this curve is concave downwards. Many runs were made at points near the anode in order to establish this fact. In drawing the curve those points were given the greatest weight which resulted from the averages of the largest number of runs. It is obvious that this D, x curve has inflection points in the neighborhood of $x=0.7$ and $x=39.4$ cm.

† The deviation D was defined by $D=V-V_0'$, where V is the observed potential with respect to cathode at the point in the electrolyte distance x from the cathode, and V_0' is the potential of that point calculated on the assumption of a strictly linear rise of potential from cathode to anode.

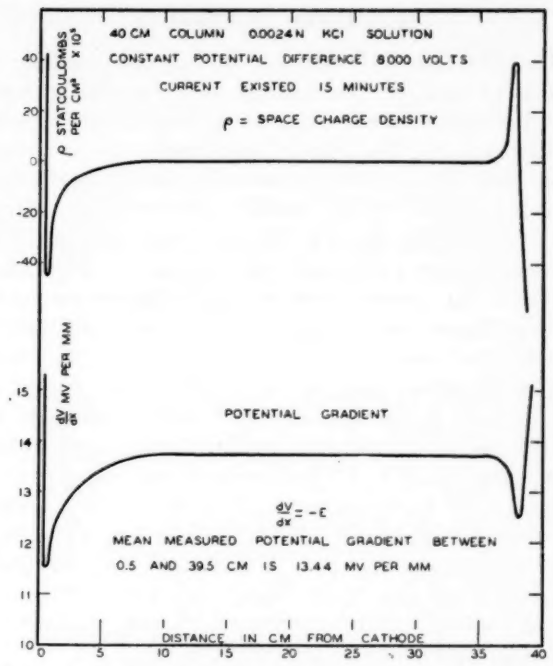
40 CM COLUMN 0.0024 N KCl SOLUTION
CONSTANT POTENTIAL DIFFERENCE 8.000 VOLTS
CURRENT EXISTED 15 MINUTES
ρ = SPACE CHARGE DENSITY
ρ STATCOULOMBS PER CM³ X 10⁵
dV/dx MV PER MM
POTENTIAL GRADIENT
dV/dx = -ε
MEAN MEASURED POTENTIAL GRADIENT BETWEEN
0.5 AND 39.5 CM IS 13.44 MV PER MM
DISTANCE IN CM FROM CATHODE

FIG. 2. Curves showing how the electric potential gradient and macroscopic space charge varied along a uniform column of KCl solution after electrolysis had taken place for 15 minutes. If there had been no space charge and no special effects very close to each electrode surface, the potential gradient would have been 20 mv/mm.

POTENTIAL GRADIENT

The potential gradient along the column of electrolyte is shown by the lower curve in Fig. 2. This curve was obtained by getting the algebraic sum of 20 mv/mm (8 v/40 cm) and the slope of the deviation-distance curve of Fig. 1 for each point. This latter slope at a particular point was determined geometrically by placing a straight edge tangent to the D, x curve at the point and then determining the slope of that straight edge from its intercepts on the two axes. Such slopes, with 20 mv/mm added, were determined at many points along the nonlinear portions of the deviation-distance curve; these values were plotted to a conveniently large scale, and a smooth curve was drawn through them. A reproduction of that curve is the one shown in Fig. 2.

SPACE CHARGE

The distribution of the space charge along the column of electrolyte is shown in the upper curve of Fig. 2. The space charge, in statcoulomb/cm³, at a point was obtained by multiplying the slope of the potential gradient curve at that point by $(-\epsilon k/4\pi)=-2.12\times10^{-3}$, where the dielectric constant ϵ was assumed to be 80 for water, and k is a constant for converting units. Here again the slopes of the curve were measured by the straight-edge-intercept method.

DISCUSSION OF RESULTS

The 0.0024 *N* KCl solution is the first solution in which the positive space charge very near the cathode and the negative space charge very near the anode, both existed out into the column sufficiently far to permit their direct detection experimentally. In previous work, only $NiCl_2$ and $CuSO_4$ exhibited positive space charges near the cathode, and only $Al_2(SO_4)_3$ exhibited negative space charge near the anode (see reference 1). The upper curve in Fig. 2 shows that the KCl solution exhibited all four space-charge regions which were alternately positive and negative in going from cathode to anode.

The maximum value of the negative space charge in the cathode region was 45×10^{-5} statcoulomb/cm^3 at $x=0.6$ cm. The maximum *positive* space charge in the anode region, 40×10^{-5} statcoulomb/cm^3, existed at a point 2.3 cm from the anode. The first of these values represents an excess of 9×10^5 Cl^- ions per cm^3, which is a relative excess of only 1 in 3×10^{12} ions originally present. These two space charges fall within the range of the maximum space charges which were observed in the first eight solutions (see reference 1).

If there had been no space-charge effects and no other effects at the electrode surfaces, the potential gradient would have had a constant value of 20 mv/mm. In the space-charge-free part of the column ($x=10$ to $x=35$ cm) the gradient was 13.75 mv/mm. The mean gradient between $x=0.5$ and $x=39.5$ cm was 13.44 mv/mm. The mean gradient in the first mm next to the cathode was 1130 mv/mm, and in the last mm next to the anode was 1200 mv/mm; these were, respectively, more than 81 and 87 times that in the space-charge-free part of the column.

Of the solutions studied thus far, KCl showed the greatest range of deviations, namely +1262 mv at $x=0.5$ cm to −1228 mv at $x=39.5$ cm. In $NiSO_4$ the range was from +500 to −1300 mv, each at a point one mm from the electrode; this was the greatest range observed heretofore.

The complicated effects which existed at, and extremely close to, each electrode surface, and which caused the very large potential gradients near the electrodes, were difficult to reproduce. Thus, reproduction of data was more difficult than it had been in those solutions in which these gradients were relatively small. On the average, measurements were reproducible to within ±10 mv in KCl.

It might be thought that the decrease in the magnitude of the deviation within a few mm of each electrode (see Fig. 1) was caused by the "shading" of the electrode by the probe. This undoubtedly was not the case, because Reed and Schriever[1] observed no decreases in 6 of their 8 solutions near the cathode, and in 7 of their 8 solutions near the anode. Their probes were equally as large as the one used for KCl.

It has been shown in this work on KCl solution, and for eight other electrolytes (reference 1), that a large fraction of the fall of potential between the electrodes in a uniform column of electrolyte, exists in the one-mm layers next to the electrodes and that this fraction varies greatly for different electrolytes having the same normality. For 0.0024 *N* solutions of KCl and $CuSO_4$ the combined falls of potential, in the one-mm layers near the two electrodes, were, respectively, 2330 mv, and 85 mv, when the total potential difference for each solution was 8000 mv across a column 400 mm long. Although no data have been published, it has been observed that this fraction also varies with concentration. Thus, if the usual two-electrode conductivity cells were calibrated by dc methods, one would expect a change in cell constant with both concentration (resistivity) and kind of electrolyte. Is it not possible that appreciable change in cell constant may occur even when ac methods are used, especially for those cells in which the electrodes are near each other?

CONCLUSIONS

It is possible to study the potential distribution along a uniform column of dilute electrolyte during electrolysis even though the electrodes do not take part in the electrolysis.

The four space-charge regions exist along a column of dilute electrolyte during electrolysis even though the electrodes do not take part.

The positive space charge near the cathode and the negative space charge near the anode may exist so far from the electrodes that they can be directly observed experimentally in the same column.

The potential gradient in a 40-cm-long uniform column of 0.0024 *N* KCl undergoing electrolysis with a current density of 5×10^{-5} amp/cm^2 between platinum electrodes is constant between points 10 and 35 cm from the cathode. Thus, Ohm's law holds in this region.

THE JOURNAL OF CHEMICAL PHYSICS VOLUME 19, NUMBER 5 MAY, 1951

The Effect of Temperature on the Photolysis of Methylamine*

CLARENCE I. JOHNSON AND H. AUSTIN TAYLOR
Department of Chemistry, New York University, New York, New York

(Received December 15, 1950)

The photolysis of methylamine has been investigated with the purpose of determining the effect of temperature. To minimize the interference due to polymeric liquid formation, the reaction was studied from −15° to 30°C. The energy of activation of amine disappearance was found to be 6 kcal, a minimum value, but which is probably caused by the effect of temperature on the light absorption. The possibility of ethylene diamine as an intermediate undergoing further decomposition or a polymerization-condensation reaction evolving ammonia is considered. The rates of hydrogen and ammonia production show previously postulated mechanisms to be untenable.

INTRODUCTION

THE mechanism suggested by Wetmore and Taylor[1] for the photolysis of methylamine attributed the low quantum yield of ~0.7, reported by Emeleus and Jolley,[2] to the recombination of the hydrogen atom and methylamino radical formed by the initial light absorption. This recombination was considered aided by the slowness of further decomposition of the radical. It was pointed out that a difference of from 10–15 kcal in the activation energies of the methylamino radical decomposition and its reaction with hydrogen to give methylamine would account for the observed quantum yield. An over-all energy of activation of methylamine photolysis should thus be observable. The present work was initiated to study this energy of activation. It soon became apparent, however, that the analytical procedures previously used to estimate ammonia in presence of methylamine were even less reliable than had been thought and had led to erroneous conclusions. By the use of an effusion method for determining ammonia and methylamine, the photolysis has been studied over a wide temperature range especially with respect to the production of hydrogen and ammonia. It will be shown that the over-all reaction is more complicated than was suspected, although its progress so far as hydrogen and ammonia production are concerned is more clearly defined.

EXPERIMENTAL

The light source was a quartz helical low pressure mercury resonance arc operated at 6000 volts from a transformer carrying 6.8–7.0 amp in the primary. The bore of the quartz tubing was ~5 mm and the helix diameter ~9 cm. In the later runs an electronic voltage regulator was used to maintain constant current in the transformer primary, and the whole lamp was placed in an air thermostat, constant to ±0.5°C, to achieve as constant light intensity as possible.

The reaction vessel in the static runs was a spherical quartz bulb of 340 ml capacity. It was held rigidly close to a quartz window in an air thermostat automatically regulated to ±0.5°C. In the low temperature runs, cooling was supplied by placing solid carbon dioxide in the air bath and supplying heat as required by the thermoregulator. Efficient air circulation was accomplished by two fans. The air bath for the lamp was joined directly to that for the reaction vessel but could be controlled independently. The distance from the lamp to the vessel was a few millimeters.

Because of a deposition on the surface of the reaction vessel during photolysis in the static system, several dynamic runs were made in an attempt to recycle undecomposed methylamine which was cleansed of the cause of the deposit by passage through glass wool. In these runs the reaction zone was a quartz tube of 1 cm bore and 10 cm long. The gas was circulated, by means of an electromagnetic mercury displacement pump with suitable mercury valves, at a rate of about 800 cc per minute. The results of these runs indicated that if success was to be achieved by this method at all, much higher flow rates would have to be used.

Methylamine was prepared from the hydrochloride purified by leaching several times with 95 percent alcohol and dried in a vacuum desiccator over concentrated sulfuric acid. The hydrochloride was treated with a nearly saturated solution of potassium hydroxide at atmospheric pressure, and the amine was collected in a trap in liquid nitrogen. Freed of air by evacuation, the amine was vaporized through a 2.5-foot column of drierite and condensed in a trap in monochlor-benzene at its melting point of −45.2°C. Several such distillations and degassing operations were carried out. Vapor pressure measurements of the amine at −45.2°C, 92.8 mm, were in good agreement with the literature value, and an infrared absorption spectrum showed only traces of ammonia in an amount less than 0.2 percent. Ammonia used in the calibration of the effusion apparatus was prepared in a similar manner from ammonium chloride.

The effusion apparatus for the analysis of methylamine and ammonia mixtures made use of a cup-shaped, single-holed spinneret of tantalum. It had a hole, 0.0076 cm in diameter, countersunk on one side to reduce viscosity effects to a minimum. The cup was mounted snugly on the outside of one glass tube and

* Abstract from a dissertation presented in partial fulfillment of the requirements for the degree of Doctor of Philosophy at New York University, October, 1949.

[1] O. C. Wetmore and H. A. Taylor, J. Chem. Phys. 12, 61 (1944).

[2] H. J. Emeleus and L. J. Jolley, J. Chem. Soc. 1615 (1935).

TABLE I.

Photolysis Rate Data[a]												
Temp. °C	−15			0			15			30		
Time (min)	29	75	120	30	90	120	30	60	90	30	90	120
Percent decomp.	12	21	29	17	38	47	26	39	51	42	77	84
ΔP (mm)	−1.1	−1.4	−2.7	1.0	1.4	2.6	3.3	5.9	8.1	8.8	16.6	15.8
Initial CH_3NH_2 (cc)	47.4	47.3	47.5	44.9	44.5	45.1	42.4	42.6	42.7	40.2	40.7	40.2
CH_3NH_2 decomp. (cc)	5.9	9.9	13.8	7.7	16.9	21.3	11.2	16.7	21.9	17.0	31.1	33.7
H_2 (cc)	2.9	5.6	8.4	4.8	12.3	15.3	8.5	13.5	17.8	14.1	27.1	29.5
NH_3 (cc) {1	0.3	0.7	1.4	0.8	2.4	4.3	1.6	2.9	4.7	2.9	7.6	7.8
NH_3 (cc) {2[b]	1.4	2.6	4.1	1.9	5.0	7.4	2.9	4.6	6.9	4.3	9.8	10.2
CH_4 (cc)	0.1	0.3	0.2	0.1	0.2	0.3	0.2	0.4	0.5	0.4	0.6	0.6
N_2 (cc)	0.1	0.2	0.3	0.0	0.2	0.1	0.2	0.0	0.3	0.3	0.3	0.6
H_2/CH_3NH_2 decomp.	0.49	0.57	0.61	0.62	0.73	0.72	0.76	0.81	0.81	0.83	0.87	0.88
H_2/NH_3	9.7	8.6	6.0	6.3	5.1	3.6	5.3	4.7	3.8	4.9	3.6	3.8
Polymer[c] m	3.9	3.7	3.4	3.4	3.1	3.0	3.0	2.9	2.4	2.8	2.5	2.5
CH_mN_n n	0.9	0.9	0.8	0.9	0.8	0.8	0.9	0.9	0.8	0.8	0.8	0.8

[a] Volumes in cc at N.T.P.
[b] Total NH_3, including NH_3 from polymer after photolysis.
[c] Calculated from C, H, N balance.

inside a second and cemented in place to make a vacuum tight seal. A volume of about 200 cc of gas was effused through the orifice and then condensed in a liquid nitrogen trap. In this manner the effusion occurred under a definite and reproducible pressure gradient measured on a closed-end manometer carrying electrical contacts in series with small light bulbs which, by their flashes, indicated fixed pressure limits. The time of effusion between these flashes was measured with a stop watch. A calibration curve was constructed by determining the effusion times of known mixtures of methylamine and ammonia. Four or more determinations were made of each effusion time by re-vaporizing the gases into the effusion reservoir and repeating the observation. The times were corrected from room temperature to 25°C using an experimentally determined correction factor of 0.175 sec/deg. This factor is only about one-third of that expected for ideal gases whose effusion times should vary inversely as the square root of the temperature. This observation, coupled with the slightly *s*-shaped calibration curve, is probably to be attributed to a deviation from ideality. The precision of the effusion times was about 0.3 percent. The effusion time of ammonia was about 300 sec; that of methylamine about 400 sec.

Hydrogen and methane were determined by combustion in oxygen over a hot platinum wire, any resulting carbon dioxide being absorbed in potassium hydroxide solution.

For the static runs, the reaction vessel, cleansed of all deposit from the previous run by successive treatment with concentrated nitric acid and water, was placed in the furnace in as nearly a fixed position as possible relative to the light source, and was thoroughly evacuated. The furnace and lamp housing were brought to the temperature desired for the run, amine was introduced into the reaction vessel to the desired pressure, usually 100 mm, and the lamp was allowed to warm up to full intensity for from 30 to 60 min while protected by a shutter. Removal of the shutter initiated photolysis, the time being observed, and pressure readings at chosen intervals were taken. After a run, the condensable products were removed to a trap in liquid nitrogen and the noncondensable fraction transferred to a gas analyzer and analyzed. The liquid nitrogen was replaced by an acetone-dry ice bath and the vaporized products distilled into the effusion analyzer.

EXPERIMENTAL RESULTS

In the earliest runs, made with the intention of studying the effect of temperature on the photolysis, rate studies were made at 40, 60, 80, and 100°C. Reproducibility was found to be very poor, attributable in the main to two causes: (1) variation of a deposit on the reaction vessel, either as droplets of liquid or as a more or less uniform film, resulting in a variable light scattering, and (2) darkening of this deposit apparently dependent on both time of exposure to the light and on temperature, resulting in a changing light intensity. The apparent effect of a temperature increase was to slow down the rate. It was in an attempt to overcome this deposition that the cyclic runs were made. Here, again, a similar result was observed in that, under otherwise identical conditions, 100 mm methylamine decomposed 31 percent at 40°C and only 19 percent at 100°C. The reaction tube was again darkened. To obviate this darkening a cyclic run at ~12°C was made, which resulted in a 23 percent decomposition with only very slight darkening. It was concluded that by working at and below room temperature, reproducibility could be achieved and reliable rate data obtained. Table I summarizes these data at −15, 0, 15, and 30°C. Ammonia and hydrogen are the principal products, with traces of methane and nitrogen. Ethane was specifically sought since it is mentioned among the products in earlier work at higher temperatures. A sample of methylamine was completely decomposed at 35°C yielding condensable hydrocarbons amounting to 0.6 percent of the noncondensable gases. This is equivalent to about one percent of the combined am-

monia plus methylamine volume. If this is assumed to be ethane, its presence in the quantities indicated would have almost no effect on the effusion determination for ammonia, but since its molecular weight is close to that of the amine, the residual amine determination would tend to be high. The amounts, however, border on the precision of the effusion determination.

The "polymer" referred to in Table I is the liquid deposit mentioned previously. It is a high boiling liquid product whose composition changes continuously during photolysis. The empirical formulas in the table were calculated from a, C, H, and N balance, but because of the complexity, they are probably not of great significance.

The ratios involving ammonia in the table are calculated from the first row of ammonia data. After a run was completed and the gaseous products had been withdrawn, a pressure increases was observed on standing at room temperature. The amount varied up to about 20 percent of the ammonia and methylamine volume. Collection of quantities of this gas from several runs showed an effusion rate equivalent to that of a 77 percent ammonia mixture, and an infrared analysis showed the presence of only ammonia and methylamine. The second row of data for ammonia are the estimated total volumes thereof derived from the reaction.

On plotting the data from Table I as logarithms of the undecomposed methylamine against time, straight lines result which correspond to first order reaction rates. The slopes of these lines yield the following specific rates in min^{-1} at $-15°$, 0.00311; at 0°. 0.00542; at 15°, 0.00875; and at 30°, 0.0157. Using the Arrhenius equation, these data correspond to an energy of activation of 6 kcal.

Since the analytical results indicate that the ratio of hydrogen produced to amine decomposed is unity for the complete reaction, the reaction rates may be calculated in terms of the hydrogen formed. Plotting the logarithms of the differences between the final hydrogen, taken as equal to the initial methylamine, and the hydrogen at various times against time, straight lines again result, and their slopes yield the following rate constants: at −15°C, 0.00189; at 0°C, 0.00362; at 15°C, 0.00638; and at 30°C, 0.0120. Although these figures do not exactly duplicate those given previously, the agreement is satisfactory. The Arrhenius plot again gives 6 kcal as the energy of activation.

In a similar manner, assuming that the ammonia produced is half the methylamine decomposed for total reaction, plots of decomposition amounts in terms of the ammonia analyses give the following rate constants: 0.000433, 0.00134, 0.00260, and 0.00470 at −15°C, 0°C, 15°C, and 30°C, respectively. These values are considerably less than those previously calculated and reflect the tendency of the ammonia analyses of the gas produced rapidly during photolysis to be less than half the amine decomposed. Even with these values, however, the Arrhenius plot gives an energy of activation of only about 8 kcal.

TABLE II. Gas production by polymer at room temperature.

Reaction conditions		Time hrs	ΔP mm	Volume of gas cc NTP	Percent of photolysis gas
°C	hrs				
−15	0.5	150	3.0	1.1[a]	3
−15	1.25	80	5.9	2.1	6
−15	2.0	77	8.9	3.1	9
0	0.5	122	3.4	1.3[a]	3
0	1.5	90	6.9	2.8[a]	9
0	2.0	168	9.3	3.5	13
15	0.5	149	4.0	1.2	4
15	1.0	140	5.2	1.9[a]	7
15	1.5	114	6.4	2.4	9
30	0.5	55	3.5	1.3	5
30	1.5	120	7.0	2.6	15
30	2.0	40	8.0	2.8	20

[a] Calculated from observed pressure.

It has not been thought necessary to give the data of runs made at higher temperatures since similar analyses to the above are in part meaningless and the rate data are definitely meaningless. Nevertheless, something may be mentioned concerning the polymer which was observed over the whole temperature range studied, −15° to 100°C. In all runs, there was observed a fog formation which set in very quickly after the start of photolysis. At 40°C, the first evidence of fog appeared in about one minute; at 100°C, after two minutes; and in a shorter time at the low temperatures. The lower the temperature the more dense the fog seemed and the longer it persisted, eventually settling out as droplets of liquid or as a continuous liquid film on the reaction vessel (more pronounced on the side adjacent to the light). A rough parallelism was always observed between the rate of reaction and the light scattering to be expected from each type of deposit. The liquid was initially colorless, but as the reaction progressed it became brown. This effect was the greater the higher the temperature. That the liquid is not a simple substance is indicated by the following observations: (1) the empirical formula changes continually during a run; with increasing decomposition the number of units of nitrogen and hydrogen per carbon unit continually decreases. (2) The polymer is only partially water soluble; in two runs at −15°C, addition of water to the polymer in the reaction vessel produced what appeared to be many small needle-like crystals within some of the yet undissolved polymer, which persisted for about a minute when the whole of the polymer had dissolved. In longer runs at higher temperatures, a portion of the polymer is always insoluble in water. Aqueous extracts of the polymer were always basic and had a *p*H of about 9. The polymer from a run at 100°C was insoluble in ether, carbon tetrachloride, benzene, and chloroform but somewhat soluble in absolute alcohol. The alcohol extract gave a basic solution after the removal of alcohol and the addition of water. The residue from the alcohol treatment was

partially water soluble, though the resulting solution was neutral to litmus. (3) Finally, as has been mentioned, the polymer undergoes a dark reaction liberating a gas at room temperature. In Table II are listed some observations on this gas production (from several runs). The volumes of gas, reported in column four, when actually measured, were found consistently to be from 10–20 percent less than those calculated from the observed pressure. This would seem to indicate the presence of an easily condensable vapor in the gas. The values quoted as derived from the pressure change have been reduced correspondingly.

It is apparent that the polymer undergoes a slow thermal decomposition involving gas production. Infrared analysis showed the presence of ammonia and methylamine in this gas. Increase of temperature caused a more rapid reaction. Thus, after a photolysis at 30°C for two hours, the gaseous products were withdrawn and the system allowed to stand at room temperature for forty-six hours. The pressure developed was 7.1 mm. The system was then heated successively for half-hour periods at 60°, 66°, 100°, and 100°C. After each heating, the vessel was brought back to room temperature and the pressure measured. The observed pressures were 8.6, 9.3, 11.5, and 13.0 mm. The volume of gas so obtained was 5.0 cc under room conditions, and all but 0.1 cc was acid soluble. It would appear possible that the gas originates from a condensation type polymerization which splits out ammonia. In two instances it was found that the polymer, after acidification with hydrochloric acid, gave a positive test with Schiff's reagent, although in neither case was Fehling's solution reduced, even on heating.

DISCUSSION

From the runs made at higher temperatures it was found that the limiting ratio of hydrogen produced to methylamine decomposed was unity. In the low temperature range where the percentage decomposition was not high, the same limiting ratio appears probable. Initially, however, two methylamines give one hydrogen and no ammonia. The limiting amount of ammonia produced is dependent on the temperature. At 80°C, the ratio of ammonia produced to methylamine decomposed was 0.5, though at lower temperatures it is less. The polymer reaction yielding ammonia after photolysis at the lower temperatures indicates that hydrogen production is complete before that of ammonia. The pressure decrease observed at −15°C is also of primary significance.

These observations suggest a primary decomposition of methylamine to give hydrogen and a substance with sufficiently low vapor pressure at −15°C to produce a pressure decrease. The over-all reaction may be written:

$$2CH_3NH_2 = H_2 + C_2H_8N_2. \qquad (1)$$

Another molecule of hydrogen and one of ammonia appear in the final products. It is apparent that $C_2H_8N_2$ undergoes further decompositions which may be written:

$$C_2H_8N_2 \rightarrow H_2 + C_2H_6N_2, \qquad (2)$$

$$C_2H_6N_2 \rightarrow NH_3 + C_2H_3N. \qquad (3)$$

Since the last two products are probably polymeric in nature, they should be more correctly written $1/n(C_2H_6N_2)_n$ and $1/n(C_2H_3N)_n$.

The mechanism of reaction (1) has already been quite well established as involving dissociation of a hydrogen atom from methylamine by the primary light absorption, and hydrogen atoms have been shown[1] to react rapidly with methylamine.

$$CH_3NH_2 + h\nu \rightarrow CH_3NH + H,$$
$$H + CH_3NH_2 \rightarrow H_2 + CH_3NH.$$

To account for the pressure decrease observed at −15°C, the methylamino radicals must be tied up effectively. That this is not dimethylhydrazine follows from the study of its photolysis[3] in which methane and nitrogen are main products, contrary to the findings here. A possible compound (with sufficiently high boiling point) to account for the pressure decrease is ethylene diamine which could conceivably arise by isomerization of the methylamino radical to CH_2NH_2 which then polymerizes. One observation offering support of this was the presence of a small amount of white solid in the trap after withdrawal of ammonia and methylamine at dry-ice temperature. On warming, the solid disappeared; ethylene diamine melts at 8.5°C. One attempt made to test specifically for ethylene diamine proved negative, possibly because the test was not sensitive enough or the quantity available was too small. Ethylene diamine would account for the fog observed in all runs. It would probably undergo further photolysis as well as react with hydrogen atoms under the experimental conditions. The finally resulting polymer could conceivably be a polyamino type polymer in the formation of which ammonia is split out, as is observed. Alternatively, ethylene diamine, through a loss of hydrogen, might yield a polymer which is unstable and liberates ammonia. The solubility tests would imply a highly polar material. Previous workers have suggested the presence of methylmethyleneimine, $CH_2{:}NCH_3$, either as an intermediate or as a substance comprising the final polymer. Its probable existence was based on a positive test for formaldehyde in an aqueous solution of the polymer and on a phenylhydrazone formation. In the present instance, although positive Schiff's tests were obtained in the cases tried, no polymer solutions were found which would reduce Fehling's solution.

Since polymer deposition tends to reduce the incident light intensity, the influence of temperature herein

[3] W. Kay and H. A. Taylor, J. Chem. Phys. **10**, 497 (1942).

observed probably represents a minimum effect. The observed energy of activation of 6 kcal is sufficiently low, however, to suggest that the temperature effect is solely one of absorption and that the thermal reactions subsequent to the initial photoreaction are almost temperature independent. Henri and Lasereff[4] have shown that the spectrum of methylamine may be divided into two groups of bands; the one between 2398 and 1986A, the other between 2525 and 2197A with an intensity from 100 to 1000 times less than that of the former at lower temperatures but markedly increasing relatively with increase in temperature. It is evident, therefore, that the only complexity in the course of the reaction lies in the identity of the polymer products, and much more work will be necessary to elucidate these products. Although the disappearance of methylamine is first order, neither hydrogen production, ammonia production, nor pressure change can be taken as an accurate measure of the amine decomposed. Finally, it may be pointed out that the rate of methane production is small though increasing with increased decomposition. This was particularly noticeable at the higher temperatures and may indicate that polymer decomposition is its source.

[4] Henri and Lasereff, Compt. rend. **200**, 829 (1935).

THE JOURNAL OF CHEMICAL PHYSICS VOLUME 19, NUMBER 5 MAY, 1951

Directional Properties of Single Crystal of Anthracene Regarding Fluorescence Phenomena

S. C. GANGULY AND N. K. CHAUDHURI
Research Laboratory, Bangabasi College, Calcutta, India

(Received September 6, 1950)

The polarization of fluorescent radiation of single crystal of anthracene has been measured and this measurement has been utilized to determine the nature and orientation of oscillators. From this measurement it has been found that the oscillators are linear oscillators and their direction is independent of the direction of the electric vector of the incident light vibration. They make an angle of 33° with the *b* axis of the crystal.

FROM magnetic studies[1] it is known that the molecules of anthracene are anisotropic in behavior; and it is known that molecules showing magnetic anisotropy may show anisotropy in optical properties, and these molecules retain their individuality regarding anisotropy in crystal state. Krishnan and others[2] have studied quantitatively the directional variation of absorption and fluorescence of chrysene molecules and naphthacene molecules in anthracene and chrysene crystal. Since the crystal structure of anthracene was determined completely by x-ray methods by Banerjee[3] and Robertson,[4] we undertook investigations to see how the directional property of a molecule may effect the absorption and fluorescence phenomenon and how they are interrelated.

The crystal is known to be monoclinic in the space group $C_{2p}^5(P\cdot 2/a)$. Its unit cell has the dimensions, $a=8.58$, $b=6.02$, $c=11.18$A, $\beta=125°$; and it contains 2 molecules of $C_{14}H_{10}$ per unit cell. The molecule has a plane structure.

[1] K. S. Krishnan, Trans. Roy. Soc. (London) **A231**, 235 (1933).
[2] K. S. Krishnan and P. K. Seshan, Indian Acad. Sci. **8A**, 487 (1938); Acta Physica Polonica **5**, 289 (1936).
[3] K. Banerjee, Nature **125**, 466 (1930), Indian J. Phys. **4**, 557 (1930).
[4] J. M. Robertson, Proc. Roy. Soc. (London) **140**, 79 (1933). Sinclair, Robertson, and Mathieson, Acta. Cryst. **3**, 251 (1950).

EXPERIMENTAL ARRANGEMENT FOR STUDYING FLUORESCENCE

The source of light used was the Hg arc (Hanovia type) which was condensed on the crystal by a condenser and the light was polarized by a Nicol with the shorter diagonal vertical. The exciting radiations were the 3650 group of a mercury arc, which were isolated with the help of a suitable filter, and polarized with the electric vector along with vertical direction. The plane of the crystal was normal to the direction of the incident ray and the *b* axis was kept vertical. The fluorescent light in the forward direction was incident on the slit of the spectrograph after passing through a double image prism, so oriented as to separate the two images verti-

FIG. 1. The fluorescence spectra of anthracene crystal: *bb* represents the component of fluorescent radiation that is vibrating along the *b* axis when the exciting light vibrations are along the same directions; *ba* represents the component of fluorescent radiation that is vibrating along the *a* axis when the exciting light vibrations are along the *b* axis.

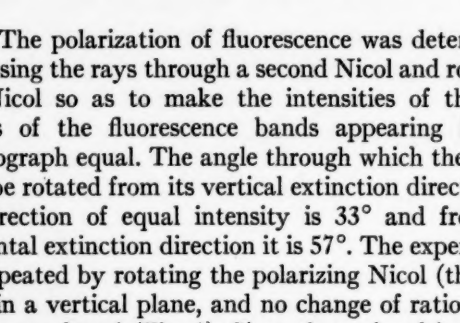

FIG. 2. By orientation of the Nicol through an angle of 33°, two component vibrations are made equally intense.

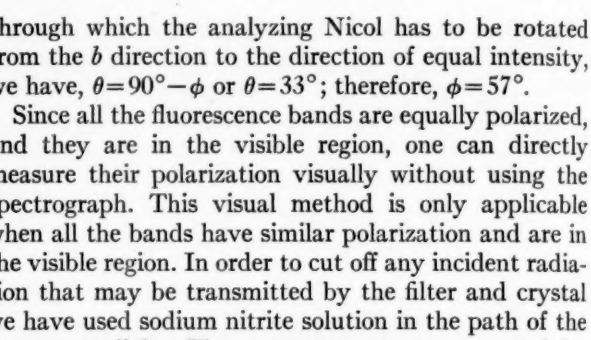

FIG. 3. Hg = mercury arc, L_1 = lens, N_1 = polarizing Nicol, F = filter C = substance, D = double-image prism, N_2 = analyzing Nicol.

cally. The polarization of fluorescence was determined by passing the rays through a second Nicol and rotating this Nicol so as to make the intensities of the two images of the fluorescence bands appearing in the spectrograph equal. The angle through which the Nicol must be rotated from its vertical extinction direction to the direction of equal intensity is 33° and from its horizontal extinction direction it is 57°. The experiment was repeated by rotating the polarizing Nicol (through 360°) in a vertical plane, and no change of ratio of intensity was found (Fig. 1). Since the ratio of intensity remains the same whether the *a* or *b* axis is vertical, we can reasonably conclude that even for unpolarized light the ratio will remain the same. Actually, by removing the polarizing Nicol altogether, we observed the same ratio.

In order to check the result, the experiment was repeated in the following way.

The exciting radiations were the 3650 group of a mercury arc, which were isolated with the help of a suitable filter and polarized with the electric vector along a direction making 45° with the vertical. It is then allowed to pass through a double-image prism so oriented as to make one image appear vertically above the other. Obviously, they will be of equal intensity. The vibration directions of the transmitted light for the two images are vertical and horizontal. Next a Nicol was introduced between the spectrograph and the double image prism, so oriented as to make the two images equally bright. Now the shorter diagonal of the Nicol makes 45° with the vertical and horizontal directions. The crystal is then introduced with the *b* axis vertical. The intensity of the two images which are due to fluorescence light is found to be unequal, and the second Nicol must be reoriented now to make them equally bright (Fig. 2). The angle through which the second Nicol must be rotated from its previous direction is found to be 12°. The shorter diagonal of the Nicol now makes an angle of $(45+12=)57_a$ from the vertical direction. Suppose θ is the angle between the oscillator and the *b* axis of the crystal, and if ϕ be the angle through which the analyzing Nicol has to be rotated from the *b* direction to the direction of equal intensity, we have, $\theta=90°-\phi$ or $\theta=33°$; therefore, $\phi=57°$.

Since all the fluorescence bands are equally polarized, and they are in the visible region, one can directly measure their polarization visually without using the spectrograph. This visual method is only applicable when all the bands have similar polarization and are in the visible region. In order to cut off any incident radiation that may be transmitted by the filter and crystal we have used sodium nitrite solution in the path of the fluorescent light. The measurement was repeated by rotating the polarizing Nicol through 360° in a vertical plane, and no change of ratio of intensity was found. The experimental arrangement used is given in Fig. 3.

RESULTS

With the incident light vibration along the *a* axis of the crystal and again along the *b* axis of the crystal, the polarization of fluorescence in the forward direction was measured. For both the excitations, the *b* vibrations in the fluorescence were found to be more intense than the *a* vibrations, and the ratio of the intensities of two vibrations was found to be the same for any direction of exciting vibration. From this we conclude that the ratio of intensities in the two directions is independent of the direction of the incident light vector and the oscillator is a linear one. If ϕ be the angle through which the analyzing Nicol has to be rotated from the *b* direction to the direction of equal intensity, $\theta=90-\phi$, where θ is the angle between the oscillator and the *b* axis. ϕ has been measured to be 57°, and hence $\theta=33°$. There are two molecules in the unit-cell equally inclined to the *b* axis at an angle of 26°; the oscillator directions are nearly along the molecular planes.

The authors wish to thank Prof. K. Banerjee for helpful discussion and the Government of West Bengal for a research grant to one of them (S.C.G.).

Time Lag in the Self-Nucleation of a Supersaturated Vapor*

RONALD F. PROBSTEIN
Department of Aeronautical Engineering, Princeton University, Princeton, New Jersey
(Received December 18, 1950)

Recent experiments have indicated that the quasi-equilibrium Volmer theory of self-nucleation fails in some cases to predict when the condensation of water vapor or the components of air will occur in the very rapid vapor expansions in a supersonic wind tunnel. By the obtaining of an approximate solution to the non-steady Becker-Döring equation for the self-nucleation of a supersaturated vapor, an attempt has been made to determine whether the time lag associated with the approach to the steady state rate of formation of condensation nuclei could account for the discrepancies between theory and experiment. A similar calculation, where the work required to form embryos of the condensing phase was neglected, has been carried out by Kantrowitz. In the present paper the work term has been taken into account to a first approximation. Also considered is the time lag arising from the heating of the nuclei due to bombardment by molecules of the condensing phase as well as the time lag resulting from an accommodation coefficient for the liquid nuclei different from unity.

Calculations of the self-nucleation of water vapor in air and nitrogen in air have been carried out. From the results it appears that the build-up time is not appreciably lengthened by inclusion of the work term to a first approximation. The results also indicate that, unless the accommodation coefficient should have a value much lower than what appears to be reasonable from meager experimental evidence, the time lag alone could not account for the existing discrepancies between theory and experiment.

I. INTRODUCTION

THE study of condensation phenomena has attracted the attention of the aeronautical engineer since it was confirmed experimentally by Hermann[1] that the crossing system of compression shocks, first noted by Prandtl,[2] downstream of the throat in a supersonic wind tunnel, was, in fact, due to the sudden condensation of the water vapor originally present in the airstream.

The first detailed theoretical consideration of the problem was given by Oswatitsch,[3] who took into account such factors as the nucleus formation, droplet growth, and collapse of the supersaturated state based on the quasi-equilibrium Volmer theory of nucleation.[4] The solution derived by Volmer on purely thermodynamical considerations was later improved by Becker and Döring,[5,6] who considered the kinetics of a quasi-stationary process, taking into account not only the condensation of vapor on the surface of a liquid droplet but also the re-evaporation. An assumption common to all these theoretical treatments is that the gas is considered to be free of foreign particles which might act as condensation nuclei and so tend to limit the attainment of high degrees of supersaturation.

For some time the results of Oswatitsch were accepted because of the good agreement between theory and experiment for the case of water vapor in air. It was not until the recent investigations of water vapor condensation in supersonic wind tunnels by Head[7] and by Eber and Wegener[8] that some doubt was cast on the validity of the Volmer theory, for in Head's experiments there appeared to be no condensation where the theory had definitely predicted it, while in Eber and Wegener's experiments condensation occurred later than was theoretically calculated.

At the same time the design of hypersonic wind tunnels with air speeds up to ten times the local speed of sound has given further rise to the need for a theory which suitably predicts whether or not condensation of the components of the air will occur. The existing theories for water vapor have been extended to try and determine whether the oxygen or nitrogen will condense out of an airstream if the temperature becomes low enough. Here as well, experiments by Bogdonoff[9] seemed to indicate an absence of condensation when it had been theoretically predicted. However, from results reported by Becker[10] and others, it appears that the presence of foreign nuclei may be the most important factor in the case of condensation of the components of air.

In an effort to resolve the apparent contradictions between theory and experiment, Lees[9] has seriously modified the Volmer theory by proposing that when the condensation nuclei become very small, they can no longer be considered as continuous liquid states. From this idea he concludes that there is a "cut-off" in the

* This work has been supported by the United States Air Force, Air Materiel Command, under Contract AF 33(038)-250. Reproduction, translation, publication, use, and disposal in whole or in part by or for the United States Government is permitted.

[1] R. Hermann, Luftfahrt-Forsch. **19**, 201 (1942).
[2] L. Prandtl, Proc. Volta High Speed Conference, Rome (1935), first edition, p. 197.
[3] K. Oswatitsch, Z. angew. Math. u. Mech. **22**, No. 1, 1-14 (1942).
[4] M. Volmer, *Kinetik der Phasenbildung* (Theodor Steinkopf, Verlag. Dresden, 1939).
[5] R. Becker and W. Döring, Ann. Physik **24**, 719 (1935).
[6] J. Frenkel, *Kinetic Theory of Liquids* (Oxford University Press, New York, 1946).
[7] R. Head, "Investigation of spontaneous condensation phenomena," Guggenheim Aero. Lab., Calif. Inst. of Tech., Ph.D. Dissertation (1949).
[8] P. Wegener and R. Smelt, "Summary of NOL research on liquefaction phenomena in hypersonic wind tunnels (NOL 159)"; NOL Memo. 10772 (February 15, 1950).
[9] S. M. Bogdonoff and L. Lees, "Study of the condensation of the components of air in supersonic wind tunnels," Princeton Univ. Aero. Eng. Dept. Report 146 (May 25, 1949).
[10] J. V. Becker, "Results of recent hypersonic and unsteady flow research at the Langley Aeronautical Laboratory," Paper presented at the fifth meeting of the Fluid Dynamics Division, Am. Phys. Soc., Charlottesville, Virginia, December 9, 1949 [Phys. Rev. **79**, 546 (1950)].

FIG. 1. Schematic representation of free energy change as a function of droplet radius.

values of the nucleus formation frequency as given by Volmer.

Kantrowitz,[11] on the other hand, suggests that the predicted values of nucleus formation frequency are too high because of a time lag associated with reaching the quasi-equilibrium distribution given by Becker and Döring. He points out that these investigators neglected the following considerations associated with time lag:

(a) The build-up to an equilibrium distribution of droplets smaller than the critical size.

(b) The heating of the nucleus due to bombardment by molecules of the condensing phase.

(c) The inability of the liquid nuclei to absorb all the molecules hitting their surface.

In the calculation carried out by Kantrowitz, very rapid expansions are considered, and the work required to form small embryos, that is, aggregates of 2, 3, or 4 molecules, is neglected.

One of the main purposes of this report is to determine if the build-up time is appreciably lengthened over that calculated by Kantrowitz if the work term is included to a first approximation. Calculations of the time lag for the expansion of a supersaturated gas through a supersonic nozzle have been carried out in two representative cases: for the nitrogen present in air and for water vapor in air having an absolute humidity of 1 part in 1000. The effects on the build-up time due to variations in the absolute humidity, the accommodation coefficient, and the initial pressure and temperature conditions are analyzed.

II. ANALYSIS

A. Modified Becker-Döring Equation

In any examination of the problem of self-nucleation it is necessary to determine the rate of formation of condensation nuclei, that is, droplets of the critical size, for it is only these droplets that are capable of growing rapidly by the addition of vapor and so cause the collapse of the supersaturated state.

The unstable equilibrium existing between the supersaturated vapor and a liquid droplet is expressed in the fact that the free energy change involved in the formation of a droplet of critical size has a maximum rather than a minimum value as in the case of stable equilibrium. This maximum value can be shown to be given by[6]

$$\Delta\phi^* = (4/3)\pi\sigma r^{*2}, \tag{1}$$

where σ is the surface tension, and r^* is the critical radius expressible by Thomson's formula:

$$r^* = 2\sigma M/dRT \ln p_s/p_\infty, \tag{2}$$

where M = molecular weight of vapor, p_s = equilibrium vapor pressure, p_∞ = saturation vapor pressure, d = liquid density, T = absolute temperature, R = universal gas constant. Since the initial phase is in a state of metastable equilibrium, droplets of critical size of the liquid phase are in a state of unstable equilibrium with the supercooled vapor owing to the forces exerted by surface tension. An examination of Fig. 1 reveals that the droplets smaller than critical, though formed more frequently, are unstable and will have a tendency quickly to re-evaporate with an accompanying reduction in the free energy change. On the other hand, for droplets greater than critical size it can be seen that their tendency is to grow with a decrease in the free energy change. From Gibbs' formula, J, the steady state rate of formation of condensation nuclei, can be shown to be given by[4,6]

$$J = C \exp(-\Delta\phi^*/kT). \tag{3}$$

Becker and Döring formulated the complete kinetic equation for the condensation of a supersaturated vapor, and then on the assumption of the existence of quasi-equilibrium conditions calculated the coefficient C. Thus, in effect, they considered the transit time from saturation to the steady state rate of formation of condensation nuclei to be large compared to the lag time. In their formulation of the kinetic equation governing the process, they assumed that the embryos grow by absorption and re-evaporation of single molecules, that the pressure remains constant, and that the velocities of the molecules both in the embryo and gas phase preserve an equilibrium distribution given by Maxwell's law. One would therefore expect that the formulation of Becker and Döring would no longer be valid for low densities where departures from the classical distribution occur.

Since Maxwell's law holds only in a force-field with no singularities in temperature, it is implied that the embryo temperature at all times is equal to the ambient temperature. Kantrowitz points out, however, that at the inception of the nucleation process, when the em-

[11] A. Kantrowitz, "Nucleation in very rapid vapor expansions"; Edwin G. Baetjer, II, Aeronautical Engineering Seminar, Princeton University, March 15, 1950; also, paper presented at Sixth Meeting of Fluid Dynamics Div., Am. Phys. Soc., Urbana, Illinois, May 13, 1950 [Phys. Rev. 77, 572 (1950)].

bryo goes from $g-1$ to g molecules, the temperature is raised to a value much higher than ambient. The tendency is, therefore, for the molecules to re-evaporate with small probability that the embryo will grow. However, as the molecules re-evaporate, they carry away more energy than they have brought in; and, in time, the tendency is to lower the embryo temperature to a value closer to ambient and so increase the probability of growth.† Thus, the build-up of the droplets less than critical size is a random process with a resulting time delay before a quasi-steady state is reached. Kantrowitz expresses this fact in a modified expression for α_g, the number of molecules evaporated from the surface of an embryo containing g molecules, per unit time and area.

The coefficient of evaporation as expressed by Becker and Döring is:

$$\alpha_{g\text{B.D.}}=\beta\exp[(\partial\Delta\phi/\partial g)(1/kT)]$$
$$=\beta\exp[-\ln(p_s/p_\infty)+2\sigma v_B/r_g kT], \quad (4)$$

where β is the number of molecules absorbed per unit time and area, k is the Boltzmann constant, and $v_B=M/dL$ is the volume occupied by one molecule in the liquid phase, L being Avogadro's number. Examination of this expression shows that since the free energy change involved in the formation of a droplet of critical size has a maximum at $g=g^*$, then $[\partial\Delta\phi/\partial g]_{g=g^*}=0$; hence, $\alpha_{g\text{B.D.}}\simeq\beta$ in the neighborhood of the critical size. By considering only the effect of the molecules of the condensing phase in this region, Kantrowitz derives a modified evaporation coefficient. His result is based on the fact that, owing to an existing statistical temperature difference, θ, between the droplet and ambient temperature, there must be a corresponding change in the evaporation coefficient. By assuming the temperature difference to be constant he arrives at the following expression:

$$\alpha_g=\alpha_{g\text{B.D.}}\left[1+\theta\left(\frac{U_\infty}{RT^2}-\frac{1}{2T}\right)\right], \quad (5)$$

where T is the ambient temperature, and U_∞ is the latent heat of vaporization of the liquid droplet. The term U_∞/RT^2 arises from an approximate integration of the Clausius-Clapeyron equation and represents the excess value of the saturation vapor pressure due to the statistical temperature difference, while the collision effect is characterized by the term $\frac{1}{2}T$. Since $\frac{1}{2}T\ll U_\infty/RT^2$, the new value of the evaporation coefficient can be written as

$$\alpha_g\simeq\alpha_{g\text{B.D.}}[1+\theta U_\infty/RT^2]. \quad (6)$$

The determination of θ is based on the fact that not only the molecules of the condensing phase but, rather, all the molecules of the gas mixture participate in the transport of heat energy away from the droplet. On this assumption Kantrowitz expresses the temperature difference as

$$\theta=\frac{J_g U_\infty}{f_g s_g \alpha_{\text{B.D.}} c_v\,\text{Ac}/h}, \quad (7)$$

where f_g represents the concentration of embryos containing g molecules, s_g is the surface area of the embryo, h is the absolute humidity of the condensing phase, c_v is the specific heat of the liquid, J_g is the nucleation rate, and Ac is the accommodation coefficient for the molecules of the condensing phase striking the droplet surface.

The kinetic equation representing the nucleation rate was given by Becker and Döring as

$$J_g=f_{g-1}s_{g-1}\beta-f_g s_g\alpha. \quad (8)$$

That is, owing to condensation of the vapor on the surface of the embryo, the molecules pass from $g-1$ to g, and owing to evaporation, they pass from g to $g-1$. If the value of α expressed by Eq. (6) is substituted in Eq. (8) and θ is eliminated by means of Eq. (7), the new nucleation rate is given by

$$J_g[1+U_\infty^2 h/c_v\,\text{Ac}\,RT^2]=f_{g-1}s_{g-1}\beta-f_g s_g\alpha_{\text{B.D.}}. \quad (9)$$

Examination of the kinetic equation for the rate of change of the number of drops of a given class, which is

$$J_g-J_{g+1}=\partial J_g/\partial g=\partial f_g/\partial t, \quad (10)$$

yields the immediate result that, if the time t is modified to some new effective time τ by the transformation

$$\tau=t/[1+U_\infty^2 h/c_v\,\text{Ac}\,RT^2], \quad (11)$$

the problem remains unchanged provided the time (t) given by Becker and Döring is replaced by the effective time (τ). From Eq. (11) it is apparent that the build-up time for droplets less than critical size is longer the lower the accommodation coefficient and the lower the ambient temperature. Also for very low absolute humidities $h\langle\langle\langle 1$, the nucleus is almost immediately cooled down to ambient and $\tau\to t$, leaving the Becker-Döring analysis unchanged.

B. Simplification of Time-Dependent Becker-Döring Equation

Becker and Döring, under the assumptions already mentioned, characterize the non-equilibrium distribution of embryos through the function $f(g,\tau)$ in the following partial differential equation:‡

$$\frac{\partial f}{\partial\tau}=\frac{\partial}{\partial g}\left(D\frac{\partial f}{\partial g}\right)+\frac{1}{kT}\frac{\partial}{\partial g}\left(Df\frac{\partial\Delta\phi}{\partial g}\right). \quad (12)$$

† E. H. Kennard [*Kinetic Theory of Gases* (McGraw-Hill Book Company, Inc., New York, 1938) p. 79] notes, however, that the experimental evidence regarding this point is still somewhat uncertain.

‡ The reader is referred to reference 6, p. 394, for the steps in proceeding from Eq. (9) to Eq. (12).

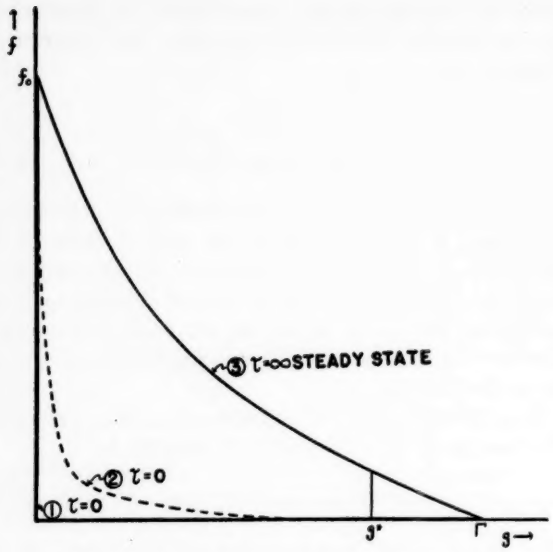

FIG. 2. Schematic representation of initial and final embryo distribution.

Here, D is a diffusion coefficient which can be written as

$$D=(4\pi)^{\frac{1}{2}}(3)^{\frac{1}{2}}v_B^{\frac{1}{2}}g^{\frac{1}{2}}p_s/(2\pi mkT)^{\frac{1}{2}}, \tag{13}$$

where m is the mass of an atom of the condensing phase.

The problem of solving Eq. (12) can be considerably simplified if one takes into consideration only the region in the neighborhood of the critical value of g (i.e., $g\simeq g^*$), and if it is assumed that the diffusion coefficient is a constant.

These simplifications can be justified by expanding Eq. (12) and rewriting it as

$$\frac{\partial f}{\partial \tau}=D\frac{\partial^2 f}{\partial g^2}+\frac{\partial f}{\partial g}\frac{\partial D}{\partial g}+\frac{1}{kT}\left[Df\frac{\partial^2\Delta\phi}{\partial g^2}+\frac{\partial\Delta\phi}{\partial g}\frac{\partial(Df)}{\partial g}\right]. \tag{14}$$

Now, as pointed out previously at $g=g^*$, $[\partial\Delta\phi/\partial g]_{g=g^*}=0$, and hence, for the critical region one can write

$$\frac{\partial f}{\partial \tau}\simeq D\frac{\partial^2 f}{\partial g^2}+\frac{\partial f}{\partial g}\frac{\partial D}{\partial g}+\frac{D}{kT}\left[\frac{\partial^2\Delta\phi}{\partial g^2}\right]_{g=g^*}f. \tag{15}$$

Since $D\sim g^{\frac{1}{2}}$ or $D=Ag^{\frac{1}{2}}$, if one arbitrarily chooses the critical value of g to be 15,§ then the coefficient $\partial D/\partial g=\frac{2}{3}Ag^{-\frac{1}{2}}\simeq 0.17A$, while D itself is approximately $6A$, and hence, $D\gg\partial D/\partial g$. From the quasi-equilibrium solution of Becker-Döring one can show that the concentration of embryos containing g molecules may be written as $f\sim\exp(-\Delta\phi/kT)$, and for a critical value of $g=15$, f can be approximated by $f\sim\epsilon^{-g/4}$. Therefore, the ratio of $\partial^2 f/\partial g^2$ to $\partial f/\partial g$ will be approximately four, in which case $D\partial^2 f/\partial g^2/(\partial D/\partial g)(\partial f/\partial g)$ would be roughly 150, and it would appear justifiable to neglect the term $(\partial D/\partial g)(\partial f\partial/g)$. This is tantamount to considering the diffusion coefficient to be constant. By factoring out the diffusion coefficient in the bracketed term of Eq. (14), it is seen that in effect one neglects the work term $(\partial\Delta\phi/\partial g)(\partial f/\partial g)$ in addition to the term $(\partial D/\partial g)\times(\partial f/\partial g)$. Since for all $g<g^*$, $\partial\Delta\phi/\partial g>0$ and $\partial f/\partial g<0$, it is apparent that both terms are negative and hence contribute to the work required to form a droplet of critical size. Thus, on the above assumptions it would appear that the time to reach a steady state distribution as calculated would be slightly shorter than the actual time.

The equation to be solved subject to the appropriate boundary and initial conditions is then

$$\partial f/\partial\tau=D(\partial^2 f/\partial g^2)-Bf, \tag{16}$$

where both D and B are positive constants, and B can be written as

$$B=(8/9)(\pi\sigma/kT)(r^*/g^*)^2D. \tag{17}$$

C. Solution to Nonsteady Distribution Equation

Equation (16) may now be solved by specifying the initial distribution of embryos to be

$$\begin{aligned} &f(g,0)=0, \quad 0<g\leq\Gamma,\\ &f(0,0)=f_0, \end{aligned} \tag{18}$$

subject to the boundary conditions

$$\begin{aligned} &f(\Gamma,\tau)=0,\\ &f(0,\tau)=f_0. \end{aligned} \tag{19}$$

This distribution is represented by curve ① in the sketch of Fig. 2. One would expect that as $\tau\to\infty$, that is, when $\partial f/\partial\tau\to 0$, a steady state solution is obtained (shown as curve ③ in Fig. 2) which is a good approximation to the Becker-Döring solution around the critical region but which is greater in error the further one goes from g^*. From the solution to Eq. (16) some insight should be afforded as to the necessary effective times required for the build-up of droplets less than critical size to an equilibrium distribution. It should then be possible to calculate the effect of different accommodation coefficients, absolute humidities, and initial pressure and temperature conditions, on the time lag. Furthermore, some idea should be obtained of the effect on the lag time of including the work term.

Examination of the initial condition chosen reveals that a more nearly correct initial distribution might be given by curve ② of Fig. 2, since at saturation there are present a certain number of embryos of all sizes. The condition used, however, may possibly compensate for the neglect of the secondary work terms in the derivation of Eq. (16).

With regard to the boundary conditions it is shown in reference 6 that for a degree of supersaturation less than critical, the concentration of embryos falls off rapidly for $g>g^*$. For all practical purposes it will be assumed in this report that f becomes 0 at a value of $g=\Gamma=(4/3)g^*$. At $g=0$, although f_0 does drop slightly with increasing

§ It will later be seen that this is a reasonable value to represent the processes involved.

time, it can be considered constant, since the decrease would be small compared to the initial value.

The solution to Eq. (16) subject to the conditions given by Eqs. (18) and (19) is most easily obtained by means of the operational calculus and is computed in the appendix.

The result is expressed by the following equation.

$$F=\frac{\sinh W(1-G)}{\sinh W}+2\sum_{n=1}^{\infty}\frac{n\pi}{(n\pi)^2+W^2}\times\sin n\pi G\left\{\exp\left(-\left[\frac{(n\pi)^2+W^2}{\Gamma^2}\right]D\tau\right)\right\}, \quad (20)$$

where $F=f/f_0$, $G=g/\Gamma$, and $W=(B/D)^{\frac{1}{2}}\Gamma$.

The first part of Eq. (20) is seen to be the quasi-equilibrium solution; it is interesting to note that for ctnh $W=1$, it reduces to the exponential e^{-W_g}. The factor W can be recognized as the direct contribution from inclusion of the work term, for as $W\to 0$, the solution becomes

$$F\to(1-G)+\frac{2}{\pi}\sum_{n=1}^{\infty}\frac{\sin n\pi G}{n}\exp\left(-\frac{n^2\pi^2}{\Gamma^2}D\tau\right), \quad (21)$$

which is the expression obtained by Kantrowitz where the work required to form the embryos is neglected.

D. Time Lag Calculations

To obtain an idea of the build-up time required to reach a quasi-equilibrium distribution of embryos for a supersaturated vapor, two cases have been chosen. The first example is the expansion of humid air, having a water vapor content of 1 part in 1000 by weight, through a supersonic nozzle to a Mach number of 1.385 from a stagnation pressure of 1.163 atmospheres and stagnation temperature of 300°K. To study the time lag involved in the build-up of nitrogen embryos, a second example is considered where dry air is expanded from a stagnation pressure of 25.82 atmospheres and stagnation temperature of 300°K to a Mach number of 5.70.

The local temperature, T, and local pressure, p, in the wind tunnel test section is given by the following isentropic relation

$$T_0/T=(p_0/p)^{(\gamma-1)/\gamma}=1+\tfrac{1}{2}(\gamma-1)M^2, \quad (22)$$

where M is the test section Mach number, and γ, the ratio of specific heats, is taken to be 1.40.

The equilibrium vapor pressure for the case of nitrogen in air will be

$$p_s=4p/5, \quad (23)$$

and for water vapor in air

$$p_s=1.607hp. \quad (24)$$

Since the saturation vapor pressure for a liquid is a function only of the local temperature, it is possible to obtain the supersaturation pressure ratio p_s/p_∞.

The following formula is used for the determination of the saturation vapor pressure for water:

$$\log_{10}p_\infty=-(2445.5646/T)+8.2312\log_{10}T-0.01677006T+1.20154\times10^{-4}T^2-6.757169, \quad (25)$$

while for nitrogen,

$$\log_{10}p_\infty=7.7818-0.006265T-341.62/T, \quad (26)$$

T in both cases being in °K, and p_∞ in mm of Hg.

It is then possible to compute the critical droplet radius by means of Thomson's formula, Eq. (2).

Having determined the critical droplet radius, it is a simple matter to calculate g^*, since

$$g^*=4\pi r^{*3}/3v_B. \quad (27)$$

Recalling that $\Gamma=(4/3)g^*$, one can show the value of W to be

$$W=(16/9)r^*(\sigma\pi/kT)^{\frac{1}{2}}. \quad (28)$$

The only problem remaining is the calculation of the undetermined constant f_0 in Eq. (20). This is to be determined by requiring $-D\partial f/\partial g=J_g$, to have the Becker-Döring steady state value at $g=g^*$. One can obtain the constant f_0 by experiment as well. The quasi-equilibrium solution for the nucleation rate derived by Volmer can be written as

$$\ln J_g=\ln 9.5\times10^{25}+\ln[\{p_\infty(\text{mm of Hg})/T\}^2(\sigma M)^{\frac{1}{2}}/d]+2\ln(p_s/p_\infty)-17.49(M/d)^2(\sigma/T)^3/[\ln(p_s/p_\infty)]^2. \quad (29)$$

Though Eq. (29) was derived on thermodynamical considerations alone, it can be shown to be equivalent to the solution of Becker and Döring, by reduction of the result given on page 397 of reference 6.

Thus, by differentiation of Eq. (20), one arrives at the result that for the critical value of g

$$J_g^*=f_0\frac{D}{\Gamma}\left[\frac{W\cosh W(1-G^*)}{\sinh W}+2\sum_{n=1}^{\infty}\frac{(n\pi)^2}{(n\pi)^2+W^2}\times\cos n\pi G^*\left\{\exp\left(-\left[\frac{(n\pi)^2+W^2}{\Gamma^2}\right]D\tau\right)\right\}\right]. \quad (30)$$

Since the first part of Eq. (30) is the equilibrium solution, insertion of the critical values in the expression of Volmer [Eq. (29)] will yield a value of J_g^* by which to determine the initial embryo concentration.

In carrying out the calculations the following significant constants shown in Table I are chosen. These values are in most cases linear extrapolations below the triple point, and must, therefore, be accepted with reservation.

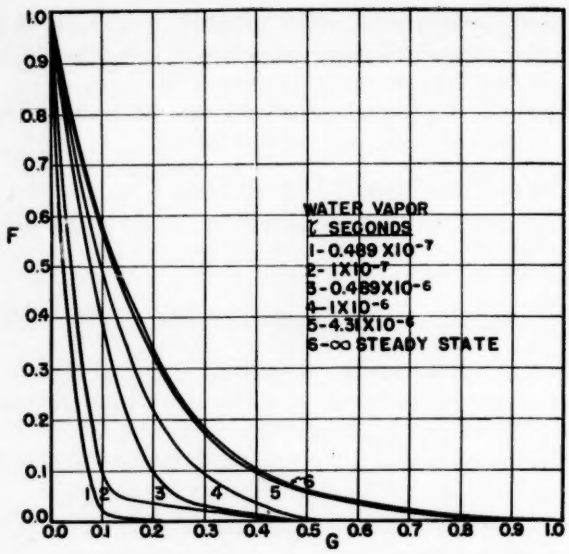

FIG. 3. Influence of effective time lag (τ) on embryo concentration distribution (F *vs* G) in the self-nucleation of water vapor.

III. RESULTS AND CONCLUSIONS

It must be pointed out before discussing the results, that because of the approximations involved and because of the uncertainty with regard to the values of the constants below the triple point, the answers must be regarded as yielding only orders of magnitude.

Illustrated in the graphs of Figs. 3 and 4 is the variation of the nondimensional embryo concentration (F) as a function of the nondimensional quantity (G) representing the number of molecules present in the embryo, for constant values of the effective time τ. The numerical results of interest are tabulated in Table II. Initial conditions of the problem were chosen so that g^* would equal 15, since this appeared to be a reasonable value to represent generally the processes involved.

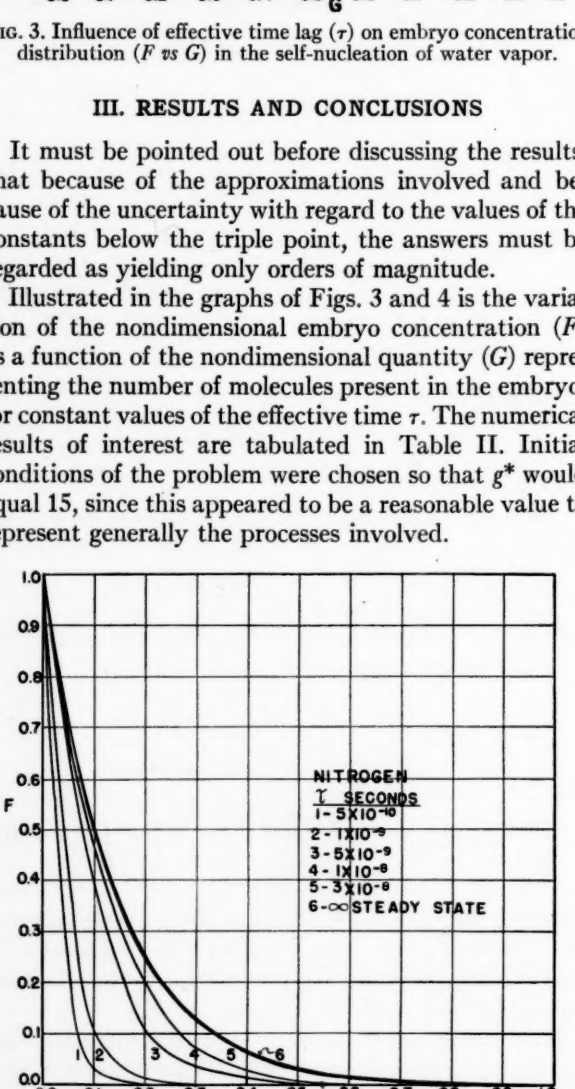

FIG. 4. Influence of effective time lag (τ) on embryo concentration distribution (F *vs* G) in the self-nucleation of nitrogen.

Examination of the curve of F *vs* G for water vapor (Fig. 3) shows that an equilibrium distribution is reached in an effective time of approximately 5×10^{-6} seconds, while in the case of nitrogen (Fig. 4) the time is of the order of 3×10^{-8} seconds. Thus, one recognizes immediately that in the critical region ($G^*=0.75$) the build-up time in both cases is extremely rapid. It is to be expected that as one departs further from the critical range, the results obtained will be greater in error. From the curves of Figs. 3 and 4 it would seem that inclusion of the work term, at least to a first approximation, does not have an appreciable effect in increasing the time lag.

A much more interesting picture, however, is afforded if one examines the curves of the critical value of the nucleus formation frequency (J_g^*/f_0) *versus* the actual lag time (t) (Figs. 5 and 6), for constant values of the accommodation coefficient. It can be seen, for example, in the water vapor case (Fig. 5) that the time lags are well within the minimum transit times of 40 microseconds achieved in Wegener's experiments[8] unless the accommodation coefficient should have a value of around 0.02. It appears very unlikely, however, that values of the accommodation coefficient are this low.

TABLE I. Constants used in evaluating results.

	Water	Nitrogen
σ(dynes/cm)	83.62	17.23
d(g/cm³)	1	0.987
U_∞(g-cal/g)	630	58
c_v(cal/g)	1	0.474

According to a recent article by Bremner[12] the observed accommodation coefficient for oxygen on tungsten at liquid oxygen temperatures is of the order of 0.2, the time intervals involved being very small and, at most, of the order of 10 microseconds. One must necessarily avoid, however, any definite conclusions because of the uncertainties attached to the value of the accommodation coefficient.

Some general conclusions can be drawn regarding the time lag. For example, in the water vapor case with low absolute humidities of, say, $h\leq10^{-3}$, from Eq. (11), $\tau\simeq t$. On the other hand, an examination of the exponent in Eq. (30) reveals that $\tau\sim1/D\sim(T)^{\frac{1}{2}}/ph$. It is therefore possible to express a general time lag for any expansion involving water vapor in air by

$$t_{H2O}/t'_{H2O}=p'_{air}h'(T)^{\frac{1}{2}}/p_{air}h(T')^{\frac{1}{2}}, \qquad (31)$$

where the primes denote the numerical values from the present paper. Considering an accommodation coefficient of 1, the lag time can be written in general as

$$t_{H2O}\simeq(T)^{\frac{1}{2}}1.3\times10^{-6}/p_{air}h, \qquad (32)$$

where t is in microseconds, p in atmospheres, and T in °K. For an accommodation coefficient different from 1,

[12] J. G. M. Bremner, Proc. Roy. Soc. (London) **A201**, 321 (1950).

the value of t'_{H2O} can be obtained from the graph of Fig. 5. By the same reasoning as above, it can be seen that the ratio of "effective times" for expansion of nitrogen in air is given by

$$\tau_{N2}/\tau'_{N2}=p'_{air}(T)^{\frac{1}{2}}/p_{air}(T')^{\frac{1}{2}}, \quad (33)$$

where primes again denote numerical values in the present paper.

It is necessary now, only to recognize that for nitrogen the term $U_\infty^2 h/c_v$ Ac RT^2 in Eq. (11) is always much greater than 1 even for an accommodation coefficient of 1. Therefore, $\tau \simeq t/(U_\infty^2 h)/(c_v \text{ Ac } RT)^2$, so that if one considers the latent heat of vaporization and the specific heat to be approximately constant, then by substitution in Eq. (31) the lag times can be related in general by the following equation:

$$t_{N2}/t'_{N2}=p'_{air}(T')^{\frac{1}{2}}/p_{air}(T)^{\frac{1}{2}}, \quad (34)$$

or for an accommodation coefficient of 1, from Fig. 6:

$$t_{N2}\simeq 18/p_{air}(T)^{\frac{1}{2}}. \quad (35)$$

TABLE II. Tabulation of significant results.

	Water	Nitrogen
p (atmos)	0.375	0.033
T(°K)	217	40
$\ln p_s/p_\infty$	3.517	5.321
r^* (cm)	4.749×10^{-8}	5.526×10^{-8}
g^*	15	15
Γ	20	20
W	5.591	6.880
D (no./sec)	7.281×10^{6}	8.070×10^{8}
Volmer J_g^* steady state (no./cm³/sec)	6.305×10^{10}	2.688×10^{9}
Present paper J_g^* steady state	$3.261\times10^{4} f_0$	$1.644\times10^{6} f_0$

One can therefore conclude for the water vapor case with low absolute humidities that, other conditions being constant, the lag time would be longer if the humidity is decreased, the initial pressure decreased, or the initial temperature raised. For the expansion of nitrogen in air, however, an increase in the time lag would result from either a lowering of the initial pressure or temperature.

IV. ACKNOWLEDGMENT

The author is deeply indebted to Professor Lester Lees of the Princeton University Aeronautical Engineering Department, without whose supervision and guidance this work would not have been possible.

Miss Carol Knoderer, Assistant in Research, carried out the numerical computations.

APPENDIX. SOLUTION TO SIMPLIFIED BECKER-BÖRING EQUATION

Consider the equation

$$\frac{\partial^2 f}{\partial g^2}-\frac{Bf}{D}-\frac{1}{D}\frac{\partial f}{\partial \tau}=0$$

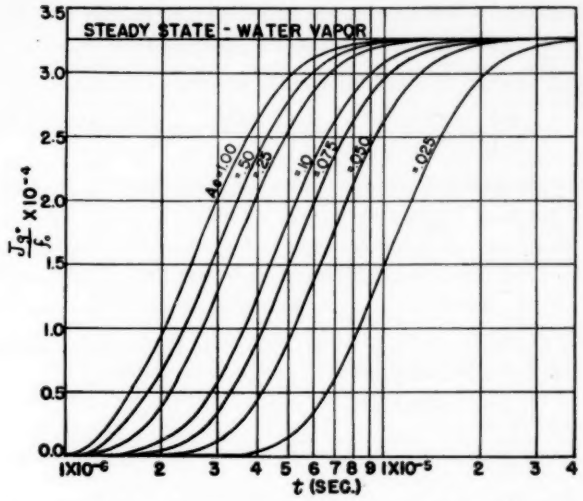

FIG. 5. Effect of accommodation coefficient (Ac) in the nucleation of water vapor on actual time lag (t) for critical values of nucleus formation frequency (J_g^*/f_0).

subject to the boundary and initial conditions specified, respectively, by

$$f(\Gamma, \tau)=0,$$
$$f(0, \tau)=f_0,$$

and

$$f(g, 0)=0, \quad 0<g\leq\Gamma,$$
$$f(0, 0)=f_0.$$

If we now define

$$\bar{f}(p)=\int_0^\infty e^{-p\tau}f(\tau)d\tau,$$

then the laplace transforms of the derivatives will be given by

$$L\{f\}=\bar{f},$$
$$L\{\partial f/\partial\tau\}=pL\{f\}-f(0),$$
$$L\{\partial^2 f/\partial g^2\}=d^2\bar{f}/dg^2.$$

The subsidiary equation can then be written as

$$(d^2\bar{f}/dg^2)-(B+p)/D\bar{f}=0, \quad 0<g<\Gamma,$$

subject to the boundary conditions satisfying the initial transform, which are

$$\bar{f}=f_0/p \quad \text{for} \quad g=0,$$
$$\bar{f}=0 \quad \text{for} \quad g=\Gamma.$$

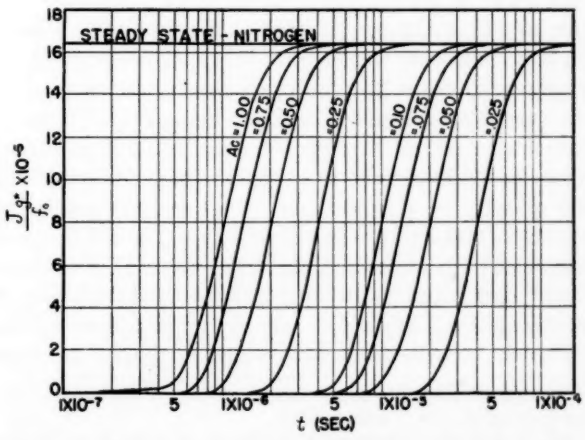

FIG. 6. Effect of accommodation coefficient (Ac) in the nucleation of nitrogen on actual time lag (t) for critical values of nucleus formation frequency (J_g^*/f_0).

The general solution to the last equation is of the form

$$\bar{f}=A\cosh[(B+p)/D]^{\frac{1}{2}}g+C\sinh[(B+p)/D]^{\frac{1}{2}}g,$$

which becomes on substitution of the prescribed conditions

$$\bar{f}=\frac{f_0}{p}\left[\cosh\left(\frac{B+p}{D}\right)^{\frac{1}{2}}g-\operatorname{ctnh}\left(\frac{B+p}{D}\right)^{\frac{1}{2}}\Gamma\sinh\left(\frac{B+p}{D}\right)^{\frac{1}{2}}g\right].$$

From the Mellin inversion theorem one can write

$$f=\frac{f_0}{2\pi i}\int_{c-i\infty}^{c+i\infty}\cosh\left(\frac{B+\lambda}{D}\right)^{\frac{1}{2}}g\,e^{\lambda\tau}\frac{d\lambda}{\lambda}$$
$$-\frac{f_0}{2\pi i}\int_{c-i\infty}^{c+i\infty}\frac{\cosh[(B+\lambda)/D]^{\frac{1}{2}}\Gamma\sinh[(B+\lambda)/D]^{\frac{1}{2}}ge^{\lambda\tau}}{\lambda\sinh[(B+\lambda)/D]^{\frac{1}{2}}\Gamma}d\lambda.$$

The first integral is seen to have only one simple pole at $\lambda=0$, while the second integral has simple poles at $\lambda=0$ and

$$\lambda=-(n^2D\pi^2/\Gamma^2)-B,\quad\text{where}\quad n=1,2,3,\cdots.$$

Evaluation of the residues from the first integral yields

$$\cosh(B/D)^{\frac{1}{2}}g,$$

while from the second integral one has, from the contribution at $\lambda=0$,

$$\operatorname{ctnh}(B/D)^{\frac{1}{2}}\Gamma\sinh(B/D)^{\frac{1}{2}}g,$$

and from $\lambda=-(n^2D\pi^2/\Gamma^2)-B$,

$$2\left\{\sin\frac{n\pi g}{\Gamma}\exp\left(-\left[\frac{n^2D\pi^2}{\Gamma^2}+B\right]\tau\right)\right\}\frac{n\pi}{(n\pi)^2+B\Gamma^2/D}.$$

Now, summing up all the residues and letting $W=(B/D)^{\frac{1}{2}}\Gamma$, $G=g/\Gamma$, and $F=f/f_0$, one has finally, that

$$F=\frac{\sinh W(1-G)}{\sinh W}-2\sum_{n=1}^{\infty}\frac{n\pi}{(n\pi)^2+W^2}$$
$$\times\sin n\pi G\left\{\exp\left(-\left[\frac{(n\pi)^2+W^2}{\Gamma^2}\right]D\tau\right)\right\}.$$

THE JOURNAL OF CHEMICAL PHYSICS VOLUME 19, NUMBER 5 MAY, 1951

Thermodynamic Investigations on Ternary Amalgams

CARL WAGNER
Department of Metallurgy, Massachusetts Institute of Technology, Cambridge, Massachusetts

(Received January 26, 1951)

Under certain conditions, interaction between positively charged metal ions in an alloy may be considered to be of minor importance as compared to interaction between conduction electrons and metal ions. Then it follows that the activity of a solute metal 2 dissolved in metal 1 will be increased by a third component if metals 2 and 3 change the valence electron/atom ratio in the same direction. Conversely, the activity of a solute metal 2 will be decreased by a third component if metals 2 and 3 change the valence electron/atom ratio in opposite directions. Reference is made to the change in the solubility of hydrogen in copper by zinc, tin, aluminum, platinum, and nickel as alloying elements, to the change in the vapor pressure of zinc dissolved in copper by aluminum and nickel, and to the change in the activity of alkali metals dissolved in mercury by thallium.

In addition, an equation is derived with the aid of which one may calculate the change in the activity of metal 2 dissolved in metal 1 due to the addition of a solute metal 3 if the changes in the activity coefficients with composition for the binary systems 1-2 and 1-3 are known and interaction between positively charged metal ions can be disregarded. This relation has been confirmed for the systems Hg-Li-Tl, Hg-Na-Tl, Hg-K-Tl, and Hg-Na-K.

1. INTRODUCTION

HUME-ROTHERY,[1] Raynor,[2] Jones,[3] and others have shown that the electron/atom ratio is a significant factor for the phase diagrams of binary and ternary alloys. In many other thermodynamic investigations, however, the electronic constitution of alloys is disregarded for the following reasons. Firstly, it is not possible to measure thermodynamic quantities of electrically charged particles such as ions and electrons. Secondly, in the limiting case of dilute solutions, the activity of a solute metal is proportional to its concentration regardless of ionization, for the electron concentration is virtually constant because of its relatively high value in the pure solvent metal. Thirdly, it is known that numerous binary liquid alloys exhibit relatively small deviations from ideality, i.e., the amount of the heat of mixing is less than $\frac{1}{2}RT$ per g-atom at a temperature somewhat above the melting point, although according to conventional assumptions the concentration of valence electrons varies considerably with composition, e.g., in the systems Bi-Pb, Bi-Sn, Pb-Tl, Sn-Tl, Pb-Sb, Sn-Sb, and Zn-Sb.

In spite of inherent difficulties, it is desirable to investigate to what extent the thermodynamic functions of an alloy are related to its electronic constitution. Special consequences are derived in the present paper and confirmed by experiments.

2. QUALITATIVE RELATIONS

Sieverts and Krumbhaar[4] have shown that the solubility of hydrogen in liquid copper is decreased considerably by tin and aluminum as alloying elements. Further results for liquid copper-tin alloys have been

[1] W. Hume-Rothery, *The Structure of Metals and Alloys* (The Institute of Metals, London, 1947).
[2] G. V. Raynor, "Progress in the theory of alloys," in *Progress in Metal Physics*, edited by B. Chalmers (Interscience Publishers, Inc., New York, 1949), p. 1.
[3] H. Jones, Proc. Roy. Soc. (London) **A144**, 225 (1934).
[4] A. Sieverts and H. Krumbhaar, Ber. deut. chem. Ges. **43**, 893 (1910).

reported by Bever and Floe.[5] Moreover, Himmler[6] has found that the solubility of hydrogen in solid copper is diminished considerably by addition of zinc. According to Himmler these findings may be interpreted as follows.

Hydrogen dissolves in palladium preponderately in the form of protons and electrons far apart from each other as is indicated by magnetic measurements[7] and by the relatively high value ($\sim\frac{1}{2}$) of the effective charge of hydrogen in transference experiments with a dilute solution of hydrogen in palladium.[8] A similar proof is not available for solutions of hydrogen in other metals. By analogy, however, we may formulate the stoichiometric equation for the dissolution of hydrogen in copper as

$$\tfrac{1}{2}H_2(\text{gas}) = H^+ + e^-. \tag{1}$$

This equation indicates that hydrogen dissolved in copper is at least in part dissociated into protons and electrons, but the "degree of dissociation" remains open to question and is not exactly definable in view of the "atmosphere" of excess electrons surrounding a proton.

The condition of thermodynamic equilibrium reads

$$\tfrac{1}{2}\mu_{H_2} = \mu_{H^+} + \mu_e, \tag{2}$$

where μ_{H_2} is the chemical potential of gaseous molecular hydrogen, μ_{H^+} is the chemical potential of protons dissolved in copper, and μ_e is the chemical potential of the electrons.

For a dilute solution we may write

$$\mu_{H^+} = \mu_{H^+}^0 + RT \ln c, \tag{3}$$

where c is the concentration of protons, i.e., the hydrogen solubility in any suitable units, and $\mu_{H^+}^0$ is the chemical potential of protons extrapolated to unity concentration. Upon combining Eqs. (2) and (3), we have

$$c = \exp[(\tfrac{1}{2}\mu_{H_2} - \mu_{H^+}^0 - \mu_e)/RT]. \tag{4}$$

Metallic copper contains essentially one valence electron per atom.[9] When copper is alloyed with elements having higher valences such as zinc, tin, and aluminum, the concentration of valence electrons per atom becomes greater than unity; and, therefore, the Fermi energy of the electrons and μ_e will increase. This increase may amount to a multiple of RT if the electron concentration is increased by as little as ten percent.

For a given hydrogen pressure corresponding to a constant value of μ_{H_2}, it follows from Eq. (4) that the hydrogen solubility is decreased by alloying elements which increase the chemical potential of the electrons, provided that the change in $\mu_{H^+}^0$ is of minor importance. Interaction between protons and electrons will be similar to the interaction between positively and negatively charged ions in an electrolytic solution. Thus, an increase in μ_e will be accompanied by a decrease in $\mu_{H^+}^0$. Consequently, we cannot conclude from Eq. (4) that an increase of the chemical potential of the electrons results necessarily in a considerable decrease of the hydrogen solubility. If, however, a considerable decrease of the hydrogen solubility is observed, we may ascribe this effect to an increase of the chemical potential of the electrons, which is compensated only in part by a decrease of $\mu_{H^+}^0$.

Likewise, we may interpret the fact that small amounts of nickel and platinum increase considerably the solubility of hydrogen in liquid and solid copper as has been reported by Sieverts and Krumbhaar,[4] Fukusima and Mitui,[10] and Himmler.[6] From magnetic measurements it is known that these elements are dissolved in copper essentially as neutral atoms.[11] Thus, the electron/atom ratio in these alloys is less than unity, and, accordingly, the Fermi energy and μ_e are lower than in pure copper. In view of Eq. (4) we conclude that the increase of the hydrogen solubility in copper by small additions of nickel and platinum is mainly due to the decrease of the chemical potential of the electrons, which is compensated only in part by an increase of $\mu_{H^+}^0$.

According to Opie and Grant,[12] the solubility of hydrogen in liquid aluminum is decreased by addition of copper. This effect cannot be interpreted on the basis of the foregoing working hypotheses and requires further consideration.

The solubility of hydrogen in palladium alloys has been discussed previously on the basis of special assumptions.[13] Further investigations are under way.

Small changes of the hydrogen solubility with alloy composition are not considered in this context, since these may be caused by other reasons than the change in the electron concentration.

The solubility of oxygen and nitrogen in alloys may be discussed in a similar way,[6] but the state of affairs is more complex owing to the large interaction energy between negatively charged oxygen or nitrogen ions and surrounding positively charged metal ions, particularly in the case of interstitial alloys with small interatomic distances.

The foregoing considerations may further be used to interpret solubility and activity changes in ternary alloys. Jellinek and Rosner,[14] Seith and Kraus,[15] Har-

[5] M. B. Bever and C. F. Floe, Trans. Am. Inst. Mining Met. Engrs. **156**, 149 (1944).
[6] W. Himmler, Z. physik. Chem. **195**, 244, 253 (1950).
[7] H. F. Biggs, Phil. Mag. (6) **32**, 131 (1916); A. E. Oxley, Proc. Roy. Soc. (London) **A101**, 264 (1922); J. H. Aharoni and F. Simon, Z. physik. Chem. **B4**, 175 (1929); E. Vogt, Ann. Physik (5) 14, 1 (1931); B. Svensson, Ann. Physik (5) **18**, 299 (1933).
[8] C. Wagner and G. Heller, Z. physik. Chem. **B46**, 242 (1940).
[9] N. F. Mott and H. Jones, *The Theory of the Properties of Metals and Alloys* (The Clarendon Press, Oxford, 1936), p. 315.
[10] M. Fukusima and S. Mitui, Science Repts. Tôhoku Imp. Univ. First Ser., Honda Annivers. Vol., 940 (1936).
[11] See reference 9, pp. 196–198.
[12] W. R. Opie and N. J. Grant, Trans. Am. Inst. Mining Met. Engrs. **188**, 1237 (1950).
[13] C. Wagner, Z. physik. Chem. **193**, 407 (1944).
[14] K. Jellinek and G. A. Rosner, Z. physik. Chem. **A152**, 67 (1931).
[15] W. Seith and W. Kraus, Z. Elektrochem. 44, 98 (1938).

TABLE I. Saturation pressure of zinc p_{Zn} over some alloys at 773°C according to Hargreaves (reference 16).

% Cu	% Zn	% Al	% Ni	p_{Zn} (mm Hg)
90	10	...	...	1.0
85.5	10	4.5	...	2.0
85	15	...	...	1.8
67	15	...	18	1.0

greaves,[16] and Schneider and Schmid[17] have found that the activity of zinc in α-brass increases quasi-exponentially with increasing zinc concentration. Birchenall[18] and Guttman[19] have interpreted these results by assuming that the bond energy between adjacent copper and zinc atoms exceeds the average of the bond energies between alike atoms. An alternative interpretation may be given on the basis of the foregoing considerations. When zinc is introduced into copper, the concentration and thus the chemical potential of the electrons increase. Consequently, if one disregards interaction between metal ions, one expects that the tendency to dissolve zinc decreases with increasing zinc concentration to a larger extent than in an ideal solution. This interpretation is substantiated by zinc vapor pressure measurements on ternary alloys by Hargreaves.[16] (See Table I.) Aluminum contributing three valence electrons increases the saturation pressure of zinc in α-brass, corresponding to a decrease of the solubility of zinc for a given partial pressure of zinc. Conversely, nickel contributing no valence electron decreases the saturation pressure of zinc in brass, corresponding to an increase of the solubility of zinc for a given partial pressure of zinc.

By and large, the activity of a solute metal 2 will be increased by a third component if metals 2 and 3 change the electron/atom ratio in the same direction. Conversely, the activity of a solute metal 2 will be decreased by a third component if metals 2 and 3 change the electron/atom ratio in opposite directions.

Since the electrical conductivity of mercury is relatively low, the effective number of electrons in mercury is considered to be small.[20] Addition of alkali metal to liquid mercury raises the concentration of conduction electrons as is indicated by the increase of the electrical conductivity by addition of sodium, potassium, rubidium, cesium, and barium.[21] (A decrease of the electrical conductivity by lithium and thallium is due to the decrease of the mean free path of the electrons as the preponderating factor.) Consequently, addition of potassium to liquid sodium amalgam is expected to increase the activity of sodium. This is in accordance with experimental data as is shown in Sec. 5. Likewise, addition of thallium to liquid alkali metal amalgams increases the activity of alkali metal as is shown in Sec. 4.

3. QUANTITATIVE RELATIONS

We consider a system consisting of metal 1 as solvent and small amounts of metals 2 and 3 as solutes with the mole fractions x_2 and x_3. Formally, we may write for the chemical potential of a dissolved substance i

$$\mu_i=\mu_i^0+RT\ln x_i+RT\ln\gamma_i, \tag{5}$$

where μ_i^0 is the chemical potential of substance i in its pure state and γ_i is the activity coefficient, which accounts for deviations from ideal behavior.

Moreover, we may resolve the chemical potential μ_i of any constituent i into the sum of the chemical potential of its ions of valence z_i and the product of valence and the chemical potential of the electrons,

$$\mu_i=\mu_{i(\text{ion})}+z_i\mu_e. \tag{6}$$

From Eq. (6) it follows that a change of the chemical potential of the electrons will affect the chemical potential of an electrically neutral component i for two reasons: (1) directly in view of the second term on the right-hand side of Eq. (6), and (2) indirectly by a change of $\mu_{i(\text{ion})}$, corresponding to a stronger or weaker interaction between positively charged metal ions and electrons when μ_e varies.

If there are only positively charged metal ions, we may assume as a limiting case that the aforementioned factors are predominant and direct interaction between metal ions can be disregarded. This assumption corresponds to Brönsted's principle of specific interaction for electrolytes in aqueous solution.[22] According to this principle, specific interaction only between ions of opposite sign of the electrical charge is taken into account, whereas specific interaction between ions of equal sign is disregarded. Consequently, it may be assumed that the term $RT\ln\gamma_i$ in Eq. (5), which accounts for deviations from ideal behavior, is mainly a function of μ_e and is affected by changes in the composition of the alloy only in so far as μ_e varies. Thus,

$$d(RT\ln\gamma_i)\cong 0 \quad \text{if} \quad d\mu_e=0. \tag{7}$$

Practically, it is not possible to vary the electron concentration independently of other changes, since only electrically neutral components can be added or removed. Theoretically, Eq. (7) may be interpreted as follows. The value of $RT\ln\gamma_i$ is not changed if combinations of elements are added in such a ratio that the Fermi energy of the electrons does not change. In the

[16] R. Hargreaves, J. Inst. Metals **64**, 115 (1939).
[17] A. Schneider and W. Schmid, Z. Elektrochem. **48**, 627 (1942).
[18] C. E. Birchenall, Trans. Am. Inst. Mining Met. Engrs. **171**, 166 (1947).
[19] L. Guttman, Trans. Am. Inst. Mining Met. Engrs. **175**, 178 (1948).
[20] See reference 9, p. 279.
[21] G. Borelius, "Grundlagen des metallischen Zustandes. Physikalische Eigenschaften" in *Handbuch der Metallphysik*, edited by G. Masing (Akademische Verlagsgesellschaft, Leipzig, 1935), Vol. 1, Part 1, p. 344.
[22] J. N. Brönsted, J. Am. Chem. Soc. **44**, 877, 938 (1922); **45**, 2898 (1923); E. A. Guggenheim, Phil. Mag. (7) **19**, 588 (1935).

case of copper as solvent, for instance, a combination of zinc and nickel may be taken.

For a ternary system involving two solute metals, 2 and 3, it then follows from Eq. (7) that

$$\partial \ln\gamma_2/\partial x_2 \cong (\partial \ln\gamma_2/\partial \mu_e)(\partial \mu_e/\partial x_2), \quad (8)$$

$$\partial \ln\gamma_2/\partial x_3 \cong (\partial \ln\gamma_2/\partial \mu_e)(\partial \mu_e/\partial x_3), \quad (9)$$

$$\partial \ln\gamma_3/\partial x_2 \cong (\partial \ln\gamma_3/\partial \mu_e)(\partial \mu_e/\partial x_2), \quad (10)$$

$$\partial \ln\gamma_3/\partial x_3 \cong (\partial \ln\gamma_3/\partial \mu_e)(\partial \mu_e/\partial x_3), \quad (11)$$

where the mole fractions x_2 and x_3 of the solute metals 2 and 3 are the independent variables for partial differentiation.

Upon multiplying corresponding sides of Eqs. (9) and (10) and of Eqs. (8) and (11) and comparing the right-hand members, we have

$$(\partial \ln\gamma_2/\partial x_3)(\partial \ln\gamma_3/\partial x_2) \cong (\partial \ln\gamma_2/\partial x_2)(\partial \ln\gamma_3/\partial x_3). \quad (12)$$

From the general equation for the Gibbs free energy F of a system consisting of n_1 moles of component 1, n_2 moles of component 2, and n_3 moles of component 3,

$$F = n_1\mu_1 + n_2\mu_2 + n_3\mu_3, \quad (13)$$

it follows by cross-differentiation that

$$(\partial^2 F/\partial n_2 \partial n_3) = \partial \mu_2/\partial n_3 = \partial \mu_3/\partial n_2, \quad (14)$$

whence in view of Eq. (5)

$$\partial \ln\gamma_2/\partial x_3 = \partial \ln\gamma_3/\partial x_2 \quad \text{for} \quad x_2 \to 0, \quad x_3 \to 0. \quad (15)$$

Substitution of Eq. (15) in Eq. (12) yields

$$\frac{\partial \ln\gamma_2}{\partial x_3} = \frac{\partial \ln\gamma_3}{\partial x_2} \cong \pm\left[\frac{\partial \ln\gamma_2}{\partial x_2}\frac{\partial \ln\gamma_3}{\partial x_3}\right]^{\frac{1}{2}} \quad \text{for} \quad x_2 \to 0, \quad x_3 \to 0. \quad (16)$$

Thus, the mutual effects of the solute metals 2 and 3 on their activity coefficients are related to the deviations of the binary systems 1-2 and 1-3 from ideality. Since the sign of the square root in Eq. (16) can be positive or negative, the sign of the mutual effects is not predicted by Eq. (16), but is given by the qualitative considerations in the foregoing section.

Equation (16) is significant only if the deviations from ideal behavior for the binary systems 1-2 and 1-3 have equal signs, since otherwise the square root in Eq. (16) is imaginary. For a given solvent metal 1, however, it can be shown that the sign of the derivative $\partial \ln\gamma_i/\partial x_i$ for any solute i must have the same sign provided that direct interaction between metal ions can be disregarded. To prove this statement, we consider formally a system consisting of n_1 moles of component 1, n_i moles of component i, and n_e moles of excess electrons. Then, considering n_1, n_i, and n_e as independent variables for partial differentiation, we have

$$\left(\frac{d\mu_i}{d\mu_e}\right)_{n_1,n_i} = \frac{(\partial \mu_i/\partial n_e)_{n_1,n_i}}{(\partial \mu_e/\partial n_e)_{n_1,n_i}}. \quad (17)$$

In analogy to Eq. (14) we have

$$(\partial \mu_e/\partial n_i)_{n_1,n_e} = (\partial \mu_i/\partial n_e)_{n_1,n_i}, \quad (18)$$

and in analogy to Eq. (8) and in view of Eq. (5) we have

$$RT\frac{\partial \ln\gamma_i}{\partial n_i} \cong RT\left(\frac{d \ln\gamma_i}{d\mu_e}\right)_{n_1,n_i}\frac{\partial \mu_e}{\partial n_i} = \left(\frac{d\mu_i}{d\mu_e}\right)_{n_1,n_i}\frac{\partial \mu_e}{\partial n_i}. \quad (19)$$

Substitution of Eqs. (17) and (18) in Eq. (19) yields

$$RT\frac{\partial \ln\gamma_i}{\partial n_i} \cong \frac{[\partial \mu_i/\partial n_e]^2}{\partial \mu_e/\partial n_e}, \quad (20)$$

whence

$$\frac{\partial \ln\gamma_i}{\partial x_i} \cong \frac{n_1}{RT}\frac{[\partial \mu_i/\partial n_e]^2}{\partial \mu_e/\partial n_e} \quad \text{for} \quad x_i \to 0. \quad (21)$$

The numerator on the right as a square is positive and the denominator is characteristic of the solvent metal. Consequently, the derivative on the left of Eq. (21) has the same sign for all solutes in metal 1 as solvent provided that interaction between ions of metal i among each other can be disregarded.

Actually, however, the sign of $\partial \ln\gamma_i/\partial x_i$ for different solutes in a given solvent is not always the same. In mercury as solvent, e.g., $\partial \ln\gamma_i/\partial x_i$ is negative for bismuth,[23] tin,[24] lead,[24] and zinc[25,26] as solutes, but positive for cadmium,[24,26] thallium,[27–29] lithium,[30] sodium,[31,33] and potassium[34–37] as solutes. This shows the limitation of Eqs. (21) and (16) and of the underlying assumption that direct interaction between metal ions can be disregarded.

Since direct interaction between metal ions is in general not equal to zero, the change in the chemical potential of the electrons can be expected to be the

[23] J. H. Hildebrand and E. D. Eastman, J. Am. Chem. Soc. **36**, 2020 (1914).
[24] Hildebrand, Foster, and Beebe, J. Am. Chem. Soc. **42**, 545 (1920).
[25] J. H. Hildebrand, Trans. Electrochem. Soc. **22**, 319 (1913).
[26] J. S. Pedder and S. Barrat, J. Chem. Soc. **1933**, 537 (1933).
[27] J. H. Hildebrand and E. D. Eastman, J. Am. Chem. Soc. **37**, 2452 (1915).
[28] T. W. Richards and F. Daniels, J. Am. Chem. Soc. **41**, 1732 (1919).
[29] G. N. Lewis and M. Randall, J. Am. Chem. Soc. **43**, 233 (1921).
[30] G. Spiegel and H. Ulich, Z. physik. Chem. **A178**, 187 (1937).
[31] H. E. Bent and J. H. Hildebrand, J. Am. Chem. Soc. **49**, 3011 (1927).
[32] H. E. Bent and E. Swift, J. Am. Chem. Soc. **58**, 2216 (1936).
[33] K. Hauffe, Z. Elektrochem. **46**, 348 (1940).
[34] R. W. Millar, J. Am. Chem. Soc. **49**, 3003 (1927).
[35] H. E. Bent and E. S. Gilfillan, J. Am. Chem. Soc. **55**, 3989 (1933).
[36] M. H. Armbruster and J. L. Crenshaw, J. Am. Chem. Soc. **56**, 2525 (1934).
[37] K. Hauffe and A. L. Vierk, Z. Elektrochem. **54**, 383 (1950).

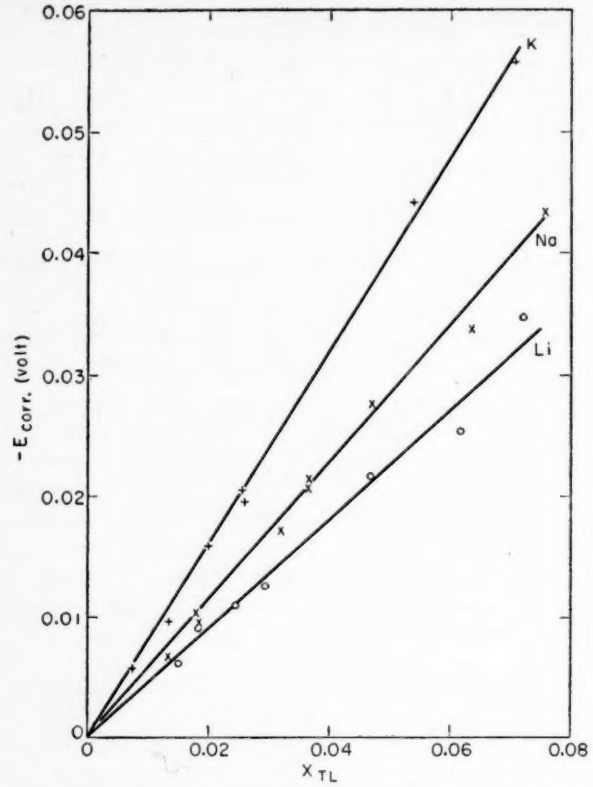

FIG. 1. Electromotive force of galvanic cells: Hg-alkali metal| alkali hydroxide (aq)|Hg-alkali metal-Tl, corrected for equal concentrations of alkali metal on either side.

predominant factor only if deviations from ideality are relatively large. Consequently, even the tentative use of Eq. (16) is to be confined to systems in which the derivatives $\partial \ln\gamma_2/\partial x_2$ and $\partial \ln\gamma_3/\partial x_3$ are considerably greater than unity.

4. EXPERIMENTAL INVESTIGATIONS ON TERNARY AMALGAMS

To check Eq. (16), the change in the activity of lithium, sodium, and potassium upon addition of thallium was determined from the electromotive force of galvanic cells of type

(Hg, alkali metal)|alkali hydroxide (aq)|
(Hg, alkali metal, Tl)

with dropping amalgam electrodes on both sides at about 25°C.

TABLE II. Evaluation of measurements on amalgams (2=Li, Na, K; 3=Tl).

System	$\partial E_{corr}/\partial x_3$, volt	$\partial \ln\gamma_2/\partial x_3$ observed	$\partial \ln\gamma_2/\partial x_3$ calc. from Eq. (15)
Hg/Li/Tl	0.45	17.5	18.7
Hg/Na/Tl	0.57	22.1	21.8
Hg/K/Tl	0.79	30.8	29.6

Amalgams of the alkali metals with about 0.05 atomic percent were prepared electrolytically. One portion was used for the left-hand electrode; another portion was mixed with a small amount of thallium amalgam containing about 35 percent of Tl and was used for the right-hand electrode.

Although the alkali metal concentration on the right is somewhat lower because of the dilution with thallium amalgam, the negative pole was always on the right-hand side, i.e., the amalgam on the right was less noble than that on the left, corresponding to an increase of the activity of alkali metal upon addition of thallium.

Since the concentrations of alkali metal in mercury were sufficiently small, the contribution of the concentration difference to the electromotive force can be calculated from Nernst's formula for amalgam electrodes. Figure 1 shows plots of the electromotive forces corrected for equal concentrations of alkali metal, E_{corr} *versus* the mole fraction of thallium. The values of E_{corr}, and thus the logarithms of the activity coefficients of alkali metal, are practically linear functions of the thallium concentration.

Values of $\partial \ln\gamma_2/\partial x_3$ (2=Li, Na, K; 3=Tl) calculated from the slopes of the lines in Fig. 1 are compiled in Table II and contrasted to values calculated from Eq. (16) with values for the binary systems available from literature:

(a) Hg-Tl[28,29]: $\partial \ln\gamma_{Tl}/\partial x_{Tl}=13.1$;
(b) Hg-Li[30]: $\partial \ln\gamma_{Li}/\partial x_{Li}=26.5$;
(c) Hg-Na[32]: $\partial \ln\gamma_{Na}/\partial x_{Na}=36.0$;
(d) Hg-K[35,36]: $\partial \ln\gamma_{K}/\partial x_{K}=67.0$.

The agreement between observed and calculated values of $\partial \ln\gamma_2/\partial x_3$ in Table II seems satisfactory in view of the approximate nature of Eq. (16) and the limited accuracy of the observed values of $\partial \ln\gamma_2/\partial x_3$, whose root-mean-square errors are 0.5, 0.3, and 0.4 for 2=Li, Na, and K, respectively.

The magnitude of these effects seems particularly important. The values of $\partial\mu_2/\partial x_3=RT\partial \ln\gamma_2/\partial x_3$ are 10,400, 13,200, and 18,300 cal for 2=Li, Na, and K, respectively, i.e., much greater than $RT=600$ cal.

5. EVALUATION OF DATA FOR SODIUM-POTASSIUM AMALGAMS

In addition, Eq. (16) is applied to the ternary system Hg-Na-K. According to Wells and Smith[38] the equilibrium of the exchange reaction

$$Na(\text{in Hg})+K^+(aq)=K(\text{in Hg})+Na^+(aq) \quad (22)$$

depends on the total concentration of alkali metal dissolved in mercury. For a given ratio Na^+/K^+ in the coexisting aqueous solution, the equilibrium condition

[38] L. S. Wells and G. McP. Smith, J. Am. Chem. Soc. **42**, 185 (1920).

for reaction (21) becomes

$$x_K\gamma_K/x_{Na}\gamma_{Na}=\text{constant}. \quad (23)$$

Since $x_{Na}+x_K$ is not higher than 0.012, we assume that the logarithms of the activity coefficients depend linearly on the concentrations of sodium and potassium,

$$\ln\gamma_{Na}=\ln\gamma_{Na}^0+x_{Na}(\partial\ln\gamma_{Na}/\partial x_{Na})+x_K(\partial\ln\gamma_{Na}/\partial x_K), \quad (24)$$

$$\ln\gamma_K=\ln\gamma_K^0+x_K(\partial\ln\gamma_K/\partial x_K)+x_{Na}(\partial\ln\gamma_K/\partial x_{Na}), \quad (25)$$

where γ_{Na}^0 and γ_K^0 are the limiting values of the activity coefficients for $x_{Na}=0$, $x_K=0$ and the derivatives refer to zero concentrations of the solutes.

Upon introduction of Eqs. (24) and (25) into Eq. (23), it follows that

$$\frac{d\ln(x_K/x_{Na})}{d(x_{Na}+x_K)}=\frac{d\ln(\gamma_{Na}/\gamma_K)}{d(x_{Na}+x_K)}=\frac{x_{Na}}{x_{Na}+x_K}\frac{\partial\ln\gamma_{Na}}{\partial x_{Na}}+\frac{x_K}{x_{Na}+x_K}\frac{\partial\ln\gamma_{Na}}{\partial x_K}-\frac{x_K}{x_{Na}+x_K}\frac{\partial\ln\gamma_K}{\partial x_K}-\frac{x_{Na}}{x_{Na}+x_K}\frac{\partial\ln\gamma_K}{\partial x_{Na}}. \quad (26)$$

In view of Eq. (15) we have

$$\partial\ln\gamma_{Na}/\partial x_K=\partial\ln\gamma_K/\partial x_{Na}. \quad (27)$$

Upon substituting Eq. (27) in Eq. (26) and solving for $\ln\gamma_{Na}/\partial x_K$,

$$\frac{\partial\ln\gamma_{Na}}{\partial x_K}=\frac{\partial\ln\gamma_K}{\partial x_{Na}}=\frac{x_{Na}+x_K}{x_{Na}-x_K}\left[\frac{x_{Na}}{x_{Na}+x_K}\frac{\partial\ln\gamma_{Na}}{\partial x_{Na}}-\frac{x_K}{x_{Na}+x_K}\frac{\partial\ln\gamma_K}{\partial x_K}-\frac{d\ln(x_K/x_{Na})}{d(x_{Na}+x_K)}\right]. \quad (28)$$

Using the values observed by Wells and Smith and the values of $\partial\ln\gamma_{Na}/\partial x_{Na}$ and $\partial\ln\gamma_K/\partial x_K$ listed above, we obtain

$$\partial\ln\gamma_{Na}/\partial x_K=\partial\ln\gamma_K/\partial x_{Na}=(1/0.38)\times[0.69\cdot36.0-0.31\cdot67.0-(-14.5)]=46.5, \quad (29)$$

whereas Eq. (16) gives a value of 49.1, which agrees satisfactorily with the experimental value.

Smith and Braley[39] and Smith and Rees[40] have reported an anomalous concentration dependence of "mass action quotients" for the reactions

$$2Na(\text{in Hg})+Sr^{2+}(aq)=Sr(\text{in Hg})+2Na^+(aq), \quad (30)$$

$$2K(\text{in Hg})+Sr^{2+}(aq)=Sr(\text{in Hg})+2K^+(aq). \quad (31)$$

The reported anomaly is due to the fact that Smith and associates expressed the concentrations of alkali metal and strontium as ratios $n_{Na}/(n_{Na}+\frac{1}{2}n_{Sr})$, etc. The observed values conform approximately to the ideal law of mass action if the concentrations in mercury and in water are expressed as mole fractions, or mole/liter; but no further conclusions can be drawn from these data.

6. CONCLUDING REMARKS

As pointed out above, Eq. (16) is not generally valid. Additional measurements are needed in order to explore the validity range of Eq. (16).

Equation (16) is based on the principle that interaction between positively charged metal ions is of minor importance as compared with effects due to a change in the chemical potential of the electrons. Deviations from this principle are indicated if Eq. (16) is found to be substantially invalid. Even if Eq. (16) holds, the validity of this principle is not strictly proven, since other assumptions may give similar relations. At the present, it can be stated only that the aforementioned principle represents a promising working hypothesis.

This work was done as a part of an investigation on the thermodynamics of metallic solutions sponsored by the Atomic Energy Commission under Contract No. AT-30-1-GEN-368.

[39] G. McP. Smith and S. A. Braley, J. Am. Chem. Soc. **39**, 1545 (1917).

[40] G. McP. Smith and E. A. Rees, J. Am. Chem. Soc. **40**, 1802 (1918).

Partition Functions of Cubic Lattices

E. FISHER
Missouri School of Mines, Rolla, Missouri

(Received August 30, 1950)

The Born-von Kármán theory of vibrational specific heats is given an analytical development that is adequate for computation even at low temperatures. Application is made to simple, body-centered, and face-centered cubic lattices.

INTRODUCTION

THE application of Blackman[1] of the Born-von Kármán theory[2] to square and simple cubic lattices, revealing the inaccuracy of the Debye theory,[2] was followed by the work of Fine[3] on the body-centered cubic and of Leighton[4] on the face-centered cubic. These applications were numerical. The only known analytical development, giving by Thirring[5] and elaborated by Montroll,[6] is limited to higher temperatures.

In the present note the analytical development is extended to lower temperatures. The partition function is worked with—rather than a specific heat—since it is the fundamental quantity from the point of view of statistical thermodynamics.[7] The usual assumptions are made: the force between two atoms (nearest or next nearest neighbors) of the lattice is linear in the displacements of the atoms from equilibrium, acts along their line of centers, is dependent of temperature, and is independent of displacements perpendicular to the atoms' line of centers. The first of these conditions fails only at higher temperatures. The second condition, that the elastic constants satisfy the cauchy relation, can be got around by an artifice.[3,4] The third assumption is justified, at present, by the lack of low temperature values of elastic constants; but the data available[8] show a variation of 10 to 20 percent in the range 0°A to room temperature. As for the fourth assumption, by using a Taylor expansion of the lattice potential energy in terms of atomic displacements, it can be shown that this amounts to neglecting $V'(a)/a$ in comparison with $V''(a)$, where V is the potential energy of two atoms, a is their equilibrium separation, and V' and V'' are first and second derivatives. Therefore, if the expressions for V known for ionic crystals[9] are used, this amounts to an initial error of roughly 10 percent. In addition, the best measurements[8] of elastic constants are not in very close agreement. All in all, therefore, computations of specific heats from elastic data cannot be expected to be correct within less than a 10 percent error. On the other hand, since a partition function changes rapidly at low temperatures, accuracy is lost when it is differentiated[7] to obtain specific heats. Therefore, partition functions are derived in this note with an error estimated at a few tenths of 1 percent. Simpler partition functions are also included in case less accuracy is needed—for example, in free-energy[7] calculations.

I. THE SIMPLE CUBIC

From Blackman,[1] the lattice energy is

$$E=N/(8\pi^3)\int_{-\pi}^{\pi}\int_{-\pi}^{\pi}\int_{-\pi}^{\pi}\times\{\sum_{i=1}^{3}h\nu_i[(e^{h\nu_i/kT}-1)^{-1}+1/2]\}d\varphi_1 d\varphi_2 d\varphi_3, \quad (1)$$

where N is the number of atoms, T absolute temperature, and h and k Planck's and Boltzmann's constants. The frequencies ν_i are given[1] in terms of the φ_i, and elastic constants as roots of

$$0=\begin{vmatrix} A(1-c_1)+B(2-c_1c_2-c_1c_3)-r_i^2 & Bs_1s_2 & Bs_1s_3 \\ Bs_1s_2 & A(1-c_2)+B(2-c_2c_3-c_2c_1)-r_i^2 & Bs_2s_3 \\ Bs_1s_3 & Bs_2s_3 & A(1-c_3)+B(2-c_3c_1-c_3c_2)-r_i^2 \end{vmatrix}$$
$$\equiv H-Gr_i^2+Fr_i^4-r_i^6, \quad (2)$$

where

$$r_i=h\nu_i/2kT, \quad c_i\equiv\cos\varphi_i, \quad s_i\equiv\sin\varphi_i,$$
$$A=(\alpha/2m)(h/2\pi kT)^2, \quad B=(\gamma/m)(h/2\pi kT)^2, \quad (3)$$

m is the mass of an atom, and α and 2γ are force constants between nearest and next nearest neighbors,

[1] M. Blackman, Proc. Roy. Soc. (London) **A148**, 384 (1935); **159**, 416 (1937).
[2] F. Seitz, *Modern Theory of Solids* (McGraw-Hill Book Company, Inc., New York, 1940), chapter III.
[3] P. C. Fine, Phys. Rev. **56**, 355 (1939).
[4] R. B. Leighton, Revs. Modern Phys. **20**, 165 (1948).
[5] H. Thirring, Physik. Z. **14**, 867 (1913).
[6] E. W. Montroll, J. Chem. Phys. **10**, 218 (1942); **11**, 481 (1943).
[7] R. W. Gurney, *Introduction to Statistical Mechanics* (McGraw-Hill Book Company, Inc., New York, 1949), chapter V.
[8] R. F. S. Hearmon, Revs. Modern Phys. **18**, 409 (1946).
[9] Reference 2, chapter II.

respectively, in the lattice. From (2) F, G, and H are determined as polynomials in the c_i.

Partition functions, P, are determined[7] from

$$E=NkT^2(d/dT)(\ln P). \tag{4}$$

Therefore,

$$P\propto T^3e^{-D}, \tag{5}$$

where

$$D=(1/\pi^3)\int_0^\pi\int_0^\pi\int_0^\pi J\,d\varphi_1 d\varphi_2 d\varphi_3, \tag{6}$$

and

$$J(\varphi_1,\varphi_2,\varphi_3)=\sum_{i=1}^{3}\ln(\sinh r_i/r_i). \tag{7}$$

Now,[10]

$$\sinh r/r=\prod_{n=1}^{\infty}[1+(r/n\pi)^2]. \tag{8}$$

Therefore,

$$J=\sum_{n=1}^{\infty}I_n(\varphi_1,\varphi_2,\varphi_3), \tag{9}$$

where

$$e^{I_n}=1+F/(n\pi)^2+G/(n\pi)^4+H/(n\pi)^6=\begin{vmatrix} a_n(1-c_1)+b_n(2-c_1c_2-c_1c_3)+1 & b_ns_1s_2 & b_ns_1s_3 \\ b_ns_1s_2 & a_n(1-c_2)+b_n(2-c_2c_3-c_2c_1)+1 & b_ns_2s_3 \\ b_ns_1s_3 & b_ns_2s_3 & a_n(1-c_3)+b_n(2-c_3c_1-c_3c_2)+1 \end{vmatrix}, \tag{10}$$

and

$$a_n=A/(n\pi)^2,\quad b_n=B/(n\pi)^2. \tag{11}$$

For temperatures satisfying

$$2\pi kT>h(\nu_i)_{\max}=k\Theta\ (\text{approx}), \tag{12}$$

where Θ is the Debye characteristic temperature, we can expand (10) in the form

$$I_n=[F/(n\pi)^2+G/(n\pi)^4+H/(n\pi)^6]-(1/2)[\ ]^2+(1/3)[\ ]^3\cdots. \tag{13}$$

Then, substituting for F, G, and H from (2) and carrying out the integration of (6) yields

$$D=A/2+B-(1/90)(9A^2/4+6AB+15B^2/2)+(1/945)(5A^3/2+9A^2B+15AB^2+57B^3/4)+\cdots. \tag{14}$$

Series (14) is no more, of course, than was obtained by Thirring[5,6] for the lattice energy, E.

Even at low temperatures, however, a small integer N can be found such that

$$2\pi(N+1)T>\Theta. \tag{15}$$

Then (13) still holds for $n>N$. Therefore, substituting in (6) as before, we get

$$D=\sum_{n=1}^{N}(1/\pi^3)\int_0^\pi\int_0^\pi\int_0^\pi I_n\,d\varphi_1 d\varphi_2 d\varphi_3+[1/6-\sum_{n=1}^{N}(1/n\pi)^2](3A+6B)$$
$$-[1/90-\sum_{n=1}^{N}(1/n\pi)^4](9A^2/4+6AB+15B^2/2)+[1/945-\sum_{n=1}^{N}(1/n\pi)^6](5A^3/2+9A^2B+15AB^2+57B^3/4)\cdots. \tag{16}$$

Disregarding for the present uncertainty of convergence, assume for the I_n in Eq. (16) a Taylor series in the variables c_i about the point $\varphi_i=\pi/2$. Then

$$(1/\pi^3)\int_0^\pi\int_0^\pi\int_0^\pi I_n\,d\varphi_1 d\varphi_2 d\varphi_3=I_n(\pi/2,\pi/2,\pi/2)+3/4\frac{\partial^2 I_n}{\partial c_1^2}(\pi/2,\pi/2,\pi/2)$$
$$+(3/64)\left(\frac{\partial^4}{\partial c_1^4}+4\frac{\partial^4}{\partial c_1^2\partial c_2^2}\right)I_n(\pi/2,\pi/2,\pi/2)+\text{sixth and higher derivatives}. \tag{17}$$

Substituting (10) in (17) gives

$$(1/\pi^3)\int_0^\pi\int_0^\pi\int_0^\pi I_n\,d\varphi_1 d\varphi_2 d\varphi_3=\ln\{(a_n+b_n+1)^2(a_n+4b_n+1)\}+\left\{\frac{3b_n^2}{(a_n+b_n+1)(a_n+4b_n+1)}\right.$$
$$-(3/4)\left[\frac{a_n(a_n+3b_n+1)}{(a_n+b_n+1)(a_n+4b_n+1)}\right]^2\Bigg\}+(3/4)\left\{\frac{2b_n^3}{(a_n+b_n+1)^2(a_n+4b_n+1)}+\frac{2a_n^3b_n+6a_n^2b_n^2-7b_n^4+2a_n^2b_n}{(a_n+b_n+1)^2(a_n+4b_n+1)^2}\right.$$
$$+\frac{7a_n^2b_n^2(a_n+3b_n+1)^2}{(a_n+b_n+1)^3(a_n+4b_n+1)^3}-(15/8)\left[\frac{a_n(a_n+3b_n+1)}{(a_n+b_n+1)(a_n+4b_n+1)}\right]^4+\frac{2a_n^2(a_n+3b_n+1)^2}{(a_n+b_n+1)^4(a_n+4b_n+1)^3}$$
$$\left.\times(a_n^3-8a_nb_n^2-6b_n^3+a_n^2-4a_nb_n-8b_n^2-2b_n)-\frac{(a_n^3-8a_nb_n^2-6b_n^3+a_n^2-4a_nb_n-8b_n^2-2b_n)^2}{2(a_n+b_n+1)^4(a_n+4b_n+1)^2}\right\}+\text{sixth-order terms}, \tag{18}$$

[10] E. T. Whittaker and G. N. Watson, *Modern Analysis* (Cambridge University Press, 1927), chapter VII.

where { } are used to separate the zeroth-, second-, and fourth-order terms.

A numerical example is instructive. For KCl[1,2]

$$\Theta=227°\text{A}, \quad \gamma/\alpha=0.128. \tag{19}$$

And from (2)

$$2(2A+4B)^{1/2}=(h/kT)\nu_{\max}=\Theta/T \text{ (approx)}. \tag{20}$$

So, the numerical example, $A=4\pi^2$, $B=\pi^2$, approximates to KCl at 10.4°A. From (15) we must take $N\geqslant 3$ in (16).

Then, for $n=1$, (18) gives

$$(1/\pi^3)\int_0^\pi\int_0^\pi\int_0^\pi I_1 d\varphi_1 d\varphi_2 d\varphi_3 = \{5.78\}-\{.21\}-\{.05\}\cdots. \tag{21}$$

The form of series (21) indicates an error $\sim$0.02. And a later calculation gives $D\sim 14$. Hence, the error in D due to (21) is $\sim$1/10 percent. Additional calculation shows: the series (18) converges more rapidly as n increases, or as T increases; in fact, the cumbersome fourth-order term is negligible for $n=3$; and if the fourth-order term is omitted completely, the total resulting error in D is $\sim$1 percent.

Inspection of (10) shows that I_n takes on simple forms for special values of the φ_i—such as $\pi/4$, $\pi/2$, $3\pi/4$, π. This suggests replacing the cumbersome derivatives in (17) and (18) with appropriate sums of these simple I_n's. The most obvious six sums to start with are

$$\begin{aligned}
&I_n(0,\pi/2,\pi/2)+I_n(\pi,\pi/2,\pi/2),\\
&I_n(\pi/4,\pi/2,\pi/2)+I_n(3\pi/4,\pi/2,\pi/2),\\
&I_n(0,0,\pi/2)+I_n(\pi,\pi,\pi/2)+2I_n(0,\pi,\pi/2),\\
&I_n(\pi/4,\pi/4,\pi/2)+I_n(3\pi/4,3\pi/4,\pi/2)\\
&\qquad\qquad +2I_n(\pi/4,3\pi/4,\pi/2),\\
&I_n(0,0,0)+I_n(\pi,\pi,\pi)+3I_n(0,0,\pi)+3I_n(0,\pi,\pi),\\
&I_n(\pi/4,\pi/4,\pi/4)+I_n(3\pi/4,3\pi/4,3\pi/4)\\
&\quad +3I_n(\pi/4,\pi/4,3\pi/4)+3I_n(\pi/4,3\pi/4,3\pi/4),
\end{aligned} \tag{22}$$

because their Taylor series in the c_i about the point, $\varphi_i=\pi/2$, involve only those derivatives that appear in (17).

Comparison of (17) and (22) yields two sums of the I_n's that are close approximations to

$$(1/\pi^3)\int_0^\pi\int_0^\pi\int_0^\pi I_n d\varphi_1 d\varphi_2 d\varphi_3:$$

$$\begin{aligned}
S_{\mathrm{I},n}&=(1/32)I_n(\pi,\pi,\pi)+(3/32)[I_n(0,0,\pi)+I_n(0,\pi,\pi)]+(3/8)[I_n(0,\pi/2,\pi/2)+I_n(\pi,\pi/2,\pi/2)]\\
&=(1/\pi^3)\int_0^\pi\int_0^\pi\int_0^\pi I_n d\varphi_1 d\varphi_2 d\varphi_3+(1/64)\frac{\partial^4}{\partial c_1^4}I_n(\pi/2,\pi/2,\pi/2)+\text{sixth-order terms},\\
S_{\mathrm{II},n}&=(1/8)[I_n(\pi/4,\pi/4,\pi/4)+I_n(3\pi/4,3\pi/4,3\pi/4)]+(3/8)[I_n(\pi/4,\pi/4,3\pi/4)+I_n(\pi/4,3\pi/4,3\pi/4)]\\
&=(1/\pi^3)\int_0^\pi\int_0^\pi\int_0^\pi I_n d\varphi_1 d\varphi_2 d\varphi_3-(1/64)\frac{\partial^4}{\partial c_1^4}I_n(\pi/2,\pi/2,\pi/2)+\text{sixth-order terms}.
\end{aligned} \tag{23}$$

The numerical example, $A=4\pi^2$, $B=\pi^2$, gives $S_{\mathrm{I},1}=5.47$, $S_{\mathrm{II},1}=5.53$, which compare satisfactorily with 5.52 from (21).

When the φ_i have the values appearing in (22) and (23), the factors of the determinants in (10) and (2) involve only square roots. This leads to more compact expressions for $S_{\mathrm{I},n}$ and $S_{\mathrm{II},n}$. For example,

$$\begin{aligned}
e^{S_{\mathrm{I},n}}=&[(1+a_n+b_n)(1+a_n+3b_n)]^{3/4}\\
&\times[(1+2b_n)(1+2a_n+2b_n)]^{9/16}\\
&\times[(1+2a_n)(1+4b_n)(1+2a_n+4b_n)]^{3/32}.
\end{aligned} \tag{24}$$

More important, it leads to simpler partition functions. First, from (6) and (9) we obtain, corresponding to $S_{\mathrm{I},n}$, $S_{\mathrm{II},n}$:

$$\begin{aligned}
D_{\mathrm{I}}=&(1/32)J(\pi,\pi,\pi)\\
&+(3/32)[J(0,0,\pi)+J(0,\pi,\pi)]\\
&+(3/8)[J(0,\pi/2,\pi/2)+J(\pi,\pi/2,\pi/2)]\\
D_{\mathrm{II}}=&(1/8)[J(\pi/4,\pi/4,\pi/4)\\
&+J(3\pi/4,3\pi/4,3\pi/4)]\\
&+(3/8)[J(\pi/4,\pi/4,3\pi/4)\\
&+J(\pi/4,3\pi/4,3\pi/4)].
\end{aligned} \tag{25}$$

A more direct derivation of the approximate D's in (25) would be made difficult by the fact that the determinant of (2) has a branch point at $\varphi_i=\pi/2$, so that

$$(\partial^2/r_i/\partial c_i^2)_{\varphi_i=\pi/2}=\infty. \tag{26}$$

The roots r_i of (2) can be substituted in the J's of (25) according to (7). Then the numerical example (slightly altered), $A=40$, $B=10$, gives $D_{\mathrm{I}}=14.363$ and $D_{\mathrm{II}}=14.426$, so that the error in each is $\sim$2/10 percent.

Finally, from (5) we obtain corresponding partition functions:

$$\begin{aligned}
P_{\mathrm{I}}=&[T\prod_{i=1}^{3}t_i\,\mathrm{csch}(t_i/T)]^{3/32}[\prod_{i=4}^{5}t_i\,\mathrm{csch}(t_i/T)]^{9/16}\\
&\times[\prod_{i=6}^{7}t_i\,\mathrm{csch}(t_i/T)]^{3/4},
\end{aligned}$$

$$t_i^2=2a,\ 4b,\ 2a+4b,\ 2b,\ 2a+2b,\ a+b,\ a+3b,$$

$i=1$ to 7, in order;

$$P_{II}=\prod_{i=1}^{2} t_i \operatorname{csch}(t_i/T)]^{1/8}\prod_{i=3}^{4} t_i \operatorname{csch}(t_i/T)]^{1/4} \times\prod_{i=5}^{10} t_i \operatorname{csch}(t_i/T)]^{3/8},$$

$$t_i^2=a[1\pm(1/2)^{1/2}]+2b,\quad a[1\pm(1/2)^{1/2}]+b/2,\quad a[1\pm(1/2)^{1/2}]+3b/2,\quad a+11b/4\pm[a^2/2+9b^2/16\pm ab/2^{3/2}]^{1/2},$$
$$i=1 \text{ to } 10, \text{ in order}; \quad (27)$$

where $a=AT^2$, $b=BT^2$.

Since the elastic constants are assumed independent of temperature, the t_i's outside the csch's can be dropped from (27). Further simplification is possible for special ranges of b/a and T by using the binomial theorem for the square roots and the series for $\sinh x$ in e^x.

Still more accurate partition functions can be derived from (22). For example,

$$\begin{aligned}S_{III,n}&=(3/14)S_{I,n}+(4/7)S_{II,n}\\&\quad+(3/56)\{2I_n(\pi/4,\pi/2,\pi/2)\\&\quad+2I_n(3\pi/4,\pi/2,\pi/2)\\&\quad-I_n(\pi/4,\pi/4,\pi/2)-I_n(3\pi/4,3\pi/4,\pi/2)\\&\quad-2I_n(\pi/4,\pi/2,3\pi/4)+I_n(0,0,\pi/2)\\&\quad+I_n(\pi,\pi,\pi/2)+2I_n(0,\pi/2,\pi)\}\\&=(1/\pi^3)\int_0^\pi\int_0^\pi\int_0^\pi I_n d\varphi_1 d\varphi_2 d\varphi_3\\&\quad+\text{eighth-order terms.}\end{aligned}\quad (28)$$

From (28), D_{III} and P_{III} can be obtained in the same way as above. And again the determinants can be factored without introducing cube roots.

To return now to (17) and the question of convergence, the above development was based on the assumptions that the I_n in the integrand of (17) can be expanded in a Taylor series, that the series converges well enough to be integrated term by term, and that the resulting series in (17) converges. The last is of most practical interest, and one sufficient condition for it, that is at the same time simple, can be obtained as follows. Write

$$\begin{aligned}I_n(\varphi_1,\varphi_2,\varphi_3)&=\ln|\varphi_1,\varphi_2,\varphi_3|_n\\&=\ln|\pi/2,\pi/2,\pi/2|_n+\ln(1+x)\\&=\ln|\pi/2,\pi/2,\pi/2|_n+x-x^2/2+x^3/3\cdots,\end{aligned}\quad (29)$$

where $|\varphi_1,\varphi_2,\varphi_3|_n$ is the determinant in (10), and

$$x=\{|\varphi_1,\varphi_2,\varphi_3|_n-|\pi/2,\pi/2,\pi/2|_n\}/|\pi/2,\pi/2,\pi/2|_n. \quad (30)$$

From (29),

$$(1/\pi^3)\int_0^\pi\int_0^\pi\int_0^\pi I_n d\varphi_1 d\varphi_2 d\varphi_3=I_n(\pi/2,\pi/2,\pi/2)+\text{descending series in } (a_n+b_n+1) \text{ and } (a_n+4b_n+1). \quad (31)$$

Series (31) is the same as (18) except for rearrangement of terms. Therefore, series (29), (31), and (17) converge absolutely provided $x<1$, that is, the greatest value of $|\varphi_1,\varphi_2,\varphi_3|_n$ in $0\leqslant\varphi_i\leqslant\pi$ does not exceed $2|\pi/2,\pi/2,\pi/2|_n$.

A faulty proof has been given[1] that $|\varphi_1,\varphi_2,\varphi_3|_n$ is greatest at one of the corners of the cell $0\leqslant\varphi_i\leqslant\pi$. However, it can be proved, by analysis too lengthy to reproduce here, that the maximum is at $\varphi_i=\pi$ provided

$$4b_n\leqslant a_n. \quad (32)$$

If (32) is assumed, the convergence condition becomes

$$(2a_n+1)^3\leqslant 2(a_n+b_n+1)^2(a_n+4b_n+1). \quad (33)$$

For KCl, where $a_n=4b_n$, Eqs. (19), (20), and (33) require that $T\geqslant 15.5°$A. Therefore, the series in (17) may not converge absolutely in the numerical example at 10°A, but only conditionally.

A more detailed investigation of the convergence is desirable, but out of place here. In any case, if the above series should diverge for very low temperatures, or large B/A, they can be replaced with convergent series simply by taking the Taylor expansions about another point than $\varphi_i=\pi/2$, for which I_n is larger—such as $\varphi_i=\pi$—and then proceeding as above. Only the resulting formulas would be more complicated.

II. THE BODY-CENTERED CUBIC

The work of Montroll and Peaslee[11] is taken as a starting point. The frequencies ν_i and the polynomials F, G, and H are determined by

$$0=\begin{vmatrix}A(1\mp c_1c_2c_3)+Bs_1^2-r_i^2 & \pm As_1s_2c_3 & \pm As_1c_2s_3\\ \pm As_1s_2c_3 & A(1\mp c_1c_2c_3)+Bs_2^2-r_i^2 & \pm Ac_1s_2s_3\\ \pm As_1c_2s_3 & \pm Ac_1s_2s_3 & A(1\mp c_1c_2c_3)+Bs_3^2-r_i^2\end{vmatrix}$$
$$=H_\pm-G_\pm r_i^2+F_\pm r_i^4-r_i^6, \quad (34)$$

[11] E. W. Montroll and D. Peaslee, J. Chem. Phys. **12**, 98 (1944).

where

$$r_i=(h\nu_i/2kT),\quad c_i\equiv\cos\varphi_i,\quad s_i\equiv\sin\varphi_i,$$
$$A=(2\beta/M)(h/2\pi kT)^2,\quad B=(\delta/M)(h/2\pi kT)^2, \quad (35)$$

where β and δ are related to the force constants between nearest and next nearest neighbors, respectively, in the lattice, M is the mass of an atom, and[11] $-\pi\leqslant\varphi_i\leqslant\pi$.

Replacing any φ_i with $\varphi_i\pm\pi$, according to whether $\varphi_i\gtrless 0$, merely interchanges the $\pm$ signs in (34). Therefore, we need consider only one of the two determinants of (34), and choose the upper sign. Then, formulas (5) to (7) of part I apply here unchanged, except that the r_i in (7) now come from (34).

Similarly, by changing from the determinant of (2) to that of (34), the Eqs. (8) to (16) can be carried over. This gives in place of (10)

$$e^{I_n}=1+F/(n\pi)^2+G/(n\pi)^4+H/(n\pi)^6$$
$$=\begin{vmatrix} a_n(1-c_1c_2c_3)+b_ns_1^2+1 & a_ns_1s_2c_3 & a_ns_1c_2s_3 \\ a_ns_1s_2c_3 & a_n(1-c_1c_2c_3)+b_ns_2^2+1 & a_nc_1s_2s_3 \\ a_ns_1c_2s_3 & a_nc_1s_2s_3 & a_n(1-c_1c_2c_3)+b_ns_3^2+1 \end{vmatrix}, \quad (36)$$

and in place of (16),

$$D=\sum_{n=1}^{N}(1/\pi^3)\int_0^\pi\int_0^\pi\int_0^\pi I_n d\varphi_1 d\varphi_2 d\varphi_3$$
$$+[1/6-\sum_{n=1}^{N}(1/n\pi)^2](3A+3B/2)$$
$$-[1/90-\sum_{n=1}^{N}(1/n\pi)^4](33A^2/16+3AB/2+9B^2/16)$$
$$+[1/945-\sum_{n=1}^{N}(1/n\pi)^6](17A^3/8+69A^2B/32$$
$$+9AB^2/8+5B^3/16). \quad (37)$$

If I_n is expanded about the point $\varphi_i=\pi/2$ as in part I, then the rest of the development for the simple cubic can be used for the body-centered cubic by replacing the determinants of (2) and (10) with those of (34) and (36), respectively.

Formula (28) was the best approximation given in part I. Substituting in it for the I_n's from (36) and factoring the determinants, we get

$$(1/\pi^3)\int_0^\pi\int_0^\pi\int_0^\pi I_n d\varphi_1 d\varphi_2 d\varphi_3+\text{eighth-order terms}$$
$$=S_{\mathrm{III},n}=(2/7)\ln\{[1+a_n(1+2^{-3/2})+b_n/2]$$
$$\times[1+a_n(1-2^{-3/2})+b_n/2]\}$$
$$+(4/7)\ln\{[1+a_n(1+2^{-1/2})+b_n/2]$$
$$\times[1+a_n(1-2^{-1/2})+b_n/2]\}+(9/112)\ln(1+2a_n)$$
$$+(9/56)\ln[(1+b_n)(1+2a_n+b_n)]$$
$$+(33/56)\ln(1+a_n)$$
$$+(3/14)\ln\{[1+a_n(1+2^{-1/2})+b_n]$$
$$\times[1+a_n(1-2^{-1/2})+b_n](1+a_n+b_n)\}$$
$$-(3/14)\ln\{[1+a_n+3b_n/4+(a_n^2/2+b_n^2/16)^{1/2}]$$
$$\times[1+a_n+3b_n/4-(a_n^2/2+b_n^2/16)^{1/2}]\}. \quad (38)$$

According to (7), (34), and (36), the corresponding approximation, D_{III}, is derived from (38) by replacing $1+a_n(1+2^{-3/2})+b_n/2$ with

$$\sinh\{[A(1+2^{-3/2})+B/2]^{1/2}\}/[A(1+2^{-3/2})+B/2]^{1/2},$$

and similarly for the rest of the factors in (38).

And from (5) a corresponding partition function is (neglecting temperature dependence of elastic constants)

$$P_{\mathrm{III}}=[T\,\mathrm{csch}(t_1/T)]^{9/112}$$
$$\times[\prod_{i=2}^{3}\mathrm{csch}(t_i/T)]^{9/56}[\mathrm{csch}(t_4/T)]^{33/56}$$
$$\times[\prod_{i=5}^{7}\mathrm{csch}(t_i/T)\prod_{i=8}^{9}\sinh(t_i/T)]^{3/14}$$
$$\times[\prod_{i=10}^{11}\mathrm{csch}(t_i/T)]^{2/7}[\prod_{i=12}^{13}\mathrm{csch}(t_i/T)]^{4/7}, \quad (39)$$

where, for $i=1$ to 13, in order,

$$t_i^2=2a,\ b,\ 2a+b,\ a,\ a+b,\ a(1\pm 2^{-1/2})+b,$$
$$a+3b/4\pm(a^2/2+b^2/16)^{1/2},$$
$$a(1\pm 2^{-3/2})+b/2,\ a(1\pm 2^{-1/2})+b/2,$$

and $a=AT^2$, $b=BT^2$ as in Part I.

An alternative development consists in using the symmetry of the determinants in (34) to obtain

$$D=(4/\pi^3)\int_0^{\pi/2}\int_0^{\pi/2}\int_0^{\pi/2}\sum_{i=1}^{3}\ln[(\sinh r_{i+}/r_{i+})$$
$$\times(\sinh r_{i-}/r_{i-})]d\varphi_1 d\varphi_2 d\varphi_3, \quad (40)$$

and

$$(1/\pi^3)\int_0^\pi\int_0^\pi\int_0^\pi I_n d\varphi_1 d\varphi_2 d\varphi_3$$
$$=(4/\pi^3)\int_0^{\pi/2}\int_0^{\pi/2}\int_0^{\pi/2}(I_{n+}+I_{n-})d\varphi_1 d\varphi_2 d\varphi_3, \quad (41)$$

where $r_{i\pm}$ denote roots of the two equations (34), I_{n+} comes from (36) directly, corresponding to the upper sign in (34), and I_{n-} comes from (36) with all the c_i's and s_i's changed in sign, corresponding to the lower sign in (34).

Assuming convergence, substitute for the $I_{n\pm}$ Taylor series in the variables φ_i about the point $\varphi_i=\pi/4$. Then, by (41)

$$(1/\pi^3)\int_0^\pi\int_0^\pi\int_0^\pi I_n d\varphi_1 d\varphi_2 d\varphi_3$$
$$=(1/2)I_{n+}(\pi/4,\pi/4,\pi/4)$$
$$+(\pi/8)^2\frac{\partial^2}{\partial\varphi_1{}^2}I_{n+}(\pi/4,\pi/4,\pi/4)$$
$$+(\pi/8)^4\left[(1/5)\frac{\partial^4}{\partial\varphi_1{}^4}+(2/3)\frac{\partial^4}{\partial\varphi_1{}^2\partial\varphi_2{}^2}\right]$$
$$\times I_{n+}(\pi/4,\pi/4,\pi/4)+\cdots$$
$$+\text{same series in } I_{n-}. \quad (42)$$

In the same way as was done in Part I, the derivatives in (42) can be replaced with appropriate sums of simple $I_{n\pm}$'s, starting from six expressions corresponding to (22):

$$I_{n+}(0,\pi/4,\pi/4)+I_{n+}(\pi/2,\pi/4,\pi/4)$$
$$+\text{same expression in } I_{n-},$$
$$I_{n+}(\pi/8,\pi/4,\pi/4)+I_{n+}(3\pi/8,\pi/4,\pi/4)$$
$$+\text{same expression in } I_{n-}, \text{ etc.} \quad (43)$$

By comparing the expansions of the expressions in (43) about $\varphi_i=\pi/4$ with (42), two approximations to

$$(1/\pi^3)\int_0^\pi\int_0^\pi\int_0^\pi I_n d\varphi_1 d\varphi_2 d\varphi_3$$

are obtained:

$$S_{\mathrm{I},n}=(1/4)[I_{n+}(0,\pi/4,\pi/4)+I_{n+}(\pi/2,\pi/4,\pi/4)]$$
$$+\text{same expression in } I_{n-};$$
$$S_{\mathrm{II},n}=(1/3)[I_{n+}(0,\pi/4,\pi/4)+I_{n+}(\pi/2,\pi/4,\pi/4)]$$
$$-(1/6)I_{n+}(0,\pi/4,\pi/2)$$
$$-(1/12)[I_{n+}(0,0,\pi/4)+I_{n+}(\pi/2,\pi/2,\pi/4)]$$
$$+(1/16)[I_{n+}(0,0,\pi/2)+I_{n+}(0,\pi/2,\pi/2)]$$
$$+(1/48)[I_{n+}(0,0,0)+I_{n+}(\pi/2,\pi/2,\pi/2)]$$
$$+\text{same expression in } I_{n-}. \quad (44)$$

$S_{\mathrm{II},n}$ is a closer approximation than $S_{\mathrm{I},n}$; but both are inaccurate in respect to fourth-order derivatives.

Substituting in (44) from (36), and factoring the determinants, yields

$$S_{\mathrm{I},n}=\ln(1+a_n+b_n/2)+(1/4)\ln[(1+a_n/2)$$
$$\times(1+b_n/2)(1+3a_n/2)(1+2a_n+b_n/2)]$$
$$+(1/2)\ln\{[1+a_n+3b_n/4+(a_n{}^2/2+b_n{}^2/16)^{1/2}]$$
$$\times[1+a_n+3b_n/4-(a_n{}^2/2+b_n{}^2/16)^{1/2}]\};$$

$$S_{\mathrm{II},n}=(1/3)\ln\{[1+a_n+3b_n/4+(a_n{}^2/2+b_n{}^2/16)^{1/2}]$$
$$\times[1+a_n+3b_n/4-(a_n{}^2/2+b_n{}^2/16)^{1/2}]\}$$
$$+(1/3)\ln[(1+a_n/2)(1+b_n/2)(1+3a_n/2)$$
$$\times(1+2a_n+b_n/2)]+(1/24)\ln(1+a_n)$$
$$+(1/16)\ln(1+2a_n)+(1/4)\ln(1+a_n+b_n)$$
$$+(7/6)\ln(1+a_n+b_n/2)$$
$$-(1/12)\ln\{[1+a_n(1+2^{-1/2})+b_n/2]$$
$$\times[1+a_n(1-2^{-1/2})+b_n/2]\}$$
$$+(1/8)\ln[(1+b_n)(1+2a_n+b_n)]$$
$$-(1/6)\ln\{[1+a_n(1+2^{-1/2})+b_n]$$
$$\times[1+a_n(1-2^{-1/2})+b_n][1+a_n(1+2^{-1/2})]$$
$$\times[1+a_n(1-2^{-1/2})]\}. \quad (45)$$

Corresponding approximations D_{I} and D_{II} are derived from (45) in the same way as D_{III} was from (38). And corresponding partition functions, from (5), are

$$P_{\mathrm{I}}=\operatorname{csch}(t_1/T)\Big[\prod_{i=2}^{5}\operatorname{csch}(t_i/T)\Big]^{1/4}\Big[\prod_{i=6}^{7}\operatorname{csch}(t_i/T)\Big]^{1/2},$$

where, for $i=1$ to 7, in order,

$$t_i{}^2=a+b/2,\ a/2,\ b/2,\ 3a/2,\ 2a+b/2,$$
$$a+3b/4\pm(a^2/2+b^2/16)^{1/2};$$

and

$$P_{\mathrm{II}}=[\operatorname{csch}(t_1/T)]^{1/24}[T\operatorname{csch}(t_2/T)]^{1/16}$$
$$\times\Big[\prod_{i=3}^{4}\operatorname{csch}(t_i/T)\Big]^{1/8}[\operatorname{csch}(t_5/T)]^{1/4}$$
$$\times\Big[\prod_{i=6}^{11}\operatorname{csch}(t_i/T)\Big]^{1/3}[\operatorname{csch}(t_{12}/T)]^{7/6}$$
$$\times\Big[\prod_{i=13}^{14}\sinh(t_i/T)\Big]^{1/12}\Big[\prod_{i=15}^{18}\sinh(t_i/T)\Big]^{1/6},$$

where, for $i=1$ to 18, in order,

$$t_i{}^2=a,\ 2a,\ b,\ 2a+b,\ a+b,\ a/2,\ b/2,\ 3a/2,\ 2a+b/2,$$
$$a+3b/4\pm(a^2/2+b^2/16)^{1/2},\ a+b/2,$$
$$a(1\pm2^{-1/2})+b/2,\ a(1\pm2^{-1/2}),\ a(1\pm2^{-1/2})+b. \quad (46)$$

For an example we take data from Fine[3] on tungsten, to get $A=B$, and $a=AT^2=9230$. Therefore, the numerical example, $A=9\pi^2=B$, corresponds to tungsten at 10.2°A. Then, substituting $a_1=9=b_1$ in (38) and (45) yields

$$S_{\mathrm{I},1}=7.71,\quad S_{\mathrm{II},1}=7.67,\quad S_{\mathrm{III},1}=7.64. \quad (47)$$

The accuracy indicated here is a little less than has been desired. Better approximations than (38) and (45)

could be obtained by the above methods but would be more complicated. It might be better, instead, to take the Taylor expansion about another point than $\varphi_i=\pi/2$ or $\varphi_i=\pi/4$. It is believed that the numerical example tests very severely the convergence of the series used in the above development. They may even diverge in this example. But if so, the agreement in (47) indicates they still possess semiconvergence in the sense that asymptotic series do.

III. THE FACE-CENTERED CUBIC

Partition functions are again derived from (5), where now

$$D=(1/\pi^3)\int_{-\pi/2}^{\pi/2}\int_{-\pi/2}^{\pi/2}\int_{-\pi/2}^{\pi/2} J\,d\varphi_1 d\varphi_2 d\varphi_3. \quad (48)$$

In (48), J is still given by (7). From the work of Leighton,[4] the frequencies ν_i and polynomials F, G, and H are determined by

$$0=\begin{vmatrix} A(2-c_xc_y-c_xc_z)+Bs_x^2-r_i^2 & As_xs_y & As_xs_z \\ As_xs_y & A(2-c_yc_z-c_yc_x)+Bs_y^2-r_i^2 & As_ys_z \\ As_xs_z & As_ys_z & A(2-c_zc_x-c_zc_y)+Bs_z^2-r_i^2 \end{vmatrix}$$
$$=H-Gr_i^2+Fr_i^4-r_i^6, \quad (49)$$

where

$$r_i=h\nu_i/2kT, \quad A=(\alpha/2m)(h/2\pi kT)^2, \quad B=(\gamma/m)(h/2\pi kT)^2,$$
$$c_x\equiv\cos x, \quad s_x\equiv\sin x, \quad \text{etc.}, \quad (50)$$

m is the mass of an atom, α and γ are force constants between nearest and next nearest lattice neighbors, respectively, and

$$x=-\varphi_1+\varphi_2+\varphi_3, \quad y=\varphi_1-\varphi_2+\varphi_3, \quad z=\varphi_1+\varphi_2-\varphi_3. \quad (51)$$

The first part of the present development follows that of part I. Equations (9), (11), and (13) are carried over unchanged. In place of (10), there follows from (48)

$$e^{I_n}=1+F/(n\pi)^2+G/(n\pi)^4+H/(n\pi)^6$$
$$=\begin{vmatrix} a_n(2-c_xc_y-c_xc_z)+b_ns_x^2+1 & a_ns_xs_y & a_ns_xs_z \\ a_ns_xs_y & a_n(2-c_yc_z-c_yc_x)+b_ns_y^2+1 & a_ns_ys_z \\ a_ns_xs_z & a_ns_ys_z & a_n(2-c_zc_x-c_zc_y)+b_ns_z^2+1 \end{vmatrix}. \quad (52)$$

From the symmetry of (49), Eq. (48) can be written

$$D=(2/\pi^3)\int_0^{\pi/2}\int_0^{\pi/2}\int_0^{\pi/2} J\,d\varphi_1 d\varphi_2 d\varphi_3$$
$$+(6/\pi^3)\int_{-\pi/2}^{0}\int_0^{\pi/2}\int_0^{\pi/2} J\,d\varphi_1 d\varphi_2 d\varphi_3. \quad (53)$$

Then, corresponding to (16), we derive from (53), (49), and (13)

$$D=\sum_{n=1}^{N}\left[(2/\pi^3)\int_0^{\pi/2}\int_0^{\pi/2}\int_0^{\pi/2} I_n\,d\varphi_1 d\varphi_2 d\varphi_3 \right.$$
$$\left.+(6/\pi^3)\int_{-\pi/2}^{0}\int_0^{\pi/2}\int_0^{\pi/2} I_n\,d\varphi_1 d\varphi_2 d\varphi_3\right]$$
$$+[1/6-\sum_{n=1}^{N}(1/n\pi)^2](6A+3B/2)$$
$$-[1/90-\sum_{n=1}^{N}(1/n\pi)^4](15A^2/2+3AB+9B^2/16)$$
$$+[1/945-\sum_{n=1}^{N}(1/n\pi)^6](51A^3/4+111A^2B/16$$
$$+9AB^2/4+5B^3/16)\cdots. \quad (54)$$

The rest is patterned after the second development of Part II. We assume for the first and second I_n in (54) Taylor series in φ_i about the point $\varphi_i=\pi/4$ and the point $(-\pi/4, \pi/4, \pi/4)$, respectively. Then, analogous to (42),

$$(2/\pi^3)\int_0^{\pi/2}\int_0^{\pi/2}\int_0^{\pi/2} I_n\,d\varphi_1 d\varphi_2 d\varphi_3$$
$$+(6/\pi^3)\int_{-\pi/2}^{0}\int_0^{\pi/2}\int_0^{\pi/2} I_n\,d\varphi_1 d\varphi_2 d\varphi_3$$
$$=\left\{1/4+(1/2)(\pi/8)^2\frac{\partial^2}{\partial\varphi_1^2}+(\pi/8)^4\left[(1/10)\frac{\partial^4}{\partial\varphi_1^4}\right.\right.$$
$$\left.\left.+(1/3)\frac{\partial^4}{\partial\varphi_1^2\partial\varphi_2^2}\right]+\cdots\right\}I_n(\pi/4, \pi/4, \pi/4)$$
$$+\left\{3/4+(\pi/8)^2\left[(1/2)\frac{\partial^2}{\partial\varphi_1^2}+\frac{\partial^2}{\partial\varphi_2^2}\right]\right.$$
$$+(\pi/8)^4\left[(1/10)\frac{\partial^4}{\partial\varphi_1^4}+(1/5)\frac{\partial^4}{\partial\varphi_2^4}\right.$$
$$\left.\left.+(2/3)\frac{\partial^4}{\partial\varphi_1^2\partial\varphi_2^2}+(1/3)\frac{\partial^4}{\partial\varphi_2^2\partial\varphi_3^2}\right]+\cdots\right\}$$
$$\times I_n(-\pi/4, \pi/4, \pi/4). \quad (55)$$

The derivatives in (55) can be replaced with appropriate sums of I_n's in the usual way, starting from expressions corresponding to (22) and (43):

$$[I_n(0,\pi/4,\pi/4)+I_n(\pi/2,\pi/4,\pi/4)]+[I_n(-\pi/2,\pi/4,\pi/4)+I_n(0,\pi/4,\pi/4)+2I_n(-\pi/4,0,\pi/4)+2I_n(-\pi/4,\pi/2,\pi/4)],\quad\text{etc.}\quad(56)$$

The determinants in some of these I_n's cannot be factored without resort to cube roots. Although this would cause no great difficulty in a numerical application, they are avoided here.

In this way two approximations are obtained for

$$(2/\pi^3)\int_0^{\pi/2}\int_0^{\pi/2}\int_0^{\pi/2} I_n d\varphi_1 d\varphi_2 d\varphi_3 + (6/\pi^3)\int_{-\pi/2}^{0}\int_0^{\pi/2}\int_0^{\pi/2} I_n d\varphi_1 d\varphi_2 d\varphi_3$$

that are inaccurate in fourth-order terms, analogous to (44):

$$S_{\mathrm{I},n}=(1/4)[I_n(0,0,\pi/2)+2I_n(0,\pi/2,\pi/2)+I_n(0,\pi/2,\pi)],$$

$$S_{\mathrm{II},n}=(1/3)[I_n(0,0,\pi/2)+2I_n(0,\pi/2,\pi/2)+I_n(0,\pi/2,\pi)]+(1/8)I_n(0,0,\pi)+(1/6)[I_n(\pi/2,\pi/2,\pi/2)-I_n(\pi/4,\pi/4,\pi/4)]-(1/2)I_n(\pi/4,\pi/4,3\pi/4),\quad(57)$$

where the arguments of the I_n's are now x, y, and z.

From (57) and (52), with the determinants factored

$$S_{\mathrm{I},n}=(1/2)\ln[(1+a_n)(1+2a_n)(1+3a_n)\times(1+a_n+b_n)(1+2a_n+b_n)(1+3a_n+b_n)],$$

$$S_{\mathrm{II},n}=(2/3)\ln[(1+a_n)(1+3a_n)(1+2a_n+b_n)\times(1+3a_n+b_n)]+(1/8)\ln(1+4a_n)+(11/12)\ln(1+2a_n)+\ln(1+a_n+b_n)+(1/6)\ln(1+4a_n+b_n)-(1/2)\ln\{[1+(3a_n+b_n)/2]\times[1+(7a_n+b_n)/2]\}-(1/3)\ln[1+(a_n+b_n)/2]-(2/3)\ln(1+2a_n+b_n/2).\quad(58)$$

The approximations D_{I} and D_{II} that correspond to the $S_{\mathrm{I},n}$ and $S_{\mathrm{II},n}$ in (58) are derived in the same way as in part II.

And from (5), the corresponding partition functions are

$$P_{\mathrm{I}}=[\prod_{i=1}^{6}\operatorname{csch}(t_i/T)]^{1/2},$$

where, for $i=1$ to 6, in order,

$$t_i^2=a,\ 2a,\ 3a,\ a+b,\ 2a+b,\ 3a+b;$$

and

$$P_{\mathrm{II}}=[T\operatorname{csch}(t_1/T)]^{1/8}[\operatorname{csch}(t_2/T)]^{1/6}\times[\prod_{i=3}^{6}\operatorname{csch}(t_i/T)]^{2/3}[\operatorname{csch}(t_7/T)]^{11/12}\times[\operatorname{csch}(t_8/T)][\sinh(t_9/T)]^{1/3}\times[\prod_{i=10}^{11}\sinh(t_i/T)]^{1/2}[\sinh(t_{12}/T)]^{2/3},$$

where, for $i=1$ to 12, in order,

$$t_i^2=4a,\ 4a+b,\ a,\ 3a,\ 2a+b,\ 3a+b,\ 2a,\ a+b,\ (a+b)/2,\ (3a+b)/2,\ (7a+b)/2,\ 2a+b/2.\quad(59)$$

From Leighton,[4] $B/A=-0.16$ and $a=AT^2=3470$ for silver, and $B/A=0.50$ and $a=7630$ for aluminum. Therefore, the numerical examples

$$A=3\pi^2=-6B,\quad A=7\pi^2=2B\quad(60)$$

correspond to silver approximately at 10.8°A and to aluminum at 10.5°A, respectively. Substituting (60) in (58) gives

$$S_{\mathrm{I},1}=5.51,\ S_{\mathrm{II},1}=5.40,\ S_{\mathrm{I},1}=8.24,\ S_{\mathrm{II},1}=8.04,\quad(61)$$

for silver and aluminum, respectively.

It is seen in (61) that (58) and (59) do not have the desired accuracy. Returning, therefore, to (56), we derive an approximation that is correct through fourth-order terms:

$$S_{\mathrm{III},n}=(1/15)\{4I_n(\pi/4,\pi/4,\pi/4)-2I_n(\pi/2,\pi/2,\pi/2)+2I_n(\pi/4,\pi/4,\pi/2)+I_n(0,\pi/4,\pi/4)+4I_n(0,\pi/4,\pi/2)+2I_n(\pi/4,\pi/2,3\pi/4)+2I_n(0,\pi/4,3\pi/4)+4I_n(0,\pi/2,3\pi/4)+I_n(0,3\pi/4,3\pi/4)\}+(4/5)I_n(\pi/4,\pi/4,3\pi/4)-(13/60)\{I_n(0,0,\pi/2)+2I_n(0,\pi/2,\pi/2)+I_n(0,\pi/2,\pi)\}-(1/10)I_n(0,0,\pi)-(1/30)I_n(0,0,0).\quad(62)$$

From (62) there follows in the usual way a corresponding partition function:

$$P_{\mathrm{III}}=T^{-1/10}[\prod_{i=1}^{4}\sinh(t_i/T)]^{13/30}[\sinh(t_5/T)]^{1/2}\times[\sinh(t_6/T)]^{7/10}[\sinh(t_7/T)]^{1/10}\times[\sinh(t_8/T)]^{2/15}[\prod_{i=9}^{14}\operatorname{csch}(t_i/T)]^{1/15}\times[\prod_{i=15}^{21}\operatorname{csch}(t_i/T)]^{2/15}[\prod_{i=22}^{27}\operatorname{csch}(t_i/T)]^{4/15}\times[\operatorname{csch}(t_{28}/T)]^{8/15}[\prod_{i=29}^{30}\operatorname{csch}(t_i/T)]^{4/5}\times[\operatorname{csch}(t_{31}/T)]^{6/5};$$

where, for $i=1$ to 23, in order,

$$t_i^2 = a,\ 2a+b,\ 3a+b,\ 3a,\ 2a,\ a+b,\ 4a,\ 4a+b,$$
$$(2\pm 2^{1/2})a,\ (1\pm 2^{-1/2})a+b/2,\ (2\pm 2^{-1/2})a+b/2,$$
$$a+b/2,\ (5\pm 3^{1/2})a/2+b/2,$$
$$2a+3b/4\pm(a^2+b^2/16)^{1/2},$$
$$5a/2+3b/4\pm(5a^2/4-ab/4+b^2/16)^{1/2},\ (2\pm 2^{-1/2})a;$$

for $i=28$ to 31, in order,

$$t_i^2=(a+b)/2,\ (3a+b)/2,\ (7a+b)/2,\ 2a+b/2;$$

and, for $i=24$ to 27,

$$t_i^2=(2\pm 2^{-3/2})a+3b/4\pm(10a^2\mp 2^{3/2}ab+b^2)^{1/2}/4, \quad (63)$$

the second $\pm$ sign being independent of the first and third.

Substituting (60) in (62) gives $S_{\mathrm{III},1}=5.46$ for Ag and 8.30 for Al.

CONCLUSION

Although the partition functions obtained in this note are accurate to within a few tenths of a percent down to temperatures much below those where previous analysis applied, they do seem to fail at very low temperatures. Now, they were derived so as to be reasonably simple; thus, Taylor series were taken about such points as $\varphi_1=\pi/2$ in order to eliminate odd derivatives. For temperatures below 10° to 15°A, it might be better to expand about a point located less symmetrically, but so as to ensure convergence, and then to simplify the resulting complicated formulas with such asymptotic approximations as $\sinh x \sim e^x/2$.

THE JOURNAL OF CHEMICAL PHYSICS VOLUME 19, NUMBER 5 MAY, 1951

Diffusivity of Water Vapor in Some Common Gases

F. A. SCHWERTZ AND JEANNE E. BROW
Mellon Institute, Pittsburgh, Pennsylvania*
(Received July 21, 1950)

From the measured rates of diffusion of water vapor into pure hydrogen, helium, methane, ethylene, nitrogen, oxygen, and carbon dioxide, the mutual coefficients of diffusion have been determined. Measurements were made at 34°, 56°, and 80°C and at atmospheric pressure employing the technique of Stefan.

INTRODUCTION

THE rate of evaporation of water into the atmosphere was first used by Stefan[1] to determine the mutual coefficient of diffusion of water vapor and air. A similar method was used in the work described here to measure the mutual coefficients of diffusion of water vapor with respect to pure hydrogen, helium, methane, ethylene, nitrogen, oxygen, and carbon dioxide.

In Sec. I of this paper, the theory of the method is presented in a more complete way than that given by Stefan. In Sec. II, the diffusion apparatus and experimental procedure are described. In Sec. III, the experimental values of the diffusion coefficients are set forth in tabular and graphical form and compared with the predictions of simple kinetic theory.

I. THEORY OF METHOD

It is convenient to discuss the theory of the method with reference to Fig. 1. This figure represents a *diffusion tube* partially filled with water. It is assumed to be immersed in an isothermal atmosphere of a test gas which is moving at a rate sufficiently large to maintain a negligible concentration of vapor at the open end of the tube. Since the concentration of vapor at the surface of the liquid corresponds to the saturation vapor pressure, the vapor diffuses up and out of the tube. This action effects a slow but steady lowering of the liquid level, the rate of lowering being simply related to the coefficient of diffusion.

The current density, $\mathbf{i}_1$, of the vapor at any point, P, in the gas-vapor phase is given by

$$\mathbf{i}_1=c_1\mathbf{v}-D\,\mathrm{grad}c_1, \quad (1)$$

where c_1 is the vapor particle density, $\mathbf{v}$ the convective velocity in the gas-vapor phase, and D the mutual coefficient of diffusion of gas and vapor. The first term on the right-hand side of Eq. (1) takes into account the transfer of vapor by the mass flow resulting from the steady lowering of the liquid level; the second term describes the transfer of vapor by diffusion in the usual way. Similarly, the current density of the gas is given by

$$\mathbf{i}_2=c_2\mathbf{v}-D\,\mathrm{grad}c_2. \quad (2)$$

For an experiment conducted at constant total pressure, the total particle density, c, is constant; that is,

$$c=c_1+c_2. \quad (3)$$

Consequently, the total current density, $\mathbf{i}$, obtained by the addition of Eqs. (1) and (2), is

$$\mathbf{i}=\mathbf{i}_1+\mathbf{i}_2=c\mathbf{v}. \quad (4)$$

The equation of continuity requires that

$$\mathrm{div}\mathbf{i}_1=-\partial c_1/\partial t, \quad (5)$$

* Industrial Fellowship on Coke-Plant Physical Technology sustained by Koppers Company, Inc., Pittsburgh, Pennsylvania.
[1] J. Stefan, Ann. Physik 41, 725 (1890).

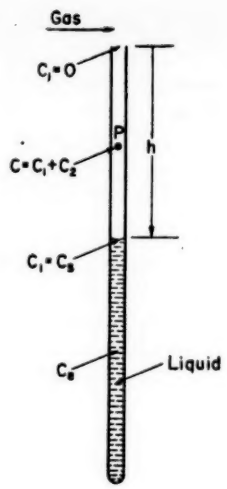

FIG. 1. Diffusion tube.

and, hence, Eq. (1) may be written in the form,

$$-\partial c_1/\partial t=\operatorname{div}(c_1\mathbf{v})-D\nabla^2 c_1. \tag{6}$$

Furthermore, since the concentration, c_1, depends only on the vertical coordinate, Eq. (6) may be simplified to

$$D\frac{\partial^2 c_1}{\partial x^2}-v\frac{\partial c_1}{\partial x}-\frac{\partial c_1}{\partial t}=0. \tag{7}$$

The velocity v is simply the rate of displacement of the gas-vapor column brought about by the evaporation of the liquid, and its value may, therefore, be obtained from the behavior of the liquid surface. If this surface moves downward an amount dh in the time dt, a number of vapor molecules equal to $c_e dh$ is formed per unit of surface area (c_e designates the liquid density). Of this number a part equal to $c_s dh$ remain behind (c_s designates the saturation vapor density), and only $(c_e-c_s)dh$ move *upward* across the surface at $x=h$. Hence,

$$\mathbf{i}_1=-(c_e-c_s)(d\mathbf{h}/dt), \tag{8}$$

where $\mathbf{h}$ is measured positively downward. Also, gas molecules must pass downward across the surface at $x=h$ at such a rate that the total particle density is increased to the number c. Hence,

$$\mathbf{i}_2=(c-c_s)(d\mathbf{h}/dt). \tag{9}$$

Summing Eqs. (8) and (9) and employing the information of Eq. (4) gives

$$c\mathbf{v}=(c-c_e)(d\mathbf{h}/dt). \tag{10}$$

The quantity $(d\mathbf{h}/dt)$ is, of course, not known, but, from dimensional arguments, it must be related to the diffusion coefficient by the expression

$$dh/dt=\alpha(D/t)^{\frac{1}{2}}, \tag{11}$$

where α is a constant of proportionality. If, for mathematical convenience, the restriction $h=0$ when $t=0$ is employed,

$$h=2\alpha(Dt)^{\frac{1}{2}}. \tag{12}$$

The theoretical problem, therefore, reduces to one of determining the value of α, and this may be done with the aid of the fundamental partial differential Eq. (7). For this purpose the substitution

$$v=-\alpha\beta(D/t)^{\frac{1}{2}} \tag{13}$$

is made, where

$$\beta=[(c_e/c)-1]. \tag{14}$$

There results

$$D\frac{\partial^2 c_1}{\partial x^2}+\alpha\beta(D/t)^{\frac{1}{2}}\frac{\partial c_1}{\partial x}-\frac{\partial c_1}{\partial t}=0. \tag{15}$$

If now it is ventured that c_1 may depend on the variables x and t and the parameter D only in the following dimensionless combination,

$$z=x/2(Dt)^{\frac{1}{2}}, \tag{16}$$

then it indeed follows from Eq. (15) that c_1 must satisfy the ordinary differential equation

$$(d^2c_1/dz^2)+(2\alpha\beta+2z)(dc_1/dz)=0, \tag{17}$$

and it is found that a solution to this latter equation can be obtained to satisfy all the boundary conditions. Two *boundary conditions* are required for the evaluation of the constants of integration of Eq. (17), and a third one permits the evaluation of α. The boundary conditions are

(a) $\quad c_1=0 \quad$ at $\quad x=0,$

(b) $\quad c_1=c_s \quad$ at $\quad x=h,$

(c) $\quad D(\partial c_1/\partial x)=c_e[1-(c_s/c)][dh/dt] \quad$ at $\quad x=h.$

The third condition is not obvious, but it may be obtained from Eq. (1) with the aid of Eqs. (8) and (10).

Equation (17) integrates immediately to

$$\ln(dc_1/dz)=-(2\alpha\beta z+z^2)+\ln A, \tag{18}$$

where A is a constant. The second integration cannot be effected in a closed form, and the solution for c_1 must, therefore, be written as

$$c_1=A\int_0^z \exp(-2\alpha\beta z-z^2)dz \tag{19}$$

since this expression satisfies boundary condition (a). Boundary condition (b) requires that

$$c_s=A\int_0^\alpha \exp(-2\alpha\beta z-z^2)dz, \tag{20}$$

since, from Eqs. (12) and (16), $z=\alpha$ at $x=h$. Furthermore, the use of boundary condition (c) in Eq. (19) leads to

$$2\alpha c_e[1-(c_s/c)]=A\exp(-2\alpha^2\beta-\alpha^2). \tag{21}$$

Eliminating the constant A between Eqs. (20) and (21)

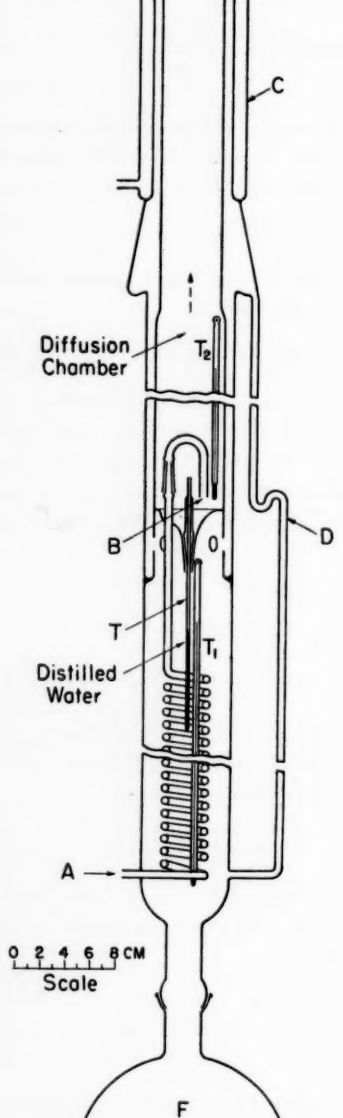

FIG. 2. Diffusion apparatus.

finally yields for α the equation,

$$\alpha \exp(2\alpha^2\beta+\alpha^2)\int_0^\alpha \exp(-2\alpha\beta z-z^2)dz = c_s/2c_e[1-(c_s/c)]. \quad (22)$$

This expression can be simplified by making use of the fact that $\beta \gg \alpha$ and $\beta \gg z$, since $\beta=[(c_s/c)-1]$ is a very large number compared to α, and z ranges from 0 to α. Equation (22) therefore reduces to

$$\alpha \exp(2\alpha^2\beta)\int_0^\alpha \exp(-2\alpha\beta z)dz = c_s/2c_e[1-(c_s/c)]. \quad (23)$$

After carrying out the indicated integration, it is found that

$$2\alpha^2 = c/(c_e-c)]\ln[c(c_e-c_s)/c_e(c-c_s)]. \quad (24)$$

Since $c_e \gg c > c_s$, this expression can be simplified to

$$2\alpha^2 = (c/c_e)\ln[c/(c-c_s)] \quad (25)$$

with very good approximation. Employing Eq. (12) gives

$$D = \frac{h^2 c_e}{2tc\ln[c/(c-c_s)]}. \quad (26)$$

Assuming that the gas and vapor behave as ideal gases,

$$c/c_s = P/P_s, \quad (27)$$

where P is the experimental pressure, and P_s the saturation vapor pressure at the experimental temperature. Equation (26) therefore becomes

$$D = \frac{h^2 c_e P_s}{2tc_s P\ln[P/(P-P_s)]}. \quad (28)$$

Finally, use is made of the fact that the magnitude of the diffusion coefficient is inversely proportional to the pressure:

$$D_0/D = P/P_0, \quad (29)$$

where D_0 is the diffusion coefficient at atmospheric pressure, P_0, and of the fact that the liquid and vapor densities are proportional to the particle densities:

$$c_e/c_s = d_e/d_s, \quad (30)$$

where d_e and d_s are the density of water and the saturated vapor, respectively, at the experimental temperature. Accordingly,

$$D_0 = \frac{h^2 d_e P_s}{2td_s P_0\ln[P/(P-P_s)]}. \quad (31)$$

If observations are made on h at times t_1 and t_2, it may be shown that it must also be true that

$$D_0 = \frac{(h_2^2-h_1^2)d_e P_s}{2(t_2-t_1)d_s P_0\ln[P/(P-P_s)]}, \quad (32)$$

where h_1 and h_2 are the values of h at t_1 and t_2, respectively. The equation for the diffusion coefficient, in this form, was used in calculating all the values of D_0 reported in this paper.

II. DIFFUSION APPARATUS AND EXPERIMENTAL PROCEDURE

The all glass diffusion apparatus is represented approximately to scale in Fig. 2. The *diffusion tube*, *T*, was about 19 cm long, had an internal diameter of 0.170 cm, and a wall thickness of 0.072 cm. It was ordinarily filled with distilled water to within 8 or 9 cm of its open end. The test gas was introduced at A, passed through a heating coil, and emptied into the diffusion chamber at B. The gas, the water, and the diffusion chamber were all maintained at a constant temperature by the condensation of vapor generated in the flask, F. This vapor was refluxed at the condenser, C, and returned to the flask via the delivery tube, D. The temperature was measured on a Bureau of Standards certified thermometer, T_1, having a minimum scale division of 0.2°C. In addition, a calibrated thermometer, T_2, was hung in the diffusion chamber, and, at the gas flow rate employed, namely 200 cm³/min, the difference between the indicated temperatures rarely exceeded a few tenths of a degree.

Observations were made on the water level in the *diffusion tube* every hour or two with the aid of a cathetometer which could be read with an accuracy of 0.005 cm. However, the first observation was made only after the diffusion equipment had been in operation at the experimental temperature for at least a half-hour. When the liquid level was determined, the temperature indications on thermometers T_1 and T_2 and the barometric pressure were also recorded. To obviate any errors which would result from a shift in the location of the *diffusion tube*, the position of its open end was checked at the beginning and end of each experiment.

There were three potential sources of error which had to be examined before systematic data were collected.

1. It was assumed that the flow rate of the test gas was not of critical importance, and, to check this assumption, the mutual coefficient of diffusion of water vapor and hydrogen was determined at 80°C and atmospheric pressure for a series of flow rates ranging from 50 to approximately 300 cm³/min. The results are summarized in Table I.

The absolute values of D_0 in this table are not important since the determinations were made before certain refinements in the diffusion apparatus were effected. They do show, however, that there is no systematic variation of D_0 with the test gas flow rate.

For one experiment the gooseneck shown at B was replaced by an adapter which blew a horizontal stream of hydrogen directly across the lip of the *diffusion tube*. The flow rate was 200 cm³/min and the temperature 80°C. In this case the diffusion coefficient was 1.19 cm²/sec, again showing that the flow conditions at the end of the tube were not critical.

2. Le Blanc and Wuppermann[2] demonstrated that certain values of *D* reported by Winkelmann[3] were too small because of the effect of supercooling at the vapor-liquid interface. This effect takes place when the liquid level is brought too near the top of the *diffusion tube*, and the vapor is carried off by diffusion faster than it can be produced by the heat conducted through the tube. In the present experiments this difficulty was obviated by keeping the liquid level at least 8 cm below the open end of the diffusion tube at all times. Actual measurements were made with the aid of a copper constantan thermocouple of the temperature above, below, and in the surface of the liquid when water was diffusing into hydrogen at 79°C. The liquid level was 10 cm below the open end of the *diffusion tube*. Although temperature differences of 0.03°C could be determined, no temperature differences were detected.

3. The position of the liquid level was determined with the aid of a heavily mounted and solidly supported cathetometer by sighting through the wall of the glass diffusion apparatus. To check the adequacy of this procedure, observations were made on an accurately calibrated, Pyrex glass scale which was mounted inside the diffusion apparatus in the environment of the heating vapors. Observations were made on the fiduciary marks at centimeter intervals over a distance of five centimeters. The distance between these marks was found to be one centimeter within the limits of accuracy of the cathetometer (0.005 cm). From these data, it was assumed that no errors would arise from inhomogeneities in the thickness of the enclosing wall or the presence of the condensed heating vapors.

The distilled water employed in the experiments was degassed by boiling immediately before the beginning of each experiment. Nevertheless, an occasional experiment had to be discontinued because of the formation of bubbles in the *diffusion tube*.

Approximately constant experimental temperatures at 34°, 55°, and 79.5°C were obtained by refluxing ether, acetone, and benzene, respectively, in the diffusion apparatus. Secular changes in the temperature of a few tenths of a degree occurred during the experiments because of slight changes in atmospheric pressure.

Bottled commercial gases were used in all of the experiments. The suppliers' analyses indicated that the hydrogen, nitrogen, and oxygen were 99.5+ percent pure. The carbon dioxide contained only trace impuri-

TABLE I. Mutual coefficient of diffusion[a] of water vapor and hydrogen at various gas flow rates.

Gas flow rate (cm³/min)	$D_0(H_2, H_2O)$ (cm²/sec)
50	1.12
77	1.28
100	1.17
220	1.19
256	1.13
291	1.18

[a] At 80°C and 760 mm Hg pressure.

[2] M. Le Blanc and G. Wuppermann, Z. physik. Chem. **91**, 143 (1916).

[3] A. Winkelmann, Wied. Ann. **22**, 152 (1884); **36**, 93 (1889).

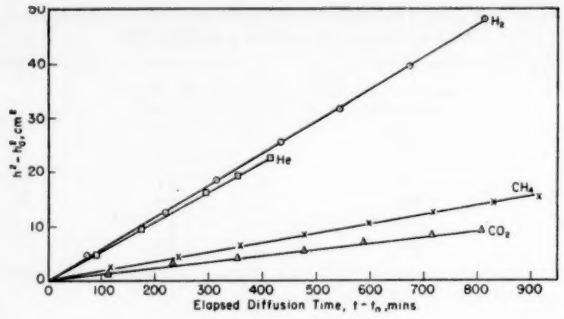

FIG. 3. Locus of liquid level.

ties. The helium was 99.8 percent pure, the impurity being principally nitrogen. The methane was 99 percent pure, and contained 0.5 percent ethane and 0.3 percent nitrogen. No estimate of the purity of the ethylene was available.

III. EXPERIMENTAL RESULTS

As mentioned above, observations were made on the liquid level, the barometric pressure, and the experimental temperature at intervals of an hour or two. The average values of the barometric pressure and the temperature were used in making the calculations. The observations on the liquid level were employed by plotting the quantity $(h^2-h_0^2)$ as ordinate against the elapsed diffusion time $(t-t_0)$ as abscissa. Here h is the distance of the liquid level below the open end of the diffusion tube at any time t_1, and h_0 is the corresponding quantity at the time the experiment was begun, that is, at t_0. According to Eq. (32) such a plot should yield a straight line. Lines of this type are depicted in Fig. 3 for the diffusion of water vapor into hydrogen, helium, methane, and carbon dioxide at atmospheric pressure and approximately 80°C. The slopes of these lines correspond to the quantity $(h_2^2-h_1^2)/(t_2-t_1)$ in Eq. (32). The values of d_e, d_s, and P_s were obtained from standard references from a knowledge of the average experimental temperature, and P from the average barometric pressure. The mutual coefficients of diffusion, D_0, were then calculated. The values obtained are set forth in Table II.

The kinetic theory of gases affords a means of investigating the internal consistency of the experimental values of the diffusion coefficients. According to this theory,[4]

$$D=\frac{3}{2(2\pi)^{\frac{1}{2}}}\frac{(kT)^{\frac{1}{2}}}{P}\left(\frac{1}{\sigma_1+\sigma_2}\right)^2\left(\frac{1}{m_1}+\frac{1}{m_2}\right)^{\frac{1}{2}} \qquad (33)$$

for rigid elastic spheres of diameters σ_1, σ_2 and molecular weights m_1, m_2 (k is Boltzmann's constant). Hence, plotting

$$D \text{ vs } \left(\frac{1}{\sigma_1+\sigma_2}\right)^2\left(\frac{1}{m_1}+\frac{1}{m_2}\right)^{\frac{1}{2}}$$

[4] S. Chapman and T. G. Cowling, *The Mathematical Theory of Non-Uniform Gases* (Macmillan Company, New York, 1939).

TABLE II. Mutual coefficients of diffusion of water vapor and some common gases (760 mm Hg).

System	Average temperature (°C)	Diffusion coefficient (cm²/sec)	Mean value (cm²/sec)
H_2-H_2O	79.5	1.197	
		1.187	
		1.215	1.200
	55.4	1.133	
		1.121	
		1.108	1.121
	34.1	1.032	
		1.026	
		1.002	1.020
$He-H_2O$	79.3	1.135	
		1.111	
		1.118	1.121
	55.3	0.979	
		1.004	
		1.050	1.011
	34.0	0.926	
		0.891	
		0.888	0.902
CH_4-H_2O	79.1	0.362	
		0.357	
		0.350	0.356
	55.6	0.331	—
	34.5	0.292	—
$C_2H_4-H_2O$	79.4	0.251	
		0.245	
		0.246	0.247
	55.3	0.234	
		0.232	0.233
	34.6	0.204	—
N_2-H_2O	79.0	0.358	
		0.366	
		0.353	0.359
	55.4	0.312	
		0.302	
		0.294	0.303
	34.4	0.264	
		0.249	0.256
O_2-H_2O	79.2	0.351	
		0.354	0.352
	55.8	0.314	
		0.316	
		0.323	0.318
	34.9	0.282	—
CO_2-H_2O	79.2	0.249	
		0.244	
		0.241	0.245
	55.4	0.211	—
	34.3	0.202	—

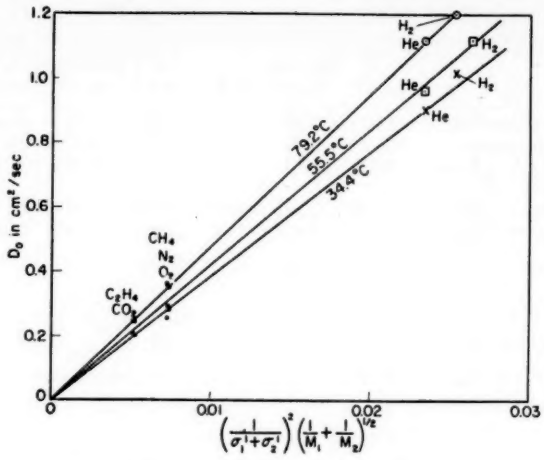

FIG. 4. Correlation of diffusion coefficients.

should yield a straight line for values of D obtained at constant temperature and pressure. Such a procedure has been used in constructing Fig. 4. The diameter $\sigma_1=2.7$A for the water molecule was calculated using the rule that the molecular diameter in Angstrom units is numerically equal to the cube root of the molecular volume of the liquid at the boiling point.[5] Values of σ_2 were obtained for the gases from viscosity data.[4] In plotting Fig. 4 the molecular diameters (σ^1) in Angstrom units were employed, and the *gram* molecular weights (M) instead of the molecular weights (m). The data are seen to produce straight lines for the experiments carried out at 34.4°C and 79.2°C. The correlation for the experiments carried out at 55.5°C was equally good, but the values of D obtained for the heavier gases at this temperature were not represented on Fig. 4 because of the clustering of the experimental points.

TABLE III.

Temperature (°C)	Experimental slope	Calculated slope (Eq. (33))
34.4	38.5	40.3
55.5	42.1	44.5
79.2	47.4	49.8

According to Eq. (33),

$$D\Big/\left[\frac{1}{\sigma_1+\sigma_2}\right]^2\left[\frac{1}{m_1}+\frac{1}{m_2}\right]^{\frac{1}{2}} \propto T^{\frac{3}{2}}.$$

Hence, the slopes of the lines on Fig. 4 should be proportional to three-halves power of the temperature. To check this point, the logarithms of the slopes were plotted against the logarithms of the corresponding temperatures on Fig. 5. The slope of the resulting line, namely 1.54, gives the exponential dependence of the diffusion coefficient on the temperature, a result in good agreement with the theoretically predicted value of $\frac{3}{2}$.

In Table III the slopes of the lines appearing on Fig. 4 are compared with values calculated by means of Eq. (33).

The experimentally determined diffusion coefficients are therefore, on the average, a few percent lower than

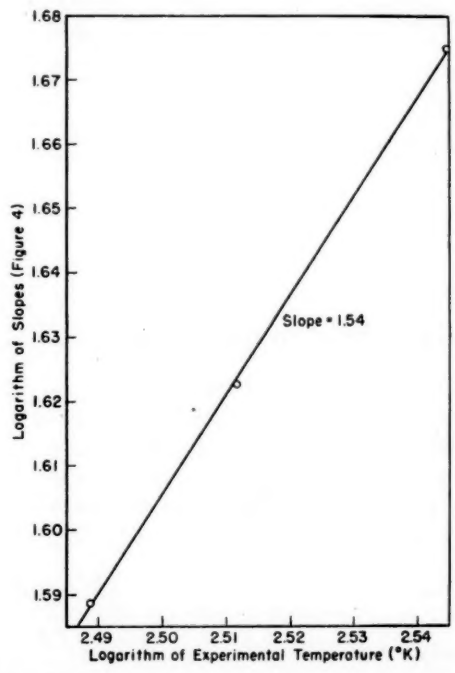

FIG. 5. Temperature dependence of diffusion coefficients.

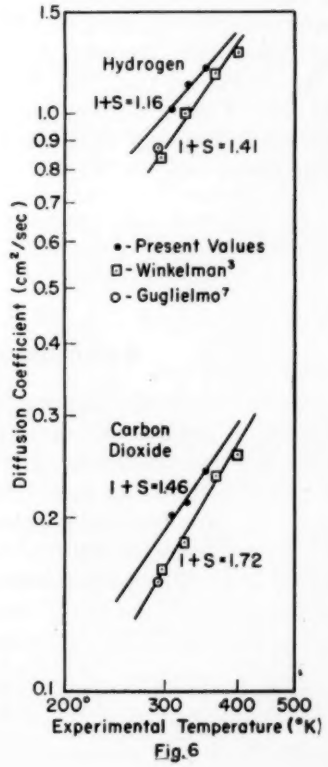

FIG. 6. Experimental diffusion coefficients.

[5] J. H. Arnold, Ind. Eng. Chem. **22**, 1091 (1930).

TABLE IV. Temperature dependence of D^0.

System	m
H_2-H_2O	1.16
$He-H_2O$	1.47
CH_4-H_2O	1.31
$C_2H_4-H_2O$	1.08
N_2-H_2O	2.04
O_2-H_2O	1.47
CO_2-H_2O	1.46
Average	1.43

those theoretically predicted on the assumption that the interacting molecules are rigid, elastic spheres.

The theoretical variation of D with temperature depends on the special molecular model employed. For unlike molecules repelling each other with a force varying inversely as the nth power of the distance,[4]

$$D \propto T^{s+1},$$

where

$$s=(\tfrac{1}{2})+2/(n-1).$$

For rigid elastic spheres, $n=\infty$ and $(s+1)=\frac{3}{2}$. However for ordinary gases s should lie between $\frac{1}{2}$ and 1. To check this prediction, the values of D have been plotted logarithmically against the logarithms of the corresponding experimental temperatures. In Fig. 6 the values for H_2-H_2O and CO_2-H_2O systems have been represented. Values of $1+s=1.16$ and 1.46 were obtained for the H_2-H_2O and CO_2-H_2O systems, respectively. Similar plots for the other gases gave the values listed in Table IV. An inspection of the table shows that the experimentally determined values of $1+s$ lie below 1.5 by appreciable amounts for the systems H_2-H_2O, CH_4-H_2O, and $C_2H_4-H_2O$. Whether these deviations are real or are a consequence of experimental error is difficult to say since small errors in D produce relatively large errors in $1+s$.

TABLE V. Comparative values of D^0.

	H_2-H_2O			CO_2-H_2O		
	34.4°C	55.5°C	79.2°C	34.4°C	55.5°C	79.2°C
Present work	1.02	1.12	1.20	0.202	0.211	0.241
Winkelmann	0.91	0.99	1.10	0.174	0.192	0.215
Elastic spheres, Eq. (29)	1.02	1.13	1.26	0.210	0.232	0.260
Arnold (calc)	0.792	0.895	1.02	0.160	0.183	0.212
Gilliland (calc)	0.827	0.911	1.01	0.189	0.208	0.231

The coefficients of diffusion for only two of the seven gas-vapor systems listed in Table II have been previously reported in the literature. Winkelmann[3] and also Guglielmo[6] published values for the H_2-H_2O and CO_2-H_2O systems. Their results are compared graphically with those of the present paper on Fig. 6. The values obtained in the present work lie roughly 10 percent above the values obtained by Winkelmann and Guglielmo. The explanation for this fact is probably the same as that already adduced by Le Blanc and Wuppermann[2] (see Sec. II) with respect to the work of Winkelmann, namely that the latter's experiments were carried out under conditions conducive to supercooling at the vapor-liquid interface, thus yielding low values of D_0.

In Table V values of D_0 interpolated from the data of Winkelmann are compared with those of the present work as well as with values of D_0 calculated according to the semi-empirical methods of Arnold[5] and Gilliland.[7]

The values for the diffusion coefficients obtained in the present work are seen to be uniformly larger than those reported by Winkelmann and those calculated by the methods of Arnold and Gilliland but are only a few percent smaller than the values predicted on the assumption that the interacting molecules behave as elastic spheres.

[6] Guglielmo, Atti Tor. **17**, 54 (1881); **18**, 93 (1882).
[7] E. R. Gilliland, Ind. Eng. Chem. **26**, 681 (1934).

Announcement: Publication Charge for Letters to the Editor

At the meeting of the Publication Board of the American Institute of Physics on January 30, 1951, a proposed publication charge for Letters to the Editor (and similar sections) was approved. The charge will be effective with the July issues and will be at a flat rate of $10.00 for each Letter. As in the case of regular articles, the charge will be made against the institution rather than the individual author and will be on a voluntary basis. When honored, 100 reprints will be provided without further cost.

The Journals affected are the following:

Physical Review
Journal of the Acoustical Society
Review of Scientific Instruments (Laboratory and Shop Notes)
Journal of Chemical Physics
Journal of Applied Physics

Transformation of Water from Covalent to Electrovalent Combination in Formic Acid-Water Mixtures

TAI-YUAN YANG
Department of Physics, Hangchow University, Hangchow, China
(Received April 26, 1949)

It was shown by the author [J. Chem. Phys. **16**, 865 (1948)] that water was necessarily a covalent compound, the molecule of which is formed by the neutralization of $2H^{+1}+2\theta+O^{+2}$; and its specific susceptibility, as we know, was -0.72 (corresponding to the molecular susceptibility -12.96) and that if it were an electrovalent compound its molecule should be formed by the neutralization of $2H^{+1}+O^{-2}$, and its specific susceptibility would have been -0.625 (corresponding to the molecular susceptibility -11.25). (Susceptibility values have been multiplied by 10^6.)

In the present paper, we shall show that, in formic acid-water mixtures, part of the water depending on the weight of formic acid in the mixtures changes its specific susceptibility from -0.72 to -0.625. This indicates that this part of the water in the process of mixing transforms from a covalent to an electrovalent combination.

1. INTRODUCTION

IT has been shown by different workers that the susceptibility of a binary mixture of liquids generally could not be expressed by the additivity law,

$$\chi_{add}=(1-w_2)\chi_1+w_2\chi_2, \tag{1}$$

where χ_1 and χ_2 are, respectively, the specific susceptibilities of the solvent and solute, and w_2 is the weight fraction of solute and equals weight of solute÷weight of solution. And, in cases where the susceptibility of the mixture deviates from this law, we will denote it by χ_{mix} and put it in the form,

$$\chi_{mix}=\chi_{add}+\chi_{dev}, \tag{2}$$

where χ_{dev} is the susceptibility arising from deviation. When the expression of χ_{dev} for a given mixture of liquids is found, the magnetic behavior of the mixture is completely known. In the case of formic acid-water mixture, the expression of χ_{dev} has been found by the author on the following assumptions: (1) When water and formic acid are mixed, with the number of water molecules in excess of formic acid molecules, there is one molecule of water for each molecule of formic acid present, which transforms from covalent to electrovalent combination. In general, for a weight fraction of formic acid w_2, there will be a part of water of which the weight fraction is kw_2, transforming from covalent to electrovalent combination, where

$$k=\frac{\text{molecular weight of water}}{\text{molecular weight of formic acid}}=0.391.$$

(2) In all mixtures, formic acid possesses the same diamagnetic susceptibility.

2. FORMULA FOR CALCULATING χ_{mix} OF ACID-WATER MIXTURES

Let us first suppose that the additivity law holds for the mixtures. Then, according to (1), we should have

$$\chi_{add}=(1-w_2)\chi_{w_c}+w_2\chi_2, \tag{3}$$

where w_2 is the weight fraction of formic acid, $(1-w_2)$ is the weight fraction of covalent water, and χ_{w_c} and χ_2 $(=-0.4464)$ are, respectively, the specific susceptibilities of covalent water and formic acid.

Now, according to the assumptions just stated, in such mixtures, covalent water and electrovalent water may coexist, the weight fraction of the former being $(1-w_2-kw_2)$ and that of the latter kw_2. Hence Eq. (3) should be replaced by

$$\chi_{mix}=(1-w_2-kw_2)\chi_{w_c}+kw_2\chi_{w_e}+w_2\chi_2, \tag{4}$$

where χ_{w_e} is the specific susceptibility of electrovalent water. By means of (3), this equation may be rewritten in the form,

$$\chi_{mix}=\chi_{add}-kw_2(\chi_{w_c}-\chi_{w_e}). \tag{5}$$

Comparing with (2), we find

$$\chi_{dev}=-kw_2(\chi_{w_c}-\chi_{w_e}). \tag{6}$$

This is the expression of χ_{dev} which enables us to predict the magnetic behavior of the formic acid-water mixtures. This relation shows that the deviation susceptibility χ_{dev} is proportional to the value of w_2 and, in the case of dilute solution, the value of χ_{dev} is negligibly small, and the additivity law holds practically. Relations (5) and (6) give

$$(-\chi_{dev}/w_2)=(\chi_{add}-\chi_{mix}/w_2)=k(\chi_{w_c}-\chi_{w_e}). \tag{7}$$

The quantity $-\chi_{dev}/w_2$ or $(\chi_{add}-\chi_{mix})/w_2$, having been proved by W. R. Angus[1] to be identical with the quantity $100(\chi_2-\chi_1)/c$ used by S. R. Rao and S. Sriraman[2] in their work, is, therefore, a constant; and since $\chi_{w_c}=-0.72$, $\chi_{w_e}=-0.625$, and $k=0.391$, we have

$$(-\chi_{dev}/w_2)=(\chi_{add}-\chi_{mix}/w_2)=-0.0371. \tag{8}$$

This result is in complete accordance with that found experimentally by Rao and Sriraman.[2] Besides, it will be noted that when the value of w_2 increases so that

$$kw_2=1-w_2 \tag{9a}$$

[1] W. R. Angus, Trans. Faraday Soc. **43**, 221 (1947).
[2] S. R. Rao and S. Sriraman, J. Annamalai Univ. **7**, 187 (1938).

TABLE I.

w_2	$-\chi_{mix}$*	$-\chi_{add}$†	$-(\chi_{add}-\chi_{mix})/w_2$ Calculated	Experimental
0.290	0.6292	0.6407	0.0371	0.040
0.360	0.6105	0.6215	0.0371	0.031
0.490	0.5701	0.5859	0.0371	0.032
0.510	0.5705 ?	0.5805	0.0371	0.020 ?
0.575	0.5414	0.5627	0.0371	0.037
0.695	0.5055	0.5299	0.0371	0.035
0.710	0.5058 ?	0.5257	0.0371	0.028 ?
0.719	—	0.5233	0.0371	—
0.730	—	0.5203	0.0352	—
0.735	—	0.5189	0.0343	—
0.740	—	0.5175	0.0333	—
0.760	—	0.5121	0.0300	—
0.790	0.4834	0.5039	0.0253	0.026
0.850	—	0.4874	0.0167	—

* The same experimental values as those contained in Table II.
† Values obtained from Eq. (3).

TABLE II.

w_2	$-\chi_{mix}$ Calculated	Experimental
0.290	0.6298	0.6292
0.360	0.6080	0.6105
0.490	0.5676	0.5701
0.510	0.5614	0.5705 ?
0.575	0.5412	0.5414
0.695	0.5039	0.5055
0.710	0.4992	0.5058 ?
0.719	0.4966	—
0.730	0.4946	—
0.735	0.4937	—
0.740	0.4928	—
0.760	0.4893	—
0.790	0.4839	0.4834
0.850	0.4732	—

or

$$w_2=(1/1+k)=0.719, \tag{9b}$$

Eq. (4) reduces to the simple form,

$$\chi_{mix}=kw_2\chi_{w_e}+w_2\chi_2, \tag{10a}$$

or by (9a),

$$\chi_{mix}=(1-w_2)\chi_{w_e}+w_2\chi_2. \tag{10b}$$

The last equation, expressing the additivity law for the susceptibility of the mixtures containing formic acid and electrovalent water, takes the same form as that of Eq. (3) which expresses the additivity law for the susceptibility of the mixtures containing formic acid and covalent water.

When the value of w_2 is given by Eq. (9b), Eq. (10b) is evidently identical with Eq. (10a). But, when w_2 increases from this value, it is only Eq. (10b) which represents the magnetic behavior of the mixtures. By means of Eq. (3), we may write Eq. (10b) in the form,

$$\chi_{mix}=\chi_{add}-(1-w_2)(\chi_{w_c}-\chi_{w_e}). \tag{11}$$

Comparing with (2), we find

$$(-\chi_{dev}/w_2)=(\chi_{add}-\chi_{mix}/w_2)$$
$$=(1-w_2/w_2)(\chi_{w_c}-\chi_{w_e}). \tag{12}$$

It is seen that the quantity $-\chi_{dev}/w_2$ or $(\chi_{add}-\chi_{mix})/w_2$ is, now, no longer a constant but a function of w_2. The calculated values obtained from this equation are collected in Table I. They show clearly how the value of the quantity $(\chi_{add}-\chi_{mix})/w_2$ decreases with increase of the value of w_2. This result has also been found by Rao and Sriraman.[2] But, owing to the unavoidable experimental error, they could not tell with certainty at what value of w_2 the quantity $(\chi_{add}-\chi_{mix})/w_2$ began to decrease. What they have found is that this quantity shows a tendency to decrease at higher concentrations corresponding to the values of w_2 greater than 0.79.

The values obtained from (4) and (10b), and the experimental values found by Rao and Sriraman are collected in Table II.

Except for the values with question marks, the agreement between the calculated and the experimental values is good. But I do not think that the observed values -0.5705 and -0.5058 or -0.020 and -0.028 are true. My opinion is quite different from that of Angus[1] who considered the value of $(\chi_{add}-\chi_{mix})/w_2 = -0.020$ as true and believed that the constancy of the quantity $(\chi_{add}-\chi_{mix})/w_2$ was somewhat ill-founded.

3. SUMMARY

(1) When the value of w_2 is less than 0.719, covalent water and electrovalent water coexist in the mixtures, and Eq. (4) is used to calculate the value of χ_{mix}, the quantity $(\chi_{add}-\chi_{mix})/w_2$ given by Eq. (7) being a constant and equal to -0.0371.

(2) When the value of w_2 is equal to 0.719, covalent water disappears from the mixture, and Eqs. (10a) and (10b) each give the value -0.4966. Equations (7) and (12) each give the value -0.0371.

(3) When the value of w_2 is greater than 0.719, Eq. (10b), or Eq. (12), represents the magnetic behavior of the mixtures.

The Calculation of Coefficients of Coulomb and Exchange Integrals in Matrix Elements Involving Polar Singlet Structures

MASSIMO SIMONETTA* AND VERNER SCHOMAKER
Gates and Crellin Laboratories of Chemistry, California Institute of Technology, Pasadena, California†
(Received December 4, 1950)

Starting from Pauling's rules for calculating matrix elements for covalent structures, it is shown how to extend the valence-bond treatment to polar structures. Attention is called to the new types of integrals which are involved and simple procedures for evaluating their coefficients are described.

THE valence-bond method for calculating molecular energy levels, first used by Heitler and London,[1] has been developed by Slater[2] and Pauling[3] for the case of singlet states in such a way as to be easily applicable to complex molecules.[4]

One of the most important criticisms of this usual valence-bond method is that the requirement of one and only one electron per orbital overemphasizes the electron-electron repulsions. It has often been stated that this deficiency could be avoided by the introduction of polar structures; however, we have found in the literature only one attempt, by Sklar,[5] to include them in an actual calculation for a complex molecule. It is not quite clear how Sklar's calculation was carried out; and, furthermore, the ionic resonance energy for an isolated double bond, the value of the single exchange integral, and the heat of hydrogenation of a pure covalent double bond were evaluated by methods which seem inappropriate. Very recently, Craig[6] has worked out the same problem but with consideration only of structures with the charges on adjacent atoms; the differences between his and our assumptions and results will be pointed out in a later paper.

THE SLATER-PAULING TREATMENT

The Slater-Pauling treatment makes use of a completely antisymmetrized product type of wave function, which for a system involving N electrons 1, 2, $\cdots$ and N specific spin-orbit functions A, B, $\cdots$, is

$$\psi=\frac{1}{(N!)^{\frac{1}{2}}}\sum_P(-1)^P PA(1)B(2)\cdots E(N). \quad (1)$$

In general, there are more than N suitable spin-orbit functions; and it is necessary to take into account the corresponding degeneracy, which can often be separated into spin degeneracy and orbital degeneracy. In case of orbital degeneracy more than one ψ, involving different combinations of orbitals, has to be considered. Orbital degeneracy occurs, for example, when there are more available atomic orbitals than electrons. There is always spin degeneracy, and it is necessary to consider all possible distributions of spin which give the desired (singlet) multiplicity. To every conventional valence-bond structure there can be assigned a combination of functions which represents a singlet state. Not all such functions are independent but they do form a complete set: Rumer[7] found that, if the orbitals are arranged in a ring and connected in pairs by nonintersecting straight lines in all possible ways, the corresponding functions form a complete, mutually independent set. These sets were called canonical by Pauling.

In order to specify the sign of the function associated with a bond diagram, it is necessary to write each bond as a vector: $a\rightarrow b$, $c\rightarrow d$, $\cdots$ then corresponds to the wave function,

$$\psi=\frac{1}{2^{n/2}}\sum_R(-1)^R R\left\{\frac{1}{(2n)!^{\frac{1}{2}}}\sum_P(-1)^P \times Pa(1)\beta(1)b(2)\alpha(2)c(3)\beta(3)d(4)\alpha(4)\cdots\right\}, \quad (2)$$

where n is the number of bonds, β and α are the two spin functions, and a, b, etc., the atomic orbital functions—so that $a\beta$ is an example of the spin-orbit functions A, B, etc., indicated in Eq. (1); P represents the $(2n!)$ permutations of the orbits and their associated spins among the electrons 1, 2, $\cdots$, $2n$; and R represents the 2^n interchanges of β and α for orbits bonded together. The factor $(-1)^R$ is equal to $+1$ for an even number of interchanges and -1 for an odd number, and $(-1)^P$ is equal to $+1$ or -1 according to whether P is an even or an odd permutation. For canonical structures the convention is adopted of initially assigning the spin function β and the tail of the arrow to orbital a, α and the arrow head to b, and so on. Then, if only spin degeneracy is involved, and only coulomb and single-exchange integrals are retained, Pauling's superposition diagrams (the arrowheads are no longer needed to define the signs) make it possible to build up the secular equation very quickly. For structures X and Y the

* Present address: Department of General Chemistry, Institute of Technology of Milan (Italy).
† Contribution No. 1495.
[1] W. Heitler and F. London, Z. Physik **44**, 455 (1927).
[2] J. C. Slater, Phys. Rev. **38**, 1109 (1931).
[3] L. Pauling, J. Chem. Phys. **1**, 280 (1933).
[4] L. Pauling and G. W. Wheland, J. Chem. Phys. **1**, 362 (1933); L. Pauling and J. Sherman, *ibid.*, **1**, 679 (1933).
[5] A. L. Sklar, J. Chem. Phys. **5**, 669 (1937).
[6] D. P. Craig, Proc. Roy. Soc. (London) **200**, 390 (1950).
[7] G. Rumer, Nachr. Ges. Wiss. Göttingen, Math-physik Klasse, p. 337 (1932); G. Rumer, E. Teller, H. Weyl, *ibid.*, p. 499 (1932).

coefficient of the coulomb integral in the matrix element H_{XY} of the hamiltonian is given by $K=\frac{1}{2}^{n-i}$ and of the single-exchange integrals by $K'=f/2^{n-i}$, where n is the number of orbitals and i the number of islands in the superposition patterns; f is a coefficient that is equal to 1 if the two exchanged orbitals are in the same island and separated by an odd number of bonds, to -2 if they are in the same island and separated by an even number of bonds, and to $-\frac{1}{2}$ if they are in different islands. A customary further simplifying assumption is that all single exchange integrals between nonadjacent atoms are disregarded (the expression "adjacent atoms" refers to the true molecule and not to the arbitrary diagrams of cannonical structures or superposition patterns). Similarly, in the evaluation of the orthogonality integral Δ_{XY}, i.e., the matrix element of unity, all terms corresponding to any exchange integral in H_{XY} are usually neglected, while the term corresponding to the coulomb integral is taken equal to 1, so that Δ_{XY} is equal to K.

INCLUSION OF POLAR FORMS

The inclusion of polar terms in the valence-bond method ought to be useful for many purposes: to obtain a better value for the principal resonance integral α; to find a better distribution of charge, thus making it possible to calculate electric moments for polar molecules; to treat ions and the molecules of heterocyclic compounds such as pyridine, pyrrole, furan, etc; and to discuss electronic spectra.

Heretofore, the valence-bond method has been applied mainly to unsaturated hydrocarbons and their radicals; it would seem that the nearly constant value found for the exchange integral α means simply that the ratio of resonance energy from covalent structures to that from polar structures is not far from constant in such molecules. But for heterocyclic compounds this cannot be true; for example, as was pointed out by Wheland,[8] furan has a much bigger resonance energy than cyclopentadiene, just because furan, in addition to structures I and II

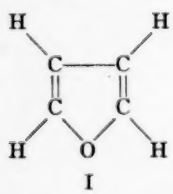

I

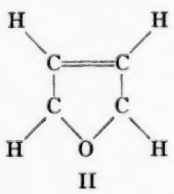

II

involves ionic structures such as III and IV

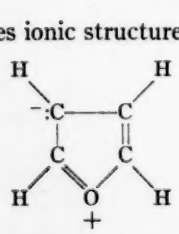

III

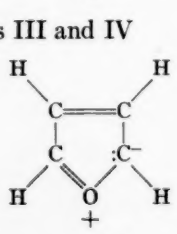

IV

[8] G. W. Wheland, *The Theory of Resonance* (John Wiley and Sons, Inc., New York, 1944), p. 62.

which may be expected to be much more important than are their counterparts for cyclopentadiene.

When polar forms are considered the first thing is to see which of all possible polar structures have to be added to the purely covalent structures to get a complete set of mutually independent singlet structures. It appears that in analogy to Rumer's theorem a complete set of structures is obtained on arranging the electrons in the available atomic orbitals in all different ways, singly or in pairs, and for each of these ways forming the canonical bond structures for the single electrons. The corresponding wave functions are given by Eq. (2) with three changes: (1) a particular orbital may appear, naturally, not only once but twice or not at all, and if it appears twice, must be associated once with spin α and once with spin β; (2) the required set of spin-orbit permutations P and spin reversals R may be achieved either by allowing all permutations of spin-orbits among the electrons and spin reversals for bonded pairs only, or by omitting those permutations which involve exchange of spin-orbits having the same orbital parts while permitting spin reversal for these pairs just as for the bonded pairs; and (3) the normalization factor becomes

$$[2^c\cdot(2n)!]^{-\frac{1}{2}}=[2^n\cdot 2^{-p}(2n)!]^{-\frac{1}{2}},$$

c, p, and $2n$ being the numbers of covalent bonds, unshared pairs, and total electrons, respectively.

When polar structures are considered, the matrix elements of **H** involve new classes of integrals besides the familiar coulomb and exchange integrals Q and α. Among these are coulomb integrals Q' for the polar structures, exchange integrals γ and γ' corresponding to an atom-atom jump by just one electron, where we call the integral γ for one covalent and one polar structure and γ' for two polar structures, and exchange integrals α' involving one or two polar structures and two electron jumps. If in this case both electrons jump from one atom to an adjacent atom, however, the integral is of the form of α and, indeed, is exactly equal to α if the two orbitals are identical. Of course, not all integrals of a class will have the same value; but we shall not discuss their differences here. Neither shall we further consider exchange integrals involving electron jumps between nonadjacent atoms or jumps of more than two electrons.

CALCULATION OF MATRIX ELEMENTS

In order to approach the problem of evaluating the coefficients of these integrals in the matrix elements we may first consider a two-electron case involving three structures,

$$\begin{array}{cccccc} 1\ 2 & & 12 & & & 12 \\ A\text{—}B, & A: & B, & \text{and} & A & B:. \\ \text{I} & & \text{II} & & & \text{III} \end{array}$$

For structure I we get

$$\psi_{\rm I}=\tfrac{1}{2}[a(1)\beta(1)b(2)\alpha(2)-b(1)\alpha(1)a(2)\beta(2)-a(1)\alpha(1)b(2)\beta(2)+b(1)\beta(1)a(2)\alpha(2)],$$

and for structures II and III

$$\psi_{\rm II}=2^{-\frac{1}{2}}[a(1)\beta(1)a(2)\alpha(2)-a(1)\alpha(2)a(2)\beta(2)],$$

and

$$\psi_{\rm III}=2^{-\frac{1}{2}}[b(1)\beta(1)b(2)\alpha(2)-b(1)\alpha(1)b(2)\beta(2)],$$

where a and b are suitable atomic orbital functions depending upon position coordinates, and 1, 2 represent the position and spin coordinates for electrons 1 and 2. The approximate hamiltonian is supposed to be of the form,

$$H=-\frac{h^2}{8\pi^2 m}(\nabla_1^2+\nabla_2^2)+e^2\left(-\frac{Z_A}{r_{A1}}-\frac{Z_B}{r_{B1}}-\frac{Z_A}{r_{A2}}-\frac{Z_B}{r_{B2}}+\frac{1}{r_{12}}+\frac{Z_AZ_B}{r_{AB}}\right).$$

We seek

$$H_{\rm II}=\int\int\psi_{\rm I}H\psi_{\rm I}d\tau_1d\tau_2.$$

Since H does not involve spin or magnetic interactions, the integrals vanish unless all the spins match; and if all the spins match, the integrals over the spin functions are equal to unity, and we obtain

$$H_{\rm II}=\frac{1}{2}\int\int a(1)b(2)Ha(1)b(2)d\tau_1d\tau_2+\frac{1}{2}\int\int a(1)b(2)Ha(2)b(1)d\tau_1d\tau_2+\frac{1}{2}\int\int a(2)b(1)Ha(1)b(2)d\tau_1d\tau_2+\frac{1}{2}\int\int a(2)b(1)Ha(2)b(1)d\tau_1d\tau_2=Q+\alpha.$$

In the same way we have $H_{\rm I\,II}=H_{\rm I\,III}=2^{\frac{1}{2}}\gamma$; $H_{\rm II\,II}=H_{\rm III\,III}=Q'$; $H_{\rm II\,III}=\alpha$; $\Delta_{\rm I\,I}=1$; $\Delta_{\rm II\,II}=\Delta_{\rm III\,III}=1$; $\Delta_{\rm I\,II}=\Delta_{\rm II\,III}=\Delta_{\rm I\,III}=0$. With these values we can set up the secular equation $|H_{XY}-\Delta_{XY}W|=0$.

For more complicated problems it is difficult to write out the functions in full in this way, and it is desirable to find a simpler notation which will serve the same purpose. The following slight modification of Pauling's arrow diagrams is convenient. For any valence bond structure, such as IV,

$$A\quad B\text{—}C\quad D\text{:}\quad \text{IV},$$

the initial disposition of the spin-orbit functions is indicated, respectively, for electrons 1, 2, 3, etc., by a row of letters, such as IVa, with both bonded and unshared pairs connected by arrows,

$$b\rightarrow c\quad d\rightarrow d,\quad \text{IVa},$$

the head of an arrow indicating initial spin function α and the tail β. The many terms of a matrix element of **H** or of unity which need to be counted can now be visualized by juxtaposing these symbols for the two structures involved, for example,

$$\frac{b\rightarrow c\quad d\rightarrow d}{b\rightarrow c\quad d\rightarrow d}\quad\text{for}\quad H_{\rm IV\,IV},$$

and imagining the spin-orbit functions to be permuted among the electrons and the arrows to be reversed, both above and below the line, in all allowed ways. (Our second prescription for the permutations and reversals, which corresponds to allowing reversal of all the arrows and ruling out permutations of identical orbitals in the symbols, turns out to be the more convenient in this connection and will be assumed in the following.) Every permutation of the spin-orbits in one of the factors can be matched by a corresponding permutation in the other so as to give rise to a number of identical contributions to the matrix element; if, therefore, we multiply by the number $(2n)!/2^{p_U}$ of allowed permutations for one of the symbols—we have arbitrarily taken the upper and designated it by the subscript U—the permutations in that symbol need not be considered further. A particular integral over the spatial coordinates, such as the integral,

$$\int b(1)c(2)d(3)d(4)Hb(1)c(2)d(3)d(4)d\tau,$$

which is directly indicated by our superposition diagram, will in general still occur a number of times, since on integrating over the spin coordinates each term which arises from the various possible reversals of arrows can only lead to the same spatial integral with a partial coefficient of ±1 or 0; furthermore, integrals which are equivalent or identical may occur a number of times corresponding to the remaining permutations, if, respectively, the molecule has symmetry or if one or more of the orbitals appears twice in the upper symbol. In any case, the coefficient of the integral which arises from a particular one of these (lower symbol) permutations is equal to the product of normalization factors,

$$2[\tfrac{1}{2}(p_U+p_L)-n]/(2n)!$$

(U and L refer to upper and lower), multiplied by $(2n)!/2^{p_U}$, and by the number of ways of matching spins, which just as in Pauling's method is 2^i, with i the number of *islands* in the juxtaposition diagram. The sign of the coefficient is given by $(-1)^{P_L+R_U+R_L}$, where P_L refers to the permutation that gives rise to the particular integral and the factor $(-1)^{R_U+R_L}$ is the same for each spin match. If we write Δp for p_L-p_U, the

coefficient may then be expressed simply as

$$2^{i-n+\Delta p/2}(-1)^{P_L+(R_U+R_L)}$$

To return to our example, the initial configuration,

$$\frac{b\to c \quad d\to d}{b\to c \quad d\to d}$$

contributes to $H_{IV\,IV}$ the integral Q' with coefficient $2^{2-2+0}\cdot(-1)^0=1$. The only permutations which lead to further important integrals are the exchange of b and c,

$$\frac{b\to c \quad d\to d}{c\leftarrow b \quad d\to d},$$

and of c with both d's,

$$\frac{b\to c \quad d\to d}{b \quad d \quad c \quad d}, \qquad \frac{b\to c \quad d\to d}{b \quad d\leftarrow d \quad c}.$$

Each resulting integral is of the class α', and the last two are identical; if, however, as we assume in the following, the two nonidentical integrals have approximately the same value, this contribution to $H_{IV\,IV}$ is

$$[2^{2+2-2+0}(-1)^{1+1}+2^{1-2+0}(-1)^{1+2}+2^{1-2+0}(-1)^{1+0}]\alpha' = (1-\tfrac{1}{2}-\tfrac{1}{2})\alpha'=0.$$

It will be noted that insofar as the desired integrals can be obtained without exchange of orbitals in the lower symbol or with only single exchanges, the arrowheads can be dropped and Pauling's familiar coefficients $\frac{1}{2}^{n-i}$ and $f/2^{n-i}$ applied. It is only necessary to make sure of the identity of the integral in question and to include the factor $2^{\Delta p/2}$. If this factor is maximized by choosing for the lower symbol the structure with the greater number of unshared pairs, the number of occurrences of identical integrals which have to be explicitly considered is, of course, minimized.

SPECIAL RULES

This method, with its use of a diagram which emphasizes the initial assignment of a labelled orbital to each electron, is very satisfactory for finding any particular coefficient; but in practice it is tedious, and we have found it profitable to derive the following more detailed but somewhat special rules, which can be used directly with the ordinary bond diagrams. No doubt more or less similar procedures useful for other cases can readily be found.

We consider a system involving an even number of electrons, and the same number of atoms arranged in a straight chain or simple ring with at most one polar bond, which may have 0, 1, or 2 atoms between the charged atoms. Those cases for the ionic structures we call ortho-, meta-, and para-, respectively.

The application of each rule is illustrated by an example taken from the benzene problem, which we have chosen for this purpose because of its general interest. It is assumed that the different integrals of each of our classes α, γ, γ', and α' are equal.

In consequence of our previous assumption that all other exchange integrals are negligible, the matrix element H_{XY} will vanish if an electron must jump to a nonadjacent atom or more than two electrons must jump to adjacent atoms in order to transform structure X into structure Y.

(I) $\dfrac{\text{non-ionic}}{\text{ionic}}$

(A) $\dfrac{\text{non-ionic}}{\text{ortho-ionic}}$ $\quad H_{XY}=\gamma 2^{i^*-i}.$

j = number of covalent bonds in ionic structure,

i^* = number of islands, with an open polygon counted as $\frac{1}{2}$ an island.

Example:

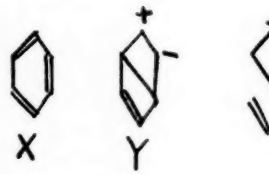

$H_{XY}=\gamma 2^{-\frac{1}{2}}=\gamma/\sqrt{2}.$

(B) $\dfrac{\text{non-ionic}}{\text{meta-ionic}}.$

For this case we have been unable to find a simple rule which is applicable to superpositions of ordinary bond diagrams, so that the matrix element has to be determined by our general method, which leads to

$$H_{XY}=\alpha' 2^{\frac{1}{2}-n+i},$$

with i the number of islands in the juxtaposition symbol.

Example:

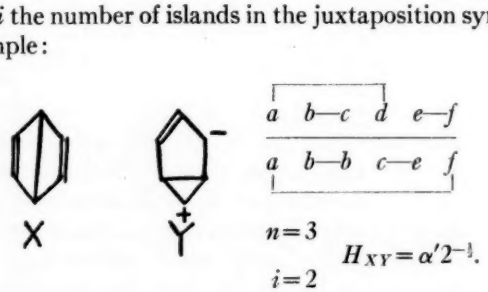

$H_{XY}=\alpha' 2^{-\frac{1}{2}}.$

(C) $\dfrac{\text{non-ionic}}{\text{para-ionic}}$ $\quad H_{XY}=0.$

Example:

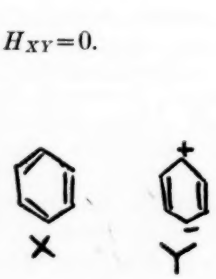

$H_{XY}=0$. (More than two electron jumps are required to change X into Y.)

(II) ortho/ortho
meta/meta
para/para

(A) Same charge distribution in both structures.

$$H_{XY}=KQ'+K'\alpha'.$$

Here K and K' are calculated with Pauling's rules, as described earlier in this paper, considering an ionic bond as equivalent to a covalent bond in the determination of n and i. There are no exchange integrals with atoms positively charged, but a double number of exchange integrals with atoms negatively charged.
Example:

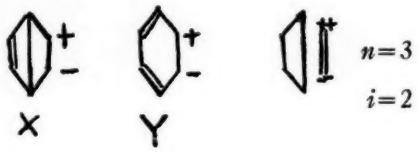

(B) Charges inverted. For ortho/ortho

$$H_{XY}=K\alpha,$$

where K is obtained in the same way as before.
Example:

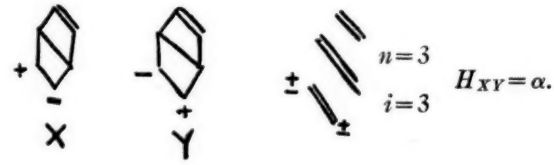

For meta/meta and para/para $H_{XY}=0$.
(C) Charges on different atoms.
(1) $H_{XY}=0$, double-jump rule.
(2) $H_{XY}\neq 0$
ortho/ortho and para/para: $H_{XY}=\alpha'2^{i-j}$.
Example:

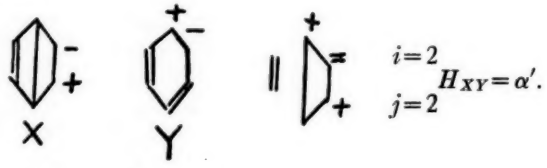

meta/meta: $H_{XY}=\alpha'2^{i'-j}$.

Here i' is calculated by connecting atoms with plus charge with each other, and atoms with minus charge with each other: if two negative charges fall on the same atom, the result is zero island; if two positive charges fall on the same atom, the result is one island; furthermore, if a bond between two atoms with minus charge is crossed by two covalent bonds, i' is diminished by 1; if the same thing happens to a bond between two positively charged atoms, i' is increased by 1.

Examples:

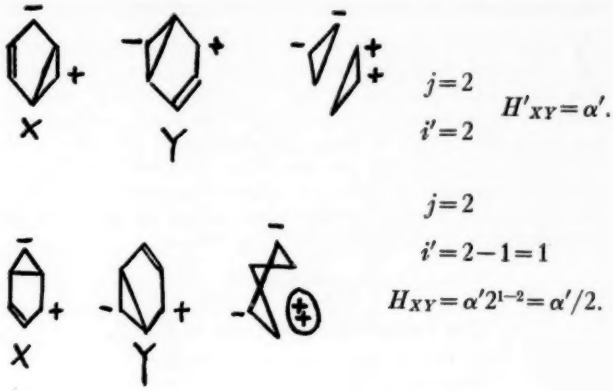

(III) ortho/meta
meta/para

(1) $H_{XY}=0$, double-jump rule.
(2) $H_{XY}=\gamma'2^{i-j}$, otherwise.
Example:

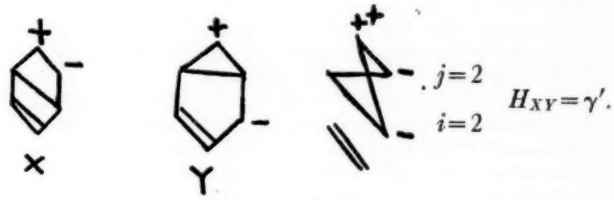

(IV) ortho/para

(1) $H_{XY}=0$, double-jump rule.
(2) $H_{XY}=\alpha'2^{i''-j}$, otherwise.
Here the number i'' is calculated by connecting plus with plus and minus with minus and counting islands. The group minus minus counts as zero island and group plus plus as one island.
Example:

The above rules have been applied to the treatment of some molecules with the assumption of reasonable values for Q, the several Q', α, α', γ, and γ'. The results are to be published soon.

ACKNOWLEDGMENTS

This problem was suggested to us by Professor Pauling, to whom we are also much indebted for many helpful discussions. One of us (M.S.) wishes to express thanks to the Italian Research Council for a grant.

Letters to the Editor

THIS section will accept reports of new work, provided these are terse and contain few figures, and especially few half-tone cuts. The Editorial Board will not hold itself responsible for opinions expressed by the correspondents. Contributions to this section should not exceed 600 words in length and must reach the office of the Managing Editor not later than the 15th of the month preceding that of the issue in which the letter is to appear. No proof will be sent to the authors. The usual publication charge ($8.00 per page) will not be made and no reprints will be furnished free.

The Infrared Spectrum of KHF_2

J. A. A. KETELAAR AND W. VEDDER
Laboratory for General and Inorganic Chemistry, University of Amsterdam, The Netherlands
(Received March 5, 1951)

THE infrared absorption (and reflection) spectra of KHF_2 show two neighboring strong fundamental frequencies at 1222 cm^{-1} and 1450 cm^{-1}, [in reflection at 1238 cm^{-1} and 1490 cm^{-1}], which have been interpreted as a doubling of the active asymmetric valency vibration ν_3 of a linear $[FHF]^-$ ion, due to a double minimum potential curve.[1]

However, as Pitzer and Westrum[2] failed to detect a peak in the heat capacity curve near 20°K, they were led to believe that these two frequencies represent the ν_3 and ν_2 fundamentals, respectively, the latter being the deformation frequency.

In order to prove definitely which of the two assignments is right, we measured the reflection spectra in polarized light of a thick crystal of KHF_2[3] from a plane cut parallel to the tetragonal C-axis (D_{4h}^{18}, $I4/mcm$). As the HF_2-groups are in a plane perpendicular to the C-axis, the vibrational moment for the valency vibration ν_3 is also at right angles to this axis. The deformation frequency ν_2, which is twofold degenerate for the free ion will at least in principle split in the crystal into two, one with the moment in the plane, the other with the moment at right angles to it, parallel to the C-axis, which we will call ν_2 and ν_2' [see also reference 4].

With the electric vector of the polarized light at right angles to the C-axis we can expect according to both our original assignment and to the interpretation of Pitzer and Westrum both frequencies just as they were observed formerly by us in reflection from the face (001). However, with the electric vector parallel to the C-axis no reflection maximum can be expected according to the first assumption, whereas according to the latter the frequency ν_2' would have to be found at about the same wavelength as observed formerly for the low frequency component.

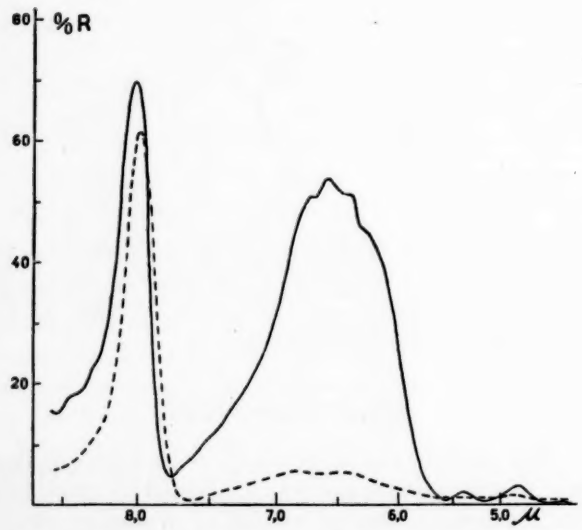

FIG. 1. Reflection from a plane of KHF_2, cut parallel to the C-axis, relative to an aluminum mirror. ——— Electric vector perpendicular to C-axis. - - - - Electric vector parallel to C-axis.

In Fig. 1 it is clearly indicated that the interpretation according to Pitzer's assignment is correct.

We now find for ν_3 1510 cm^{-1} (formerly 1490 cm^{-1}, a broad maximum) and for the deformation frequency we find as expected a small difference for both components ν_2: 1245 cm^{-1} (formerly 1238 cm^{-1}) and ν_2': 1250 cm^{-1}. Thus there is no indication of a double minimum character with the FHF potential as supposed formerly by the first of us.

The very small remnant of ν_3 in the reflection curve, with the electric vector deviation parallel is probably due to the deviation of 7° from right angle incidence. The faint structure in the band at 1510 cm^{-1} is not real, but due to incomplete correction for the water absorption in the long optical path.

The frequency of the inactive fundamental ν_1, given formerly as 550–580 cm^{-1} from combination overtones has been essentially conformed by the investigation of the Raman effect by Mathieu and Couture[4] which revealed two frequencies 595 cm^{-1} and 604 cm^{-1} doubled by the interaction between two HF_2-groups in the elementary cell.

The further assignment of the many absorption maxima will be made when also the absorption spectra in polarized light of slabs cut parallel to the C-axis are completed.

[1] J. A. A. Ketelaar, Rec. Trav. Chim. **60**, 523 (1941); J. Chem. Phys. **9**, 775 (1941).
[2] K. S. Pitzer and E. F. Westrum, J. Chem. Phys. **15**, 526 (1947). Also D. Polder [Nature **160**, 870 (1947)] failed to observe an abnormal behavior in the dielectric constant.
[3] We thank L. Couture-Mathieu for setting at our disposal a thick crystal of KHF_2.
[4] L. Couture and J. P. Mathieu, Compt. rend. **228**, 555 (1949). J. P. Mathieu and L. Couture-Mathieu, Compt. rend. **230**, 1054 (1950).

Mass Spectrometer Resolution of Ion Pairs of Similar m/e

DUANE V. KNIEBES AND SIDNEY KATZ
Institute of Gas Technology, Chicago, Illinois
AND
RICHARD B. BERNSTEIN
Chemistry Department, Illinois Institute of Technology, Chicago, Illinois
(Received March 14, 1951)

AN investigation has been undertaken to determine the limits of mass resolution of the consolidated mass spectrometer, Model 21–103. Mixtures of "isobaric" pairs of ions were scanned with the instrument modified for very low scanning speeds and set for maximum resolution. Table I lists the pairs studied in the

TABLE I.

Ion pair[a]		ΔM[b]	$(\Delta M/M)\times 10^3$
He^{++}	H_2^+	0.0144	7.14
He^+	D_2^+	0.0255	6.33
O^+, O_2^{++}	CH_4^+	0.0363	2.26
A^{++}	D_2O^+	0.0416	2.08
A^+	$C_3H_4^+(C_3H_6)$	0.0685	1.71
CO_2^+	$C_3H_8^+$	0.0727	1.65
$NO^+(HNO_2)$	$C_2H_6^+$	0.0490	1.63
$OH^+(NH_4OH)$	$NH_3^+(NH_4OH)$	0.0238	1.40
$C^{13}O^+(C^{13}O_2)$	$C_2H_6^+(C_2H_6)$	0.0409	1.40
CO^+	$C_2H_4^+$	0.0363	1.29
H_2CO^+	$C_3H_8^+$	0.0363	1.21
N_2^+	$C_2H_4^+$	0.0251	0.90
N^+, N_2^{++}	$CH_2^+(CH_4)$	0.0126	0.90*
$C_2O^+(n-C_4H_9OH)$	$C_4H_4^+(C_4H_6)$	0.0364	0.1*
D^+	H_3^+	0.0016	0.79*
$CS^+(CS_2)$	CO_2^+	0.0191	0.43*
CO^+	N_2^+	0.0112	0.40*

[a] Terms in brackets indicate the parent molecules.
[b] M values are atomic weight units divided by the number of charges.

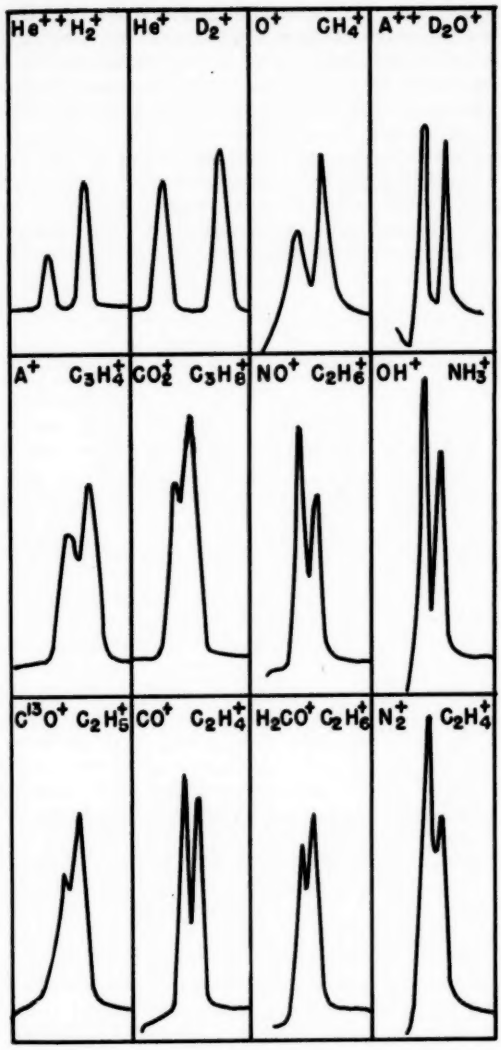

FIG. 1.

approximate order of decreasing ease of resolution, together with the mass differences (ΔM) in atomic weight units[1] and the ratios of mass difference to mass, $(\Delta M/M)\times 10^3$. The galvanometer tracings for the pairs for which separation was effected are shown in Fig. 1. It was noted that negative ion peaks[2] usually occurred in the region immediately before the region under study. Pairs for which measurable separation was not obtained are designated with asterisks.

The implications of these results with respect to analytical mass spectrometry are apparent.

[1] Sullivan, *Trilinear Chart of Nuclear Species* (John Wiley & Sons, Inc., New York, 1949).
[2] A. G. Sharkey and R. A. Friedel, J. Chem. Phys. **17**, 998 (1949).

The Interpretation of Intermolecular Force Parameters

S. D. HAMANN
C.S.I.R.O. Division of Industrial Chemistry, High Pressure Laboratory, Sydney University, Australia
(Received February 26, 1951)

A RECENT article by Bird, Spotz, and Hirschfelder[1] referred to earlier observations of Hirschfelder *et al*[2] on the relationship between the critical volume of a nonpolar gas and the molecular volume calculated from second virial coefficient data. For spherical molecules these two quantities are in the ratio predicted by theory. For ellipsoidal molecules, however, the molecular volumes derived from virial coefficients are considerably larger than the theoretical relationship requires. The explanation given by these authors was that an ellipsoidal molecule in a dilute gas describes, in rotating, a sphere with diameter equal to the molecular length. Its effective volume is therefore greater than it is when the molecules are packed together in the critical state.

Some quantitative evidence supporting this view is found in a comparison of the equilibrium intermolecular separations r^* (from virial coefficient data) and the calculated lengths of some nearly ellipsoidal nonpolar molecules. This comparison is made in Table I. The column r^* lists the equilibrium intermolecular distances derived from second virial coefficient data assuming the applicability of the Lennard-Jones intermolecular field defined by:

$$E=E^*[(r^*/r)^{12}-2(r^*/r)^6], \qquad (1)$$

where E is the mutual potential energy of two molecules separated by a distance r, and E^* is the maximum interaction energy corresponding to $r=r^*$. The first three molecules of Table I are spherically symmetrical and the values listed under l are the intermolecular distances in their close-packed crystals. The remaining molecules are linear and their lengths l have been calculated from the observed internuclear distances together with the atomic van der waals radii which Pauling[3] based upon crystallographic data (with the additional value of 1.57A for carbon).

TABLE I.

	r^*(A)	l(A)		r^*(A)	l(A)
Ne	3.08[a]	3.20	O_2	4.02[e]	4.00
A	3.83[a]	3.83	CO	4.10[d]	4.10
CH_4	4.28[b]	4.16	NO	4.29,[f] 3.56[b]	4.04
H_2	3.28[c]	3.14	N_2O	5.15[b]	5.21
N_2	4.10[d]	4.09	CO_2	5.13[b]	5.13

[a] R. A. Buckingham, Proc. Roy. Soc. (London) **A168**, 264 (1938).
[b] See reference 2.
[c] J. de Boer and A. Michels, Physica **5**, 945 (1938).
[d] J. Corner, Proc. Phys. Soc. (London) **58**, 737 (1946).
[e] J. O. Hirschfelder and W. E. Roseveare, J. Phys. Chem. **43**, 15 (1939).
[f] Calculated from data measured by H. L. Johnston and H. R. Weimer, J. Am. Chem. Soc. **56**, 625 (1934).

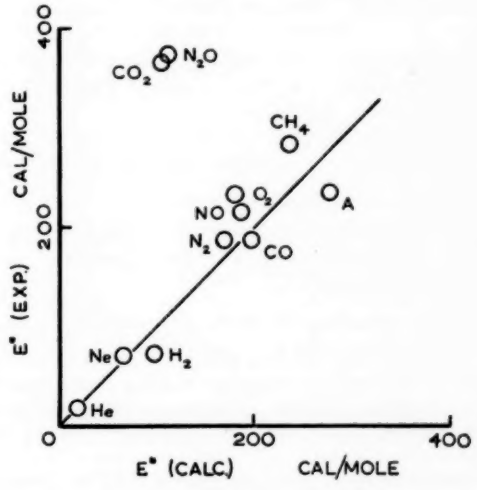

FIG. 1.

It is seen that, except in the case of NO, r^* agrees with l to within 0.15A, that is, almost to within the uncertainty of the summed van der waals radii. It is from 20 to 40 percent higher than the mean diameter calculated from the volume of the van der waals model (except, of course, for Ne, A, and CH_4).

The identity of r^* and l allows the calculation of E^* from molecular parameters which can be observed independently of gas be-

havior. This is done by writing, from Eq. (1):

$$-E^*=c/2r^{*6}$$

where c is the coefficient of the r^{-6} term in the intermolecular potential. For the almost nonpolar molecules considered here only dispersion forces contribute to c. It is convenient to use the derivation of these forces by Slater and Kirkwood and by Kirkwood,[4] which gives:

$$c=3eh(N\alpha^2/m)^{\frac{1}{2}}/8\pi\cdots \quad (2)$$

in which e and m are the electronic charge and mass, h is Planck's constant, α is the polarizability of the molecule and N is the number of electrons in the molecule. In the present calculations the molecular polarizabilities have been estimated from the refractive indices of the gases and the values l (Table I) have been used for r^*.

The figures for E^*(calc) determined in this way have been plotted against E^*(exp) (from second virial coefficient data references as in Table I) in Fig. 1. The extent of agreement between the experimental and calculated values is remarkable considering that Eq. (2) is only approximately applicable to many-electron molecules and that E^* is enormously dependent upon the value chosen for r^*. The outstanding failures of the theory occur for the linear triatomic molecules N_2O and CO_2 and may be due to the rather wide departure of these molecules from spherical symmetry.

[1] Bird, Spotz, and Hirschfelder, J. Chem. Phys. **18**, 1395 (1950).
[2] Hirschfelder, McClure, Curtiss, and Osborne, N.D.R.C. Rep. A116 (1942).
[3] L. Pauling, *Nature of the Chemical Bond* (Cornell University Press, Ithaca, New York, 1940), p. 189.
[4] J. C. Slater and J. G. Kirkwood Phys. Rev. **37**, 682 (1931). J. G. Kirkwood, Physik. Z. **33**, 57 (1932).

The Effect of Halogenation on the C—Br Bond Dissociation Energy in Halogenated Bromomethanes

M. SZWARC AND A. H. SEHON
Chemistry Department, University of Manchester, Manchester, England

(Received March 13, 1951)

THE pyrolyses of methyl bromide and of the halogenated bromomethanes: CH_2ClBr, CH_2Br_2, $CHCl_2Br$, $CHBr_3$, CF_3Br, CCl_3Br, and CBr_4 were investigated by the use of the "toluene carrier" technique. It was shown that all these decompositions were initiated by the unimolecular dissociation process

$$R.Br\rightarrow R\cdot+Br. \quad (1)$$

Since these reactions were carried out in the presence of an excess of toluene, the bromine atoms produced in process (1) were removed by the fast reaction (2)

$$C_6H_5.CH_3+Br\rightarrow C_6H_5.CH_2\cdot+HBr. \quad (2)$$

Hence, the rate of the unimolecular dissociation process (1) was measured by the rate of formation of HBr. Furthermore, the formation of dibenzyl in the pyrolysis of each of these bromomethanes revealed clearly the radical mechanism of the over-all decomposition.

The kinetics of these pyrolyses showed that the investigated processes were essentially homogeneous gas reactions of the first order with respect to the bromide. The rate constants were affected, however (except in the case of CCl_3Br and CBr_4), by the pressure of toluene. The dependence of the rate of decomposition on the toluene pressure forced us to abandon the calculation of activation energies from the temperature coefficients of the respective rate constants. The relevant bond dissociation energies were calculated, therefore, by using the Arrhenius expression for the rate constant of a unimolecular decomposition

$$k=\nu.e^{-D/RT}.$$

The values of k used in this computation were obtained from experiments carried out at the lowest temperatures. The frequency factor, ν, which was *assumed to be constant* throughout the whole series, was estimated at 2.10^{13} sec^{-1} from the results of the pyrolysis of methyl bromide, $D(CH_3-Br)$ being taken at 67.5 kcal/mole. The latter value was determined from thermochemical data in conjunction with the well-established values for $D(CH_3-H)$. This particular estimate of ν compares well with the value of 1.10^{13} sec^{-1} for the frequency factor of the pyrolysis of Cl_3CBr, which was determined experimentally from the temperature coefficient of the rate constant. The close agreement between these two values of ν is our justification for assuming that the frequency factor remains constant throughout the whole series. The C—Br bond dissociation energies obtained on this basis are listed in Table I.

TABLE I.

Compound	D(C—Br) kcal/mole	Compound	D(C—Br) kcal/mole	Compound	D(C—Br) kcal/mole
CH_3Br	(67.5)	CH_2Br	(67.5)	CH_3Br	(67.5)
...	...	CH_2ClBr	61.0	CH_2Br_2	62.5
...	...	$CHCl_2Br$	53.5	$CHBr_3$	55.5
CF_3Br	64.5	CCl_3Br	49.0	CBr_4	49.0

For polybromomethanes the experimental rate constants were divided by the appropriate statistical factor, i.e., the number of bromine atoms in the molecule. These rate constants per bromine atom were used in the above calculations.

The outstanding feature of this investigation is the striking decrease in the C—Br bond dissociation energy along the series from CH_3Br to CX_3Br, where X designates a chlorine or bromine atom. One would anticipate a decrease in the C—Br bond dissociation energy with increasing degree of halogenation on account of the increasing steric repulsion between the bulky halogen atoms. To illustrate the steric interaction between the various halogens in these compounds, we have given in Fig. 1 the schematic model of a halogenated bromomethane molecule, the circles representing the accepted van der waals radii[1] for fluorine, chlorine, and bromine. This diagram reveals clearly that while the overlapping between the fluorine and bromine atoms in CF_3Br is negligible, the overlapping between the chlorine and bromine atoms or two bromine atoms in chlorinated or brominated methyl bromides is quite considerable. Furthermore, it is evident that the extent of the overlap between a chlorine and a bromine atom differs only slightly from that between two bromine atoms. It is also apparent that this steric repulsion becomes more pronounced as the number of chlorine or bromine atoms increases.

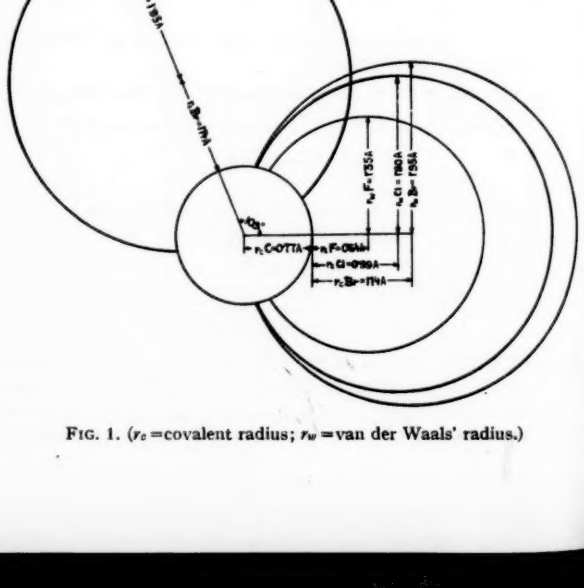

FIG. 1. (r_c = covalent radius; r_w = van der Waals' radius.)

One would expect, therefore, that as a result of this steric repulsion the C—Br bond in Cl_3CBr and CBr_4 would be longer than in CH_3Br. Inspection of the available data on interatomic distances[2] does not indicate, however, any significant change in the C—Br bond distance in bromomethanes. We conclude, therefore, that there must be another factor compensating for the expected lengthening of the bond due to steric repulsion and leaving the bond strength unaffected.*

It seems that this "compression" factor can be interpreted in terms of the results of a recent study of bond energy-bond length relationship by Warhurst and Scanlan.[3] These workers proposed a theoretical treatment for molecules of the type MXn, where the M—X bond has a partially ionic character. Assuming that the strength of the M—X bond is unaffected by the number of X atoms in the molecule they deduced that the M—X bond length decreases with increasing value of n. This result is a mathematical consequence of the increasing degeneracy of the system. We suggest, therefore, that the Scanlan-Warhurst effect might account for the observed constancy of the C—Br bond length in bromomethanes.

The observed variation in the C—Br bond dissociation energy along the series CH_3Br to CX_3Br might be attributed, therefore, to the increasing steric repulsion. In addition to this factor, we have to consider the effect of resonance stabilization of the relevant radicals on the C—Br bond dissociation energy. It was suggested[4,5] that the stabilization of a radical R might be measured by the difference $D(CH_3—H)-D(R—H)$. On the basis of this assumption we deduce that the stabilization of the Cl_3C. radical amounts to ~12 kcal/mole,† this value being the difference between $D(CH_3—H)$ and $D(Cl_3C—H)$.

The additional decrease of the C—Br bond dissociation energy in Cl_3CBr as compared with that in CH_3Br would then measure the steric repulsion between the bromine and chlorine atoms which is removed during the dissociation of the Cl_3CBr molecule. We are, however, unable to assess the correction which ought to be introduced in order to account for the possible change in the ionic character of the C—Br bond in Cl_3CBr with respect to that in CH_3Br.

A full account of this work is in course of preparation.

One of us (A.H.S) wishes to thank Monsanto Chemicals, Ltd., Ruabon, for a maintenance grant.

[1] L. Pauling, *The Nature of the Chemical Bond* (Cornell University Press, Ithaca, New York, 1945).
[2] P. W. Allen and L. E. Sutton, Acta Cryst. **3**, 46 (1950).
* See also R. M. Badger, J. Chem. Phys. **3**, 710 (1935).
[3] J. Scanlan and E. Warhurst, Trans. Faraday Soc. **45**, 1000 (1949).
[4] Baughan, Evans, and Polanyi, Trans. Faraday Soc. **37**, 377 (1941).
[5] M. Szwarc, J. Chem. Phys. **18**, 1660 (1950).
† This amount measures the total stabilization of the $Cl_3C\cdot$ radical which might be made up of two contributions: (i) the "electronic" stabilization, and (ii) the decrease in the repulsion energy during the process of dissociation, when the closely packed tetrahedral Cl_3C group opens to give the probably planar configuration of the $Cl_3C\cdot$ radical.

The Influence of Aromatic Substitution on the C—Br Bond Dissociation Energy

M. Szwarc, C. H. Leigh, and A. H. Sehon
Chemistry Department, University of Manchester, Manchester, England

(Received March 13, 1951)

THE investigation of the thermal decompositions of benzyl and allyl bromides[1] showed that the respective C—Br bond dissociation energies could be determined by pyrolysing these compounds in an excess of toluene. Under the experimental conditions used in these investigations the bromide molecule dissociates according to Eq. (1)

$$R.Br \rightarrow R\cdot + Br. \qquad (1)$$

The bromine atom formed in this process is removed rapidly by reaction (2)

$$C_6H_5.CH_3 + Br \rightarrow C_6H_5.CH_2\cdot + HBr. \qquad (2)$$

Hence, the rate of the initial dissociation (1) is measured by the rate of formation of HBr, and the formation of dibenzyl is considered proof of the radical character of reaction (1).

Assuming that the recombination process

$$R + Br \rightarrow R.Br$$

does not require any activation energy, it was concluded that the C—Br bond dissociation energy, $D(R—Br)$, is measured by the activation energy of the unimolecular dissociation process (1).

In the present study this same technique was used for the determination of the changes in the C—Br bond dissociation energies of the substituted benzyl bromides: *p*-, *m*-, and *o*-xylyl bromides, *p*-, *m*-, and *o*-chlorobenzyl bromides, *p*- and *m*-bromobenzyl bromides, *p*- and *m*-nitrobenzyl bromides, and *p*- and *m*-nitrilebenzyl bromides. The difference between $D(Ph.CH_2—Br)$ and $D(Ph_s.CH_2—Br)$ was measured by the difference in activation energies of reactions (3) and (4)

$$Ph.CH_2.Br \rightarrow Ph.CH_2\cdot + Br, \qquad (3)$$

$$Ph_s.CH_2.Br \rightarrow Ph_s.CH_2\cdot + Br, \qquad (4)$$

$Ph_s.CH_2\cdot$ denoting here the substituted benzyl radical. Assuming that the frequency factor of these unimolecular reactions is not affected by substitution,* we calculated the differences, ΔD's, between $D(Ph.CH_2—Br)$ and the values for $D(Ph_s.CH_2—Br)$ by using the relation

$$\Delta D = 2.3.R.T.\log_{10}(k_s/k_u).$$

k_u and k_s denote the unimolecular rate constants of reactions (3) and (4), respectively. The results obtained by this method are listed in Table I.

The data listed in Table I seem to indicate that the substitution of a hydrogen atom in the benzene ring by a chlorine or bromine atom does not affect the C—Br bond dissociation energy in $Ph_s.CH_2.Br$, particularly if the substituting halogen atom is in the para or meta position. The apparent increase in ΔD observed in the case of *o*-chloro-benzyl bromide might be due to ortho-effect affecting the frequency factor, which would then invalidate the calculation for ΔD. The results obtained for the chloro and bromo derivatives are in agreement with the conclusions drawn from the investigation of the pyrolyses of the fluorotoluenes.† It appears, therefore, that the influence of the field effect on a bond dissociation energy is negligible even for so highly a polar bond as that in $Ph_s.CH_2—Br$.

The substitution of a hydrogen atom in the benzene nucleus by a methyl group in the meta position seems to have no effect on $D(Ph_s.CH_2—Br)$. On the other hand, the introduction of a methyl group in the ortho or para position seems to weaken the corresponding C—Br bond strength. The calculated values for ΔD are 2.0 kcal/mole for *o*-xylyl bromide and 1.4 kcal/mole for *p*-xylyl bromide. These two results should be treated however with some reservation, since the ortho-effect might invalidate the calculation in the case of ortho-xylyl bromide and the pyrolysis of *p*-xylyl bromide exhibited some peculiarities. In this connection it is worth mentioning that the C—H bond dissociation energy in *m*-xylene was found to be the same as that in toluene, while $D(o\text{-}CH_3.C_6H_4.CH_2—H)$ and $D(p\text{-}CH_3.C_6H_4.CH_2—H)$ were

TABLE I.

Substituted benzyl bromides	ΔD kcal/mole
o-chloro	0.9
m-chloro	0.1
p-chloro	0.4
m-bromo	0.3
p-bromo	0.3
o-methyl	2.0
m-methyl	0.0
p-methyl	1.4
m-nitro	2.1
p-nitro	1.1
m-nitrile	1.4
p-nitrile	0.7

The values of ΔD are given to the nearest 0.1 kcal/mole.

found to be smaller than $D(C_6H_5.CH_2-H)$ by 3.5 kcal/mole and 2.5 kcal/mole respectively.[2]

The results obtained for nitro- and nitrile-benzyl bromides indicate a small decrease in the corresponding C—Br bond dissociation energies. Although it seems premature to analyze further the factors responsible for these small changes in bond dissociation energies, it is to be stressed that these substituents have a considerable effect on the rate of ionic reactions, e.g., Hammett's σ-factor for the *p*-nitrile and *p*-nitro groups have the extremely high values of +1.00 and +1.27 respectively.[3]

In conclusion we would like to point out that the effects of substitution on bond dissociation energies are to be attributed to different factors from those affecting the rates of ionic reactions. Thus the present study reveals that the effect of substitution in the benzene nucleus on $D(Ph_5.CH_2-Br)$ is very small indeed.

A detailed account of this investigation is in course of preparation.

[1] Szwarc, Ghosh, and Sehon, J. Chem. Phys. **18**, 1142 (1950).
* The justification for this assumption was discussed elsewhere. M. Szwarc, Chem. Revs. **47**, 75 (1950).
† The latter investigation had shown that $D(C_6H_5.CH_2-H)$ is approximately equal to $D(C_6H_4F.CH_2-H)$ irrespective of the position of the fluorine atom in the benzene ring. M. Szwarc and J. S. Roberts, J. Chem. Phys. **16**, 609 (1948).
[2] M. Szwarc, J. Chem. Phys. **16**, 128 (1948).
[3] L. P. Hammett, *Physical Organic Chemistry* (McGraw-Hill Book Company, Inc., New York, 1940).

Combination Bands of Ethylene

EARLE K. PLYLER
National Bureau of Standards, Washington, D. C.
(Received March 5, 1951)

THE fundamental vibrational frequencies of ethylene have been often studied. Recently Arnett and Crawford[1] have made a reassignment of the fundamental bands. We have observed the fine structure of a number of combination bands in the region 1.6 to 2.5μ and wish to present a preliminary report at this time as the results seem to require a revision of the assignment of the above-named authors. In the present work the absorption spectrum of C_2H_4 has been measured with an infrared spectrometer using a 15,000 line/in. grating. The path length was 60 cm, and the pressure varied from 10 cm Hg to 57 cm Hg. Sixteen bands have been observed, and there are several weaker bands which are so much overlapped that they could not be measured accurately.

Our assignment, given in Table I, accounts for all expected binary combinations except $\omega_1+\omega_{11}$ and $\omega_1+\omega_9$ which are believed to be present but overlapped. Further careful measurements will be made to determine their existence. It will be noted that a number of the strong bands involve ω_5. The ternary combinations are not always certain.

TABLE I. The assignments of the bands of C_2H_4 observed in the region from 1.6 to 2.5μ.

In cm^{-1} in vacuum	Type	Intensity	Assignment
4206	*B*	S	$\omega_6+\omega_{11}$
4323	*A*	S	$\omega_3+\omega_{11}$
4328	*A*	M	$\omega_6+\omega_9$
4411	*A,B*	W	$(\omega_1+\omega_{12})(\omega_3+\omega_9)$
4514	*B*	S	$\omega_5+\omega_{12}$
4728	*B*	S	$\omega_2+\omega_9$
4949	*B*	M	$\omega_5+\omega_7+\omega_8$
5059	*A*	W	$\omega_1+\omega_6+\omega_{10}$
5802	*B*	W	$\omega_2+\omega_6+\omega_{11}$
5918	*C*	W	$\omega_1+3\omega_7$
5929	*A*	M	$\omega_2+\omega_3+\omega_{11}$
5995	*B*	M	$\omega_9+2\omega_{12}$
5997	*C*	W	$\omega_2+\omega_4+\omega_5$
6029	*A*	S	$\omega_1+\omega_{11}$
6071	*A*	M	$\omega_1+\omega_2+\omega_{12}$
6150	*A*	VS	$\omega_5+\omega_9$

In making the assignments the values of the fundamentals of Rank, Shull, and Axford[2] and of reference 1 are adopted except that ω_5 must be lowered from their value of 3272.5 cm^{-1} to the neighborhood of 3075 cm^{-1}. This follows unequivocally from the occurrence of the strong bands at 6150 and 4514 cm^{-1} which cannot otherwise be accounted for. The combination $\omega_5+\omega_9$ is also very strong in C_2D_4. With $\omega_5=3075$ cm^{-1} the anharmonic term $X_{5,9}$ is of comparable magnitude in C_2H_4 and C_2D_4; with $\omega_5=3275$ cm^{-1} an abnormally high anharmonicity would be indicated. As pointed out by Arnett and Crawford, the Raman line observed in the liquid by Rank, Shull, and Axford at 3075 cm^{-1} is depolarized and could well be the ω_5 fundamental.

The fine structure of the bands shows considerably more detail than was reported in the bands studied by Gallaway and Barker.[3] In addition to the two principal spacings of about 8.1 cm^{-1} in types *B* and *C* bands and about 1.8 cm^{-1} in type *A* bands, many weaker lines, some as close as 0.12 cm^{-1} have been resolved. This additional structure probably arises from the facts that the molecule only approximates a symmetric rotor and that vibration-rotation interactions, Fermi and Coriolis resonances, exist among the many possible upper-state levels.

[1] R. L. Arnett and B. L. Crawford, J. Chem. Phys. **18**, 118 (1950).
[2] Rank, Shull, and Axford, J. Chem. Phys. **18**, 116 (1950).
[3] W. S. Gallaway and E. F. Barker, J. Chem. Phys. **10**, 88 (1942).

Equation of State for Liquids

FRANK MASLAN AND ETIENNE ABERTH
Chemical Engineering Department, New York University, University Heights, New York, New York
(Received March 5, 1951)

IN a recent paper, De Boer and Lunbeck[1] discussed the Lennard-Jones and Devonshire theory of liquids in terms of a molecular law of corresponding states. According to this law, reduced liquid volume, $V_1^*=V_1/Nr_0^3$, is a unique function of reduced temperature, $T^*=kT/\epsilon$, providing there is no quantum-mechanical effect in the liquid. They showed that theoretically all liquids require a quantum effect correction. The parameter for this is $\Lambda^*=h/r_0(m\epsilon)^{\frac{1}{2}}$, and V_1^* is a function of (Λ^*).[2]

Their curves of V_1^* *versus* $(\Lambda^*)^2$ for experimental volumes of H_2, He, Ne, A, and Kr are straight smooth lines which confirm the dependence of V_1^* on Λ^*. For the heavy molecular weight Lennard-Jones liquids, they found that Λ^* approaches zero. The values of r_0 and ϵ used in these calculations were obtained from the following intermolecular field equation:

$$\phi(r)=4\epsilon[(r_0/r)^{12}-(r_0/r)^6]. \quad (1)$$

We applied their theory to experimental volume and molecular data of other liquidified gases:[2,3] CH_4, N_2, O_2, C_2H_6, N_2O, C_3H_8, SO_2, and CO_2 and found poor correlation. Reference to Table I shows that V_1^* has no uniform dependence on $(\Lambda^*)^2$. Furthermore, the V_1^* values are all considerably lower than those predicted from De Boer and Lunbeck's curves. According to their curves, the

TABLE I. Reduced liquid volume.

Gas	$(\Lambda^*)^2$	V_1^* $T^*=0.8$	$T^*=0.9$	$T^*=1.0$
CH_4	0.0582	1.062	1.115	1.177
N_2	0.0552	1.132	1.190	1.263
O_2	0.0449	1.150	1.215	1.300
C_2H_6	0.0142	1.060	1.115	1.185
N_2O	0.0132	0.956	1.022	1.100
C_3H_8	0.0067	0.925	0.966	1.020
SO_2	0.0065			0.910
CO_2	0.0014			0.904
Ne[a]	0.349	1.37	1.45	1.58
A[a]	0.035	1.26	1.33	1.47
Kr[a]	0.0104	1.24	1.32	1.44
Classical[a]	0	1.23	1.31	1.41

[a] See reference 1.

limiting values for V_1^* at $T^*=0.8$, 0.9, and 1.0 are 1.23, 1.31, and 1.41, respectively. This is for a molecule obeying the classical statistical mechanics. However, all of our values are below these.

There are several reasons for these departures from their theory. First, the quantum corrections are numerically small at temperatures above 15°K[3]. Second, the molecules which we have considered are not spherical. Hence Eq. (1) is probably not an accurate representation of molecular interaction in the liquid state. Hirschfelder, *et al.*[3] found that use of Eq. (1) gave excellent results when applied to the gaseous viscosity of these gases. However, in the liquid state the molecules are much closer together and departure from the Lennard-Jones law is probable.[4] Third, the gases which we considered are much more complex than those of De Boer and Lunbeck. It seems likely that other correction parameters must be considered which take into account the various distributions of energy in the more complex molecules.

[1] J. De Boer and R. J. Lunbeck, Physica **14**, 520 (1948).
[2] J. H. Perry, Editor, *Chemical Engineers' Handbook*, Third Edition (McGraw-Hill Book Company, Inc., New York, 1950).
[3] Hirschfelder, Bird, and Spotz, Chem. Revs. **44**, 205 (1949).
[4] Buehler, Wentorf, Jr., Hirschfelder, and Curtiss, J. Chem. Phys. **19**, 61 (1951).

A Property of the Mass-Ratio $m_{Cl^{35}}/m_{O^{16}}$

P. TORKINGTON
British Rayon Research Association, Urmston, Lancaster, England
(Received February 26, 1951)

WHILE engaged on calculations of the properties of vibrations of the chlorine monoxide molecule, a property of the mass-ratio $\mu=m_{Cl^{35}}/m_{O^{16}}$ was observed which may be of interest. It is found that for these masses $\mu(1+2\mu)=11.746_4$ and $1+2(1+2\mu)=11.745_4$. This appears rather a remarkable coincidence. In the present instance it led to misapplication of formulas—it was some time before the identity was established. If the two functions are equated, then the mass-ratio arises as the (positive) root of the equation $(1+2\mu)(\mu-2)=1$, or $2\mu^2-3(\mu+1)=0$. It would be of interest if either such identities existed.

A New Viewpoint in Computing Crystal Frequencies

W. A. NIERENBERG
Department of Physics, University of California, Berkeley, California
(Received February 27, 1951)

AS a result of some observations on the eigenvalues of certain infinite matrices, the problem of finding the distribution of characteristic vibration frequencies in crystals can be viewed from an entirely different aspect. The characteristic infinite matrices governing the motion of the atoms of a crystal have the simplifying property that the matrix elements which lie on a diagonal parallel to the main diagonal have a simple periodicity which is the same for all diagonals. The eigenvalues of such a matrix can be written down at sight. As an example, consider the matrix N whose matrix elements are given by the complex numbers

$$(N)_{m,m+n}=c_n. \tag{1}$$

This matrix has all elements on the diagonal "n off the main diagonal" equal to the same constant c_n. The eigenvalues of this matrix are given by

$$\lambda=\sum_{-\infty}^{\infty} c_n e^{inx}, \quad 0\leq x\leq 2\pi, \tag{2}$$

where x is a continuous parameter and the eigenvalues are uniformly distributed with respect to x. As an application consider the two-dimensional lattice whose atoms are vibrating perpendicularly to the plane:[1]

$$M\ddot{u}_n=\alpha[(u_{n-1}-2u_n+2u_{n+1})+(u_{n-L}-2u_n+u_{n+L})] +\gamma[(u_{n+L-1}-2u_n+u_{n+L+1})+(u_{n-L-1}-2u_n+u_{n-L+1})]. \tag{3}$$

There are L^2 atoms in the square network, and they are ordered linearly and next nearest neighbors are taken into account. The frequencies are therefore given by

$$\omega^2=4\alpha+4\gamma-2\alpha\cos x-2\alpha\cos Lx -2\gamma\cos(L-1)x-2\gamma\cos(L+1)x, \tag{4}$$

where $L\to\infty$ and $0\leq x\leq 2\pi$. Whereas the usual procedure involves ω^2 as a given function over an area, this method determines ω^2 as a function of the points of a line. The inversion problem changes character. With the usual procedure, it is essentially geometric. Now it is essentially analytic. As in illustration, consider Eq. (4) with $\gamma=0$. A given value of ω^2 corresponds to a large number of values of x, x_i. The density function $g(\omega^2)$ is

$$g(\omega^2)=\Sigma_i\left|\frac{d(\omega^2)}{dx}\right|^{-1}_{x=x_i}. \tag{5}$$

This is easily evaluated and yields

$$g(\tilde{\omega}^2)=\frac{4}{\pi^2\omega^2}K\left(\frac{1-\tilde{\omega}^2}{\tilde{\omega}^2}\right), \quad \tilde{\omega}^2\leq\tfrac{1}{2}, \tag{6}$$

where $\tilde{\omega}^2$ is normalized to unit range. This agrees with Eq. (9c) for $\alpha=0$ in reference 1.

In application to a real, two-dimensional, monatomic crystal, there are two branches of form similar to Eq. (4) with, however, a quadratic radical, and the analytic problem is more difficult. Similarly, the three-dimensional, diatomic crystal has six branches given by the roots of a sixth-degree equation.

A detailed comparison of this procedure with the more classical methods[2] emphasized the fact that the main achievement is the statement of the problem in completely analytic form without any recourse to geometric methods. In particular, it would appear that this method is basically suited to numerical computations of crystal frequencies.

The author is grateful to Professors G. C. Wick, R. Serber, and C. Kittel for useful discussions of the problem.

[1] W. A. Bowers and H. B. Rosenstock, J. Chem. Phys. **18**, 1056 (1950).
[2] The author gratefully acknowledges the stimulation of discussions with Professor E. W. Montroll in making these comparisons.

The Raman Spectra of Hexamethylcyclotrisiloxane and Octamethylcyclotetrasiloxane

HIROMU MURATA
The Osaka Municipal Technical Research Institute, Osaka, Japan
(Received March 13, 1951)

IT was shown by C. W. Young, P. C. Servais, C. C. Currie, and M. J. Hunter,[1] experimenting on the infrared absorption spectra of the trimer and tetramer most frequently obtained during the preparation of cyclic disubstituted siloxanes by the hydrolysis of R_2SiCl_2-type compounds in organic solutions, how infrared absorption spectra may be used to distinguish between these two forms of polysiloxanes. However, the spectra of these polymers were almost identical, and there was a difference only near the region of $\Delta\nu=1000$–1100 cm^{-1} attributed to ring distortion.

I have found moderate difference existed in the Raman spectra of hexamethylcyclotrisiloxane and octamethylcyclotetrasiloxane. The samples are prepared as follows: dimethyldichlorosilane is hydrolyzed by adding it slowly to vigorously stirred water at a temperature of 0–10°C. On fractional distillation, trimer and tetramer are isolated, and purified by redistillation. They have following physical properties: trimer, m.p. 65°, b.p. 134°; tetramer, m.p. 18.5°, b.p. 175°. The Raman spectra of these compounds are given in Table I. The Si—O ring of the trimer takes a planar structure;[2] but since it is predictable that probably this is not the case for the tetramer, difference in the modes of ring distortion between these polymers may be expected. Therefore, I believe that the work to distinguish between cyclic trimer and tetramer must be done in the smaller $\Delta\nu$-range.

TABLE I. Raman spectra of hexamethylcyclotrisiloxane and octamethylcyclotetrasiloxane (cm^{-1}).

	Trimer			Tetramer		
skeletal vibration				147	(3b)	(ek)
	193	(9b)	(e)	193	(7b)	(e)
				250	(2b)	(ek)
	457	(6s)	(ek)	474	(6b)	(ek)
	586	(6s)	(ek)	710	(6b)	(ek)
	650	(2s)	(ek)			
	731	(3b)	(ek)			
	791	(3s)	(ek)	787	(3b)	(ek)
	883	(2b)	(ek)	875	(2b)	(ek)
	1046	(0b)	(e)	1040	(2b)	(ek)
inner vibration	1260	(2s)	(ek)	1260	(2s)	(ek)
	1327	(5s)	(e)	1323	(5b)	(ek)
	1395	(5s)	(ek)	1396	(5b)	(ek)
	2783	(4s)	(ek)	2788	(1s)	(e)
	2903	(10s)	(ek)	2902	(10b)	(ek)
	2972	(9s)	(ek)	2961	(10b)	(ek)

I am indebted to Dr. H. Tani (Osaka University) for the samples.

[1] Young, Servais, Currie, and Hunter, J. Am. Chem. Soc. **70**, 3958 (1948).
[2] E. H. Aggarwal and S. H. Bauer, J. Chem. Phys. **18**, 42 (1950).

Determination of an Isotope Effect in the Decarboxylation of Malonic-1-C^{14} Acid

ARTHUR ROE AND MAX HELLMANN
Radioisotope Laboratory and Venable Chemical Laboratory, University of North Carolina, Chapel Hill, North Carolina
(Received March 5, 1951)

YANKWICH and Calvin[1] studied the decarboxylation of malonic acid containing C^{14} in only one carboxyl group and reported an isotope effect which they expressed as the ratio of frequency of rupture of a $C^{12}-C^{12}$ bond to that of a $C^{12}-C^{14}$ bond; the magnitude of this ratio was 1.12 ± 0.03. In a later communication Bigeleisen[2] calculated the theoretical isotope effect for this reaction and obtained a value of about 1.04. In support of the correctness of this calculation Bigeleisen and Friedman[3] determined the isotope effect in the decarboxylation of malonic acid of normal isotopic composition by measuring the fractionation of $C^{13}O_2$. The experimental results obtained were in close agreement with the theoretical prediction.

In view of the discrepancies in the magnitude of the calculated and observed isotope effect for malonic-1-C^{14} acid the decarboxylation studies were repeated in this Laboratory by using a method somewhat different from that of Yankwich and Calvin.[1]

The malonic acid was prepared by an adaptation of the method of Baumgarten and Hauser;[4] the decarboxylations were performed at constant temperatures (usually 153–154°C). The acetic acid formed was separated by collecting it in dry ice traps and the carbon dioxide was frozen out in liquid air traps. The amount of carbon dioxide present was then determined by transferring it to a calibrated measuring system; subsequently it was passed directly into an ionization chamber. The malonic and acetic acids were assayed by converting them to carbon dioxide by the wet oxidation method of Van Slyke and Folch[5] and introducing the carbon dioxide into an ionization chamber. All activity measurements were taken on a vibrating reed electrometer[6] by using the rate of drift method. This instrument is reported to give a higher efficiency than G-M counters and has the further advantage that samples of very low activities can be used.

The processes involved in the decarboxylation of malonic acid are as follows:

$$CH_2(CO_2H)_2 \xrightarrow{k_1} CH_3CO_2H+CO_2$$

$$CH_2(C^{14}O_2H)(CO_2H) \xrightarrow{k_2} CH_3CO_2H+C^{14}O_2$$

$$\xrightarrow{k_3} CH_3C^{14}O_2H+CO_2.$$

The magnitude of the isotope effect was calculated by using the equation developed by Bigeleisen[2] which for $t=\infty$ can be simplified to

$$\text{Act.}_{\text{M.A.}}/\text{Act.}_{CO_2}=(k_2+k_3)/k_2, \quad \text{or}$$
$$\text{Act.}_{\text{HOAc}}/\text{Act.}_{CO_2}=k_3/k_2.$$

A large number of determinations was made. Some inconsistencies in the results were noted but from ten determinations performed with samples of different activities the isotope effect expressed as k_3/k_2 was found to be 1.06 ± 0.02 which is smaller than the results reported by Calvin and Yankwich and approaches the theoretical value.

In addition to the complete decompositions described above several experiments have been performed in which samples of CO_2 were withdrawn at various stages of the decomposition. A kinetic formula has been developed to express the activity of these increments of CO_2 as a function of time. This treatment would make it possible to evaluate the ratio k_1/k_2+k_3, i.e., the relative rates of decarboxylation of the labeled and unlabeled acids. A detailed summary of this work will be presented at a later date when more reliable experimental data have been accumulated.

We wish to acknowledge the generous support of this research by the Research Corporation and by the Atomic Energy Commission (Contract AT-(40–1)–270).

[1] Yankwich and Calvin, J. Chem. Phys. **17**, 109 (1949).
[2] Bigeleisen, J. Chem. Phys. **17**, 425 (1949).
[3] Bigeleisen and Friedman, J. Chem. Phys. **17**, 998 (1949).
[4] Baumgarten and Hauser, J. Am. Chem. Soc. **66**, 1037 (1944).
[5] Van Slyke and Folch, J. Biol. Chem. **136**, 509 (1940).
[6] Palevsky, Swank, and Grenchik, Rev. Sci. Instr. **18**, 298 (1947).

Carrier-Free Radioisotopes from Cyclotron Targets. XVI. Preparation and Isolation of Pd^{103} from Rhodium*

JEANNE D. GILE, HERMAN R. HAYMOND, WARREN M. GARRISON, AND JOSEPH G. HAMILTON
Crocker Laboratory, Radiation Laboratory, and Divisions of Medical Physics, Experimental Medicine, and Radiology, University of California, Berkeley and San Francisco, California
(Received March 23, 1951)

THE 17-day Pd^{103} was prepared[1] from rhodium by the nuclear reaction $Rh^{103}(d, 2n)Pd^{103}$ using the 20-Mev deuteron beam of the 60-inch cyclotron at the Crocker Laboratory. In the procedure described below, the Pd^{103} is isolated in the carrier-free state from the target element and from the 41-day Ru^{103} which is produced concurrently in low yield by the (n, p) reaction. "Palladium-free" rhodium foil,[2] 20 mil thick, was clamped to a water-cooled aluminum target plate and bombarded for a total of 155 μa-hr at an average beam intensity of 10 μa. The bombarded rhodium metal (approx. 1 g) was fused with excess potassium acid sulfate and the resultant mass was leached with water. A small amount of insoluble material which did not carry activity was removed by centrifugation. The supernatant solution was made 6*N* in hydrochloric acid by the addition of appropriate amounts of 12*N* hydrochloric acid and sodium chloride. Five milligrams of selenium as selenous acid was added, and the solution was saturated with sulfur dioxide. The resultant precipitate

of elemental selenium, which carried over 99 percent of the Pd^{103}, was separated from solution by centrifugation, washed with water, dissolved, and reprecipitated. The final selenium precipitate containing the Pd^{103} was dissolved in 36*N* sulfuric acid, transferred to an all-glass distilling flask, and distilled at 200°C with the addition of 9*N* hydrobromic acid. The residue which contained all of the Pd^{103} activity was evaporated to dryness on 40 mg of sodium sulfate. The activity dissolved quantitatively in 5 ml of water.

The activity was followed for 80 days and showed only the assigned 17-day half-life.[3,4] The *x*-radiation had a half-thickness in aluminum of 200 mg/cm², which agrees closely with the previously observed value.[5] The activity was further identified by chemical separation through the use of added palladium, rhodium, and ruthenium carriers.

We wish to thank Professor G. T. Seaborg for helpful suggestions; Mr. T. Putnam, Mr. B. Rossi, and the crew of the 60-inch cyclotron for bombardments; and Miss Margaret Gee for assistance in counting.

* This document is based on work performed under Contract No. W-7405-eng-48-A for the AEC.

[1] G. T. Seaborg and I. Perlman, Revs. Modern Phys. **20**, 585 (1948).
[2] Spectrographic analysis showed less than 0.01 percent palladium.
[3] A. R. Brosi, Plutonium Project Report, Mon N-150 (July, 1946).
[4] D. E. Mathews and M. L. Pool, Phys. Rev. **72**, 163 (1947).
[5] H. F. Gunlock and M. L. Pool, Phys. Rev. **74**, 1264 (1948).

The Infrared Spectrum of $H_2C=CD_2$

JOHN E. LANCASTER, RICHARD G. INSKEEP, AND BRYCE L. CRAWFORD, JR.
School of Chemistry, University of Minnesota, Minneapolis, Minnesota
(Received March 5, 1951)

IN the study of the planar vibrations of ethylene, we have prepared asymmetrical $C_2H_2D_2$ and have observed its infrared spectrum. The sample contained approximately 5 percent monodeuteroethylene. The spectrum of a second preparation containing CH_2CD_2, C_2H_3D, and C_2H_4 in a ratio of 4:4:1 facilitated the identification of monodeuteroethylene bands in the first sample.

Table I lists the observed bands and their band type together with a tentative assignment.

Our observations confirm the assignment of the nonplanar fundamentals of this molecule which were made by Arnett and Crawford.[1] We are also in essential agreement with the reported results of Courtoy, de Hemptinne, and Migeotte[2] on the spectrum of C_2H_3D.

Work is now in progress on the spectra of the *cis-* and *trans-*dideuteroethylenes, and on the determination of the in-plane force constants of ethylene.

TABLE I. Bands observed in the infrared spectrum of $CH_2=CD_2$.

$\bar{\nu}$	Type	Intensity	Possible assignment
700?	*B*	w	ω_{10} (Band center not certain)
752	*C*	s	ω_7
808	*C*	w	ω_7 of C_2H_3D
944	*C*	s	ω_8
1000	*C*	w	ω_4 of C_2H_3D
1032	*A*	m	ω_3
1150	*B*	vw	ω_6
1291	*A*	w	C_2H_3D
1384	*A*	m	ω_{12}
1484	*B*	w	$\omega_7+\omega_{10}$ Coriolis perturbed
1585	*A*	w	ω_2
1711	*B*	vw	$\omega_3+\omega_{10}$
1840	*A*?*C*?	vw	$\omega_6+\omega_{10}$
1879	*A*	m	$2\omega_8$
2031	*A*?*C*?	vw	$\omega_4+\omega_6$
2091	*A*?*C*?	vw	$2\omega_3$
2131	*A*	vw	?
2231	*A*	m	ω_{11}
2335	*B*	m	ω_9
2526	*B*	vw	$\omega_6+\omega_{12}$
2754	*B*	vw	$\omega_2+\omega_6$
2955	*A*	w	$\omega_2+\omega_{12}$
3019	*A*	m	ω_1
3095	*B*	m	ω_5
3169	*A*?	vw	$2\omega_2$
3369	*B*	vw	$\omega_3+\omega_9$
3467(center) 3492(*Q*)	*A*	vw	$\omega_6+\omega_9$
3609	*A*	vw	$\omega_{11}+\omega_{12}$
3718	*B*	vw	$\omega_9+\omega_{12}$
4152	*B*	vw	$\omega_3+\omega_5$ or $\omega_1+\omega_6$
4228(center) 4237(*Q*)	*A*	vw	$\omega_3+\omega_6$
4464	*B*	vw	$\omega_5+\omega_{12}$

Errata: Radiotracer Studies of Cationic Surface-Active Agents by Measurement of Gegenion Adsorption

[J. Chem. Phys. **19**, 378 (1951)]

CHARLES M. JUDSON, ANN A. ARGYLE, J. K. DIXON, AND D. J. SALLEY
Stamford Research Laboratories, American Cyanamid Company, Stamford, Connecticut

THE coordinate labels were omitted in the two figures of the letter cited above. The abscissa in Fig. 1 should be labeled "Aerosol *SE* sulfate concentration" with values from 0 to 400 $\times 10^{-5}$ equivalents/liter, and the ordinate should be labeled "Sulfate adsorbed" with values from 0 to 120×10^{-11} equivalents/cm². The abscissa in Fig. 2 should be labeled "Sulfate concentration" with values from 0 to 400×10^{-5} equivalents/liter, and the ordinate should be labeled "Sulfate adsorbed" with values from 0 to 140×10^{-11} equivalents/cm².

Interpretation of the Infrared and Raman Spectra of Mixed Crystals

HENRY J. HROSTOWSKI AND GEORGE C. PIMENTEL
Department of Chemistry and Chemical Engineering, University of California, Berkeley, California
(Received March 22, 1951)

INTEREST in the infrared and Raman spectra of solids has been stimulated by recent contributions to the theoretical aspects of their interpretations.[1-3] Solid phase spectra differ from the gas phase spectra because of alteration of selection rules and/or shift of the fundamental frequencies. These spectral changes accompanying solidification may be conveniently attributed to two distinguishable influences of the lattice.

1. The molecular symmetry may be perturbed by the crystal's potential field with the local symmetry of the site group.

2. The molecular vibrations may be perturbed by coupling with identical molecular systems, with the symmetry of the coupling appropriate to the space group.

In veryifying the theory and in experimentally determining the relative importance of the two perturbations, it would be convenient to study these perturbations individually. It is possible to eliminate the coupling with identical molecular systems by studying molecule *A* in a *dilute* solid solution with an isomorphous molecule *B*. If the crystal parameters of solids *A* and *B* are quite close, if *A* fits into the *B* lattice, and if the *B* lattice has the same site symmetry as *A*, it is possible to study the influence of site symmetry alone on the spectrum of *A*. This corresponds to partial or complete elimination of the potential term V_{mm}', the coupling of the internal modes of different molecules, in the potential function proposed by Hornig.[2] (In the weak fields of most molecular crystals, only identical vibrational modes of adjacent molecules will couple appreciably.) Multiplicities introduced by the molecular coupling (as indicated by the space group analysis) should be lost. Band structure caused by coupling with lattice modes should be altered, since the lattice modes will no longer be those of the *A* lattice. Dichroism should pass from that of the components of the space group multiplets (if resolved) to that of *A* molecules held in the site positions of the *B* lattice; roughly the dichroism of a gas whose molecules are oriented in space as in the unit cell.

[1] R. L. Arnett and B. L. Crawford, Jr., J. Chem. Phys. **18**, 118 (1950).
[2] Courtoy, de Hemptinne, and Migeotte, J. Chem. Phys. **19**, 137 (1951).

Of particular interest in mixed crystal systems would be a dilute solid solution of a deuterated compound in the corresponding undeuterated compound (or vice versa). In this case, the crystalline forces would be virtually identical to those in either of the pure crystals. Hence, the influence of site group symmetry in the mixed crystal should be identical to that in the pure crystal and *all* spectral changes must be caused by disturbance of the coupling among molecules of the unit cell. Spectroscopic studies of such mixed crystals are in progress in this laboratory.

Raman studies of mixed crystals have been reported earlier for the systems paradichlorobenzene-paradibromobenzene,[4] sodium chloride-potassium chloride,[5] and potassium nitrate-sodium nitrate.[6] In the first system, the only molecular crystal investigated, the solid solutions were not studied at concentrations sufficiently low to provide a clear-cut test of this proposal. Saksena[7] proposes an explanation of the apparent shift of the torsional lattice modes for this mixed dihalobenzene system. The mixed crystal frequencies are calculated using a statistical average of the moments of inertia, a proposal which would not be expected to apply to vibrational modes of molecular crystals. Matossi[8] also attacks the problem of lattice vibrations of mixed crystals but considers in detail only ionic crystals.

[1] R. S. Halford, J. Chem. Phys. **14**, 8 (1946); H. Winston and R. S. Halford, *ibid.* **17**, 607 (1949).
[2] D. F. Hornig, J. Chem. Phys. **16**, 1063 (1948).
[3] R. Newman and R. S. Halford, J. Chem. Phys. **18**, 1276 (1950).
[4] S. C. Sirkar and I. C. Bishur, Indian J. Phys. **6**, 327 (1937) and references there cited.
[5] Krueger, Reinkobes, and Koch-Holm, Ann. Physik **85**, 110 (1928).
[6] M. K. Raju, Proc. Indian Acad. Sci. **22A**, 150–6 (1946) and references there cited.
[7] B. D. Saksena, J. Chem. Phys. **18**, 1653 (1950).
[8] F. Matossi, J. Chem. Phys. **19**, 161 (1951).

Relations between Dye Phosphors and Hydrogen Bonds of Rigid Media or Surface of Adsorbents

DAIJIRO YAMAMOTO AND RYOJIRO IWAKI
Department of Chemistry, Tokyo University of Education, Otsuka, Tokyo, Japan
(Received March 19, 1951)

THERE are many studies on the phosphorescence of dyes dissolved in rigid media and adsorbed on the surface of some solid materials. It was, however, G. N. Lewis, D. Lipkin, and T. Magel[1] who suggested that through hydrogen bonds the solvent molecules were clamped tightly, not only to one another, but often to the dye molecules as well.

The authors examined the contribution of hydrogen bonds to the dye phosphors, using the well-known phosphorescent dye "Trypaflavin." In the case of adsorbents of organic high molecular compounds, celluloses (Cellophane, paper, cotton, and linen), starch, dextrin, agar-agar, and solid proteins (gelatin, silk, wool, and solid egg-albumin) were good ones for dye phosphors. Some of them checked well with the work of H. Kautsky.[2] It was interesting that such nitrocelluloses as trinitrocellulose, solid collodion, and celluloid were not phosphorescent adsorbents. In the case of adsorbents of organic low molecular compounds, we used the crystallization method from saturated solutions of the dye in ethyl alcohol or water, dissolving the examined materials in them. Good phosphorescent adsorbents are summarized in Table I. In this case, the sorts of solvents for the dye were important to make phosphors. For example, in the case of glucose, powders obtained from water solution were good phosphors, but from alcoholic solution not. This may depend on, perhaps, the solubility of materials in each solvent.

Those materials have hydrogen bonds in crystals or molecules. Other materials like hydroquinone, pyrogarol, *p*-phenylendiamin, monomethyl-*p*-amidphenol sulfate, diphenylamine, and stearic acid did not make phosphors. In the case of inorganic adsorbents, boric acid crystal obtained from both water and alcoholic solutions of the dye was remarkable, but intensity of phosphorescence was less than the one dissolved in the glassy boric acid.

TABLE I.[a]

	Materials	Solvent of dye	Intensity of phosphorescence
1	Oxalic acid	*A*, *W*	strong
2	Tartaric acid	*A*, *W*	strong
3	Citric acid	*A*, *W*	strong
4	Potassium bitartarate	*W*	weak
5	Benzoic acid	*A*	strong
6	Salicylic acid	*A*	strong
7	Resorcinol	*A*	moderate
8	Glucose	*W*	moderate
9	Dextrose	*W*	strong
10	Lactose	*W*	moderate
11	Glycine	*W*	feeble
12	Alanine	*W*	feeble
13	Saccharin	*A*, *W*	strong
14	Dulcin	*W*	feeble
15	Urea	*A*, *W*	strong

[a] In the table *A* means the one obtained by using alcoholic solution, *W* by water solution, and *A*, *W* by both solutions.

From the experimental results, it is considered that hydrogen bonds of adsorbents or rigid media are important factors to the dye phosphors. The nature of combination between solvents and dye molecules in the case of acridine dyes may be the type of $-OH\cdots N\lessdot$ and $>NH\cdots N\lessdot$, or such resonance combination as dye-polypeptide interaction as suggested by S. Mizushima *et al.*[3] This consideration may give us a new suggestion on the triplet state of π-electron as a phosphorescent state. Detailed discussion will be reported in another paper.

[1] Lewis, Lipkin and Magel, J. Am. Chem. Soc. **63**, 3005 (1941).
[2] Kautsky, Hirsch, and Baumeister, Ber. **64**, 2053 (1931).
[3] S. Mizushima and T. Shimanouchi, Bull. Chem. Soc. Japan, **21**, 1 (1948).

Erratum: On the Viscosity of Liquid Hydrocarbon Mixtures

[J. Chem. Phys. **19**, 137 (1951)]

FAUSTO W. LIMA
Escola Politécnica, Department of Chemistry, University of São Paulo, São Paulo, Brazil

FORMULA (1) should be written

$$\log\log\eta=(x_1I_1+x_2I_2)d/(x_1M_1+x_2M_2)-k,$$

and formula (2) should be written

$$\log\log\eta=(I_1+I_2)d/(M_1+M_2)-k.$$

Erratum: Suggested Structures of Water in Inert Gas Hydrates

[J. Chem. Phys. **19**, 259–60 (1951)]

W. F. CLAUSSEN
Illinois State Water Survey, Urbana, Illinois

ON page 260, lines 15 and 19, the number of pentagonal dodecahedra is 16, not 12; the hypothetical hydrating number calculation for small molecules is thus 136/24, or $5\frac{2}{3}$.